2010-06-08

# Development of Novel Image Analysis Methods for the Morphological Quantification of Filamentous Fungi

David Barry
*Technological University Dublin*, david.barry@tudublin.ie



## Recommended Citation

Barry, D. J. (2010). *Development of Novel Image Analysis Methods for the Morphological Quantification of Filamentous Fungi*. Doctoral Thesis. Technological University Dublin. doi:10.21427/D7730D

# Development of Novel Image Analysis Methods for the Morphological Quantification of Filamentous Fungi

**David J Barry, BE**

School of Biological Sciences

School of Electrical Engineering Systems

Dublin Institute of Technology

Republic of Ireland

A thesis submitted in fulfilment of the requirements for the degree of

Doctor of Philosophy

Supervisors:

Dr. Gwilym A. Williams, Dr. Raymond Ryan and Prof. Jonathan M. Blackledge


Submitted: 31st March 2010

Defended: 8th June 2010

## Abstract

Mycelial morphology is a critically important process property in fermentations of filamentous micro-organisms, as particular phenotypes are associated with maximum productivity. The design of systems capable of rapidly and accurately characterising morphology within a given process represents a significant challenge to biotechnologists, as the complex phenotypes that are manifested are often not easily quantified.

A system has been developed for high-resolution characterisation of filamentous fungal growth, using membrane immobilization and fully-automatic image-processing software. The system has been used to quantify the early-stage hyphal differentiation of *Aspergillus oryzae* on solid substrates, by measuring spore projected area and circularity, the total length of a hyphal element, the number of tips per element, and the hyphal growth unit. Spore swelling expressed as an increase in mean equivalent spore diameter was found to be approximately linear with time. Widespread germination of spores was observed by 8 h after inoculation. From approximately 16 h, the number of tips was found to increase exponentially. The specific growth rate, maximum hyphal tip extension rate and specific branching frequency of a population of hyphae were calculated as approximately 0.27 $h^{-1}$, 27 $\mu m\ tip^{-1}\ h^{-1}$ and $2.3 \times 10^{-3}$ tips $\mu m^{-1}\ h^{-1}$ respectively. The robustness of the image-analysis system was verified by testing the effect of small variations in the input parameters.

Subsequent experimentation focussed on investigating the morphological development of *A. oryzae* in submerged culture and the associated influence on $\alpha$-amylase production. The temporal variation in pellet structure and $\alpha$-amylase production over time was quantified and the potential for the use of membrane-immobilisation in submerged culture was examined. Variation in carbon source type had little

morphological impact, although increasing starch concentration caused a shift from a pelleted form to dispersed, 'pulp-like' growth. Increasing inoculum concentration was found to result in a decrease in mean pellet diameter and an increase in $\alpha$-amylase production. The supplementation of fermentation media with non-ionic detergents caused a significant increase in $\alpha$-amylase production (up to 149%), but this increase did not seem to be related to observed morphological variation.

Recently, fractal geometry has been employed in the study of filamentous microbes, but a clear link between fractal dimension and branching behaviour has not been demonstrated. This thesis presents an alternative means of enumerating the fractal dimension of fungal mycelial structures, by generating a 'fractal signal' from an object boundary. In the analysis of a population of *A. oryzae* mycelia, both fractal dimension and hyphal growth unit were found to increase together over time, while cultivating populations of *Penicillium chrysogenum* and *A. oryzae* mycelia under a variety of different conditions revealed a strong correlation between fractal dimension and hyphal growth unit. The technique has the potential to be adapted and applied to any morphological form that may be encountered in a fermentation process, providing a universally-applicable parameter for more complete data acquisition.

## Declaration

I certify that this thesis, which I now submit for examination for the award of Doctor of Philosophy, is entirely my own work and has not been taken from the work of others, save and to the extent that such work has been cited and acknowledged within the text of my work.

This thesis was prepared according to the regulations for postgraduate study by research of the Dublin Institute of Technology and has not been submitted in whole or in part for another award in any Institute.

The work reported on in this thesis conforms to the principles and requirements of the Institute's guidelines for ethics in research.

The Institute has permission to keep, lend or copy this thesis in whole or in part, on condition that any such use of the material of the thesis be duly acknowledged.

David J. Barry

Signature:  Date: 31st March 2010

"*We must not forget that when radium was discovered, no one knew that it would prove useful in hospitals. The work was one of pure science and this is a proof that scientific work must not be considered from the point of view of the direct usefulness of it. It must be done for itself, for the beauty of science, and then there is always the chance that a scientific discovery may become, like the radium, a benefit for humanity.*"

Marie Curie

## Acknowledgements

Firstly, thanks to my supervisors, Dr. Gwilym Williams for his valiant attempts to make a biologist out of me over the course of this work, Dr. Raymond Ryan for his invaluable input on all matters biochemical and Prof. Jonathan Blackledge for introducing me to the wonderful world of fractals. I would also like to thank Dr. Cecilia Chan for her guidance in the project's early stages.

To all of the staff, past and present, in the School of Biological Sciences, DIT. In particular, Ms. Bríd Ann Ryan for her assistance when it was required.

The technical support staff, especially Ms. Patricia Taylor for her patience in answering my every conceivable question.

Thanks to all the students whose projects I have been involved with. Your efforts provided valuable insights for my own research.

To the considerable number of undergraduate and postgraduate students who have passed through Lab 230 over the course of my work.

To my friends and family.

And finally, to Zara, my supervisor outside DIT, for a seemingly limitless supply of support and encouragement.

## List of Publications

1. D. J. Barry, C. Chan, and G. A. Williams, "Nitrocellulose as a general tool for fungal slide mounts," *J Clin Microbiol*, vol. 45, no. 3, pp. 1074-5, 2007, doi: 10.1128/JCM.01609-06.

2. D. J. Barry, C. Chan, and G. A. Williams, "Kinetic analysis of fungal differentiation in solid state culture via a novel image analysis method," in *Abstracts of European BioPerspectives*, Köln, Germany, May 2007.

3. D. Barry, C. Chan, and G. Williams, "Morphological quantification of filamentous fungal development using membrane immobilization and automatic image analysis," *J Ind Microbiol Biot*, vol. 36, no. 6, pp. 787-800, 2009, doi: 10.1007/s10295-009-0552-9.

4. D. J. Barry, O. C. Ifeyinwa, S. R. McGee, R. Ryan, G. A. Williams, and J. M. Blackledge, "Relating fractal dimension to branching behaviour in filamentous microorganisms," *ISAST T Elec Sig Proc*, vol. 1, no. 4, pp. 71–76, 2009.

## Notation & Abbreviations

### Fungal growth

| | |
|---|---|
| $E$ | Mean rate of hyphal extension ($\mu$m tip$^{-1}$ h$^{-1}$) |
| $k_b$ | Specific branching constant (tips $\mu$m$^{-1}$ h$^{-1}$) |
| $k_{tip}$ | Maximum tip extension rate ($\mu$m h$^{-1}$) |
| $K_r$ | Colony radial expansion rate ($\mu$m h$^{-1}$) |
| $K_t, K_g, K_s$ | Monod saturation constants |
| $l_{germ}$ | Germ tube length ($\mu$m) |
| $q_{germ}$ | Germ tube extension rate ($\mu$m h$^{-1}$) |
| $q_{tip}$ | Mean hyphal tip extension rate ($\mu$m h$^{-1}$) |
| $s$ | Nutrient concentration (L$^{-1}$) |
| $t$ | Time (h) |
| $w$ | Colony peripheral growth zone width ($\mu$m) |
| $x$ | Biomass (mg mL$^{-1}$) |
| $Y_{X/S}$ | Yield coefficient |
| $\mu$ | Specific growth rate (h$^{-1}$) |
| $\mu_{max}$ | Maximum specific growth rate (h$^{-1}$) |

### Morphological parameters

| | |
|---|---|
| $A_c$ | Convex projected area ($\mu$m$^2$) |
| $A_f$ | Area of pellet filamentous region ($\mu$m$^2$) |
| $A_p$ | Projected area ($\mu$m$^2$) |
| $A_{p,\,min}$ | Minimum projected area ($\mu$m$^2$) |
| $C$ | Circularity |
| $C_{h,\,max}$ | Maximum hyphal circularity |
| $C_{s,\,min}$ | Minimum spore circularity |

| | |
|---|---|
| $D_p$ | Pellet diameter (mm) |
| $D_s$ | Spore diameter ($\mu$m) |
| $L_{hgu}$ | Hyphal growth unit ($\mu$m) |
| $L_{b,\,min}$ | Minimum branch length ($\mu$m) |
| $L_{th}$ | Total hyphal length ($\mu$m) |
| $L_{mh}$ | Main hyphal length ($\mu$m) |
| $n$ | Population size |
| $N$ | Number of hyphal tips per mycelium |
| $P$ | Perimeter ($\mu$m) |
| $P_c$ | Convex perimeter ($\mu$m) |
| $r$ | Radius (mm) |
| $V$ | Volume (mm$^3$) |

**Other image processing & mathematical symbols**

| | |
|---|---|
| $D$ | Fractal dimension |
| $F(\omega)$ | Fourier transform |
| $P(\omega)$ | Power spectrum |
| $R^2$ | Coefficient of determination |
| $T$ | Grey-level threshold |
| $\overline{x}$ | Mean |
| $\Delta f$ | Laplacian operator |
| $\sigma$ | Standard deviation |
| $\sigma^2$ | Variance |
| $\ominus$ | Erosion |
| $\oplus$ | Dilation |

**Abbreviations**

| | |
|---|---|
| ANN | Artificial neural network |
| CCD | Charge-coupled device |
| CMC | Carboxymethylcellulose |
| DAPI | 4',6-diamidino-2-phenylindole |
| DCW | Dry-cell weight |
| DEAE | Diethylaminoethyl cellulose |
| EDCF | Energy dissipation/circulation function |
| EDM | Euclidean distance map |
| FITC | Fluorescein isothiocyanate |
| LPCB | Lactophenol cotton blue |
| PBS | Phosphate-buffered saline |
| RBBR | Remazol brilliant blue R |
| RGB | Red-green-blue colour space |
| ROI | Region-of-interest |
| SmF | Submerged fermentation |
| SSF | Solid-state fermentation |

# Contents

# List of Figures

# List of Tables

# Chapter 1

# General Introduction

Filamentous microorganisms are exploited in industry for the production of a wide range of compounds of economic importance, including enzymes, organic acids, vitamins, antibiotics and, increasingly, various compounds of medicinal value [6–8]. Historically, the fermentation of such microbes has been associated with the production of traditional oriental foods such as *miso*, *shōyu* (soy sauce) and *tempeh*, which involves the cultivation of organisms such as *Aspergillus oryzae* (*kōji* mould) on solid substrates. While this practice is still common in the Far East, the submerged culture format became increasingly popular for industrial processes during the course of the 20$^{\text{th}}$ century, primarily due to reduced space requirements, and is now the more commonly employed culturing method.

During cultivation in submerged fermentation, there are a range of phenotypes that can be manifested (Fig. 1.1), depending on the physiology of the organism and the prevailing environmental conditions. Furthermore, there is significant evidence that the morphological form adopted by a microbe during the course of a submerged process can have a considerable influence on the level of metabolite produced, both directly and indirectly [8]. As such, developing a thorough understanding of the role of environmental variables in structural variation and the subsequent impact on productivity is a key target in the optimisation of fermentation processes.

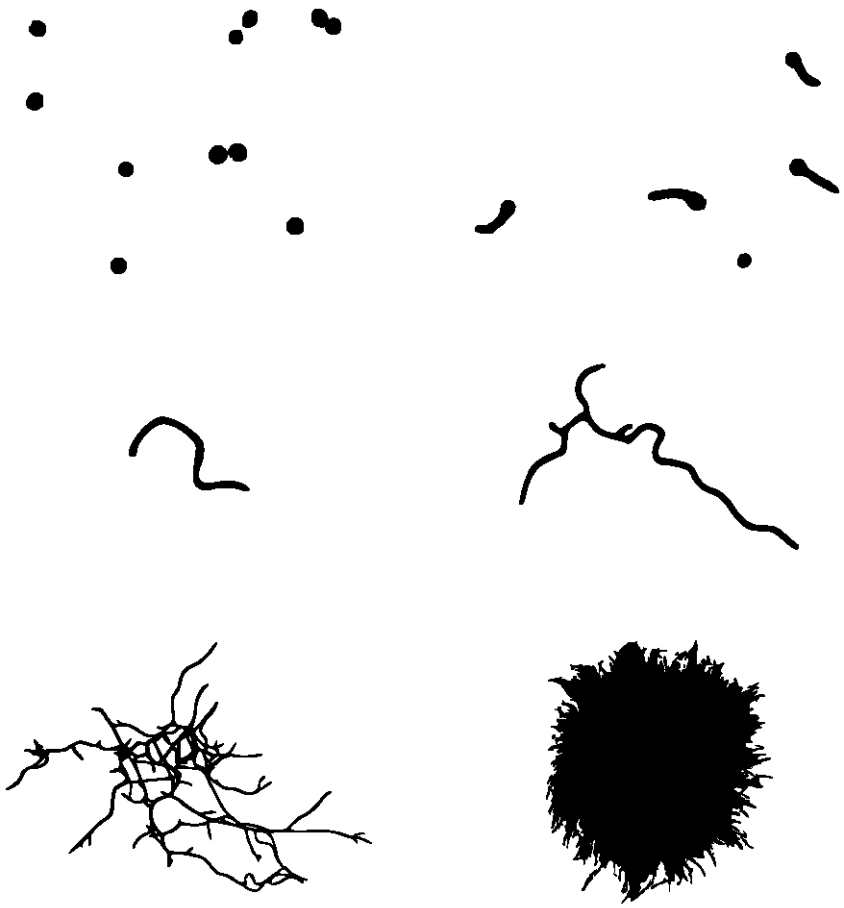

**Figure 1.1:** Different morphological forms of filamentous microbes. Growth commences from approximately spherical spores (typically $< 10$ $\mu$m in diameter), which, over time, produce simple branched hyphal structures (hyphal diameter is generally $< 10$ $\mu$m). These can, in turn, develop into complex, composite architectures termed mycelia, while the agglomeration of biomass in submerged culture can result in the formation of dense, approximately spherical configurations termed 'pellets', which may be up to several millimetres in diameter.

Prior to the advent of the digital era, fungal architecture was often characterised using subjective, qualitative descriptions. However, with the proliferation of personal computers and digital cameras in the 1990's came the application of image processing techniques to the characterisation of morphology; systems capable of unsupervised, fully automated analysis of mycelial structures were soon realised [5, 9]. However, despite this early progress, many of the image processing systems described in recent studies are not fully automated and rely on some degree of manual operation for the production of accurate data [10–13]. Furthermore, other recent studies still lack quantitative data, reporting ambiguous, qualitative descriptions of macroscopic forms such as 'pulpy growth', 'smooth pellets' and 'fluffy pellets' [14, 15]. There is therefore a pressing need for further development of automated imaging systems for this purpose.

## 1.1 The fungi

As saprotrophs, fungi play an important role in nutrient cycling in a variety of ecosystems, degrading organic matter to inorganic molecules, which may subsequently be exploited by other organisms [16]. Although traditionally included in many botany curricula and textbooks, fungi are evolutionarily more closely related to animals [17]; green plants are phototrophic autotrophs (producing complex organic compounds from simple inorganic molecules via photosynthesis), whereas fungi, like animals, are chemotrophic heterotrophs (organic compounds, such as glucose, are metabolised to release energy and obtain carbon for growth). The Kingdom Fungi consists solely of hyphal species, or those closely related to hyphal species, that are exclusively absorptive in their mode of nutrition [7]. However, there is no unique, generally accepted classification system at the higher taxonomic levels and there are frequent name changes at every level, from species up to phylum

(or division). For example, the phylum designation of the Zygomycota is controversial and it was not included as a formal taxon in the 'AFTOL classification' of Fungi [18]. Efforts to establish and encourage usage of a unified and more consistent nomenclature are ongoing [18, 19].

The major phyla of fungi have been classified mainly based on the morphology of sexual reproductive structures. However, asexual reproduction, via efficient dispersal of spores or spore-containing propagules from specially-adapted structures or through mycelial fragmentation, is common; it maintains clonal populations adapted to a specific niche, and allows more rapid dispersal than sexual reproduction [20]. Some species may allow mating only between individuals of opposite mating type, while others can mate and sexually reproduce with any other individual or itself. In sexually reproducing fungi, compatible individuals may combine by fusing their hyphae together into an interconnected network; this process, anastomosis, is required for the initiation of the sexual cycle. Sexual reproduction exists in all fungal phyla (with the exception of the Glomeromycota), but differences exist between fungal groups, which have been used to discriminate species by morphological differences in sexual structures and reproductive strategies [21, 22].

The Ascomycota (commonly known as the 'sac fungi') are the largest phylum of Fungi, with over 64,000 species, which may be either single-celled (yeasts), filamentous (hyphal) or both (dimorphic). The defining feature of this fungal group is the 'ascus', a microscopic sexual structure in which non-motile spores, called ascospores, are formed. However, many species of the Ascomycota are asexual, meaning that they do not have a sexual cycle and thus do not form asci or ascospores. Instead, asexual reproduction occurs through the dispersal of conidia, produced from fruiting bodies termed conidiophores, the morphology of which can vary extensively from species to species. Perhaps the most famous member of this phylum is the mould *Penicillium chrysogenum* (formerly *Penicillium notatum*), which, through

the production of the antibiotic penicillin, triggered a revolution in the treatment of bacterial infectious diseases in the 20$^{\text{th}}$ century. Some ascomycetes (*Penicillium camemberti*, *Penicillium roqueforti* and *A. oryzae*, for example) have been employed for hundreds or even thousands of years in the production of various foods. More recently, ascomycete fungi (the genus *Aspergillus* in particular [23]) have proved to be suitable candidates for heterologous protein expression, enabling large-scale microbial production of therapeutic proteins such as insulin and human growth hormone.

Basidiomycota is one of two large phyla that, together with the Ascomycota, comprise the sub-kingdom Dikarya (often referred to as the 'higher fungi'). The most conspicuous and familiar Basidiomycota are those that produce mushrooms, on which are sexual reproductive structures called basidia that bear basidiospores, although this phylum also includes some yeasts and asexual species. Among the 'lower fungi', the traditional division of the Zygomycota ('pin' or 'sugar' moulds) consists of organisms typically found in soil and animal dung, as well as on fruits high in sugar content, such as strawberries. Among the more extensively studied fungi in this (disputed) taxon are the Mucorales, containing genera such as *Mucor*, *Rhizopus* and *Mortierella*. Zygomycota are defined and distinguished from all other fungi by sexual reproduction via zygospores and asexual reproduction by sporangia, within which non-motile, single-celled sporangiospores are produced. Most Zygomycota, unlike the so-called 'higher fungi', form hyphae that generally lack septae.

## 1.2 Fungal growth

The life cycle of filamentous microorganisms typically begins and ends as a spore, which are produced from the microbe's fruiting bodies and dispersed by air, water, or possibly by animals. The spore will usually remain dormant until the necessary

environmental conditions for activation are met, but how this dormancy is maintained is poorly understood. There is evidence that low levels of metabolic activity are necessary to maintain spore viability; $O_2$ consumption and $CO_2$ production by *Neurospora* ascospores were found to be 1 – 4% that of vegetative cells [7]. However, prolonged viability has been demonstrated in the absence of metabolism; fungi have been grown from glacial ice cores estimated to be up to 140,000 years old [7].

Various physical agents, such as light, temperature and chemical compounds, can cause activation of fungal spores [24]. Of most importance however is the availability of water and a minimum water activity[1] of approximately 0.65 is required for growth of most fungi [25]. The germination rate of *P. chrysogenum* spores has been demonstrated to be highly dependent on water activity [26], while both temperature and water activity were shown to be significant in determining the germination rate of *Aspergillus ochraceus* spores [27]. Some microbes may also require nitrogen or carbon sources for spore activation [28], while others can germinate in pure water, the growth being supported by endogenous reserves [7]. Large numbers of spores in close proximity may fail to germinate (self-inhibition); in some species, the frequency of germination increases as the concentration of spores is decreased [29]. Some species require a 'trigger', such as heat or chemical stimulus, that may not necessarily be required to maintain vegetative growth, to initiate spore germination. For example, exposure to temperatures of 50 – 60°C for approximately 20 minutes is required by ascospores of *Neurospora* to initiate germination [29]. Germinative potential has implications for industrial processes, as variations in the number of viable spores in the inoculum can have a considerable influence on the outcome of a fermentation (Section 1.4.1).

Once the conditions for activation have been met, spores undergo a swelling

[1] $a_w$; ratio of vapour pressure of water in a substance to the vapour pressure of pure water at the same temperature

process, during which their size may increase up to four-fold due to the uptake of water [30]. Trinci reported that during the first 4 hours after inoculation, *Rhizopus stolonifer* sporangiospores increased linearly in diameter [31]. In their analysis of the development of *A. oryzae*, Spohr and colleagues found that the spores remained approximately spherical during enlargement, although it was difficult to differentiate between exponential growth in the spore volume and a linear increase in the spore equivalent diameter [4]. The swelling process culminates in the emergence of one or more germ tubes from the spore, the extension rate of which increases exponentially until a constant rate is attained [31], which varies between species and is also dependent on the prevailing environmental conditions. The extension of the germ tube ($q_{germ}$) may be described by the following empirical, Monod-type expression [4]:

$$q_{germ} = k_{germ} \cdot \frac{l_{germ}}{l_{germ} + K_{germ}} \tag{1.1}$$

where $k_{germ}$ is the maximum extension rate and $K_{germ}$ is a saturation constant. Alternatively, the length of the germ tube ($l_{germ}$) at time $t$ is given as follows [32]:

$$l_{germ} = \begin{cases} l_0 e^{k_1 t} & t \leq t_l \\ l_l + k_2 t & t > t_l \end{cases} \tag{1.2}$$

where $k_1$ and $k_2$ are constants, $t_l$ represents a point in time when $l_{germ} >> K_{germ}$ ($\therefore q_{germ} \approx k_{germ}$) and $l_0$ and $l_l$ are germ tube lengths at $t = 0$ and $t = t_l$ respectively. Such empirical kinetic expressions are generally based on experimental data, with little or no knowledge of the underlying growth mechanisms. This is as opposed to mechanistic models, which are typically more complex to enable quantitative consideration of assumptions on growth [32].

Extension of the germ tube, or hypha, is confined to the apical region; extension occurring in sub-apical regions would result in 'buckling' and distortion of the hypha.

Early studies of this mechanism involved 'dusting' sub-apical hyphal regions with particles and noting any displacement of these particles over time as the growth of the organism proceeded; those particles that adhered to hyphae did not alter their position [7]. Apical advancement is a result of internal hydrostatic pressure within the hypha forcing the thin, plastic apical cell wall outward; hyphae contain high concentrations of solutes, resulting in water entering the cells by osmosis and generating positive turgor pressure [33]. As growth proceeds, the cell wall in sub-apical regions becomes thicker, more rigid and more resistant to turgor pressure [34], restricting hyphal growth to the apical region. The advancement of apical cells often occurs at the direct expense of cytoplasm in sub-apical cells, resulting in the formation of vacuoles, which are typically not seen in the proximity of hyphal tips [35]. The cell wall formation driving hyphal extension is a vesicle-based process, with the vesicles[2] (containing the precursors required for cell wall formation) believed to be supplied by the Vesicle Supply Centre (VSC) [36], also known as the apical body or Spitzenkörper. The VSC, visible under phase-contrast microscopy as a dark region located just behind an advancing hyphal tip, has been implicated in 'guiding' hyphal growth. The formation of a new branch is preceded by the formation of a new Spitzenkörper, while a change in direction in hyphal growth is preceded by a displacement of the apical body [7].

In the higher fungi, internal cross-walls termed septae are formed at regular intervals as the hypha extends, sub-dividing the hypha into individual cells. In the event that a breach of the cell wall occurs, the pores within these septae are 'plugged', so that loss of cytoplasm is confined to one particular cellular compartment and death of the entire hypha does not occur. It has been demonstrated that cutting a sub-apical compartment does not result in the death of the apical cell, although a reduction in extension rate may be observed [37].

[2]A vesicle is a sac that stores or transports substances intra-cellularly

When a hypha has attained a certain length, a branch is formed laterally to the parent, typically towards the end of the period of exponential extension [1, 32]. An expression similar to Equation (1.1) may be used to describe the extension of branches, but the value of the saturation constant, $K_i$, may vary significantly within a single mycelium; there is evidence suggesting $K_i$ is proportional to the distance between a newly-formed branch and the tip of the 'primary' hypha [4]. The process of branching is poorly understood, although a correlation with septation has been proposed, as branches often form just behind septae [7]. It has been postulated that a hypha will produce a branch if the material supply to a hypha exceeds that required for the maintenance of growth of a single hypha, or, when transport of material distant from the tip becomes limited. This may be explained by the formation of a septum behind the advancing tip, after which extension is dependent on biosynthesis within the apical region [32]. Branches are typically formed in acropetal succession behind the primary tip, with the formation of a new branch preceded by a softening of the rigid sub-apical cell wall at the location where the new branch emerges [29].

The critical branch length that results in a new branch being spawned is referred to as the hyphal growth unit ($L_{hgu}$), which is approximately equal to the total hyphal length ($L_{th}$) divided by the total number of tips ($N$) on any given element. First proposed by Plomley [38], this represents the mean length of hypha required to support tip growth. If mycelial growth involves the duplication of a 'growth unit', it follows that $L_{th}$ and $N$ increase exponentially at approximately the same specific growth rate. That is, branching attains an exponential rate, with each individual branch growing at approximately the same linear rate, resulting in a similar exponential increase in biomass. This was first demonstrated experimentally by Trinci in a study of *Neurospora crassa*, *Aspergillus nidulans*, *Geotrichum candidum*, *Mucor hiemalis* and *P. chrysogenum* [1]. Colonies were cultivated on cellophane-covered

media (to restrict growth to two dimensions) and measures of the dimensions were made on enlarged photographic prints. After an initial period of discontinuous branch production, exponential growth was observed (Fig. 1.2), although a wide variation in the growth rate of individual branches was noted. Measured specific growth rates varied from approximately 0.25 $h^{-1}$ for *A. nidulans* up to 0.60 $h^{-1}$ for *M. hiemalis*. The growth unit was also studied in batch cultures of *G. candidum* by Caldwell and Trinci, who reported that total hyphal length and the number of branches per mycelium increased exponentially with biomass, suggesting that the ratio of total mycelium to number of tips was constant [39]. Furthermore, it was found that the hyphal growth unit remained relatively constant for specific growth rates ranging from 0.173 to 0.385 $h^{-1}$, supporting the hypothesis that the mould had a functional unit of hyphal growth.

In young mycelia exhibiting undifferentiated growth, the mean rate of hyphal extension ($E$; $\mu$m $tip^{-1}$ $h^{-1}$) may be calculated as follows [32]:

$$E = \frac{2(L_{th} - L_{th0})}{N_t + N_0} \tag{1.3}$$

where $L_{th0}$ and $L_{th}$ are the total hyphal lengths at time $t = 0$ and 1 hour later, while $N_0$ and $N_t$ are the respective number of hyphal tips. The mean extension rate may then be related to the specific growth rate ($\mu$; $h^{-1}$) as follows:

$$E = \mu L_{hgu} \tag{1.4}$$

Over time, nutrient limitations will arise at the centre of the colony, where germination occurred, eventually resulting in the cessation of growth at this location (and often sporulation occurs) [32]. A differentiated colony is thus formed, in which growth is restricted to the colony periphery, where abundant nutrients are still available. The active region is referred to as the peripheral growth zone, the width of which ($w$) may be determined by modifying the formula proposed by Trinci [37]:

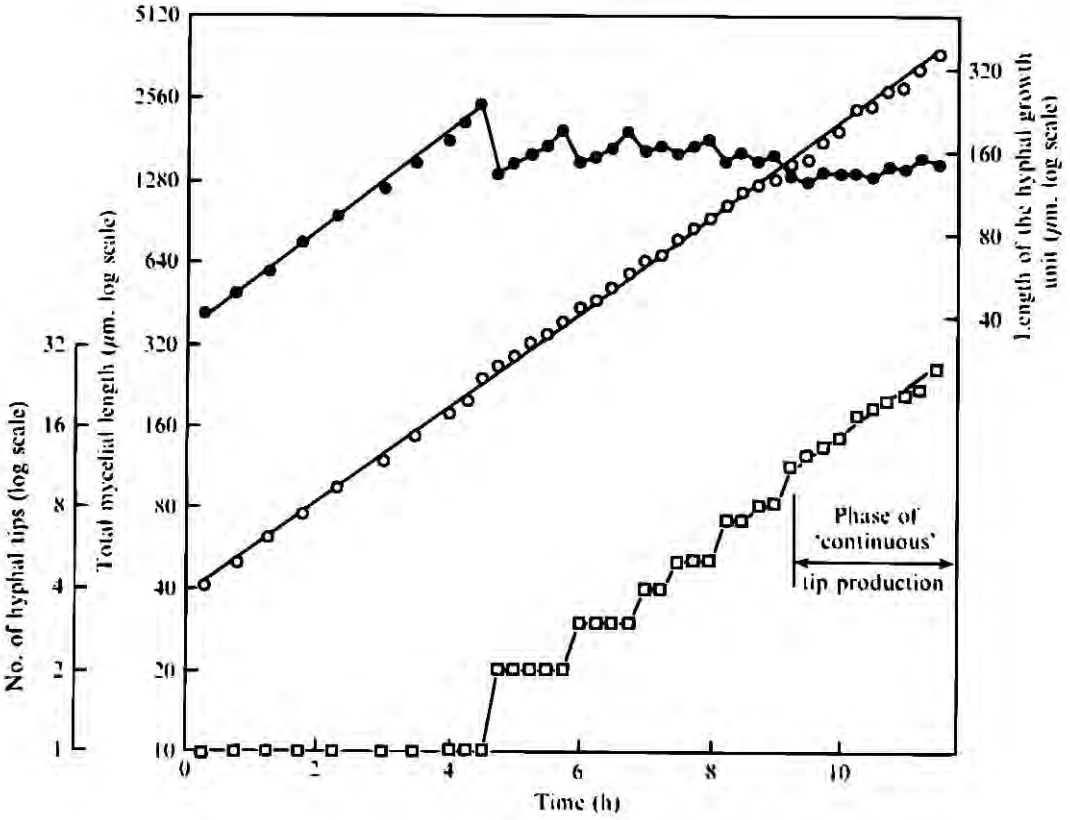


**Figure 1.2:** Growth of a mycelium of *Geotrichum candidum* on solid medium, as described by Trinci [1], showing number of tips (□), total hyphal length (○) and hyphal growth unit (●). Reproduced with permission from the Society for General Microbiology.

$$w = \frac{K_r}{\mu} \tag{1.5}$$

where $K_r$ is the radial expansion rate of the colony ($\mu$m h$^{-1}$). Alternatively, if an estimate for $w$ is known, then $\mu$ may be calculated by measuring the change in colony radius over time. However, such an approach would not take into consideration aerial hyphae or hyphae growing into media substrata [29]. Furthermore, variations in the direction of growth of individual hyphae will affect their contribution to radial extension [32].

Growth in such a manner results in the formation of a 'sink', into which nutrients

diffuse, and a 'source', from which metabolites effuse, and, consequently, concentration gradients develop within the medium. An analysis conducted by Olsson showed graphically that such gradients existed in medium supporting the growth of *Fusarium oxysporum* colonies [40], with a particularly steep decline in glucose and phosphate concentration at the colony edge, while the concentration of both nutrients was virtually zero at the colony centre. Radially-directed growth away from the colony centre is probably a consequence of such gradients [7], but the mechanism by which fungi grow in such patterns, efficiently exploiting the available substrate, is not fully understood. The tendency of hyphae to avoid each other is particularly evident at the edge of a colony, where branches are formed at acute angles, and may be a response to a signalling metabolite secreted by the hyphae themselves (autotropism) or a localised depletion of oxygen (or higher concentration of carbon dioxide) around the hyphae (chemotropism) [30].

### 1.2.1 Growth in submerged batch culture

In a closed, 'batch' system, a volume of media is inoculated and growth proceeds until the concentration of an essential nutrient becomes limiting, or toxic compounds have reached a critical, growth-inhibiting level. A stationary liquid culture will result in the formation of a fungal 'mat' on the media surface. Agitation results in the formation of submerged culture, in which the growth form varies between a homogeneous suspension of dispersed hyphae and discrete pellets (Fig. 1.1). Non-septate organisms typically grow poorly in such environments, as the shear forces caused by agitation result in excessive loss of cytoplasm from cells.

The early stages of growth of filamentous microbes in submerged liquid culture are similar to those described above for an undifferentiated mycelium. The growth is well described using kinetic equations derived from unicellular bacterial studies, such that biomass, substrate and product are assumed to be uniformly distributed

[32]. Following an initial lag phase[3], during which the organism acclimatises to a new environment after inoculation, branching attains an exponential rate. The rate of change of biomass ($x$) may therefore be described as:

$$\frac{dx}{dt} = \mu x \tag{1.6}$$

Integrating yields:

$$\ln x_t = \ln x_0 + \mu t \tag{1.7}$$

where $x_t$ is the level of biomass at time $t$ and $x_0$ is biomass at time $t = 0$. This equation may also be written as:

$$x_t = x_0 \; e^{\mu t} \tag{1.8}$$

This growth phase, following the initial lag, is thus termed the exponential growth phase (Fig. 1.3) and will continue as long as the necessary environmental conditions to support it exist (nutrients in excess, adequate aeration, favourable temperature and pH). In industry, this growth phase is of interest for the production of biomass and growth-associated metabolites, such as amylases, cellulases and proteases, which are typically required for the synthesis of nutrients. The secretion of these metabolites can be influenced by the media composition, as the production of certain enzymes may be induced by the presence of a particular substrate. Furthermore, if a mixture of sugars is present in the medium, low-molecular weight substrates, such as glucose in particular, will typically be preferentially consumed by the organism. This is typically achieved by the inhibition (or repression) of the synthesis of enzymes involved in the catabolism of other carbon sources (known as catabolite repression) [29].

[3]If the fermentation was inoculated with an exponentially-growing culture, growth continues exponentially and no lag phase occurs

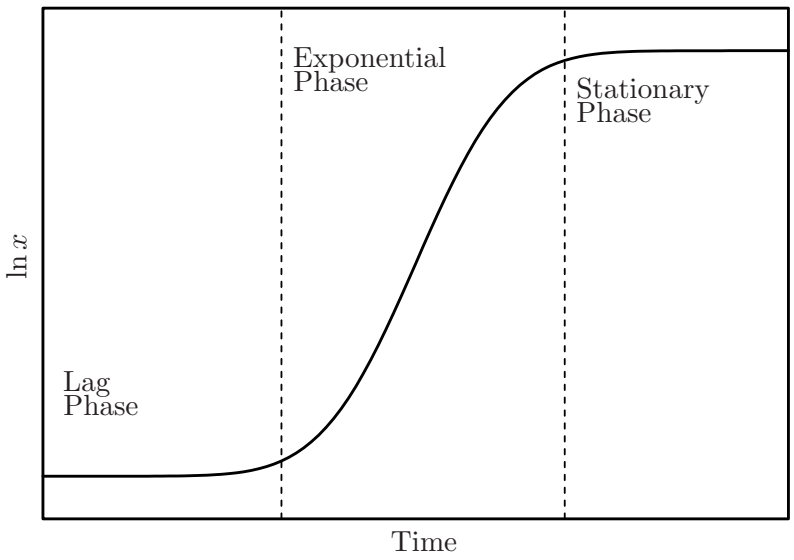


**Figure 1.3:** Typical growth profile of a microorganism grown in submerged culture, where $x$ denotes biomass.

The specific growth rate attained during the exponential phase is dependent on nutrient concentration; if all nutrients required for growth are present in excess, then the specific growth rate attains a maximal value ($\mu_{max}$). The empirical relationship between $\mu$ and nutrient concentration ($s$) may be expressed in terms of Monod kinetics (Fig. 1.4):

$$\mu = \mu_{max} \cdot \frac{s}{s + K_s} \tag{1.9}$$

where $K_s$ is a saturation constant, which is typically very small relative to the concentration of the relevant nutrient in the media. As such, in a laboratory environment in which a chemically-defined medium is used, all nutrients will typically be present in amounts vastly greater than the respective saturation constants and the specific growth rate will approximate $\mu_{max}$ during the exponential phase.

The exponential growth phase is ended as a result of the exhaustion of a nutrient required for growth or the accumulation of growth-inhibiting compounds. The culture then enters the stationary phase of growth, the transition involving substantial

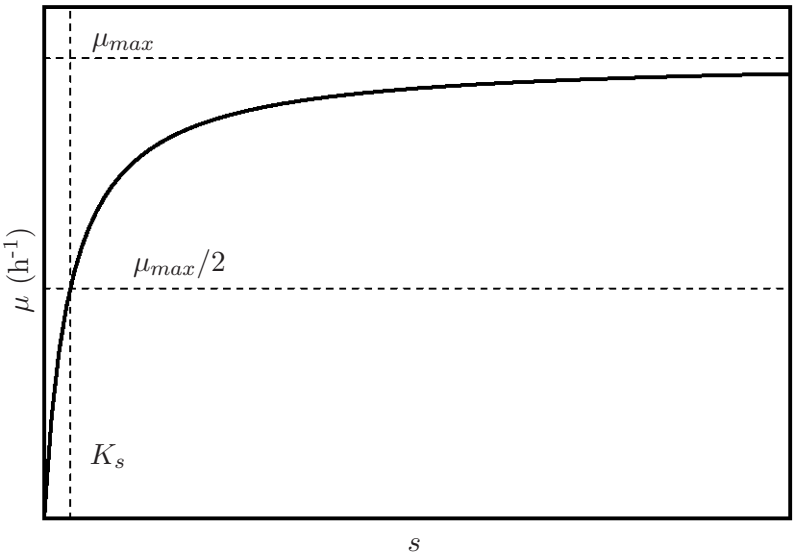


**Figure 1.4:** Specific growth rate ($\mu$) versus nutrient concentration ($s$) according to Monod kinetics. Half of the maximum specific growth rate ($\mu_{max}$) is attained when $s$ is equal to the saturation constant $K_s$.

physiological changes, which again, may be influenced by media composition. During the stationary phase, cell growth is balanced by cell death, but compounds of industrial interest, such as organic acids, vitamins and lipids, may be accumulated in the culture. A fourth growth phase, termed the decline phase, may follow the stationary phase, during which cell growth is outpaced by cell death and biomass declines as a result.

An important variant of the batch culture format is 'fed-batch culture', in which biomass is initially grown in a batch system until a pre-determined point in time, perhaps relating to the exhaustion of a chosen medium component. Fresh nutrient is then added, typically as a concentrated form of a component of the original medium. Conducting fermentations in this manner may be used to, for example, minimise medium viscosity in the event that a starch substrate is employed, or, if glucose is utilised as substrate, to maintain the concentration below repressing levels. The fed-batch format may also be used to add an inducer to initiate secretion of a particular

metabolite, or to maintain the limiting nutrient conditions necessary for secondary metabolite production. The majority of large-scale industrial fungal fermentations are of the fed-batch variety.

*Growth in the form of pellets*

Depending on the organism, pellet formation can result from the aggregation of spores prior to germination, aggregation of spores and germ tubes or, less commonly, the aggregation of mycelia [32]. A wide range of physiochemical parameters may affect the pellet formation process, some of which will be discussed in Section 1.4.

Pelleted cultures have long been assumed to follow cube root kinetics [41, 42]:

$$x^{1/3} = {x_0}^{1/3} + kt \tag{1.10}$$

where $x$ is biomass at time $t$, $x_0$ is biomass at time $t = 0$ and $k$ is a constant. The growth of fungi in the form of pellets is somewhat analogous to colony growth on solid substrates; over time, growth of the pellet will be restricted to an outer 'active layer' (the width of which, $w$, is dependent on the diffusional properties of the mycelium [32]) as the core of the pellet suffers from diffusion limitations [43]. Changes in the pellet radius may be described by:

$$r = r_0 + w\mu t \tag{1.11}$$

If the pellet is assumed to be spherical with a constant biomass density ($\rho$), increase in biomass can be rewritten as follows:

$$x = x_0 + \left(\frac{4}{3}\pi\rho n\right)^{1/3} w\mu t \tag{1.12}$$

where $n$ is the number of pellets. Exponential growth is predicted (while $r \leq w$) until restrictions to diffusion of nutrients through the pellet mass reduce growth

rates in the centre of the pellets ($r > w$); subsequent growth will then follow cube-root kinetics.

Over time, diffusion limitations will lead to a cessation of biomass production at the pellet core and the onset of autolysis. This leads to a reduction in stability and the pellet becomes more susceptible to damage by mechanical forces. Furthermore, hyphal elements at the pellet surface become weakened by ageing and vacuolation, making them more susceptible to shearing. Consequently, the macroscopic morphology can change considerably [44]. Pellet break-up often results in growth renewal, provided nutrient requirements are met (the medium will be enriched by nutrients from autolysed biomass), since fragments can act as centres for new growth [8]. This complex relationship between pellet growth, fragmentation and regrowth has been studied in a variety of organisms (Table 1.1).

The growth of *A. oryzae* in the form of pellets was studied in detail by Carlsen and colleagues [45]. In the time period of 18 to 32 hours post-inoculation, the number of pellets was almost constant and the pellet radius increased with a constant rate of 37.5 $\mu$m h$^{-1}$, which was very similar to the value of 35 $\mu$m h$^{-1}$ reported for the hyphal tip extension rate in freely dispersed cultures. After 35 hours of cultivation, the pellet concentration rapidly increased, whereas the mean pellet radius decreased, but the growth in biomass was described very well by the cube-root law prior to pellet break-up ($t > 35$ h). Thereafter, a smaller fraction of the biomass was mass-transfer limited, resulting in an increase in $\mu$. Oxygen limitation in pellet cores set in approximately 23 hours after inoculation and, after 35 hours, approximately 50% of the biomass was estimated to be limited by oxygen. The concentration of ethanol in the media was found to increase with the estimated oxygen-limited biomass concentration, while no ethanol production was detected in batch cultivations grown as freely dispersed hyphal elements.

**Table 1.1:** Recent reports in the literature on the development of fungal pellets in batch cultivations.

| Organism | Report | Reference |
|---|---|---|
| *A. oryzae* | Pellet radius increased linearly up 35 hours before onset of fragmentation | [45] |
| *A. niger* | Pellet formation completed 15 h post-inoculation - pellets increased in size but not in numbers. Active region of pellets decreased from 20 h | [46] |
| *A. terreus* | Pellet size increased up to approximately 75 h and remained relatively constant thereafter in shake-flasks inoculated with pellets, although free mycelia were visible after 120 h | [47] |
| *A. niger* | Pellet size increased continuously with cultivation time in shake-flask culture | [48] |
| *A. niger* | Pellet diameter levelled off between approximately 50 and 100 h cultivation, depending on the inoculum concentration | [49] |
| *C. militaris* | Pellet size increased over the course of 8-day fermentation, but sucrose concentration was high (40 g/L) | [50] |
| *A. terreus* | Pellets in stirred-tank reactors increased in size before falling in later stages | [51] |
| *A. niger* | Approximately 50 hours post-inoculation, a transition from 'smooth' to 'hairy' pellets took place, indicated by a decline in fullness ratio (area/convex area) | [35] |
| *P. baumii* | Small pellets with filamentous growth changed into 'feather-like' mycelial clumps. Diameter declined from 5.2 to 2.6 mm after 12 days | [52] |
| *P. gilvus* | Pellets were compact and smooth until latter stages of fermentation when hollow cores formed and diameter declined | [52] |
| *P. linteus* | Pellets exhibited compact central cores with loose filamentous outer zones. Diameter, core area and circularity increased during fermentation | [52] |

## 1.3 Industrial fermentation of fungi

Filamentous microbes, and fungi in particular, are perhaps traditionally associated with destructive and parasitic behaviour, incurring immense economic losses in the process. Their invasive growth strategies enable colonisation of a wide variety of plants, trees, insects, fish, animals and even humans. Some of the most devastating crop failures in recorded history have been attributed to fungal disease, such as the Irish potato famine of 1845 (*Phytophthora infestans*) and the Bengal rice famine of 1943 (*Cochliobolus miyabeanus*).

However, the saprophytic mode of nutrition of many filamentous microbes has been exploited to produce a wide range of compounds of economic significance, such as enzymes, antibiotics, plant growth regulators and vitamins (Table 1.2). This list is by no means exhaustive and in fact the range of products obtainable from filamentous fungi is frequently expanded upon. For example, investigations into the use of fungi for the production of diesel-like compounds ('myco-diesel') are well underway [53], while the utilisation of novel cultivation formats can result in increased productivity [48] or even the discovery of new metabolites of potential utility [54]. The future economic potential of industrial biotechnology has been outlined in several reports, with the British Department of Business Enterprise and Regulatory Reform (BERR) recently estimating that the global market for bio-based products will grow to US$250 billion by 2020 [55].

The exploitation of fungi by man is by no means a recent phenomenon, with processes such as the fermentation of alcoholic beverages dating back to ancient times. Some authors have suggested that the beginnings of biotechnology were coincident with the dawn of agriculture; the advent of large-scale grain production and the domestication of cows and goats was probably quickly followed by early forays into the production of alcoholic beverages and fermented milk products [56].

**Table 1.2:** A selection of metabolites produced in industry by fungi, their uses and some of the organisms used in their production [6–8].

| Metabolite | Uses | Producer organisms |
|---|---|---|
| Biomass | Food industry | *A. bisporus*, *F. venenatum* |
| Amylases | Food industry, detergents | *A. niger*, *A. oryzae*, *A. awamori*, *R. oryzae*, *T. viride* |
| Glucoamylases | Food industry | *A. niger*, *A. awamori*, *A. oryzae*, *R. oryzae* |
| Cellulases | Food processing, pulp & paper industry | *A. niger*, *A. terreus*, *T. reesei*, *T. viride* |
| Lipases | Detergents | *A. niger*, *A. oryzae*, *R. arrhizus* |
| Phytases | Animal feedstuffs | *A. niger* |
| Ethanol | Chemical industry, biofuels | *S. cerevisiae* |
| Organic acids (citric, gluconic, itaconic) | Food, soft drinks and pharmaceutical industries | *A. niger*, *A. terreus*, *T. viride* |
| Riboflavin | Food supplement, various clinical applications | *A. gossypii* |
| Penicillins | Antibiotics | *P. chrysogenum* |
| Cephalosporins | Antibiotics | *C. acremonium* |
| Statins | Cholesterol-lowering drugs | *P. citrinum*, *M. ruber* |
| Cyclosporin A | Treatment of organ-transplant patients | *T. inflatum* |
| Gibberellins | Fruit cultivation | *G. fujikuroi* |
| Lactones, peptides, terpenoids | Food industry (flavourings) | *T. viride*, *G. fujikuroi*, *M. circinelloides*, *P. blaksleeanus* |
| Heterologous proteins | Healthcare industry | *A. niger*, *A. oryzae*, *A. nidulans*, *T. reesei* |

Many traditional Japanese foods, such as soy sauce and miso, have been produced in fermentation processes for thousands of years [57] and the Japanese biotechnology industry has used this vast experience to establish itself as a world-leader in the production of fungal metabolites. Fungi have also been traditionally utilised as sources of food themselves, as is the case with mushrooms (*Agaricus bisporus*, for example). More recently, *Fusarium venenatum* has been developed as single-cell protein for human consumption under the trade name of Quorn$^{TM}$, the protein of which is comparable in nutritional quality to that of chicken. However, the conversion of 'feedstock' into protein is more efficiently achieved by *F. venenatum* than by chickens [58]. A chicken gains approximately 49 g of protein per kilogram of protein-containing feed consumed and the animal doubles in weight in 3 weeks. However, *F. venenatum* requires just a simple feed consisting of glucose and some inorganic salts, each kg of which is converted into 136 g of protein, with biomass doubling every 6 hours!

Up to the early 1980's, the majority of products derived from microbial fermentation were for use in the food industry, making up an estimated 80% of the market value of biotechnology applications in 1981 [58]. However, since the use of microbes for the production of therapeutic compounds was clinically approved in 1982 (initially for the production of insulin by *Escherichia coli*), successful attempts have been made to exploit fungi as expression hosts of heterologous proteins [59], due to their capacity for high levels of excretion and the GRAS status[4] obtained by many (such as *A. oryzae*). This has resulted in many compounds of medicinal value, previously only obtainable from mammals, being produced using microbes. Diabetics, for example, were previously prescribed insulin derived from animal pancreatic tissue, which occasionally provoked immune responses in patients, but also carried a risk of infection from harmful pathogens [60]. Recombinant microbes have

[4]'Generally regarded as safe'; US Food and Drug Administration

also been used to produce factor IX, a deficiency of which causes hemophilia B, obviating the requirement for blood transfusions and the associated risks of infection [60]. The production of these proteins was initially conducted using *E. coli*, but the intra-cellular accumulation of the proteins of interest by the bacterium requires the use of expensive extraction techniques, which result in the inactivation of a portion of the product [6]. Filamentous microbes, however, secrete enzymes prodigiously in their natural environment and, as such, they are a more suitable choice of host organism for such processes. Research into microbial development of vaccines against human diseases such as hepatitis, influenza, rabies and HIV is also underway [58].

### 1.3.1 Submerged industrial processes

Production facilities typically employ 'trains' of bioreactors ranging from 20 to 250,000 L (or even larger for some processes) [2], although it is desirable to keep the number of reactors to a minimum, as the costs associated with a reactor increase in proportion to (reactor volume)$^{0.7-0.8}$ [61]. Culturing begins in the smallest vessel and at a predetermined point in time during the exponential growth phase, the contents are used to inoculate the next fermenter in the chain (each vessel is usually approximately ten times larger than its predecessor). When the biomass level has increased sufficiently, the culture is transferred to the next fermenter in the chain, continuing in successive stages until the largest vessel (the production fermenter) is reached. This inoculum 'work-up' avoids the long lag phase that would otherwise result from inoculating a large vessel with a relatively low level of biomass. Furthermore, inoculating with exponentially-growing cultures minimises any lag in growth at each stage in the chain. At the end of the process, the biomass is separated from the medium and the metabolite of interest is extracted. Industrial fermentations are commonly conducted on a large scale in a stirred-tank bioreactor, although airlift and bubble column reactors are also used extensively [2].

The bioreactor was first introduced in the 1940's for the large-scale production of penicillin from *P. chrysogenum* (known at the time as *P. notatum*) [7] and the basic design remains unaltered, although monitoring equipment has increased in sophistication. In addition to the those components shown in Figure 1.5, reactors are also fitted with side ports for pH, temperature and $dO_2$ probes as minimum requirements, in addition to connections above the liquid level for acid and alkali addition (for pH control), antifoam addition and inoculation. A foam breaker or foam rake will sometimes be fitted in the headspace above the liquid for processes where the use of antifoam is unacceptable. The exterior of the vessel is typically fitted with a water jacket to dissipate the heat of metabolism and that generated from culture agitation. Temperature control in this manner can be problematic in large vessels, as surface area for heat transfer decreases with increasing volume, and, as such, larger vessels will often be equipped with internal heat exchanger coils.

Most industrial fermentation processes are aerobic, air typically being introduced via a sparger with small holes below the impeller shaft. This facilitates the production of small air bubbles whose presence in the medium is prolonged as a result of the turbulent flow created by the impellers, aiding convective mixing and maximising their residence time. The combination of small bubbles (large total surface area) and long residence time maximises the diffusion of oxygen from the bubble into the medium and carbon dioxide from the medium into the bubble. Introducing air at the foot of the vessel also takes advantage of a relatively high hydrostatic pressure, which reduces bubble volume, therefore increasing surface-to-volume ratio, and maximising diffusion. Maintaining a positive pressure within the bioreactor can also aid diffusion.

Mechanical agitation, which also aids in the convective mixing of nutrients present in the media, is typically provided by Rushton impellers mounted on a

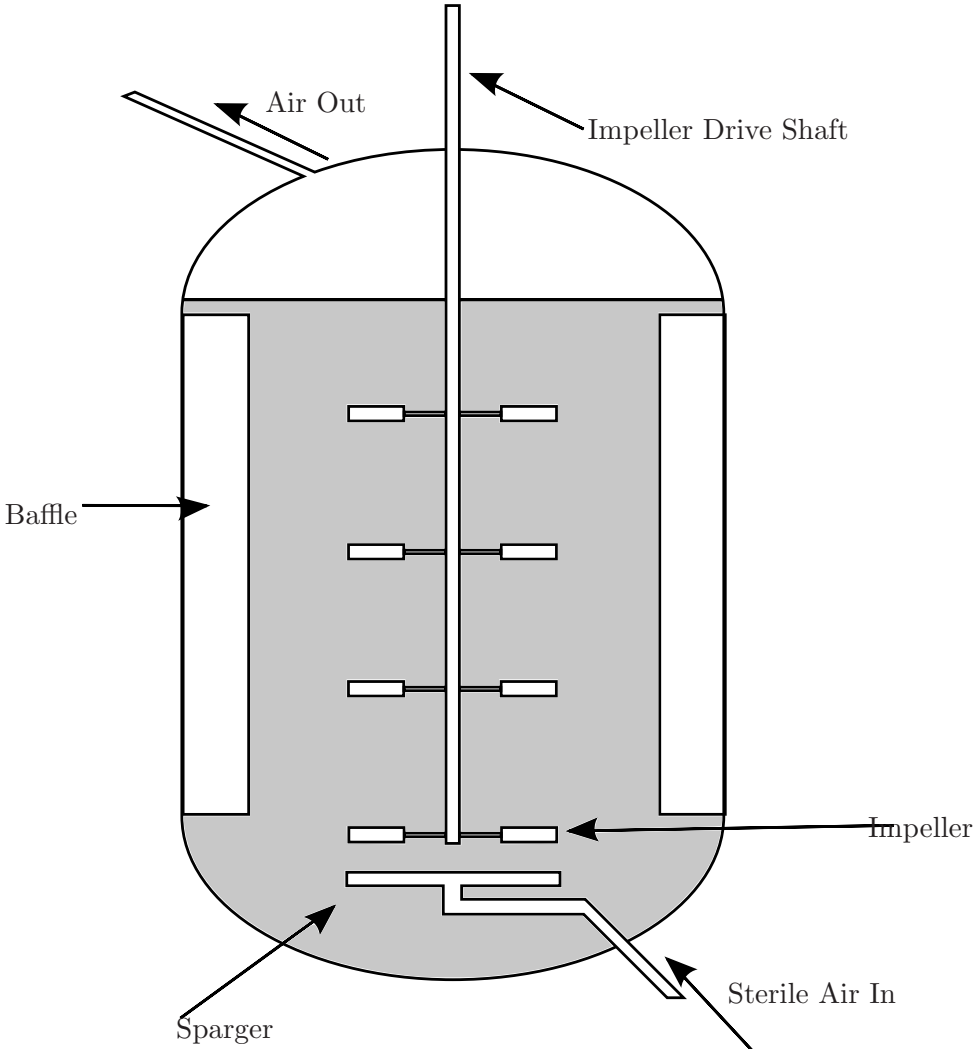


**Figure 1.5:** Schematic of a typical stirred-tank bioreactor. Four baffles are usually used to prevent vortexing, with the baffle width ranging from $D/10$ to $D/12$, where $D$ is the vessel diameter. The number of impellers used is determined by the aspect ratio of the vessel, which is typically $\sim 3.5$. The lower-most impeller is located $\sim D/3$ from the bottom of the reactor, with additional impellers spaced $\sim 1.2$ impeller diameters ($d$) apart, where $d \approx D/3$ (dimensions from [2]).

central vertical shaft[5]. Together with medium sterilisation, culture mixing is one of the most energy-intensive aspects of fermentation, but the power requirement for agitation depends greatly upon the rheological properties of the broth, which in turn depends upon the growth form of the cultivated organism; pelleted structures will typically result in a Newtonian fluid[6], but filamentous growth often results in a pseudo-plastic, non-Newtonian fluid (viscosity decreases with increasing shear). For some processes, in which the cost of power required for mechanical agitation is deemed to be prohibitive, 'tower' fermenters are employed, in which agitation is provided by supply of compressed air. Agitation can also have a significant impact on the morphology of the organism (Section 1.4.2).

Other significant costs associated with fermentation processes are raw materials for use as substrate and transport of same. In a laboratory environment, medium composition is typically strictly defined with the use of pure chemicals. However, on an industrial scale, this is not practical as the volume of media required is several orders of magnitude greater than that used in a bench-top fermenter. A cheap, carbon-rich feedstock must therefore be sourced and quite often, waste products from other industries, such as molasses (waste liquor from sugar refineries), are well-suited. The costs associated with transporting large quantities of these raw materials can often be considerable and, as a result, the fermentation plant may be sited near the source of raw materials. Medium ingredients alone can represent up to 60% of operating costs, with the carbon source alone constituting up to 90% of raw material expenditure [61].

[5]A Rushton impeller consists of six to twelve flat, rectangular plates mounted perpendicularly on a horizontal disc, with the plates' horizontal alignment being radially coincident with the disc.

[6]A Newtonian fluid is characterised by a linear relationship between stress and strain rate, the constant of proportionality being the viscosity. The flow properties of a non-Newtonian fluid are not described by a single constant value of viscosity.

### 1.3.2 Solid-state processes

Solid-state fermentation (SSF) involves the cultivation of microbes on solid particles, typically under conditions of low water activity. The majority of SSF processes are aerobic, involve filamentous fungi (although some involve bacteria and yeasts), and may be classified as either natural (indigenous), such as ensiling or composting, or pure culture, using individual or mixed strains [62, 63].

The success of submerged culturing (SmF) during the 20$^{\text{th}}$ century has led to a decline in the use of SSF. However, the practice is still ongoing and has shown promise for the production of many enzymes, acids and bioactive compounds, leading to increased research interest [62, 64]. However, due to the different physical nature of SSF compared to SmF (particularly, the presence of solid-air interfaces in SSF), hyphal extension and branching patterns in mycelial organisms may be quite different between the two systems [62]. Recent studies have indicated differential protein expression in solid culture by several organisms [59, 65], exemplifying future potential application of this fermentation format. There is also evidence that solid-state cultivation can result in higher biomass yields and higher enzyme titres compared to submerged fermentation [66, 67], possibly due to the closer resemblance to the natural environment of the microbes [68]. Furthermore, different products may be produced in SSF. For example, Ruijter and colleagues found that *A. oryzae* accumulates polyols (glycerol, erythritol and arabitol) at low water activity on a solid substrate [69]. It was suggested that this might be typical for SSF due to the specific growth conditions present during growth on a solid substrate. However, much of this investigative work remains confined to laboratories; the potential of SSF to operate reliably at a large scale has not been investigated to the same degree as the SmF format [64]. However, examples of production-scale SSF facilities do

exist, such as that operated by Alltech[7] in Serdan, Mexico, claimed to be the first in enzyme technology based on SSF.

Traditionally associated with the production of oriental foods, the use of solid media has certain merits, such as low energy requirements, abundance of cheap raw materials and a low water requirement [66]. Agro-industrial crop waste and residues are typically utilised as substrates and, while wheat bran has proved to be the most popular choice, a variety of other substances have been investigated, such as cassava, soya bean, sugar beet, potato, crop residues and residues of the fruit-processing, coffee-processing and oil-processing industries (reviewed extensively by Pandey and colleagues [64]). However, the substrate may require chemical or mechanical pre-treatment prior to fermentation [70] and the sterilisation of a solid substrate is typically more difficult to achieve than a liquid medium. However, SSF often involves an organism capable of tolerating low water activity, and, if an active inoculum is added to a (cooked) substrate, the process organism is able to outcompete potential contaminating organisms, meaning that strict aseptic operation of the bioreactor may not be essential [64].

However, SSF is often slower, is difficult to control due to the lack of suitable sensors and probes and the dissipation of metabolic heat is often problematic [66]. Environmental parameters in SSF, such as temperature, pH, concentrations of oxygen and nutrients, porosity and other physical properties of the solid matrix as well as fungal biomass are difficult or even impossible to measure online due to the lack of free liquid, the complexity and heterogeneity of the solid material as well as the intimate interactions between the microorganisms and their substrates [71]. Furthermore, there may be severe restrictions in the supply of $O_2$ to a significant proportion of the biomass, large nutrient concentration gradients can exist within solid particles and the movement of solid particles can cause impact and

[7] http://www.alltech.com

shear damage to hyphae [62]. SSF is also generally more labour-intensive, although a fully automated system for soy sauce production has been developed in Japan [67] and several commercial enzymes are produced using solid substrates [68]. However, while a variety of computational and modelling methods have been applied to the study of solid-state fermentations, experimental data on this culture format is still lacking [71].

## 1.4 Influence of process variables on morphology and metabolite production in submerged fermentations

The diffusional limitations associated with pelleted growth would perhaps suggest that a dispersed mycelial morphology is preferable for increased product yield. However, while a pelleted form typically results in a broth exhibiting Newtonian properties, facilitating easier mixing, dispersed growth often results in non-Newtonian broth behaviour. This results in mixing problems within the bioreactor, often leading to substrate gradients and oxygen limitations, which can require substantial power inputs to overcome. For example, Papagianni and Mattey reported that when dispersed or clumped growth of *Aspergillus niger* predominated, dissolved oxygen levels did not exceed 80% of saturation, while 100% saturation was maintained for pelleted cultures [72]. The factors that determine the growth form are many and varied, some of which will now be considered, together with the techniques utilised in morphological quantification.

### 1.4.1 Inoculum concentration

The initial inoculum concentration can have a significant influence on the gross morphology of a process (Table 1.3). A very large concentration of spores provides a large number of growth centres and a very limited amount of growth from each

can result in nutrient exhaustion. Conversely, if the initial spore concentration is low, substantial growth may be required before nutrient exhaustion occurs. The distribution of biomass may thus be varied between a large number of small elements and a small number of large elements. However, in practice, the relationship is often considerably more complex and while simple, linear correlations between inoculum size and pellet diameter have been reported for some organisms, more abrupt, step-change phenotypic shifts have been described for others.

A direct linear relationship between the number of pellets formed per unit volume and the initial spore concentration was proposed by Bizukojc and Ledakowicz for *Aspergillus terreus* cultivations [47]. It was estimated that approximately 10,400 spores formed a single pellet and, therefore, a higher inoculum concentration resulted in a greater number of smaller pellets (diameter $< 1.5$ mm), which were favourable for mevinolinic acid (lovastatin) production. A methyl blue-staining and subsequent cross-sectioning technique was used to visualise intra-structural regions of different metabolic activity within pellets. The fraction of actively growing cells at the pellet periphery was correlated with mevinolinic acid production, while the specific (+)-geodin formation rate was found to increase as the size of the active region declined. However, the methodology involved in the preparation of pellets for microtome sectioning was laborious and time-consuming and does not lend itself to high-throughput processing.

A decrease in pellet size for increased inoculum concentration was also obtained by Xu and colleagues in cultures of a recombinant *A. niger* strain [74]. An unusual means of evaluating mean pellet diameter (according to Jianfeng and colleagues [78]) was employed, which involved filtering culture samples through a set of sieves with pore sizes in the range 0 – 6 mm, resulting in pellets being divided into six fractions. The mean diameter ($D_p$) of the population was estimated as:

**Table 1.3:** Reports in the literature indicating a link between morphology and initial inoculum concentration

| Organism | Report | Reference |
|---|---|---|
| *A. awamori* | Increased $L_{hgu}$ and faster growing hyphal tips at higher inoculum concentrations | [73] |
| *A. niger* | Reduction in pellet size for increasing inoculum concentration. Pellets were optimal for minimising protease production while maximising green fluorescent protein yield | [74] |
| *A. niger* | Increases in inoculum concentration induced dispersed morphology. Increase in $L_{hgu}$ also noted as inoculum concentration was increased | [72] |
| *A. terreus* | Mean pellet diameter was inversely proportional to initial spore concentration, with pellet count per unit volume directly proportional to inoculum concentration | [47] |
| *P. chrysogenum* | Transition from cultures containing large, smooth and compact clumps to more dispersed growth as inoculum level increased. Sharp transition observed from $5 \times 10^4$ to $5 \times 10^5$ spores ml$^{-1}$. | [75] |
| *R. chinensis* | A 10-fold increase in spore concentration sufficient to shift morphology from single agglomerate to dispersed growth | [76] |
| *R. nigricans* | Reduction in pellet size for increasing inoculum concentration. | [15] |
| *S. hygroscopicus* | Increasing spore concentration from $10^4$ to $10^5$ spores ml$^{-1}$ caused a slight increase in pellet diameter. Further increase to $10^6$ spores ml$^{-1}$ resulted in a decrease | [77] |

$$D_p = \frac{1}{2}\sum_{i=0}^{5} E_i(2i+1) \tag{1.13}$$

where $E_i$ is the dry-cell weight of pellets in fraction $i$. A sharp reduction in $D_p$ from 3.6 to 0.5 mm was observed when the inoculum level was increased from $10^5$ to $10^7$ spores ml$^{-1}$, with free mycelia also discernible at high inoculum concentrations. Protease activity increased approximately 3-fold and green fluorescent protein (GFP) production declined approximately 64% when the morphology shifted from pelleted to free mycelial growth. Biomass yield increased 29% as pellet size decreased, indicating the influence of mass transfer limitation on cell growth; $O_2$ limitation within pellets was suggested to be responsible for the reduction in protease activity. However the accuracy of $D_p$ estimates is questionable and, as no microscopic analysis was conducted, microscopic structural variations cannot be ruled out.

Larger increases in inoculum concentration were demonstrated by Papagianni and Mattey to induce a completely dispersed growth form in *A. niger* [72]. As the inoculum level was increased from $10^4$ to $10^9$ spores ml$^{-1}$, a large decrease in the size and 'compactness' (ratio of area of hyphae in clump/pellet to total area enclosed by perimeter) of pellets and mycelial clumps was found, accompanied by an increase in 'roughness' (circularity). Morphological variation was also reported at the microscopic level, with increases in the mean main hyphal length, mean total length and branching frequency of mycelia observed as the inoculum level was increased from $10^4$ to $10^8$ spores ml$^{-1}$. Large pellets (approx. 1.0 to 1.2 mm$^2$) were associated with maximal glucosamine production and it was suggested that a relationship between dissolved oxygen levels ($dO_2$) and ammonium ion uptake, which reflects biosynthesis of glucosamine, may have existed.

Sharper transitions in growth form have been reported in other studies. For example, Teng and colleagues found that a ten-fold increase in initial spore concentra-

tion was sufficient to shift the morphology of *Rhizopus chinensis* from a single large agglomerate (described as '*fully entangled mycelia*') to dispersed mycelial growth [76]. Furthermore, large agglomerates were found to be optimal for mycelium-bound lipase production compared to other phenotypes. An inoculum of $3.3 \times 10^9$ spores $ml^{-1}$ resulted in dispersed mycelia, but large agglomerates were obtained for inocula between $3.3 \times 10^7$ and $3.3 \times 10^8$ spores $ml^{-1}$. A micro-morphological influence was also observed, with the mean hyphal length of individual mycelia being lower when large agglomerates formed, while the number of tips per mycelium was higher. However, the prevalence of free mycelia in cultures containing large agglomerates was not specified and, as such, it is not clear what population size these results were based on.

A micro-morphological influence of variation in inoculum concentration was also noted by Johansen and colleagues in their study of *Aspergillus awamori* [73]. Different values of total hyphal length ($L_{th}$) were obtained for different inoculum concentrations in the early stages of fermentation; a lower inoculum resulted in a lower rate of sugar consumption and a larger value of $L_{th}$ per element before the onset of substrate exhaustion. A lower inoculum concentration also resulted in a greater degree of branching and lower tip extension rates, although a limited effect on cutinase production was observed. It was suggested that a constant number of vesicles were supplied per unit length of hypha and therefore a greater number of tips results in a lower number of vesicles supplied to each individual tip and, consequently, a lower tip extension rate. Assuming enzyme production to be coupled to specific growth rate, it was proposed that lower production per tip may have been related to slower growing tips, although 'artificial tips' resulting from fragmentation may have biased measurements. Furthermore, derived trends were based on a limited number of data points and large standard deviations were evident, possibly owing to the low number of tips ($5 - 7$) measured per hyphal element.

Other studies have suggested that the influence of inoculum concentration can vary depending on medium composition. Domingues and colleagues reported that higher protein and cellulose levels were produced using a more concentrated inoculum (attributed to the absence of pellet formation) in cultures of *Trichoderma reesei* [14]. However, when the media was supplemented with Tween-80, yeast extract and peptone, it was found that a lower inoculum concentration produced higher protein and cellulase yields; a more concentrated inoculum resulted in a higher initial growth rate and nutrient exhaustion in the early stages of fermentation, which may have resulted in lower metabolite yields. However, morphological classification was limited to the description of growth as either pelleted or 'pulpy' and, as such, the full extent of structural variation that may have occurred (and the effect on production) is not known.

### 1.4.2 Mechanical agitation

Mechanical agitation is a general requirement in the fermentation of filamentous microbes in order to ensure adequate mixing and aeration. However, the turbulent flows generated, together with the shearing forces of impellers, can have a significant influence on morphology (Table 1.4). Stress-inducing localised pressure variations in the fluid cause mycelial fragmentation if the tensile strength of the hyphae is exceeded, while the peripheral regions of pellets can be sheared away if sufficient force is applied, dispersing the biomass and creating new centres of growth. Papagianni and colleagues demonstrated that increased agitation in batch cultures of *A. niger* can reduce hyphal vacuolation [79]. In batch cultures, both clump perimeter and filament length decreased with increasing agitation, while the percentage of vacuolated hyphal volume, as well as the mean diameter of vacuoles, were higher at lower agitation speeds. This suggested that higher levels of hyphal fragmentation occurred at higher agitation levels, which caused a reduction in vacuolated hyphae,

indicating that fragmentation can aid in regrowth and limiting of vacuolation. However, high levels of agitation can cause excessive levels of mycelial damage, reducing biomass yield and compromising productivity [46].

A relationship between agitation intensity and the growth form of *A. niger* was described by Papagianni and colleagues, who proposed the 'relative mixing time' (derived from analysis of pH response to an alkali pulse in both tubular-loop and stirred-tank reactors) as a significant process-controlling factor [80]. As agitation intensity was increased, the perimeter length of mycelial clumps decreased, while citric acid production increased. The increased citric acid yield was attributed to morphological variation, but reduced dissolved oxygen concentration was noted at lower agitation speed, which may have influenced metabolite production. Increased agitation was also found by Park and colleagues to cause a reduction in the size of *Cordyceps militaris* pellets [50]. Pellets were found to be larger and 'fluffier' at low agitation intensity (50 rpm); at high agitation intensity (300 rpm), the outer filamentous regions were sheared off, resulting in a decrease in pellet size and circularity, defined as the ratio of the minimum Feret's diameter[8] to the maximum. It was suggested that the larger pellets formed at low agitation intensity were probably oxygen-limited at their cores, resulting in autolysis at an earlier stage of fermentation and subsequent formation of hyphal 'fragments'. Maximum exo-biopolymer production (15 g $L^{-1}$) was obtained at 150 rpm, which was attributed to the compact, spherical nature of the pellets obtained at this agitation intensity.

The influence of shearing forces on pellet morphology was further investigated by Rodríguez-Porcel and colleagues in fermentations of *A. terreus* [51]. Following inoculation of fluidised-bed reactors (FBR's) and stirred-tank reactors (STR's) operated at 300 rpm with a culture of pellets approximately 1,200 $\mu$m in diameter, the pellets grew to a steady state diameter of approximately 2,300 $\mu$m. However,

[8]The perpendicular distance between parallel tangents touching opposite sides of the perimeter

**Table 1.4:** Reports in the literature indicating a link between mechanical agitation and morphology

| Organism | Report | Reference |
|---|---|---|
| *A. niger* | Increased agitation speed resulted in decreasing mean perimeter length of mycelial clumps. 'Relative mixing time' proposed as significant process-controlling factor | [80] |
| *A. niger* | Increased agitation inhibited pellet growth in shake-flask cultures. Small pellets were associated with maximum phytase production | [81] |
| *A. niger* | Increased agitation caused reduction of pellets to 'micro-pellets' and filamentous growth, resulting in increased glucose oxidase yield | [46] |
| *A. niger* | Linear relationship between energy dissipation and pellet count per unit volume | [82] |
| *A. oryzae* | Direct relationship derived between projected area of mycelial clumps and EDCF, while $L_{hgu}$ was relatively independent of agitation intensity | [83] |
| *A. oryzae* | Amyloglucosidase production found to be approximately proportional to the number of 'active' tips in a culture | [84] |
| *A. terreus* | Steady-state mean pellet diameter correlated with power input per unit volume. Pellets also became more compact at higher agitation speeds | [51] |
| *C. militaris* | Increased agitation resulted in smaller, more spherical (quantified in terms of circularity) pellets | [50] |
| *T. harzianum* | Linear relationship between power input (EDCF function) and mean clump diameter | [85] |
| *T. harzianum* | Reduction in the diameter of mycelial clumps for increasing agitation intensity in shake flasks | [86] |

for more intensely agitated STR cultures (600 and 800 rpm), pellet size declined from inoculation to an average steady state diameter of approximately 900 and 700 $\mu$m respectively, which was attributed to 'erosion' of the pellet surface. Steady-state values of mean pellet diameter in all reactors was found to correlate well with total power input ($P_g$; including that from expansion of sparged gas) per unit volume ($P_g/V$). For all operating regimens and reactors, the filament ratio ([area of peripheral 'hairy surface']/[total projected area]) declined to 0.4 during the first 72 hours of fermentation; agitation that did not result in a reduction in pellet size still caused a decrease in the filament ratio. This was attributed to fluid eddies 'folding' the peripheral hyphae onto the pellet, compacting the structure. Highly agitated (800 rpm) STR cultures were an exception, in which a lower stable value of 0.2 was obtained.

The duration of shearing forces was found to be a significant morphological influence by Wongwicharn and colleagues in chemostat cultures of *A. niger* [87]. Values of mean hyphal length, mean tip number and $L_{hgu}$ all rose up to a dilution rate ($D$) of 0.08 $h^{-1}$ before falling. This was explained by the greater residence time at low $D$; the average length of time hyphal elements were exposed to hydro-mechanical damage was greater than at high $D$, so in general a shorter, more compact 'organism' resulted. Pellet core diameter also increased with $D$, due to increased growth rate and decreased mean residence time (less shear damage) as $D$ rose, which emphasises that duration of exposure to shearing forces can have a discernible effect on growth form.

The morphological influence of sudden 'step' changes in agitation, and associated implications for metabolite production, were investigated by Paul and colleagues [44]. In a fermentation inoculated with pellets, diameter increased slightly (up to approximately 1.5 mm) before decreasing following a step increase in agitation from 500 to 800 rpm. Circularity increased slowly with time, indicating increasingly ir-

regular pellets, probably due to fragmentation. During most of this fermentation the citric acid titre was comparable to that in another fermentation inoculated with spores and cultivated as a dispersed phenotype; evidence that the pellets were too small for significant diffusional limitations to have occurred. The overall yield however was greater from the dispersed fermentation (0.74 compared to 0.58 g citric acid/g glucose). A second fermentation inoculated with pellets was initially maintained at 300 rpm, which resulted in a rapid increase in diameter (up to 3.1 mm) with circularity increasing slowly - a step increase in agitation up to 500 rpm had little effect. A subsequent step increase to 800 rpm resulted in a rapid decrease in pellet diameter, accompanied by an increase in circularity, carbon dioxide production rate, oxygen uptake rate and a slight increase in growth rate, suggesting increased agitation caused a reduction in substrate-limited biomass. This fermentation resulted in the lowest yield of citric acid on glucose (0.49), probably owing to diffusional limitations in large pellets, reflected in a lower rate of glucose uptake, decreased specific growth rate, decreased specific uptake of oxygen and decreased specific production of carbon dioxide.

The work of Paul and colleagues suggests that increased agitation can result in a greater degree of biomass dispersal, a reduction in the fraction of unproductive biomass and, consequently, an increase in metabolite production. This hypothesis was further supported by El-Enshasy and colleagues, who reported a reduction in pellet size and an increase in the fraction of 'active' biomass for increased agitation levels [46]. Agitation speeds of 200, 500 and 800 rpm resulted in mean pellet diameters of 1,500, 400 and 24 $\mu$m respectively, although the latter were described as '*micro-pellets embedded in a filamentous mesh*', which may have complicated their measurement. The yield of glucose oxidase increased with increasing power input and the shift from pelleted to filamentous growth. Staining with acridine orange indicated that active protein production was restricted to free filamentous

elements and the outer, peripheral region of pellets. It was also shown that the active region decreased in size with cultivation time in tandem with a decline in the specific glucose oxidase production rate. A comparison of cultures grown at 200 and 800 rpm showed similar specific glucose oxidase activities and production rates, when calculated based on the active fraction of biomass.

However, in their study of *A. oryzae*, Amanullah and colleagues found that although increased agitation resulted in a decrease in the projected area of mycelial clumps, no increase in metabolite production was observed [83]. Steady-state values of mean projected area of biomass (clumps and freely dispersed elements) correlated well with the Energy Circulation/Dissipation Function (EDCF[9]). However, no significant difference in the hyphal growth unit ($L_{hgu}$) was measured and agitation speed did not have an appreciable effect on production rates (of $\alpha$-amylase and amyloglucosidase), although fewer tips per element were measured at higher agitation. It was proposed that because $L_{hgu}$ was relatively independent of agitation speed, and assuming that the tip extension rate (which is coupled to enzyme synthesis) was also constant (influenced by dilution rate rather than agitation), the total number of 'active' tips in the culture was approximately independent of agitation speed. This suggested that, within certain limits, agitation could be modified to regulate mixing and morphology without compromising metabolite production. In a subsequent study, Amanullah and colleagues used calcofluor white staining to distinguish between active and non-active tips in *A. oryzae* [84]. A dependence of amyloglucosidase production on agitation intensity was found, which was attributed to the presence of a larger number of active tips at higher agitation speeds; an approximate correlation ($R^2 = 0.65$) between specific amyloglucosidase production and % active tips was illustrated.

[9] $P/(KD^3t_c)$, where $P$ is the power input, $D$ the impeller diameter, $t_c$, the mean circulation time, and $k$ is a geometric constant for a given impeller.

Further physiological influences of mechanical agitation were reported by Rocha-Valadez and colleagues in cultures of *Trichoderma harzianum* [85]. While a linear relationship between power input (EDCF function) and mean clump diameter was discerned, production of 6-Pentyl-$\alpha$-Pyrone, which increased with ECDF before decreasing, was not directly linked to the observed morphological shift. It was proposed that, given the observation of a linear increase in specific $CO_2$ production and a linear decrease in specific growth rate, a metabolic shift had occurred in response to increased hydrodynamic stress, reducing biomass synthesis and metabolite production.

In addition to influencing hyphal fragmentation and shearing of pellet peripheral regions, mechanical agitation can also affect the extent of cellular aggregation. Amanullah and colleagues found that a 'step-down' in agitation speed resulted in substantial aggregation of *A. oryzae* mycelia [88]. An increase in mean projected area from $17,800 \pm 1,500$ to $25,000 \pm 2,300$ $\mu m^2$ and from $12,000 \pm 1,300$ to $17,000 \pm 2,000$ $\mu m^2$, at biomass concentrations of 5.3 and 11.2 g $L^{-1}$ respectively, was observed between 5 and 15 minutes after a lowering of the EDC from 800 to 50 $kWm^3s^{-1}$. It was estimated that 85 – 115 minutes would have been required if mycelial growth alone was responsible for these size increases. However, a significant increase in mean projected area was not measured in the absence of dissolved oxygen at either biomass concentration, suggesting that aggregation requires aerobic metabolism. It was also shown that an increase in the mean total length of the freely dispersed biomass fraction was faster than that in the mean projected area of clumps, leading the authors to speculate that small hyphal elements had a greater tendency to aggregate than larger elements, possibly due to their larger contact areas. These findings have implications for processes conducted in large-scale, aerated fermenters, as mycelia may be repeatedly fragmented and aggregated as they circulate through a large volume.

Variations in agitation intensity can also significantly affect spore agglomeration and subsequent pellet formation. Kelly and colleagues reported that increasing energy dissipation caused an initial decrease in the diameter and growth rate of *A. niger* pellets [82]. However, after reaching a minimum, the pellet diameter and the growth rate both increased again at a higher specific energy dissipation, but the overall concentration of pellets decreased linearly. It was suggested, perhaps counter-intuitively, that greater aggregation of spores at the beginning of cultivation due to higher agitation rates was responsible, resulting in fewer pellets. Each pellet therefore had a greater amount of substrate available and, in addition, higher agitation rates improved mass transfer, which together could have explained the increased growth rate and pellet diameter at higher energy dissipations. This assumes that increased agitation results in increased particle-to-particle interaction and that spore-spore 'bonding' forces are sufficiently strong to withstand increased external shearing forces at higher agitation levels.

However, in their study of shake-flask cultures of *A. niger*, Papagianni and colleagues reported that increased agitation resulted in the inhibition of pellet formation [81]. A fermentation conducted at 150 rpm resulted in a mixture consisting of pellets (average diameter 0.5 mm) and a small number of mycelial clumps. At higher agitation (300 rpm), no pellets were detected, with the culture consisting entirely of 'loose' clumps and 'free' mycelial trees, suggesting that increased agitation inhibited cellular aggregation. The effect of medium viscosity (regulated with the addition of guar gum) was also investigated and, at 150 rpm, pellet formation tended to reduce with increasing gum concentration; no pellets appeared at a gum concentration of 1 g $L^{-1}$. The morphological shift was attributed to the lower dissolved oxygen concentration in the presence of gum [81].

### 1.4.3 Carbon and nitrogen sources

Certain nutrients are required by most fungi to maintain growth, but the general composition of the media can be altered to affect metabolism. This is common practice in industrial fermentation processes, as certain media components are often required in order to induce production of the metabolite of interest. An organic source of carbon and a source of nitrogen are almost always required; carbon typically constitutes approximately 50% of dry-cell weight, while nitrogen is required to synthesise amino acids and proteins [7]. While fungi are typically capable of producing a large number of enzymes for the extra-cellular degradation of substrates, sugars such as glucose, maltose and starch are commonly used as carbon sources, although some fungi can metabolise organic acids and even hydrocarbons [89]. There also exists evidence that variations in media composition, and the subsequent influences on metabolism, can result in changes in morphology (Table 1.5).

Papagianni and Mattey found that increasing glucose concentration resulted in a decrease in the diameter of *A. niger* pellets and an increase in citric acid production in immobilised cultures [48]. At low glucose concentration (50 g $L^{-1}$), 'hairy' pellets predominated with long, thin, unbranched filaments at the surface, but at higher concentrations (100 and 150 g $L^{-1}$), pellets were compact with short, thick filaments with swollen tips (based on SEM images). The rates of citric acid production increased with glucose level and were always higher with immobilized mycelium. The increased yield was attributed to the greater mean diffusion path in pellets compared to the immobilized system; immobilised biomass was considered to be maximally productive, while pellets were substrate-limited below the surface. However, the study suffered from a lack of quantitative methods for the microscopic analysis of filaments, although the routine imaging of immobilised mycelia may be challenging.

**Table 1.5:** Reports in the literature indicating a link between medium composition and morphology

| Organism | Report | Reference |
|---|---|---|
| *Aspergilli* | Correlation between volume of apical compartment and specific growth rate, regulated by glucose concentration | [90] |
| *A. niger* | Increasing glucose concentration resulted in decrease in pellet diameter and increase in hyphal apical volume | [48] |
| *A. niger* | Hyphae more susceptible to fragmentation at low glucose levels - increase in vacuolation also noted | [79] |
| *A. oryzae* | Pulsed addition of carbon during fed-batch fermentation reduced mean projected area of mycelial elements, reducing broth viscosity | [91] |
| *M. alpina* | Increasing carbon to nitrogen ratio ($C/N$) resulted in increase in total pellet area ($A_m$) and size of pellet annular region ($A_f$) for $C/N > 20$, but $A_f/A_m$ remained constant | [92] |
| *M. alpina* | Enriching media by increasing both $C$ and $N$ (with $C/N = 20$) resulted in decrease in pellet size | [93] |

The manner in which substrate is added to a fermentation has also been determined to be an important influence on growth. Bhargava and colleagues have shown that the pulsed addition of substrate during fed-batch fermentations of *A. oryzae* can reduce the mean projected area of mycelial elements, reducing broth viscosity and increasing productivity [91]. Viscosity was found to be inversely proportional to cycle time ($t_c$; the length of time between pulsed additions of substrate) with cultures produced with a high value of $t_c$ exhibiting viscosities approximately 5 times lower than a continuously fed batch. The reduction in viscosity was likely a result of changes in morphology, with the average size of fungal elements (clumps or free mycelia; measured by projected area) decreasing approximately linearly with $\log t_c$. However, this structural variation did not result in a significant impact on

glucoamylase production (for $t_c \leq 300$ s), indicating that culture viscosity could be reduced (reducing requisite power input) without compromising metabolite production. However, for longer cycle times ($t_c \geq 900$ s), a marked reduction in glucoamylase levels was observed (approximately 50%), which was likely related to the increased occurrence of sporulation noted by the authors, caused by low substrate levels. Low levels of carbon substrate have also been demonstrated to result in increased hyphal vacuolation and fragmentation in fed-batch cultures of *A. niger* [79]. Reducing the glucose concentration from 70 to 17 g $L^{-1}$ resulted in an increase in the percentage vacuolated volume of hyphae as well as a reduction in the mean length of hyphal filaments, suggesting an increase in fragmentation at lower glucose concentrations.

Müller and colleagues also quantified a micro-morphological and physiological influence of substrate concentration in cultures of *A. oryzae* and *A. niger* [90]. The average number of nuclei in the apical compartment was found to increase for increasing specific growth rate, but little or no change was observed in sub-apical compartments. The average length and diameter of an apical compartment also increased for increasing specific growth rate (the length of sub-apical compartments was only slightly affected); this increase in volume may have been required to accommodate an increase in cytoplasmic mass, so as to maintain a constant cytoplasm to nucleus ratio. An increase in apical volume in response to increased glucose concentration was also noted by Papagianni and Mattey in cultivations of *A. niger* [48].

While it has been suggested that a balanced medium will contain ten times as much carbon as nitrogen [7], varying this ratio can have a significant influence on morphology. Park and colleagues found that increasing the carbon to nitrogen ratio ($C/N$) in cultivations of *Mortierella alpina* resulted in both an increase in total pellet area, $A_m$, and an increase in the size of the pellet annular region, $A_f$ (for

$C/N > 20$), but the filamentous fraction ($A_f/A_m$) remained constant [92]. The pellet core size was 0.45 mm$^2$ on average, and did not change for $C/N < 20$, with the filamentous mycelial area displaying a similar trend (1.1 mm$^2$ on average). The ratio of the filamentous mycelial area to the whole mycelial area was 0.82 and was independent of the consumed $C/N$ ratio. When the medium was enriched 3-fold, the filamentous mycelial area and pellet core size increased 8.6- and 4.7-fold compared to the control. The ratio of the filamentous mycelial area to the whole mycelial area was 0.76, which was independent of the consumed $C/N$ ratio despite the use of enriched media.

However, Koike and colleagues found that enriching medium at a fixed $C/N$ ratio resulted in a decrease in the whole pellet size and the width of the pellet annular region in *M. alpina*, but variations in morphology similar to those described by Park and colleagues were reported for variations in the $C/N$ ratio [93]. The whole pellet size ($A_m$) did not change for $C/N < 20$, but then increased gradually with an increase in the consumed $C/N$ ratio. The width of the annular region remained approximately constant for $C/N < 20$ and then increased linearly with increasing $C/N$ ratio.

### 1.4.4 Culture pH

The medium pH is an important environmental factor that can significantly influence the outcome of a fermentation. While filamentous fungi can grow over a wide range of pH (typically 4 – 9), maximal growth is often found near neutral pH [7] and minimising pH drift is often a target in bioprocess design. However pH has also been shown to impact morphology and, in particular, pellet formation (Table 1.6).

In batch cultivations of *A. oryzae*, Carlsen and colleagues reported that at pH 3.0 – 3.5 freely dispersed hyphal elements predominated, with pellets becoming more common as acidity was reduced [45]. At very low pH ($\leq$ 2.5) the mycelium was

**Table 1.6:** Reports in the literature indicating a link between pH and morphology

| Organism | Report | Reference |
|---|---|---|
| *A. nidulans* | Reduction in electrophoretic mobility of conidiospores for increasing pH, which was subsequently shown to increase pellet formation | [94] |
| *A. oryzae* | At pH 3.0 – 3.5 freely dispersed hyphal elements predominated, with pellets becoming more common as acidity was reduced | [45] |
| *Phellinus* | Macro-morphological effect of pH variation on different species, but not expressed quantitatively | [52] |
| *R. nigricans* | Growth suppressed below pH 2. Clumpy growth noted at pH 3 or above 7, otherwise pelleted growth prevailed | [15] |

vacuolated with swollen cell walls, resulting in poor growth, but at pH 3.0 to 3.5, freely dispersed hyphal elements resulted. As pH was increased further, pellets became more prevalent, with no free elements discernible at high pH ($\geq 6$) and pellet radius increasing with medium alkalinity. At relatively high pH ($> 4$), agglomerates containing 10 to 100 spores were observed approximately 10 hours post-inoculation, whereas at low pH (2.5 to 3.5) only freely dispersed spores were found. When cultivations were inoculated with freely dispersed hyphal elements no pellets were witnessed and it was therefore concluded that pellet formation in *A. oryzae* resulted from coagulation of spores, which was dependent on medium pH. While no micro-morphological influence of pH was found (based on measures of total hyphal length and number of tips per element), the effect of pH on the growth kinetics was studied and a broad optimum between pH 3 and 7 was found, while the specific $\alpha$-amylase production rate had an optimum in the range pH 5 to 7.

Dynesen and Nielsen demonstrated a reduction in the electrophoretic mobility of *A. nidulans* conidiospores for increasing pH, which was subsequently shown to in-

crease pellet formation, although the influence of hydrophobicity was also reported as significant [94]. Contact angles[10] (determined using water droplets on layers of conidiospores) for strains lacking hydrophobins were lower than those of the control strain and for all strains, electrophoretic mobility decreased from positive to negative with increasing pH. The percentage of free mycelia in shake flasks 19 hours post-inoculation increased with decreasing pH and for all pH values studied (except pH 5.8), the percentage of free mycelia increased with decreasing hydrophobicity. Disruption of genes encoding hydrophobins did not affect the surface charge of the conidiospores, so the reduced pellet formation by the mutant strains could not be attributed to differences in electrostatic interactions and it was therefore suggested that a high surface hydrophobicity of *A. nidulans* conidia favoured pellet formation. However, since pellet formation by the mutant strain exhibiting the lowest hydrophobicity was observed at low pH values, the authors concluded that agglomeration of *A. nidulans* conidia could not be attributed to hydrophobic and electrostatic interactions alone; possible chemical interactions such as polysaccharide bridging, may also have been at play.

Hwang and colleagues displayed the macro-morphological effect of pH level on different *Phellinus* species, although the variation was not expressed quantitatively [52]. *P. baumii* produced high amounts of free mycelium as the culture pH shifted to neutral and alkaline ranges. In contrast, *P. gilvus* displayed pelleted growth at low pH (4 and 5) whereas free mycelia were predominant at pH 9. *P. linteus* showed spherical pellet growth with lesser amounts of free mycelia irrespective of culture pH.

[10]The contact angle is the angle at which a liquid/vapour interface meets a solid surface.

### 1.4.5 Supplementation with metal ions

Certain essential metals are required for fungal growth and their absence from nutrient media can result in developmental abnormalities, while excess levels of certain ions can induce morphological variation (Table 1.7). For example, omission of $Mn^{2+}$ ions were found to have a significant impact on the morphology of *A. niger* by Kisser and colleagues, although the assessment of variation in form was limited to qualitative descriptions [95]. In the presence of manganese ($5 \times 10^{-5}$ M), growth was initiated by the emergence from spores of germ tubes after 18 – 20 hours. The germ tubes were thin, had very few branches (described as 'filamentous' growth) and citric acid production was poor (44 mM after 150 h). However, in the absence of manganese, considerable swelling of spores occurred prior to germ tube formation and hyphae were characterised as 'squat, bulbous cells', which were preferable for a high citric acid yield (286 mM). An intermediate level of manganese ($4 \times 10^{-7}$ M $L^{-1}$) resulted in both the 'filamentous' and 'bulbous' phenotypes. The addition of iron ($> 5 \times 10^{-4}$ M) also resulted in filamentous growth in the absence of manganese, while the addition of copper ($10^{-4}$ – $10^{-3}$ M) reduced the influence of manganese.

The addition of metal ions has also been used to influence the hydrophobicity of cells, which subsequently affected cellular aggregation. Dobson and O'Shea found that the hydrophobicity of *Streptomyces hygroscopicus* cells could be influenced with the addition of calcium or magnesium ions [97]. Cultures supplemented with $Ca^{2+}$ ions were found to be hydrophobic, which resulted in cellular aggregation, while the addition of $Mg^{2+}$ ions resulted in hydrophilic cells with the organism growing as freely dispersed filaments, with shorter, more branched hyphae visible, although these dispersed elements were not morphologically analysed. Increasing the concentration of $Ca^{2+}$ from 0.01 to 0.5 g $L^{-1}$ resulted in a 40% increase in pellet diameter and a decrease of approximately 70% in the number of pellets per ml, which reflected

**Table 1.7:** Reports in the literature indicating a link between metal ion supplementation and morphology.

| Organism | Report | Reference |
|---|---|---|
| *A. niger* | Omission of $Mn^{2+}$ ions resulted in '*squat, bulbous hyphae*' | [95] |
| *A. niger* | Addition of $Fe^{2+}$ and $Zn^{2+}$ ions resulted in diffuse pellets | [96] |
| *R. nigricans* | Increase in mean pellet diameter observed in presence of $Ca^{2+}$ ions | [15] |
| *S. hygroscopicus* | Cultures supplemented with $Ca^{2+}$ ions were hydrophobic, resulting in cellular aggregation. Addition of $Mg^{2+}$ ions resulted in hydrophilic cells and freely dispersed filaments | [97] |

the extent of aggregation. This increase in pellet size coincided with a decrease in geldanamycin yield of 85%. Evaluation of the cell-surface hydrophobicity (CSH), by measuring of contact angles, determined that control cultures were hydrophilic (contact angle of $37.65 \pm 4.1°$), whereas pelleted cultures containing $Ca^{2+}$ ions were strongly hydrophobic ($76.64 \pm 5.5°$). In contrast, $Mg^{2+}$-supplemented cultures growing as dispersed filaments were classed as hydrophilic ($22.89 \pm 4.9°$). A relationship between pellet size and CSH was demonstrated, with increasing hydrophobicity instigating aggregation and pellet formation.

Metal ion supplementation was also explored by Couri and colleagues in cultures of *A. niger*, who found that the addition of $Fe^{2+}$ and $Zn^{2+}$ ions resulted in diffuse pellets compared to the control [96]. Pellet diameter ($D$), perimeter and pellet core diameter ($d$) were measured manually and other measures, such as pellet area ($A_p$) and pellet core area ($A_c$), were derived. The addition of $Fe^{2+}$ and/or $Zn^{2+}$ resulted in smaller pellets with smaller cores, while the ratio of $D/d$ was higher and

$A_c/A_p$ lower in pellets incubated in the presence of both ions, compared to those fermentations supplemented with just one ion. Polygalacturonase production was higher in the presence of both ions compared to the control, but specific activity was higher in control cultures, even though morphologies were similar. However, control pellets were larger and probably autolysed at the core (based on measures of weight and volume), which possibly biased measures of specific activity.

### 1.4.6 Supplementation with surface active agents and polymers

Various surface active agents (surfactants) have also been investigated in attempts to disrupt cellular aggregation in submerged processes. Žnidaršič and colleagues found that the supplementation of *Rhizopus nigricans* cultures with Tween-80 caused a slight increase in pellet diameter, but higher concentrations (1 – 2 g $L^{-1}$) also produced some clumped growth [15]. The increase in pellet size, which was accompanied by an increase in biomass, was attributed to increased cell membrane permeability, facilitating more efficient mass transfer of nutrients. Other factors were also investigated, such as culture pH and the influence of $Ca^{2+}$ ions, but the morphological assessment was rather qualitative in nature, with pellets classified as either 'smooth' or 'fluffy'. Conversely, Domingues and colleagues reported that Tween-80 inhibited pellet formation in *T. reesei* [14]. Inoculation with $10^5$ spores $ml^{-1}$ resulted in pellet formation in a control media, but filamentous growth resulted in the presence of Tween-80, although only qualitative morphological descriptions were produced. A more concentrated inoculum ($10^7$ spores $ml^{-1}$) resulted in filamentous growth in both media. Supplementation with Tween-80 also resulted in elevated yields of both protein concentration and cellulase production at both inoculum concentrations, with increased permeability of the cell membrane again suggested as the cause, allowing more rapid secretion of enzymes which in turn leads to higher enzyme synthesis.

Supplementation of *S. hygroscopicus* cultures with Tween-80 was reported by

**Table 1.8:** Reports in the literature indicating a link between surfactant and/or polymer supplementation and morphology

| Organism | Report | Reference |
|---|---|---|
| *A. niger* | Addition of kaolin resulted in small, compact pellets | [98] |
| *A. niger* | Carboxymethylcellulose shifted morphology from pelleted to filamentous | [99] |
| *R. nigricans* | Supplementation with Tween-80 caused slight increase in pellet diameter | [15] |
| *S. hygroscopicus* | Supplementation with Tween-80 had minimal influence on morphology, but Triton X-100 resulted in significant increase in pellet size | [100] |
| *S. hygroscopicus* | Concentrations of carboxymethylcellulose up to 3.0% resulted in decrease in pellet size. Reduction in 'wall growth' also observed | [101] |
| *T. reesei* | Tween-80 inhibited pellet formation | [14] |
| *T. harzianum* | Tween-40 resulted in reduction in pellet size, with more dispersed growth | [102] |

Dobson and colleagues to have a minimal impact on morphology, but the inclusion of 0.01% (v/v) Triton X-100 resulted in a considerable increase in pellet size [100]. Further increases in the concentration of Triton X-100 (up to 1.0% v/v) resulted in a subsequent decrease in pellet size (to control levels). While the addition of Tween-80 did not have a significant influence on pellet size, an increase in concentration did result in an increase in pellet count per ml, which was accompanied by an increase in geldanamycin production. However, control cultures produced a greater or equal yield of geldanamycin compared to all surfactant-supplemented cultures. Silicone antifoam was also found to be influential, with an increase in the concentration present in the medium causing an increase in the dispersion of pellets; pellet sizes decreased by more than 50% in those cultures supplemented with 5% (v/v) silicone

antifoam. Antibiotic synthesis appeared to be repressed by the formation of large pellets, implying that cultures with smaller pellet sizes are optimal for geldanamycin production.

Supplementation of *T. harzianum* cultures with Tween-40 also resulted in a reduction in pellet size, together with more dispersed growth, and a linear relationship between Tween-40 concentration and biomass yield was also reported [102]. In the absence of Tween-40, large, 'star-like' pellets were formed, while supplementation with 0.2 ml $L^{-1}$ Tween-40 resulted in the formation of spherical pellets, typically exhibiting a smooth, compact structure and a narrow filamentous outer region, reflected in the lower roundness value. With respect to the control, a narrower particle size distribution resulted in the presence of Tween-40, indicating greater pellet homogeneity. A rapid transition from pelleted to dispersed/clumped morphologies at Tween-40 concentrations above 0.4 ml $L^{-1}$ was observed, although a small number of pellets were still present at this concentration. It was suggested that high Tween-40 concentrations may have resulted in the incorporation of Tween molecules into the cell wall, influencing spore aggregation.

Other studies have explored the influence of polymers on culture conditions. Ilić and colleagues described the effect of carboxymethylcellulose (CMC) supplementation on cultures of *S. hygroscopicus*, with concentrations of up to 3.0% resulting in a decrease in pellet size, a significant increase in biomass levels and a reduction in wall growth [101]. In the absence of CMC, large pellets ($\sim$ 4.1 mm in diameter) developed and '*extra heavy*' wall growth was observed. With the addition of CMC, pellet diameter decreased to a minimum of approximately 0.7 mm at a concentration of 3.0% (w/v) and wall growth was reduced to low levels. An increase in metabolite production in the presence of CMC was also noted, with the maximum concentration of hexaene H-85 obtained at 3.0% CMC (146.7 mg $dm^{-3}$ versus 94.58 mg $dm^{-3}$ in control culture) and the maximum concentration of azalomycine was obtained

at 1.0% CMC (188.6 mg $dm^{-3}$ versus 115.7 mg $dm^{-3}$ in control culture). It was therefore concluded that smaller pellets favoured elevated antibiotic production. However, pellet diameters were determined in a crude manner, with measurements obtained from microscope images using a ruler; only ten pellets were analysed for each sample. CMC supplementation was also reported to induce filamentous growth in *A. niger*, but the morphological variation was not assessed quantitatively [99].

O'Cleirigh and colleagues regulated the apparent viscosity of *S. hygroscopicus* broths with the addition of xanthan gum, increased concentrations of which (up to 3 g/L) resulted in a decrease in pellet size [103]. The pellet count increased to a maximum (by a factor of 4 relative to the control) at a concentration of 3 g $L^{-1}$ xanthan gum and then decreased in excess of that point, whereas the mean pellet volume decreased (by a factor of 3.5) with respect to increasing xanthan gum concentration. An increase in biomass production of up to 2.5-fold was also recorded. This data suggested that, by inhibiting particle aggregation, the development of individual spores into smaller pellets was achieved. It was also found that the addition of xanthan gum resulted in an increase in gas-liquid mass transfer ($K_L a$), increasing the oxygen transfer to pellets. Increased broth viscosity was also determined to inhibit pellet growth in *A. niger*, but reduced dissolved oxygen concentration was assumed to be responsible [81].

The addition of kaolin[11] to cultures of *A. niger* was reported by Ali to promote the formation of small, compact pellets [98]. When a 15 ppm aqueous suspension of kaolin was added to the fermentation, citric acid yield peaked at 74.62 g $L^{-1}$ 96 hours post-inoculation, compared to a peak of 40.94 g $L^{-1}$ 168 hours post-inoculation in the control culture, with morphology shifting from 'mixed mycelia' (1.10 - 1.75 mm in size) to 'small pellets' (1.12 mm). Process performance was further enhanced by delaying the addition of kaolin (15 ppm) until 24 hours post-inoculation, which

[11] A common mineral (also known as kaolinite) widely referred to as 'China clay'.

resulted in a citric acid yield of 96.88 g $L^{-1}$, which resulted in a 'mixed pellet' (1.08 - 1.28 mm) growth form. However, the methodology employed in determining 'mycelial size' was not specified.

### 1.4.7 Significance of branching

In investigating the role of different environmental variables in microbial development, many researchers have demonstrated reproducible relationships between macro-morphology and product yield for a particular process (Table 1.9). Often, however, micro-morphological variation has been overlooked. Fundamental to furthering the understanding of morphological influence on product yield is the eliciting of a link between hyphal branching and metabolite production, as there is considerable evidence in the literature that protein secretion occurs almost exclusively at the hyphal apex (Table 1.10).

Wösten and colleagues developed a technique for the localisation of glucoamylase around the hyphal tips of *A. niger* [105]. A polycarbonate membrane was centrally placed on the surface of solidified medium and topped with an agarose layer (approx. 0.3 mm thick), which was inoculated with a small piece of mycelium. The surface was then topped with a second polycarbonate membrane, causing colonies to grow approximately two-dimensionally. When 4-day-old colonies were transferred from xylose to starch and incubated overnight, starch-degrading activity (detected with Lugol's iodine) was localized at the colony periphery; prolonging growth for another 8 hours resulted in virtually all starch under the colony being degraded. It was also found (using immunodetection) that enzymes were mainly secreted at the periphery of the colony; glucoamylase was observed around the tips of leading hyphae, but little was seen surrounding subapical regions. When colonies were transferred to a cold environment (4°C) for 10 minutes before being re-transferred to the original plate at 25°C, labelling with N-acetylglucosamine showed that all hyphae had

**Table 1.9:** Recent reports in the literature indicating a relationship between macromorphology and productivity

| Organism | Report | Reference |
|---|---|---|
| *A. niger* | Small pellets optimal for minimising proteases and maximising green fluorescent protein yield | [74] |
| *A. niger* | Small pellets preferable for polygalacturonase synthesis | [96] |
| *A. niger* | Reduced pellet size provided increase in glucose oxidase production | [46] |
| *A. niger* | Large pellets associated with maximal glucosamine production | [72] |
| *A. oryzae* | Filamentous growth optimal for $\alpha$-amylase production | [45] |
| *C. militaris* | Compact pellets favourable for exo-biopolymer production | [50] |
| *P. chrysogenum* | Filamentous growth favourable for penicillin production | [104] |
| *R. chinensis* | Mycelium-bound lipase production increased from 101.2 to 691 U $g^{-1}$ with a change in morphology from dispersed mycelia to large agglomerates | [76] |
| *S. hygroscopicus* | Dispersed growth synthesised geldanamycin at an optimal rate | [97] |

stopped growing and immunosignals of glucoamylase could no longer be detected. No interference with growth and secretion occurred when colonies were transferred to a fresh agar medium at 25°C and after 10 minutes re-transferred to the original plate. It was therefore concluded that glucoamylase was secreted exclusively by actively growing tips of *A. niger*.

However, Müller and colleagues contended that during growth on solid medium, secreted proteins will always be found surrounding the hyphae and, therefore, studies localising metabolite excretion in mycelia grown on agar are inconclusive [107]. Their work focussed on submerged culturing of *A. oryzae* and FITC labelling of

**Table 1.10:** Reports in the literature indicating a link between branch formation and productivity

| Organism | Report | Reference |
|---|---|---|
| *A. niger* | Localisation of glucoamylase secretion at hyphal tips | [105] |
| *A. niger* | High citric acid productivity characterised by swollen hyphal tips | [48] |
| *A. niger* (B1-D) | Correlation between 'percentage active length' of hyphae and total soluble protein concentration | [87] |
| *A. oryzae* | Correlation between amyloglucosidase production and number of active tips | [84] |
| *A. oryzae* | Densely branched strain favourable for $\alpha$-amylase production | [106] |
| *A. oryzae* | Localisation of $\alpha$-amylase in apical cell walls | [107] |
| *A. oryzae* | Strains with lower $L_{hgu}$ values produced higher yields of $\alpha$-amylase, glucoamylase and proteases | [108] |
| *A. oryzae* | Lipase production coincided with swelling of hyphal tips | [109] |
| *P. cinnabarinus* | Correlation between branching and phenol-oxidase secretion | [110] |

antibodies suggested that $\alpha$-amylase resided in the cell walls of hyphae. Fluorescence was greatest in new tips or extending hyphae, while older hyphae (more than 100 $\mu$m from the tip) did not fluoresce as strongly, supporting the hypothesis that $\alpha$-amylase is secreted from the hyphal apex. However, a comparison of three different strains of *A. oryzae* showed similar levels of amylase productivity, despite differing branching patterns; the $L_{hgu}$ of a mutant strain was 52% lower than a wild-type. However, it was also determined that the estimated maximum tip extension rate and average tip extension rate were reduced by 20 – 80% in the mutant strains, which may explain the lack of an increase in amylase yield for increased branching. A similar conclusion was reached by Johansen and colleagues in their study of *A.*

*awamori* [73]. A higher inoculum concentration resulted in lower values of $L_{hgu}$ and lower tip extension rate; if enzyme secretion is coupled to growth (as reported by Carlsen and colleagues in the case of $\alpha$-amylase production by *A. oryzae* [111]), this would result in less metabolite production per tip, offsetting the increase in the number of tips per mycelium.

Further evidence of metabolite secretion at hyphal tips was reported by Haack and colleagues, who observed changes in apical volume in *A. oryzae* in response to elevated production of lipase [109]. During the fed-batch phase of fermentation, during which high lipase production was evident, the ratio between the diameter of the hyphal tip and the diameter of the hypha (measured 20 $\mu$m from the apex) increased from less than 1.0 during the exponential phase to 2.5 at the end of the fed-batch phase. A cessation of cell growth and lipase production were coincident with a return to a normal diameter of hyphal tip. Changes in apical volume have also been described in *A. niger* in response to elevated production of citric acid [48].

More significantly, other studies have documented associations between the extent of mycelial branching and productivity. Jones and Lonergan proposed a link between the branching complexity (quantified as the fractal dimension) of *Pycnoporus cinnabarinus* and phenol oxidase expression [110]. Solid media was supplemented with different concentrations of Remazol Brilliant Blue R (RBBR) to induce variation in branching patterns and it was reported that higher $D$ values correlated with increasing tip and sub-apical branching. A trend was observed in $D$ values for differing RBBR concentrations, although the associated errors in the mean $D$ values were relatively large (and often overlapped), possibly due to the small number of colonies analysed at each RBBR concentration ($\geq 10$). However, variation in oxidase activity in submerged culture, in response to differing RBBR concentrations, followed similar trends to fractal dimension in solid culturing, demonstrating a positive correlation between branching complexity and oxidase enzyme expression.

A proxy indicator of branching complexity was also employed by Papagianni and colleagues, who demonstrated a dependency between citric acid titre and the length of filaments at the periphery of *A. niger* mycelial clumps, independent of the reactor used for cultivation (stirred-tank or tubular loop reactor) [112]. Decreasing the circulation time in either a tubular loop reactor (TLR) or a stirred tank reactor (STR) resulted in an increase in citric acid titre, while clump perimeter ($P1$) and the length of filaments arising from the clump core ($l$) both decreased. A correlation between hyphal diameter ($d$) and citric acid titre was also evident in the TLR, although no clear relationship was identified in the STR. Since $l$ had a direct influence on $P1$, it was therefore concluded that a single parameter, $l$, could be directly coupled to citric acid production.

A more direct link between metabolite production and hyphal tips was demonstrated by Wongwicharn and colleagues in deriving a correlation between the 'active length' of hyphae (determined by calcofluor white staining [113]) and total soluble protein concentration in chemostat cultures of *A. niger* [87]. A close relationship between the mean number of tips versus total extracellular protein was observed, while a linear dependency of total extracellular protein on mean total concentration of tips (biomass concentration $\times$ mean number of tips per organism) was found; a link between % active length and protein secretion was also derived. A similar result was derived by Amanullah and colleagues between the number of active tips of *A. oryzae* and amyloglucosidase production [84].

Other studies have suggested that morphological mutants are preferable for high levels of protein secretion. For example, Spohr and colleagues observed increased productivity in a densely-branched mutant strain of *A. oryzae* compared to a wild-type [106]. Comparison of two recombinant strains showed that the morphological mutant exhibited substantially higher $\alpha$-amylase production, possibly indicating that changes in branching behaviour influenced enzyme production; a dense

mycelium with many tips may be able to secrete protein at a higher rate than a less branched mycelium. It is possible that physiological changes may have been responsible for this increase in production, although it was concluded that based on the combination of physiological and morphological characterization presented, there did not seem to be a significant difference in the physiology of the two strains. Increased productivity in densely-branched mutant strains of *A. oryzae* (compared to a wild-type) was also recognised by te Biesebeke and colleagues [108]. The different strains were cultivated for up to 24 hours in a 1 – 2 mm layer of wheat-based solid medium (WSM) and the mutant strains exhibited an average $L_{hgu}$ 50 – 74% that of the wild type. When subsequently grown on wheat kernels (WK), the $\alpha$-amylase activities measured in the media extracts were at least 50% higher in the mutant strains compared to that of a wild-type, glucoamylase activities more than 100% higher and protease activities more than 90% higher. Increased biomass did not seem likely to be responsible for the increase in protein production, as biomass yields on WSM were similar for all strains. However, the manner in which the morphology was quantified on WSM was not made clear, the authors stating that analysis was conducted using ImageJ [114] '*according to the manufacturer's protocol*'.

However, there are other reports of a disconnect between branching complexity and metabolite production in certain processes. For example, Jayus and colleagues contended that hyphal branching frequencies had no discernible effect on productivity in fermentations of *Acremonium* sp. IMI 383068 [115]. $L_{hgu}$ fell from $93 \pm 13$ $\mu$m to $64 \pm 16$ $\mu$m as the agitation speed was increased from 100 to 200 rpm respectively, but remained approximately constant ($55 \pm 14$ $\mu$m) as agitation was increased up to 600 rpm. For the same increases in agitation speed, $(1 \rightarrow 3)$-$\beta$-glucanase yields fell substantially. However, the manner in which the morphology was quantified was not presented. Furthermore, the authors described difficulty in differentiating be-

tween mycelial branches representing 'true vegetative hyphae' and those that would eventually form conidiophores, which represents a potential source of error in the estimations of $L_{hgu}$.

Other authors have hypothesised that, in certain filamentous microbes, metabolite excretion does not occur at hyphal tips. Martin and Bushell proposed that antibiotic secretion from *Saccharopolyspora erythraea* occurred at sites a fixed distance *behind* the advancing hyphal tip, rather than from the tip itself [116]. By comparing the specific erythromycin yield from two different mycelial populations with different size distributions, it was concluded that a minimum particle diameter of 88 $\mu$m (determined by circumscribing circles around images of mycelia) was required for antibiotic production - '*particles below the critical size would grow but not produce antibiotic until they had increased in size sufficiently to include the hypothetical antibiotic secretion site*'. It was also found that particle size distributions were significantly influenced by agitation speed, with the mean diameter increasing from 70 to 124 $\mu$m when agitation was reduced from 1,500 to 750 rpm, causing an increase in specific antibiotic production rates from 0.867 to 0.913 mg $g^{-1}$ $h^{-1}$.

## 1.5 Morphological quantification of filamentous microbes

Many attempts have been made to express the product yield from an organism in a given process in terms of the morphological form adopted [8]. Of fundamental importance to the elucidation of such relationships is the ability to accurately and unambiguously quantify structural variation in microbial conformations. Early investigations involved the manual measurement of morphological features either directly using a microscope (and a graticule, for example) or indirectly by photography. Trinci studied the growth kinetics of various filamentous moulds by imaging cellophane-immobilised cultures (to restrict growth to two dimensions) in inverted

Petri dishes with a 35 mm camera and then taking manual measurements from enlarged prints [1]. Although extensive data (total hyphal length and number of tips versus time, specific growth rate, specific branching rate and mean tip extension rate) was presented on the development of *G. candidum*, *A. nidulans*, *M. hiemulis*, *P. chrysogenum* and *N. crassa*, such a procedure would be extremely laborious and time-consuming, even with modern digital cameras, meaning only a small number of mycelia could be studied (3 – 5 per organism in the case of Trinci).

### 1.5.1 Development of image processing systems for mycelial analysis

The application of image processing, defined as '*the conception, design, development and enhancement of digital imaging programmes*' [117], to the study of filamentous microbes was, until recently, limited by the available computer hardware - many 'personal computers' of the late 1980's were not equipped with the necessary capability to load into memory a single image from a modern digital camera. Image processing has clear advantages in terms of speed and lower labour intensity and imaging systems also have the potential to be automated, reducing the workload still further and permitting online analysis of samples. Digital images may also be transferred electronically to a location remote from the laboratory for analysis if required.

A typical imaging system utilised for the quantification of fungal morphology might consist of a standard bright-field microscope onto which a digital camera is mounted. Studies employing image analysis techniques often mounted video cameras on microscopes and then captured images on a PC by way of a frame-grabber [118, 119]. However, the proliferation of universal serial bus-enabled devices largely negates the need for such a set-up in the modern laboratory. Once the image has been transferred to the PC, some form of image processing application is required to extract the relevant data. There are commercially available image processing

packages that may be used for this task, but many are expensive and are not application-specific. Alternatively, open-source applications such as ImageJ [114] may be extended by way of plug-ins, permitting the user to adapt the pre-existing functionality of the application to their needs, or incorporate wholly original algorithms as is necessary. Considerations of computer specifications, such as processor speed and memory capacity, are also now largely unnecessary, as a typical desktop or laptop PC will almost certainly be equipped with the necessary functionality to run most image processing tasks.

The first attempts to represent filamentous microbes digitally were described by Metz and colleagues, who projected magnified images of mycelia onto a digitising table (graphics tablet) [3]. Touching a point on the digitiser with stylus caused the $(x, y)$ coordinates of that point to be output to an attached computer (IBM 1130), which estimated the length of a hypha by calculating the distance between this series of points (Fig. 1.6). The particle dimensions were subsequently output (punched on paper tape) by the computer and fed into an IBM mainframe (370-158) for statistical analysis. Extensive data was presented on morphological parameters such as main hyphal length ($L_{mh}$), total hyphal length ($L_{th}$) and the hyphal growth unit ($L_{hgu}$). However, the method was very time-consuming and labour-intensive, permitting the examination of a relatively small population (10 – 20 mycelial elements per sample), resulting in large errors in the estimation of parameter means in an assessment of the development of *P. chrysogenum*. Furthermore, mycelial clumps were not considered due to their complexity and measures of hyphal diameter were unreliable, due to the poor resolution of the digitiser. Nevertheless, this represented an important step toward the digital quantification of filamentous microbes.

Martin and Bushell proposed an alternative method for the quantification of hyphal fragments of *S. erythraea*, which involved circumscribing a circle around each object in an image [116]. The diameter of the circle was then interpreted as

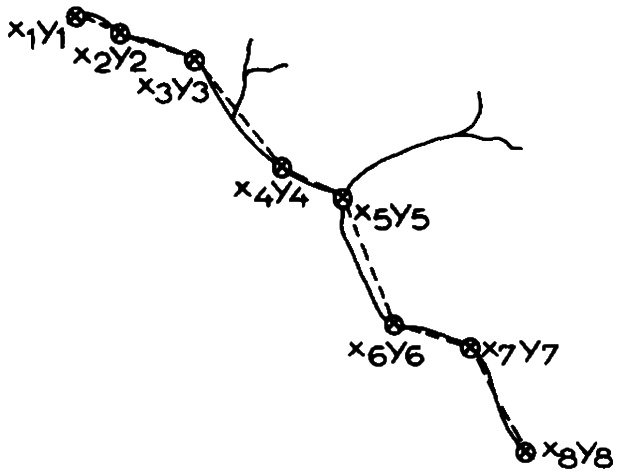


**Figure 1.6:** Calculation of hyphal length by means of a digitising table according to Metz and colleagues [3]. Reproduced with permission from John Wiley and Sons.

the 'maximum diameter' of a hyphal fragment. Stained slides were imaged with a phase-contrast microscope and the resulting photographs were examined using a stencil containing circles of various diameters; the maximum mycelial diameter was determined as the diameter of the smallest circle that completely enclosed the object. It may be possible to automate such a procedure, but fitting circles around irregular objects such as mycelia would be computationally expensive and the net benefit of the maximal diameter parameter over conventional measures such as projected area is questionable.

The first significant advance on the digitising table method was proposed by Adams and Thomas, who described a semi-automatic image processing system to derive similar measurements of hyphal filaments [120]. The performance of their image analysis system was compared to that of a digitising method, similar to that described by Metz and colleagues [3]. Manual editing of the binary images produced by the imaging system was necessary (elimination of artifacts, separation of branches from main hypha) and although the total time required to quantify a single hyphal element was substantial by modern standards (approximately 1 minute), the

digitising method was estimated to be up to five times slower. Furthermore, image processing was shown to be more accurate for the determination of hyphal lengths, as 'arcs' in the hyphae were more accurately represented and the subjectivity surrounding the location of branch-points was removed. Image processing was also far more convenient, as it obviated the requirement for photographic film development.

Packer and Thomas later described a fully-automated system that produced similar metrics, but also considered 'clumped' biomass for the first time [9]. The program (implemented on a Magiscan 2A image analyser) required the manual setting of certain application-specific parameters: a grey-level threshold for image segmentation, a circularity threshold, the specification of a 'measuring frame' to exclude truncated structures at the image boundary and a maximum length threshold for the identification of artifactual branches (caused by debris). Once these parameters were established, the system proceeded automatically to segment the input image (to produce a binary image), eliminate artifact using a circularity test and skeletonise the remaining objects. The dimensions of each hyphal element were subsequently evaluated ($L_{mh}$, $L_{th}$, $N$ and $L_{hgu}$) and the percentage of clumped material was also calculated (clumps were identified as relatively circular objects containing 'holes'). The results produced by the automated system, on the development of *Streptomyces clavuligerus* in submerged culture, were in close agreement with those produced using a manual image processing method, which involved manual editing of binarised images (filling 'false' holes, eliminating hyphal crossovers, removing debris) and manual selection of mycelia. However, the automated method was only marginally faster than the manual method. This was attributed to the time-consuming nature of the skeletonisation algorithm, but employing modern hardware should alleviate this problem. Furthermore, it was demonstrated that the percentage of biomass present in the form of clumps in a given sample was dependent on sample dilution, which tended to disperse entangled mycelia. Given this sensitivity,

it was concluded that proportion of material present in the form of clumps may not be a reliable morphological indicator, unless excessive dilution was employed and long processing times were acceptable. However, subsequent studies have utilised analysis systems that extracted similar metrics to those described above [104].

Tucker and colleagues expanded upon the work of Packer and Thomas by including measures of clump 'roughness' (circularity) and 'fullness' (ratio of projected area to convex area) [5]. The set-up (on a Leica Quantimet 570) used was similar to that described by Packer and Thomas. Following image segmentation and the production of a binary image, artifacts were removed using a combination of morphological ('opening') and size/circularity thresholds. Clumps were identified by 'ultimate skeletonisation'; successive removal of pixels until either a single point or a 'loop' (resulting from a background region enclosed within an object, characteristic of clumps) remained. In addition to projected area and perimeter (both determined by pixel counts), clumps were characterised in terms of circularity and compactness, which was measured in two ways: the ratio of pixel area to total area enclosed by the perimeter and the ratio of area to convex area ($A_c$; area enclosed by convex perimeter). Following the removal of small, 'artificial' branches, free hyphal elements were subjected to a 'shrink-back' algorithm, involving the iterative 'pruning' of mycelia to identify branch-points, to classify branches as zero-order, first-order, and so on. This permitted a more detailed examination of mycelial structures beyond the conventional hyphal growth unit. However, this additional processing resulted in a substantial increase in execution time from approximately 41 seconds per field of view (Packer and Thomas) to 67 seconds. However, subsequent studies have employed the same methodology to extract similar features to those described above [119, 121, 122].

The method of Tucker and colleagues was further improved upon by Paul and Thomas [35]. The production of a skeletonised image was performed as described

by Tucker and colleagues, with remaining artifacts removed based on an evaluation of the 'fullness' ratio ([projected area prior to skeletonisation]/[convex area]), which was typically lower for mycelia. Mycelial trees were then quantified according to $L_{th}$, $N$, $A$, branch order and length and inter-nodal distances; similar measures were applied to 'simple' clumps or loose entanglements (clumps containing only 1 – 3 'holes', resulting from hyphal crossovers). Clumps were analysed on the basis of maximum dimension, roughness, fullness ratio and area. The system was used to monitor the development of *P. chrysogenum* in submerged fermentation and it was found that a significant reduction in clump size occurred from 24 hours post-inoculation, in tandem with a reduction in the total length of and number of tips per free mycelial element. It was postulated that this may have been partly a result of hyphae being sheared off the periphery of clumps.

A more complete description of clumped morphology was proposed by Papagianni and colleagues [112]. The perimeter of mycelial clumps ($P1$) was measured by joining the tips of the filaments that arose from the core of the clump. The perimeter of the clump core ($P2$) was estimated by drawing lines around the core and measuring their length. The total length of filaments and their branches that arose from the core ($l$) were also measured, although how this was achieved was not specified. Furthermore, the high degree of entanglement at the core periphery made it impossible to distinguish between main filaments and their branches and it was therefore suggested that $l$ indicated the degree of branching. However, precisely what dimension $l$ corresponded to was not made clear. The hyphal diameter ($d$) was also determined, by joining two opposite points on the hyphal wall and estimating the distance. The image analysis method was described as automatic, although based on the description, it would appear that significant manual intervention was required.

One of the limitations associated with the systems described above is the inabil-

ity to analyse the ultra-structure of mycelial trees while simultaneously extracting information on hyphal width from the same image. This difficulty stems from the considerable difference in scale between the width of a hypha and the width of a mycelium (2 – 3 orders of magnitude). A possible solution to this problem may be the use of a motorised stage to construct a matrix of high-resolution images, such as that which was employed by Müller and colleagues to extract information on septum and nuclei positions in *A. niger* and *A. oryzae*, while also quantifying large hyphal arrangements using the same set of images [90]. Samples were stained with calcofluor white and 4',6-diamidino-2-phenylindole[12] then imaged with a $\times 100$ objective. By forming a $9 \times 9$ array with the resultant images, a sufficient resolution was obtained to simultaneously visualise sub-cellular details and ultra-structural variation, although significant user intervention was required, with distances between the apical tip, nuclei and septae all measured manually.

*Online monitoring of mycelial development*

One of the principal advantages of image processing systems is their potential use in conducting online assessment of hyphal extension, whereby images may be routinely captured and analysed automatically in tandem with development. Spohr and colleagues described such an online system [4] based on a small 'flow-through cell', consisting of a microscope slide above a Perspex base, separated by a Parafilm$^{TM}$ spacer, mounted on a microscope stage (Fig. 1.7). Liquid media was pumped through an inlet valve on one side of the cell and removed through another. By fixing fungal spores to the inside of the slide (using Poly-D-lysine) and circulating nutrient media through the cell, the growth of the organism could be monitored using phase-contrast optics.

[12]DAPI: a nucleic acid stain, which binds strongly to DNA, used in multicolour fluorescent techniques.

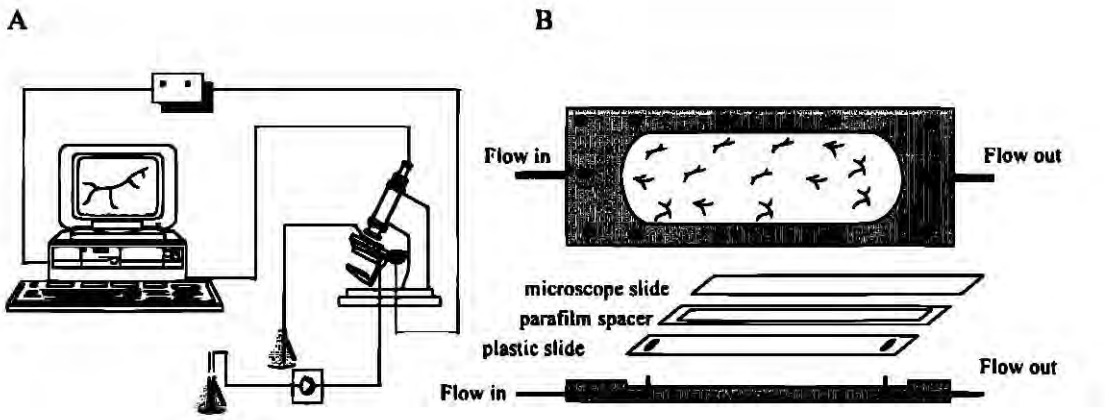


**Figure 1.7:** Schematic of the online imaging system employed by Spohr and colleagues [4]. **A.** The system consisted of an image analyser, a CCD-camera, a phase-contrast microscope and a flow-through cell mounted on the microscope, all of which were enclosed in a thermostated cupboard to ensure a constant temperature. The temperature sensor was located in the proximity of the chamber. **B.** Construction of the flow-through cell. Reproduced with permission from John Wiley and Sons.

The data produced by Spohr and colleagues on the development of *A. oryzae* mycelia was similar to that produced earlier by Trinci [1] (albeit with a greater number of data-points), permitting the calculation of the specific growth rate and branching rates. In general agreement with the work of Trinci, it was found that the extension rates of different branches within a single mycelium varied, with the extension rate postulated to be proportional to the position of the branch relative to the primary tip. Evidence was also presented for the secretion of growth-stimulating compounds by *A. oryzae*; high flow rates resulted in poor growth, which was not evident when 'recycled' media was used. In addition, Spohr and colleagues presented data on the swelling of spores; circularity remained approximately constant during the swelling process, while measures of projected area over time suggested that spore volume increased exponentially prior to germination.

The advantage of such a system is the ability to monitor the growth of individual elements, and even individual hyphae, from a single spore, up to a mycelium several

millimetres in length. However, the methodology employed by Spohr and colleagues was perhaps slightly inefficient; analysis of images was conducted post-cultivation rather than simultaneously, requiring the use of a storage device for the large number of images captured. Quantification of morphological parameters post-cultivation was necessary as user intervention was required to identify the formation of a new branch in the image sequence for each mycelium, resulting in increased processing time. Similar systems have since been used to assess the development of *Mucor circinelloides* [13, 123] and various *Mortierella* species [124, 125].

*Sub-cellular analysis*

A limited number of studies have focussed on the analysis of sub-cellular hyphal features. Paul and Thomas developed one such system, designed to quantify vacuolation and 'active' growing regions in neutral red-stained *P. chrysogenum* mycelia [35]. Their elegant routines comprised a series of grey-scale and binary morphological operations to extract vacuoles and active hyphae from an image, although some manual editing was required. The objects of interest (hyphae, vacuoles, active tips) all exhibited different grey levels and each could be segmented from the input image using different grey-level thresholds. Artifacts in the resulting binary images could generally be identified based on size and circularity. Their results showed that the percentage of vacuolated hyphae increased (and vacuoles became larger and less circular) during the course of a fed-batch fermentation. It was also shown that hyphal width increased rapidly up to approximately 30 hours post-inoculation, after which time the width of active regions declined rapidly, whereas the width of inactive regions remained relatively constant. However, the total execution time was long: 25 – 35 minutes per sample, depending on the type of sample and the level of manual editing required.

A semi-automatic method for the characterisation of vacuoles in *A. niger* hy-

phae was developed by Papagianni and colleagues [79]. Samples were imaged with a phase-contrast microscope at a magnification of ×400 and vacuoles were segmented from the image by grey-level thresholding. Artifacts could generally be removed from the resulting binary image using pre-set size and circularity filters. However, some vacuole-like artifacts could remain, but these objects could be removed by logically adding the image with a mask of the mycelium - only those objects coincident with hyphae could be considered vacuoles. It is implied that the detection of vacuoles involves some form of manual intervention, but what level of user involvement was required is not clearly specified. The vacuoles were subsequently quantified automatically in terms of perimeter, diameter, circularity and area, from which the volume of the vacuoles was estimated (assuming the hyphae to be cylindrical) and the percentage of vacuolated volume of filaments calculated.

*Use of fluorescence microscopy techniques*

Fluorescence microscopy has also proved useful for identifying 'active tips' on individual mycelia. Amanullah and colleagues used calcofluor white staining [113] to distinguish between active and non-active tips in *A. oryzae* [84]. Actively growing tips appeared intensely bright when stained (the brightness extending to 6 – 8 $\mu$m from the hyphal apex), while 'inactive' tips did not fluoresce, nor did 'artificial' tips resulting from hyphal fragmentation. However, a significant amount of manual image processing was required to quantify the active tips within a sample, with tips manually 'cut' from an image by the user. The calculation of a user-defined grey-level threshold was also required to distinguish between active and non-active tips. In addition to an increase in processing time, this introduces a degree of human error into the analysis as, for example, in the case of fluorescing tips, the point at which fluorescence was deemed to have 'terminated' may have varied. Furthermore, tips within mycelial clumps could not be observed and taken into consideration. Cal-

cofluor white staining was also employed by Wongwicharn and colleagues to identify the 'active length' of *A. niger* hyphae [87]. However, manual measurements were also required, made using a mouse to determine the main hyphal length, total branch length and number of tips. The percentage 'active length' was defined as the sum of the mean of the length between the hyphal apex and the start of the vacuolated zone divided by mean total hyphal length, which may have been a source of error.

Agger and colleagues used a double-staining method involving fluorescence microscopy to estimate the percentage of active cells in a culture of *A. oryzae* [126]. The hyphae were stained with both calcofluor white and $DiOC_6$, which stained organelles within the cells. The fraction of active cells within a hyphal element could then be determined by using separate filter blocks to view fluorescence from each stain.

### 1.5.2 Analysis of macroscopic pellets

In the analysis of macroscopic aggregates such as pellets, compromise is often required between microscopic assessment of hyphae at the pellet periphery and macroscopic examination of the pellet ultra-structure, as the pellet diameter is typically 2 – 3 orders of magnitude greater than that of hyphae. Consequently, the simultaneous observation of both micro- and macroscopic pellet morphology is often not possible; different means of image capture are often required. For example, in their study of *A. niger*, Paul and Thomas suspended pellets in a cavity slide (depth 1 mm) suitable for mounting on a microscope stage [35]. However, for larger pellets (greater than approximately 0.6 mm in diameter), a macro-viewer attached to a camera was required. Following the removal of small artifacts from binary images by opening, pellets were identified by the presence of a solid 'core', the existence of which was ascertained by ultimate erosion of the pellet to a single point (opening operations were used to remove peripheral hyphal 'loops' if necessary). Further opening oper-

ations were used to separate the core from the annular region; objects for which no core could be identified were classified as clumps. Similar means of evaluating the 'filamentous fraction' of pellets was employed by Park and colleagues, who removed the pellet annular region in binary images by repeated opening cycles until only the pellet core remained [92]. The filamentous mycelial area, $A_f$, was then calculated by subtracting the pellet core area ($A_{pc}$) from the total mycelial area ($A_m$) and the filamentous fraction expressed as $A_f/A_m$.

An alternative method for pellet analysis, proposed by O'Cleirigh and colleagues, aimed for a high-speed, high-throughput quantification of pellets of *S. hygroscopicus* [77]. Safranin-stained pellets were suspended in distilled water in a Petri dish and an image acquired using a flatbed scanner. Following noise removal and conversion to a monochrome image, a binary mask was produced using a pre-defined threshold and objects were measured according to area equivalent diameter, number of particles per ml and volume of particles per ml. Testing of the method using size calibration particles showed a high level of accuracy. However, a relatively high resolution (21 $\mu$m per pixel) was used, producing extremely large 58 Mb images (when stored in TIFF format), resulting in relatively long processing times (approximately 2.5 minutes, plus 2.6 minutes for image capture). Although this could have been reduced by converting to a monochrome image prior to processing, it is also questionable whether such a high resolution is necessary for macroscopic objects such as pellets, depending on pellet size. A similar method was employed by Bizukojc and Ledakowicz in their assessment of *A. terreus* pellets, although the dish was photographed rather than scanned and manual editing of images was required for separation of touching objects and selection of a region of interest [47].

Similar methods have been employed by other authors. For example, in their study of *Coprinopsis cinerea*, Rühl and Kües suspended shake-flask cultures in water on a large glass plate bordered by a silicon frame to contain the liquid [127].

The plate was subsequently illuminated from below and imaged with a camera and the images subjected to automated image analysis. However, the resultant data (mean grey value, area, convexity, shape factor, sphericity) was filtered to remove measurements relating to any objects, including mycelial clumps, that did not conform to a pre-determined description of a pellet. This lead to as much as 20% of objects being excluded from the results.

*Visualisation of pellet interior*

Fluorescent stains have been widely employed in the study of filamentous microbes, but their use in conjunction with image processing has been limited. Hamanaka and colleagues utilised fluorescence microscopy and image analysis to determine that lipid synthesis occurred at the edge of *M. alpina* pellets [128]. Microtomed sections of fluorescein isothiocyanate-labelled (FITC[13]) and Nile red-stained[14] pellets were imaged using fluorescence microscopy and a 'cavity ratio' estimated based on the average FITC staining intensity ($I$) across the section diameter ($D$):

$$I_{avg} = \frac{1}{D} \int_0^D f(I)\ dl \tag{1.14}$$

Their results showed that FITC staining was typically low at the pellet centre, particularly in the later stages of fermentation, indicative of a hollow core, the size of which correlated with total pellet volume. Nile red staining was also restricted to the pellet periphery, evidence that intracellular lipids were not present in the pellet core.

A similar technique was employed by Bizukojc and Ledakowicz to estimate the 'active' region in *A. terreus* pellets [47]. Methyl blue-stained[15] pellets were solidified in paraffin before cross-sectioning with a microtome. When viewed with fluorescence

[13]Binds non-specifically to cell surface proteins (fluoresces when binding occurs).

[14]Nile red stains intracellular lipid droplets

[15]Also known as 'cotton blue', stains fungal cell walls.

microscopy, the active region at the pellet periphery appeared reddish-violet, while the interior exhibited a greyish-white colour. These two regions were subsequently segmented and the volume ($V$) of active biomass in each pellet was estimated based on the radius of the whole pellet ($R$) and the radius of the inactive region ($L$):

$$V = \frac{4}{3}\pi[R^3 - (R - L)^3] \tag{1.15}$$

While these studies provide valuable information on the influence of pelleted growth on fungal physiology, the preparation of samples for microtome cross-sectioning was laborious and time-consuming and does not lend itself to high-throughput processing.

Fluorescence microscopy was also employed by El-Enshasy and colleagues to estimate the 'productive' fraction of biomass in pellets of *A. niger* [46]. Samples were heat-fixed on microscope slides before staining with acridine orange (fluoresces orange-red when bound to ribonucleic acid (RNA), indicative of active protein synthesis). When subsequently viewed under fluorescence microscopy, the 'unproductive', central region of pellets fluoresced green, whereas the productive outer region exhibited a strong red-orange colour. Images were subsequently analysed manually by drawing diameters and estimating the depth of the productive fraction and the volume of productive biomass was calculated using an expression similar to Equation (1.15). The method could be improved by using a multi-spectral segmentation routine to discriminate between the two regions and subsequent measures of projected area would provide a more accurate determination of active/non-active biomass.

### 1.5.3 Analysis of spores and germination rates

The application of image processing to the analysis of spores has received surprisingly little attention given the influence of inocula on fermentation outcomes. Many

measures of germinative potential, for example, are still performed by way of manual counts [26, 27]. However, Paul and colleagues developed a system to automatically distinguish between germinated and non-germinated spores, allowing an accurate quantification of the number of spores that had germinated within a population [129]. Image pre-processing was similar to that described above [44], the resulting binary image containing non-germinated spores, germinated spores and unwanted artifacts.

Initially, artifacts were eliminated based on size and a circularity threshold was then used to extract non-germinated spores. Germ tubes were removed from germinated spores by iterative opening - subsequent subtraction of the resultant 'germ tube spores' from the binary image produced an image consisting exclusively of germ tubes. The germ tube image was then segmented to separate any objects that may have been in contact with the germ tubes. Some of these separated objects may have been spores, which could be identified based on size and circularity - all others were removed. 'Germ-tube-like' artifacts could also be removed based on their position relative to 'germ-tube spores'.

The system did have some difficulty in separating 'chains' of spores, resulting in an underestimation in spore concentration of approximately 7%. In addition, the presence of solid particles in media resulted in a significantly reduced system performance (evaluated by comparison to manual-editing method). Perhaps an initial watershed operation to separate all 'touching' objects (including germ tubes and their parent spores), which could be subsequently classified according to size and circularity, would have been a more efficient approach.

Oh and colleagues developed a system with a similar function, although it was successfully applied to a variety of spore species with different morphological characteristics [130]. A micro-well chamber containing fungal spores in liquid medium was mounted on a microscope stage and imaged at regular intervals. The resulting

images were automatically analysed to determine whether spores had germinated or not. Following manual image capture, images were subjected to edge enhancement (Laplacian operator) followed by noise suppression (median filtering) and artifact removal (using an area threshold). From a binary image, the object boundary was sampled and low-pass filtered in Fourier space[16] to produce a smooth representation of the shape contours. The contour $C$ was parameterised by the arc length $t$ and expressed in terms of $x(t)$ and $y(t)$. The curvature ($K$) of a function $y(x)$ was then calculated as follows:

$$K = \frac{d^2y}{dx^2}\left(1 + \frac{dy}{dx}\right)^{-\frac{3}{2}} \tag{1.16}$$

The contour could thus be reduced to a set of shape 'primitives' based on local values of $K$; rapidly changing convex curves (characteristic of hyphal tips), slowly changing convex curves (characteristic of spores), concave curves (where a spore 'meets' a germ tube) and straight lines. Such a methodology is highly flexible and can be adapted to spores of different morphological characteristics. Counts of germinated spores compared well with those obtained manually except for high spore concentrations, when system performance deteriorated due to the overlapping of germ tubes. However, the minimum inhibitory concentrations of amphotericin B necessary for complete inhibition of germ tube formation were determined for *Aspergillus fumigatus*, *Curvularia lunata* and *Fusarium solani*. While the processing time of approximately one minute per well could undoubtedly be improved upon with modern hardware, the high level of accuracy obtained in this study suggests that the system represents a potentially powerful laboratory diagnostic tool, particularly if used in conjunction with automated image capture.

[16] A frequency-domain representation of a function $f(x)$ can be obtained using the Fourier Transform ($F(\omega)$)

### 1.5.4 Other applications of image processing to the study of filamentous microbes

*Colorimetric assay quantification*

Other studies have aimed to quantify metabolic activity directly using image processing. Jones and colleagues used image analysis to evaluate dye bio-transformation by white rot fungi [131]. Agar was supplemented with Remazol Brilliant Blue R (RBBR) and inoculated centrally with either *P. cinnabarinus* or *Phanerochaete chrysosporium*, then imaged every 24 hours for 7 days. By calculating the area ($A$) of dye remaining in a given image captured at time $t$, the specific enzyme diffusion or activity coefficient ($\nu$) was calculated as:

$$\nu = \frac{\ln A - \ln A_T}{t} \tag{1.17}$$

were $A_T$ was the total dye area at $t = 0$. An alternative method analysed dye biotransformation by identifying the shift in the mean peak of the image histogram (with respect to an uninoculated control plate). Results showed that *P. cinnabarinus* converted the chromophores of RBBR more rapidly than *P. chrysosporium*.

Olsson described a colorimetric method for measuring concentrations of glucose and phosphorus in agar medium supporting growth of *F. oxysporum* colonies [40]. Colonies were cultivated on cellophane-covered agar for seven days before removal and development of the agar with Sandell's solution or molybdate to show the presence of glucose or phosphate respectively. Subsequent imaging (by illumination with a light-box) and analysis revealed steep phosphate and glucose gradients at colony edges, while the concentration of both nutrients was virtually zero at the colony centre; the profiles were virtually identical regardless of the carbon to phosphate ratio present in the media. Correlations between mean pixel intensity ($I$) in images of colonies and dry cell weight ($X$) were also derived using transmitted ($I = e^{aX}$)

and reflected ($I = aX$) light measurements and it was demonstrated that biomass distribution within the colony was affected by glucose concentration.

*Use of in situ probes*

*In situ* probes have proved successful for the monitoring of certain processes. Wei and colleagues developed an *in situ* dark-field microscopy probe (IDMP) for the monitoring of cell cultures [132]. The probe consisted of an illumination unit at the bottom and a CCD camera at the top of a single, partially-submerged tube. Just above the illumination unit (which consisted of a light-emitting diode, a collimating lens and a condenser), separated by a window, was an opening in the tube allowing the culture to enter a sampling region, just above which was positioned a $\times 10$ objective lens behind a second window. In the analysis of cultures of *Saccharomyces cerevisiae*, results provided by the IDMP and imaging system, based on training set data, were in close agreement with manual counts for both total cell density and cell viability. However, it is unlikely that such a system could be easily adapted for the study of filamentous microbes. Unicellular organisms are approximately ellipsoidal and are presented as simple, regular shapes in a single focal plane; subsequent detection may be achieved using techniques such as the Hough Transform [133], ellipse detection [134], or some variant thereof. However, the morphology of filamentous microbes in a submerged suspension is significantly more complex, the capture of which within a single focal plane would be challenging.

## 1.6 Conclusions

Filamentous microbes are industrially important organisms used to produce a wide range of compounds for a variety of applications. While solid-state fermentations involving such micro-organisms have been conducted by humans for perhaps thou-

sands of years, submerged culturing became the dominant industrial format over the course of the 20$^{th}$ century, primarily due to reduced space requirements, but also the greater ease with which such processes may be controlled. However, productivity may be significantly influenced, both directly and indirectly, by the complex, three-dimensional phenotypes that are manifest in submerged culture, the specific form of which is a result of a variety of factors. The advent of the digital era provided the necessary tools for researchers to develop image processing systems to quantify these elaborate conformations, but fully-automated systems are still rare and many studies still rely on qualitative morphological descriptions.

## 1.7 Aims of this study

- The principal aim of this study was the design of an automated image analysis system for the rapid and accurate characterisation of fungal morphology.
- In parallel with this, it was required that a means of sampling fungal cultures be developed that would present the organism in an essentially two-dimensional format for imaging purposes, whilst preserving the fragile fungal architecture.
- Finally, this system was to be applied to the study of a model organism, *A. oryzae*, and relationships between micro-morphology, macro-morphology and metabolite production investigated.

### 1.7.1 Thesis overview

**Chapter 2** provides details on the most commonly used protocols and techniques used throughout the study.

**Chapter 3** describes the development of an integrated application, based on the ImageJ platform, that may be used as a means of automatically analysing a

two-dimensional representation of filamentous fungal micro- or macro-morphology, generating data on populations of spores, mycelia or pellets. In the design of this system, speed-of-execution was prioritised to provide a system capable of near-real-time analysis.

**Chapter 4** describes the investigation of a two-dimensional growth assay by immobilising fungal spores on cellulose nitrate membranes, using *A. oryzae* as the model organism. The suitability of the assay for producing samples appropriate for the image analysis system developed in Chapter 3 was examined. Efforts to optimise the assay were undertaken, concentrating specifically on minimising processing time.

In **Chapter 5** the kinetic development of *A. oryzae* on a solid substrate was analysed using the systems described in chapters 3 and 4 to establish the basic kinetic parameters for this system and investigate whether a change in media composition results in a change in any of these kinetic parameters.

In **Chapter 6**, morphology and $\alpha$-amylase production in shake-flask cultures of *A. oryzae* was characterised. Attempts were then made to perturb the system, through variation in inoculum concentration, carbon source type and concentration and surfactant supplementation. Resultant changes in macro-morphology were quantified and related to concomitant changes in amylase production. Attempts were made to derive simple correlations between pellet size and $\alpha$-amylase yield.

**Chapter 7** describes an alternative means of quantifying the branching behaviour of filamentous microorganisms using fractal geometry. The fractal dimension of different populations of mycelia was related to the conventional hyphal growth unit and the potential for future use of fractal geometry in the analysis of fungi is discussed.

**Chapter 8** outlines the overall conclusions derived from this study and discusses the relevance of the results with regard to the literature. Potential future investigations are also considered.

# Chapter 2

# General Materials & Methods

## 2.1 Preparation of spore inoculum

Conidial suspensions were prepared in one of two ways. In the first method, standardised *Aspergillus oryzae* (ATTC 12891) conidial suspensions were prepared from malt agar (Lab M LAB037) slant cultures (after incubation for 7 days at 25°C) by the addition of 5 ml phosphate-buffered saline (PBS) containing Tween 80 (0.1% v/v; PBS-Tween-80). The cultures were briefly vortexed and the suspensions recovered by aspiration with a Pasteur pipette. Conidium concentration and the absence of hyphal elements were assessed using a Neubauer chamber, and the conidia were subsequently pelleted by centrifugation at 3,000 rpm for 30 min at 4°C. The pellet was then re-suspended in PBS-Tween-80 and glycerol (20% v/v, final concentration) to yield $1 \times 10^6$ spores $ml^{-1}$ and stored at $-20$°C.

The second method is similar to that described by O'Cleirigh and colleagues [77]. *A. oryzae* was grown on malt agar in 250 ml Erlenmeyer flasks for 7 days at 25°C. A spore suspension was prepared by washing the surface of the culture with 25 ml (PBS-Tween-80) containing approximately 3 g glass beads (BDH) and agitating at 120 rpm, 25°C for 30 minutes. The suspension was filtered through sterile glass wool to remove hyphae and the conidia were subsequently pelleted by centrifugation at

3,000 rpm for 20 minutes at 4°C. Conidium concentration was standardized using a Neubauer chamber to yield a stock concentration of $1.8 \times 10^8$ spores $ml^{-1}$ and aliquots were stored in glycerol (20% v/v) at −20°C.

### 2.1.1 Assessment of spore viability

The viability of spores after freezing was determined using the pour plate method [135]. Vials containing spore suspension were thawed from frozen at 37°C and serially diluted with sterile PBS-Tween-80 to yield suspensions of approximately $5 \times 10^3$, $1 \times 10^3$ and $1 \times 10^2$ spores $ml^{-1}$. An aliquot (1 ml) of each spore concentration was transferred to the centre of a separate sterile Petri dish and immersed in approximately 25 ml of molten malt agar (40°C). Each spore concentration was plated in triplicate. The dish was gently swirled to disperse the spores and allowed to cool at room temperature for 1 hour. Once the agar had set, the dishes were incubated at 25°C for approximately 36 hours and any visible colonies were manually counted. The percentage mean spore viability ($v$) was calculated according to:

$$v = \frac{100}{C} \sum \frac{c_i}{3d_i} \tag{2.1}$$

where $C$ is the nominal spore concentration in the frozen stock, $c_i$ is the mean colony count for each plated spore concentration and $d_i$ is the corresponding dilution factor for that concentration (1/10, 1/100, etc.). The resultant values are referred to in individual experiments.

## 2.2 Preparation of buffers

Phosphate-buffered saline was routinely prepared by dissolving one tablet (Oxoid Dulbecco 'A' BR0014) in 100 ml of distilled water. Where specified, Tween-80 was added at a concentration of 0.1% (v/v). All conidium dilutions used in the

experiments described were performed in sterile PBS-Tween-80.

## 2.3 Basal medium for microorganism cultivation

The basal medium used for both submerged and solid state fermentation of *A. oryzae* was a modification of that described by Amanullah and colleagues [122]: Citric Acid, 2.0 g $L^{-1}$; $MgSO_4.7H_2O$, 2.0 g $L^{-1}$; $KH_2PO_4$, 2.0 g $L^{-1}$; $(NH_4)_2SO_4$, 3.0 g $L^{-1}$; $CaCl_2.2H_2O$, 1.1 g $L^{-1}$; $K_2SO_4$, 2.0 g $L^{-1}$. A trace metal solution was added (0.5 ml/L), consisting of: Citric acid, 3.0 g $L^{-1}$; $ZnSO_4.7H_2O$, 0.5 g $L^{-1}$; $FeSO_4.7H_2O$, 0.5 g $L^{-1}$; $CuSO_4$, 0.25 g $L^{-1}$; $MnSO_4.H_2O$, 0.28 g $L^{-1}$; $NiCl_2.6H_2O$, 0.09 g $L^{-1}$. Media pH was adjusted using either 2 M HCl or NaOH as required using an electronic pH metre (Hanna Instruments 8519 or pH210) calibrated against standard buffer solutions (AVB Titrinorm 32044.268 & 32045.262). All media were sterilised by autoclaving at 121°C and 1 atm for 15 minutes.

## 2.4 Optimised protocol for membrane immobilisation of culture and subsequent visualisation

### 2.4.1 Cell immobilisation and solid-state cultivation

The basic conidiospore immobilisation procedure consisted of filtering a suspension (25 mL of approximately 400 spores $ml^{-1}$) through a cellulose nitrate membrane (Sartorius Stedim 11306-47-ACN, Millipore HAWG 047 SO or Pall 66278) using a membrane filtration device (Millipore) connected to a vacuum pump. A spore concentration of this magnitude was found by trial-and-error to be optimum in preventing over-crowding of mycelium on the membrane upon germination, while suspension volumes in excess of 20 ml were adequate to ensure a uniform spore coverage of the membrane. After washing with PBS-Tween-80 (for removal of any

wall-adherent cells) and sterile water (removal of excess PBS-Tween-80), the membrane was overlaid evenly on to the surface of malt agar and incubated at 25°C.

### 2.4.2 Processing of culture for image analysis

In the optimised procedure derived from the experiments described in subsequent chapters, the membrane was removed from the agar after a suitable period of time and replaced in a filtration device where it was exposed to fixative solution (phenol 20% w/v, glycerol 40% v/v, lactic acid 20% v/v in distilled water) for 5 minutes. Following washing with PBS-Tween-80 and then water, the membrane was placed in a Petri dish and dried at 65°C (75 min). After staining with lacto-phenol cotton blue, the membrane was rinsed with PBS-Tween-80 (5 min) and distilled water, followed by cutting and mounting on a microscope slide and drying at 65°C (75 min). The membrane was rendered transparent and suitable for imaging by treatment with microscopy immersion oil (Olympus AX 9602).

### 2.4.3 Microscopic visualisation of submerged culture

Samples (1 ml) were taken from shake-flasks and added to approximately 25 ml PBS-Tween-80 before filtering through a cellulose nitrate membrane using a filtration device. The membrane was then fixed, stained and dried as described above.

For fluorescence microscopy, samples were diluted approximately as necessary with PBS-Tween-80. The diluted sample (1 ml) was added to 4 ml of calcofluor white (0.01% w/v; Sigma F3543) and incubated at room temperature for 10 minutes, before filtration through a cellulose nitrate membrane and drying at 65°C (75 minutes).

## 2.5 Microscopy and image capture

Light microscopy was performed with a Leica DMLS2 microscope, with the condenser and aperture fully opened and maximum illumination. The microscope is fitted with a ×10 eyepiece lens, four standard objective lenses (×4, ×10, ×20 and ×40) and a single oil-immersion objective (×100). All lenses, filters and light-sources were cleaned thoroughly with lens tissue prior to use. Standard glass microscope slides were used in all experiments.

All images were captured using a Canon Powershot S50 camera attached directly to the microscope. The camera could be controlled remotely from a PC using Canon's *RemoteCapture* utility. The camera lens was cleaned with lens tissue prior to use. Images were stored in JPEG format with minimal image compression. The image resolution used is referred to in individual experiments.

Inter-pixel distances were calibrated by imaging a stage graticule, from which a standard scale factor (0.138 $\mu$m pixel$^{-1}$ for 2592 × 1944 image captured at ×400) was calculated that was subsequently used in all experiments.

Images of fluorescent samples were captured with a Canon PowerShot S50 digital camera attached to a fluorescence microscope (Leitz Laborlux S) fitted with an epifluorescence illuminator (307-148.002 514687, Leitz Wetzlar). Images were captured at ×100 magnification.

### 2.5.1 Visualisation of fungal macro-morphology

Fungal macro-morphology was visualised using a method similar to that described by O'Cleirigh and colleagues [77]. Samples (approximately 10 ml) were decanted from shake flasks and centrifuged at 1,000 rpm, 4°C for 35 minutes. Supernatant was removed and the biomass was immersed in lactophenol cotton blue with gentle agitation to ensure stain uptake. Distilled water was added to a volume of 30 ml and

the contents gently agitated before being subjected to centrifugation (1,000 rpm, 4°C for 20 minutes). The supernatant was replaced with distilled water before further centrifugation. This process was repeated until excess stain was removed and the supernatant became clear. The stained biomass was then transferred to a Petri dish and diluted to yield a coverage of approximately 1 $cm^2$ biomass per 20 $cm^2$. The contents of the Petri dish were then scanned with a Hewlett Packard Scanjet G4010 flatbed scanner, with the images stored as 24-bit bitmaps (300 dpi).

# Chapter 3

# Development of an Automated Image Analysis System for the Morphological Quantification of Filamentous Microbes

## 3.1 Introduction

The need to precisely quantify morphological variation in mycelial structures as a means of control in industrial fermentations has led to the deployment of computer-aided image processing as a tool for the study of microbial culture systems [136]. The detailed assessment of limited numbers of hyphal elements in both submerged [4] and solid state systems [118, 137] has contributed much to the understanding of apical growth mechanisms, while the derivation of average data from the monitoring of large cell populations [45, 106] is aimed at process optimization within bioreactor systems. Early progress in the development of automated routines [5] led Thomas and Paul to declare in 1996 that '*it is probable that fully automated image analysis will soon be used to gather the large amounts of data needed for both model extension and verification*' [138]. However, many studies of morphology still rely on significant manual intervention [10, 87, 123, 139, 140], which increases execution time and reduces throughput. There is therefore a pressing need for further development of

automated image analysis systems for application in this field.

### 3.1.1 Basic concepts of digital image processing

The application of image analysis permits the translation of readily recognisable qualitative traits into actionable, quantitative data (Fig. 3.1). The derivation of accurate data is dependent on the capture of representative images, as the integrity of the results will be compromised by low-quality input. The input process commences when the projection of a three-dimensional object is captured on a charge-coupled device (CCD) array, such as that contained within a digital camera or a flat-bed scanner, and is subsequently digitised. This digitisation causes the original two-dimensional, continuous, analogue representation of the image to be quantised at each point on the array, resulting in a digital representation of the field of view. The resolution (the number of pixels) of the resultant image is dependent on the size of the array on which the image was captured. Quantisation is generally performed uniformly, whereby the intensity at some point $(x, y)$ within the image is linearly translated to some integer value between 0 and $2^M$, where $M$ is referred to as the bit depth of the resulting digital image. In most applications (and in most images used in this thesis) $M = 8$, so each pixel is represented by an intensity value between 0 and 255 (Fig. 3.2). Colour images generally have a bit-depth of 24, 8 bits for each colour component, red, green and blue.

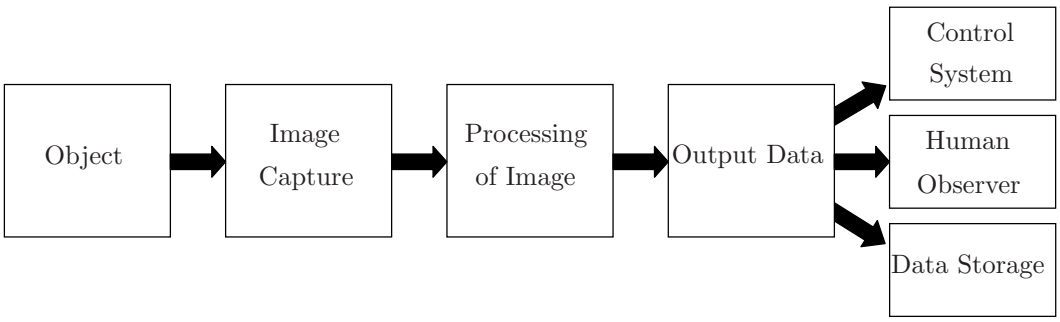


**Figure 3.1:** Schematic representation of a typical image analysis system.

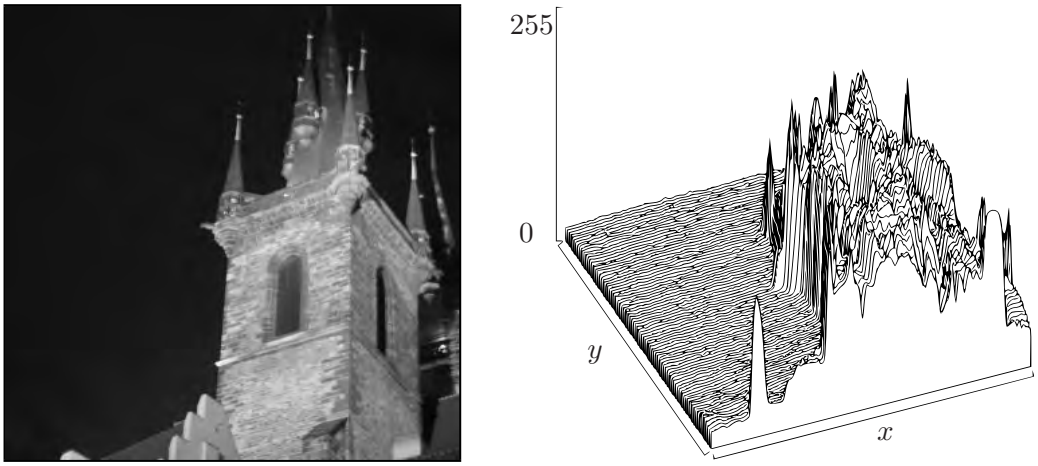


**Figure 3.2:** Quantisation of intensity levels. Each $(x, y)$ coordinate in the image has an associated integer value between 0 and 255.

Following image capture and digitisation, there are various forms of low- and high-level processing that may be performed. Roerdink categorised these as image pre-processing, segmentation, object description and finally, interpretation [141]. Pre-processing is based on the premise that the image contains both an object of interest and an added unwanted noise component, which may, for example, result from electrical disturbances in the CCD on which the image was captured. Other unwanted features that may require correction include non-uniform image background, poor image contrast or blurring. Once the image has been optimised, attempts are made to group together regions within the image based on some property, such as the intensity of the pixels. Image segmentation typically aims to separate objects of interest from the image background, but more generally, it is a means of identifying different regions. Common forms of segmentation are grey-level thresholding and edge detection and the result of segmentation is often the output of a binary image (Fig. 3.3). Description then seeks to characterise the different regions identified by the segmentation stage using various properties: projected area, perimeter length, centre of mass, bounding rectangle, Feret's diameter, and radius of gyration, among

**Figure 3.3:** Binary image of Figure 3.2, in which only two grey levels are present.

others. Finally, it may be required that the various region descriptions be interpreted in some way, so as to, for example, eliminate a particular region from further analysis, or, to assign a particular classification to a region.

### 3.1.2 Morphological classification of filamentous microbes

A wide variety of parameters have been utilised in the study of microbial spores, hyphal elements, aggregates and pellets [142], although many are derived from simple measures such as projected area ($A_p$) or perimeter length ($P$). Means of identification of different structures have also received considerable attention and some of the different techniques utilised are outlined here.

*Analysis of spores*

Typical measures utilised in the analysis of spores include projected area and circularity ($C$), particularly in cases where the spores in question are approximately spherical [4]. Teliospores and pycniospores of certain *Puccinia* species are approximately ellipsoidal and have been quantified in terms of their major and minor axes [12]. Other studies have utilised Fourier descriptors for more complex spore

morphologies that cannot easily be described in terms of ellipsoids or spheres [143].

Investigations into the influences on rates of spore germination have often relied on manual observation and counting to determine the percentage of germinated spores within a population [26, 27]. However, the use of a simple parameter such as circularity can prove useful in differentiating between germinated and non-germinated spores, as was demonstrated by Paul and colleagues [129]. The germinated spores were subsequently subjected to morphological filtering to separate the germ tube from the parent spore for analysis of each structure. An automated method was also developed by Jones and colleagues, although the intended use was enumeration of spores in a haemocytometer for inoculum standardisation, rather than morphological quantification [144].

*Enumeration and analysis of hyphae*

While the study of hyphal development has taken on several different forms, the challenges associated with the quantification of these structures may be resolved into three general approaches: high-magnification assessment of individual hyphae, quantification of mycelial 'trees' or free mycelial elements and the identification and subsequent analysis of mycelial aggregates. Determination of measures such as the hyphal growth unit ($L_{hgu}$; ratio of total hyphal length to number of hyphal tips) and hyphal width is generally not possible from the same image given the differences in scale[1] and capture of images at different magnifications is typically required for this purpose [109, 145].

At the high-magnification level, Bartnicki-García and colleagues used computer enhanced video-microscopy to map the trajectory of cell surface markers in growing hyphae of *Rhizoctonia solani* to determine the pattern of cell wall expansion during apical growth [118]. McIntyre and colleagues estimated lengths of apical compart-

[1]Generally 2 – 3 orders of magnitude between hyphal width and mycelial width

ments in hyphae by determining the distance between the apex and first septum (apical compartment) and between subsequent septa of each hyphal element [146]. Other studies have yielded information on sub-cellular hyphal details. For example, Pollack and colleagues measured the percentage of vacuolated area as the total vacuole size per total mycelium size [147]. Vacuolation was also used to differentiate between active and non-active hyphal regions of *A. niger*, permitting estimations of the percentage of active biomass [87, 148].

Numerous studies of mycelial architectures have been reported, but one of the earlier systems was developed by Packer and Thomas, which permitted the determination of total hyphal length, main hyphal length (by determination of the longest connected path), hyphal branch length and hyphal growth unit in mycelial 'trees' [9]. An estimation of the percentage of biomass occurring in clumped form was also included. This system was later enhanced to include a novel means of first identifying, then characterising, clump morphology in terms of projected area, circularity and convex perimeter ($P_c$; Fig. 3.4) [5]. Similar approaches to the quantification of mycelial trees and clumps have been employed in several other studies [104, 119, 121, 122]. Lecault and colleagues proposed an intermediate classification between free elements and clumps, termed an entangled mycelium, identified based on the number of 'holes' in the structure [10]. They also produced more extensive data on dispersed growth forms, including the mean, minimum and maximum branch lengths, as well as the mean, minimum, and maximum inter-nodal distances and the number of inter-nodal units. The branching order was determined by calculating the number of iterations required to subtract all of the end points, similar to the method described by Tucker and colleagues [5]. Other studies have adopted a more general approach, measuring all biomass present in terms of projected area, as constant hyphal width implies area is proportional to biomass, so specific biomass fractions can be derived [91, 119, 149, 150].

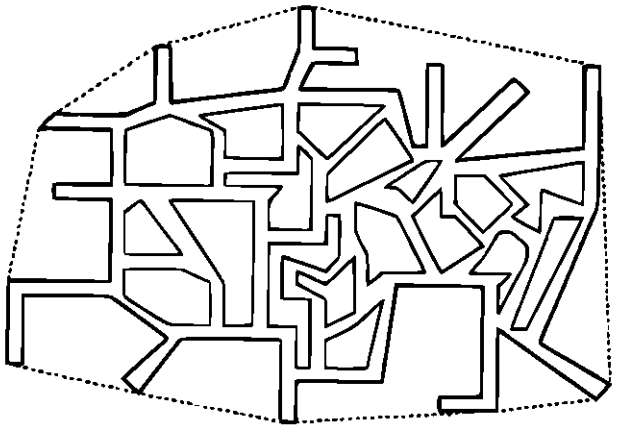

**Figure 3.4:** A mycelial clump, as illustrated by Tucker and colleagues, with the convex perimeter ($P_c$) indicated by the dotted line [5]. Reproduced with permission from John Wiley and Sons.

*Classification of dense aggregates and pellets*

Conventional measures of dense, pellet-like aggregates (Table 3.1) include projected area, equivalent diameter ($D_p$), circularity, perimeter, projected convex area (area including holes; $A_c$) and convex perimeter [136]. Various other metrics have been employed, which generally involve some combination of the above, such as 'roughness' [151], 'compactness' [50, 107, 152] and 'convexity' [48, 49]. Lucatero and colleagues used a combination of shape factors to distinguish between free hyphae, clumps and pellets [102]. Objects exhibiting a mean diameter of less than 0.3 mm were considered dispersed mycelia. Clumps were considered to be particles larger than 0.3 mm and of compactness (estimation of density) lower than 0.99, while pellets were defined as particles having a compactness between 0.99 – 1 and roundness (deviation from a circle) less than 6. Similarly, a clump was defined by Müller and colleagues as a structure with $D_p > 40$ $\mu$m and $A_p/A_c > 0.55$ [107].

The mean grey-level intensity of regions has been utilised as an effective means of discriminating between dense aggregates, such as pellets, and less compact structures, such as mycelial aggregates or clumps [49, 76]. Similarly, a difference in grey

**Table 3.1:** Some commonly used parameters in the morphological description of mycelial aggregates and pellets.

| Parameter | Definition | Description |
|---|---|---|
| Projected Area | $A_p$ | Number of pixels representing an object. |
| Equivalent Diameter | $D_p = 2\sqrt{A_p/\pi}$ | Diameter of a circle with area equivalent to $A_p$. |
| Perimeter | $P$ | The pixel length of an object boundary. |
| Circularity | $C = (4\pi A_p)/P^2$ | A measure of deviation from a circle. |
| Roughness | $R = P^2/A_p$ | |
| Projected Convex Area | $A_c$ | Number of pixels representing an object, including any enclosed 'holes'. |
| Convex Perimeter | $P_c$ | Perimeter of an object with all concavities filled (Fig. 3.4). |
| Compactness | $M = A_p/A_c$ | |
| Convexity | $E = P/P_c$ | |

levels between pellet core and periphery has been employed to distinguish between the two regions and derive separate measures of each [153, 154]. Subsequent quantification of the pellet cores is thus possible, based on, for example, the ratio of the minimum Feret's diameter to the maximum [50, 52]. Others have operated on binary images with morphological filters to 'erode' the annular region in both pellets [92, 93] and clumps [155], producing binary representations of aggregate cores. For example, Rodríguez-Porcel and colleagues expressed pellet morphology as a ratio between the filamentous area and the total pellet area [51], while Papagianni and Moo-Young included measures of the average length of the filaments that protruded from the core of clumps in their characterisation of *A. niger* [49].

*Other macroscopic analyses*

Macroscopic and low-magnification microscopic analysis of mycelial growth on solid substrates has generally been restricted to measures of hyphal coverage or projected area of biomass [156, 157]. However, a significantly more detailed system was developed by Dörge and colleagues for the identification of different species of *Penicillium*, based on colony colour distribution, colony dimensions and texture measurements [158]. Image processing was also utilised in the evaluation of dye biotransformation by the white rot fungi *Pycnoporus cinnabarinus* and *Phanerochaete chrysosporium* [131].

### 3.1.3 Development platform

ImageJ is a public domain, Java image processing program designed with an open architecture that provides extensibility via Java plug-ins [114]. It comes pre-equipped with many standard image processing capabilities, such as image segmentation (thresholding, edge detection), various linear and non-linear filter implementations, frequency-domain operations and limited object classification and measurement. The ImageJ platform has previously been utilised in the study of filamentous microorganisms [108, 140, 159].

### 3.1.4 Aims of the work in this chapter

Extensive work on the classification of filamentous microbial morphology using digital image processing is evident in the literature, but fully automated systems are still rare. A wide range of approaches have been adopted during the course of these studies, but many studies have been specific to the analysis of one particular growth form or used a limited number of morphological parameters.

The aim of this chapter was to develop an integrated application, based on

the ImageJ platform, that may be used as a means of quantifying any form of filamentous fungal morphology. The programme would proceed automatically and generate data on the population of spores, mycelia or pellets analysed and output this data to the user. In the design of this system, speed-of-execution was prioritised to provide a system capable of near-real-time analysis.

The design drew on many established methods in digital image analysis, for image pre-processing in particular, which were deemed suitable for this application. A survey of some popular pre-processing techniques was conducted and the most appropriate for this application selected. The morphological parameters incorporated into the design were based largely on the review of the literature. However, a more extensive quantification of hyphal elements in particular was targeted, so as to permit the compilation of data beyond the conventional hyphal growth unit and provide more detailed information on the branching strategies of filamentous micro-organisms.

## 3.2 Materials & methods

Mycelial samples were produced by culturing membrane-immobilised *A. oryzae* on malt agar and processing as described in Section 2.4. Microscopic images were subsequently acquired as described in Section 2.5. Pellet samples were obtained by submerged culturing of *A. oryzae* in basal medium (BM; see Section 2.3) supplemented with 1.0% (w/v) soluble starch (Sigma S-9765, Lot 93H0243 or Difco 0178-17-7, Lot FJ0041XA) and adjusted to pH 6.0. Erlenmeyer flasks (250 mL), with a working volume of 20%, were incubated in a Lh Fermentation Mk X Incubator Shaker at 30°C and 200 rpm. Inoculum consisted of 500 $\mu$L of $1 \times 10^7$ spores ml$^{-1}$. Images of pellet macro-morphology were acquired according to the method described in Section 2.5.1.

## 3.3 System development I: Image pre-processing

Described in this section are the approaches considered for noise removal, image segmentation and binary image pre-processing, most of which were pre-existing within ImageJ. As one of the initial aims in designing the system was minimisation of execution time, speed of execution was prioritised when selecting a method for each pre-processing stage.

### 3.3.1 Low-frequency noise removal

The first stage in any image processing algorithm generally involves an attempt to minimise any unwanted noise or distortion present in a given image. Low-frequency noise is typically characterised by a gradient across the image plane, resulting from, for example, non-uniform illumination. Removing this gradient results in a more homogeneous background, which is preferable for image segmentation (see below), and may be accomplished in a variety of ways.

*Mean filtering and background subtraction*

A mean filter is a form of smoothing filter that can be used to suppress high-frequencies in an image. A simple example of a mean filter kernel is as follows:

$$G_{n,n} = \frac{1}{n^2} \begin{bmatrix} 1 & 1 & \cdots & 1 \\ 1 & 1 & \cdots & 1 \\ \vdots & \vdots & \ddots & \vdots \\ 1 & 1 & \cdots & 1 \end{bmatrix} \tag{3.1}$$

where $G_{n,n}$ is a square matrix and $(n-1)/2$ is the filter radius. If $G$ is convolved with an image ($I$), each pixel in the output image ($J$) is therefore defined as:

$$J(x,y) = \frac{1}{n^2} \sum_{j=-m}^{m} \sum_{i=-m}^{m} I(x+i, y+j) \tag{3.2}$$

where $2m = n-1$. By forming a duplicate of the image to be filtered and smoothing over a sufficiently large radius, all details (high frequencies) in the image are suppressed and an approximation of the image background results. This 'background image' may then be subtracted from the original, leaving the object(s) of interest intact against a uniform background. However, convolution with a smoothing filter with a large kernel is computationally expensive, with the processing time being proportional to $n^2 \times$ image area.

*Frequency-domain filtering*

Noise removal may also be effected by filtering in the frequency domain rather than using spatial filtering. The Fourier transform of an image is computed, the result convolved with the desired filter and the inverse-Fourier transform calculated, resulting in the original image with noise removed. However, this approach is also very time-consuming, particularly for large images.

*Rolling ball background subtraction*

This approach to background removal may be conceptualised as follows. If the image to be filtered is considered to be three-dimensional, the third dimension being the luminous intensity at each pixel, the image will resemble a surface with depressions (Fig. 3.5). If the filter kernel is considered to be a ball of radius $r$ that traverses this surface, the background is defined as any part of the surface that contacts the ball. The objects within the image, represented by 'holes' in the surface plot, will be unaffected if $r$ is sufficiently large. The ImageJ implementation is based on Sternberg's rolling ball algorithm [160] and, as it is far less time-consuming than

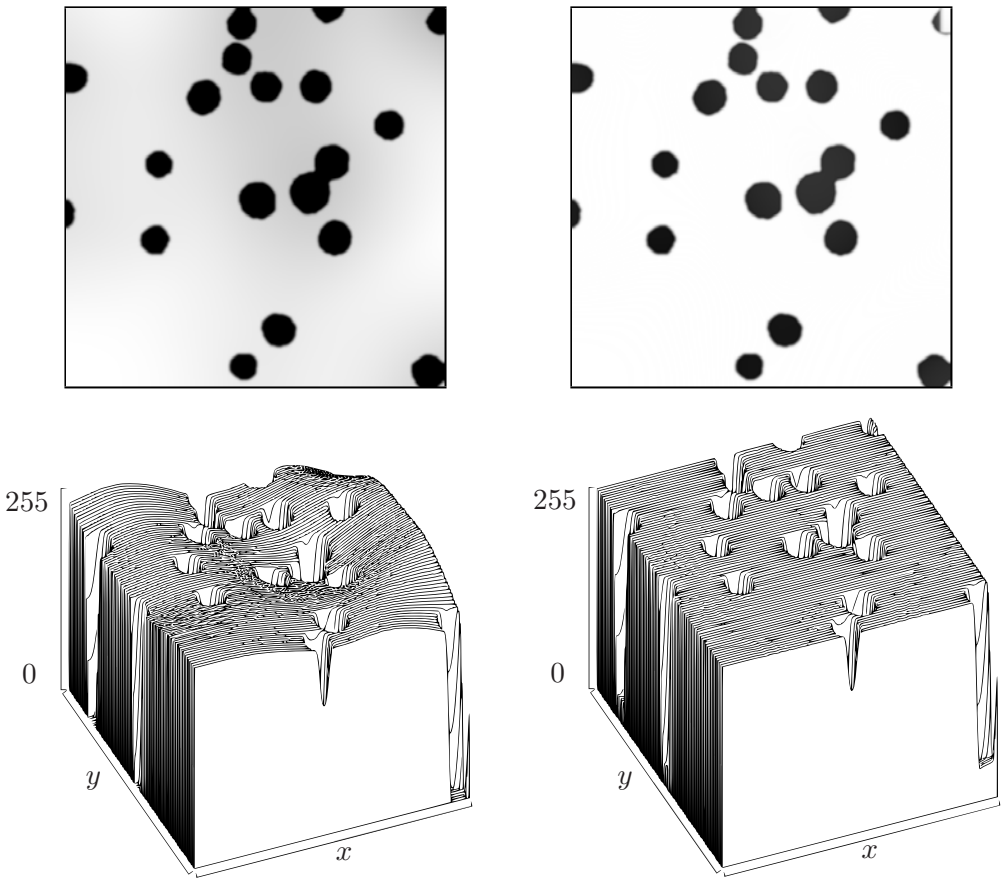


**Figure 3.5:** Surface plots of an image, before (left) and after (right) background subtraction, showing objects as depressions in the surface.

smoothing or frequency-domain filtering, was selected as the preferred means of background removal.

### 3.3.2 High-frequency noise removal

High-frequency 'speckle' noise can result from, for example, electrical noise in the CCD array on which the image was captured and is characterised by individual pixels within an image that are noticeably different in intensity from their immediate neighbours, resulting in a 'granular' appearance (Fig. 3.6a). A common approach to alleviating this problem is median filtering, a form of 'rank filtering', so called

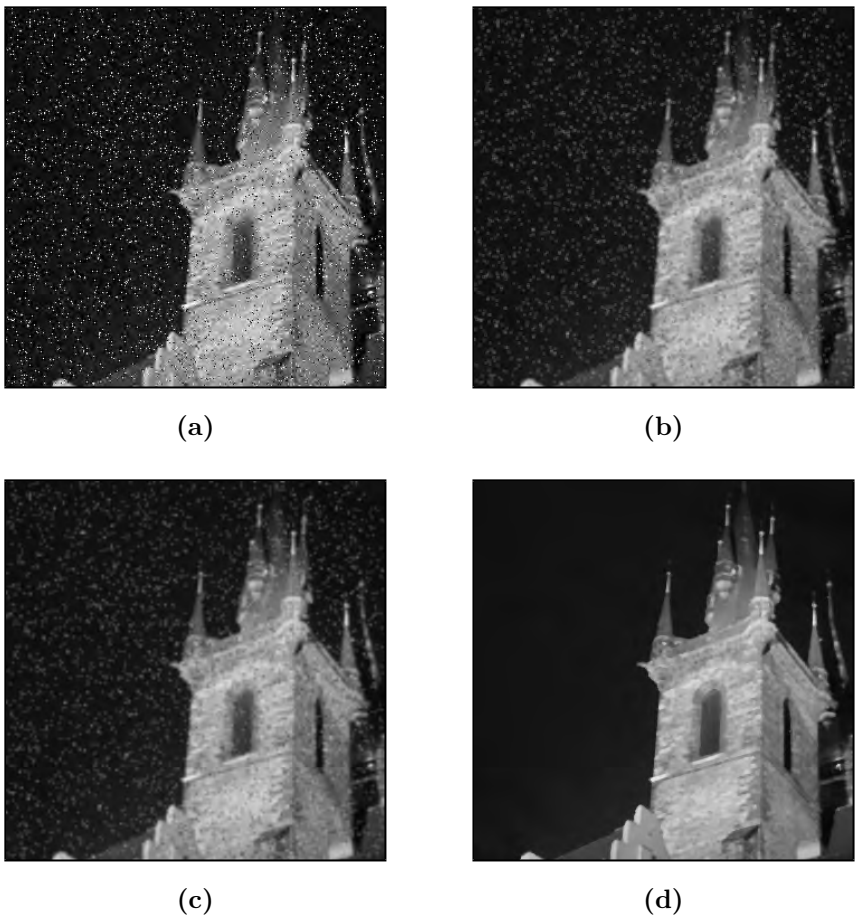


**Figure 3.6:** (a) Image in Figure 3.2 with added 'salt and pepper' noise (b) Result of mean filtering (c) Result of Gaussian filtering (d) Result of median filtering. In all cases, the filter radius was 1 pixel.

because the pixel values within a specified radius are 'ranked' according to their intensity values and the median selected as the filter output. This is a more effective form of high-frequency noise removal than smoothing, as fine details such as edges and region boundaries are preserved (Fig. 3.6). Median filtering was therefore chosen as the means of high-frequency noise removal for this study.

### 3.3.3 Image segmentation

Image segmentation, in the simplest sense, refers to the separation of objects of interest from the background. This is achieved by specifying regions within the image, based on a particular property, with each region being relatively homogeneous with respect to the chosen property and differing from the other regions of the image. One of the simplest means of implementing image segmentation is grey-level thresholding, which defines different regions within an image based on the grey level of individual pixels. A binary image, $g(x, y)$, may be generated from a grey-level image, $f(x, y)$, as follows:

$$g(x,y) = \begin{cases} 1 & \text{for} \quad f(x,y) \geq T \\ 0 & \text{for} \quad f(x,y) < T \end{cases} \tag{3.3}$$

where $T$ is some pre-determined 'threshold' that results in optimal separation between object and background. A value of $T$ may be calculated for the entire image (a global threshold) or $T$ may vary between different areas of the image, being dependent on image properties within a specified window (local or 'adaptive' thresholding [161]). The calculation of a value for $T$ based on the image histogram (i.e., the grey-level distribution of the image) is a common approach [161]. If both the object of interest and the image background have relatively homogeneous grey levels (and no other regions are present in the image), then the image histogram should be approximately bi-modal (Fig. 3.7). In this scenario, the calculation of a threshold is intuitive and will lie approximately at the location of the local minimum between the two modes.

Real images rarely exhibit such ideal characteristics and as a result, the calculation of a threshold is non-trivial in many cases. Often there may be no discernible peaks or valleys in the image histogram or there may be considerable overlap between modes representing object and background. The choice of algorithm for

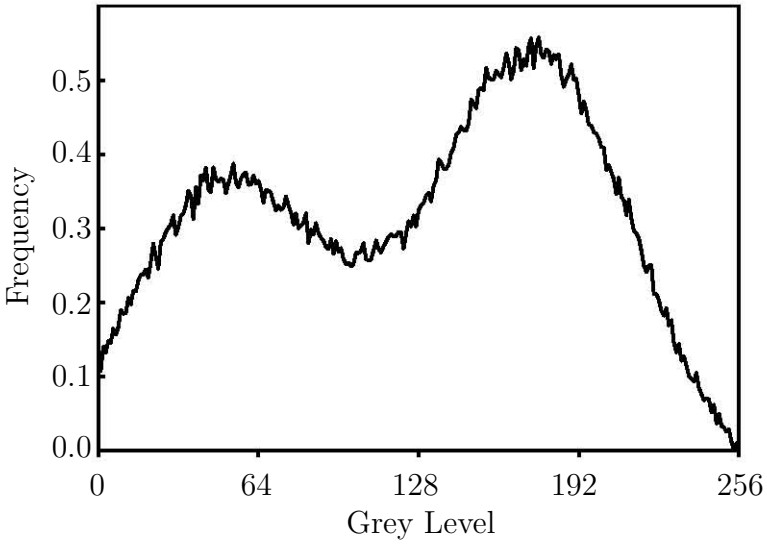


**Figure 3.7:** A bi-modal image histogram, representing two distinct regions within the image with differing grey-level distributions.

threshold computation therefore depends very much on the nature of the image and the shape of the histogram. For example, the 'triangle' thresholding technique [162] is quite effective for histograms in which the background mode is significantly larger than that of the object, characteristic of a large image containing small, low-contrast objects. However, this approach requires 'smoothing' of the image histogram for accurate segmentation, necessitating the estimation of further variables (the width of the smoothing kernel and the number of smoothing iterations), and is biased toward computing relatively high threshold values (Fig. 3.8b).

Another useful technique is that proposed by Otsu, which seeks to maximise the inter-regional variance ($\sigma^2$) in the segmented image [161]:

$$\sigma^2(T) = \frac{[\overline{I}_t P(T) - \overline{I}(T)]^2}{P(T)[1 - P(T)]} \tag{3.4}$$

where $\overline{I}_t$ is the mean grey value of the entire image, $P(T)$ is the probability of a pixel having a grey level $\leq T$ and $\overline{I}(T)$ is the mean grey level of those pixels.

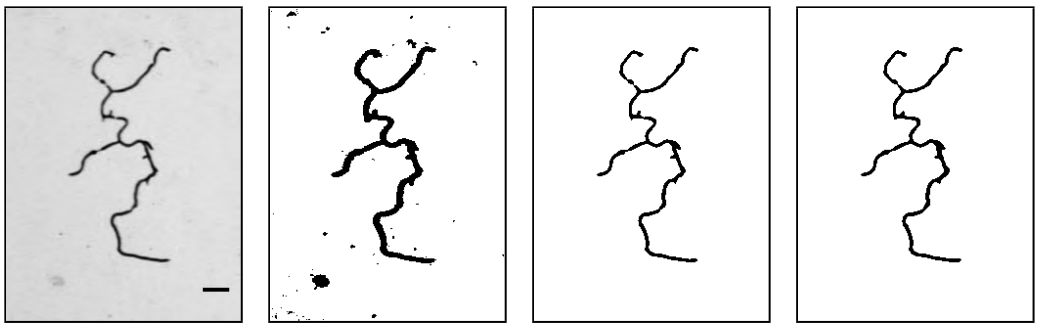

**(a)** **(b)** **(c)** **(d)**

**Figure 3.8:** (a) Original image of stained mycelium (Bar 30 $\mu$m) with binary images resulting from application of (b) triangle-thresholding (c) Otsu thresholding and (d) iso-data thresholding.

The optimum threshold is determined as that which maximises $\sigma^2(T)$. While this approach yielded acceptable results in the case of mycelial images (Fig. 3.8c), the computational overhead is relatively large.

The iso-data algorithm [163], the default thresholding method in ImageJ, determines a threshold by selecting an initial value (such as the minimum grey level in an image) and then calculating the mean values of all pixels above this value (the 'background' pixels) and all pixels below (the 'object' pixels). The value of $T$ is increased until the following condition is met:

$$T \geq \frac{\text{object mean} + \text{background mean}}{2} \tag{3.5}$$

This method of thresholding proved effective provided that the hyphae were contiguously stained a uniform colour and they were presented against a homogeneous background (Fig. 3.8d).

### 3.3.4 Pre-processing of binary images

*Morphological filtering*

Once thresholding is complete and a binary image has been generated, a degree of enhancement is required using morphological filters prior to object classification and subsequent measurement. For example, such processing may be necessary to remove small, unwanted objects (artifacts) or fill small holes or gaps within objects of interest. Small artifacts may be removed from an image by one or more *erosion* operations, while the quasi-inverse is termed *dilation*, both of which are illustrated in Figure 3.9. In simple terms, *erosion* may be considered to 'shrink' objects, while *dilation* causes them to 'grow'. More specifically, *erosion* may be explained as follows. Let $H$ be a structural element consisting of some arrangement of foreground pixels. An image ($I$) is traversed by $H$ and each pixel $(i, j)$ in the output image ($J$) is defined as follows for every $(i, j) \in I$:

$$J(i,j) = \begin{cases} 0 & \text{if } H_{i,j} \subseteq O \\ 1 & \text{otherwise} \end{cases} \tag{3.6}$$

where $O$ is a foreground object and $H_{i,j}$ represents $H$ centred on $(i, j)$. Put simply, if $H$ is entirely contained within $O$ when centred at a position $(i, j)$, then $(i, j)$ is defined as foreground in the output image. Otherwise it is denoted as background. *Dilation* is somewhat the reversal of *erosion*:

$$J(i,j) = \begin{cases} 0 & \text{if } (i,j) \in H_{m,n} \text{ for any } (m,n) \in O \\ 1 & \text{otherwise} \end{cases} \tag{3.7}$$

$H$ is centred on each foreground pixel in $O$ and any background pixels in $I$ overlapped by $H$ are designated as foreground pixels in $J$.

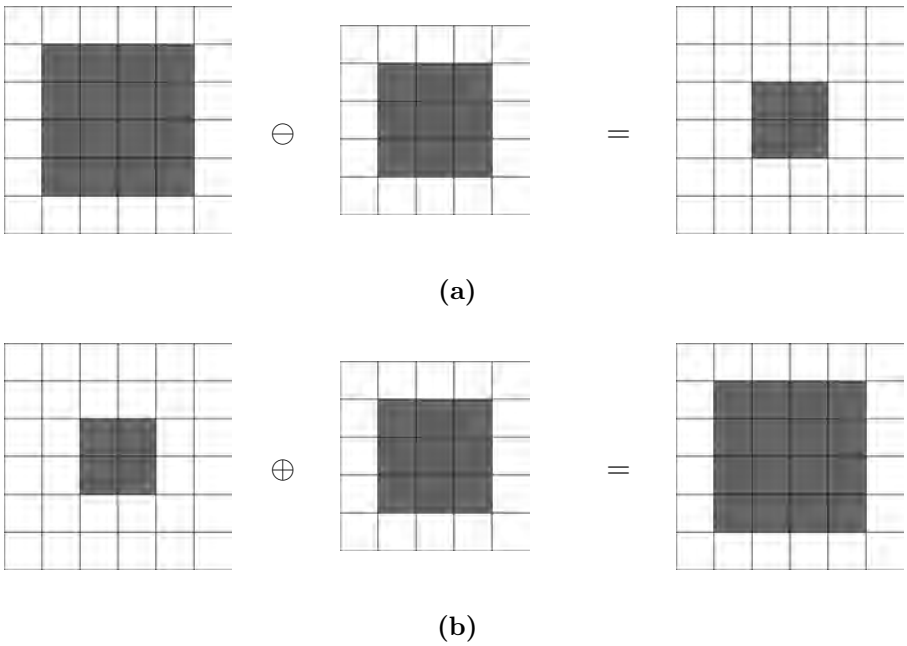


**Figure 3.9:** Effect of (a) *erosion* (denoted by ⊖) and (b) subsequent *dilation* (denoted by ⊕) on a binary object. This combined sequence is commonly termed an *open* operation.

*Watershed segmentation*

It is often the case that objects within binary images are in contact with one another (Fig. 3.10a). In the case of binary images of relatively spherical structures (such as fungal spores or pellets), some form of *watershed* segmentation may be employed to separate touching objects, which is based on the concept of constructing boundaries ('watersheds') between adjacent objects or regions. The ImageJ implementation is based on the generation of a Euclidean Distance Map (EDM) [164], a visual representation of the distance between each foreground pixel and the nearest background pixel (Fig. 3.10b). Each foreground pixel is assigned an integer value (represented by different grey levels in the visual representation) corresponding to the number of pixels separating it from the nearest background pixel. Alternatively, this value could be considered the number of *erosion* operations that would be re-

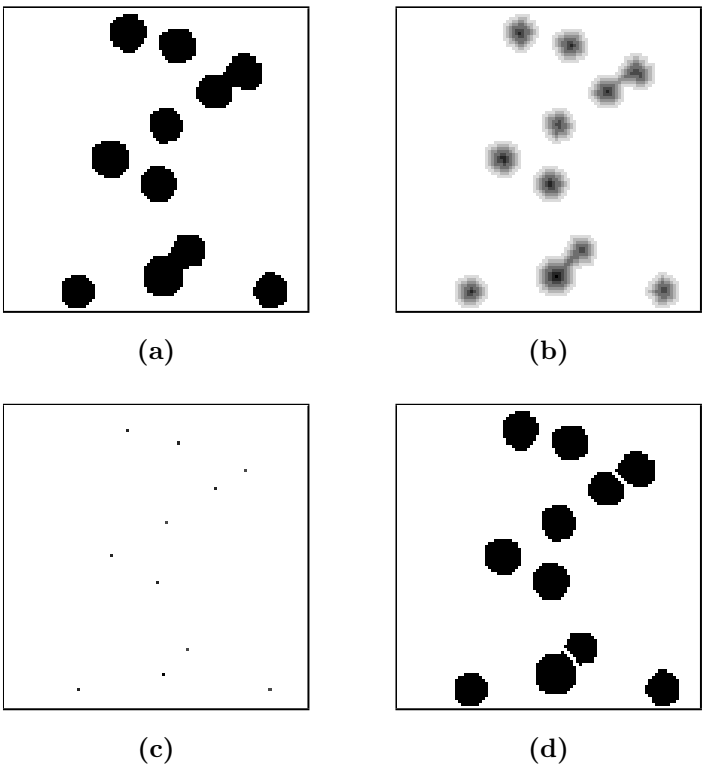


**Figure 3.10:** (a) Original image containing conjoined objects (b) Euclidean Distance Map (c) Ultimate Points (d) Segmentation of objects following conditional *dilation*.

quired to remove this pixel from the image. From the EDM image, a further image is generated, displaying the 'ultimate points', or the local maximum values for each EDM (Fig. 3.10c). These 'ultimate points' can be thought of as approximations to the centre of each object. It remains to reconstruct the original image by way of conditional *dilation*; that is, a number of *dilations* are performed on each object, sufficient to restore the object to its original size, on condition that *dilation* causes no two objects to come into contact with each other (Fig. 3.10d). *Watershed* segmentation has been utilised in other studies of fungal morphology [47, 77] and was deployed in this study to separate touching objects in images of spores and pellets.

*Object classification*

Prior to measurement, it is necessary to identify different objects within the image, such as spores, hyphae and any remaining unwanted artifacts. This may be achieved by assigning certain descriptors to each object, such as the projected area, perimeter length, equivalent diameter or some measure of boundary curvature, the most common form of which in the study of microbes is circularity. Other parameters, such as Fourier descriptors [143] and chain codes [165], may also be of value.

To maximise the accuracy of object classification, a training set can be utilised, the establishment of which requires each object in an image to be quantified in terms of $A_p$ and $P$, for example, which subsequently form the elements of a feature vector for that object [166]. The object is then classified as a spore, hypha, mycelium or artifact by a human observer and this process continues until a sufficiently large knowledge base has been established. When a test object is subsequently presented, a feature vector is formed and, for example, the Euclidean Distance calculated between the vector of the test object and those in the knowledge base. The test object is classified according to the 'winning' vector in the knowledge base, that is, the vector within the knowledge base containing the features that best describe the test object. However, such an approach involves a large number of calculations and requires time devoted to the establishment and maintenance of the knowledge base. A similar approach involves the implementation of some form of Artificial Neural Net (ANN), such as that adopted by Papagianni and Mattey for the classification of fungal structures [72].

However, the most common (and least time-consuming) means of discriminating between objects of differing classes in the quantification of fungal morphology is the use of threshold values [12, 167]. In this study, minimum and/or maximum values were set for projected area ($A_{p,\,min}$) and circularity ($C_{s,\,min}$, $C_{h,\,max}$) and these

values were refined by analysing the distribution of $A_p$ and $C$ within a population (see Section 5.3.1). Establishment of values for these variables will be discussed in Section 5.3.1 and the effect of small variations in these values is investigated in Sections 5.3.1 and 5.3.2.

*Pre-processing of hyphal structures*

Prior to the measurement of hyphal architecture, it is common for the associated binary images to be subjected to some form of thinning algorithm to produce a skeletal structure [4, 5, 168]. This facilitates the rapid determination of parameters such as the total length of the mycelium, the total number of tips and the location of branch-points. For relatively low-resolution images of mycelia, in which the hyphae are typically just a few pixels in diameter, *skeletonisation* may be achieved quickly and accurately. However, such an approach may not be suitable for higher resolution images, resulting in large hyphal 'objects' or regions, small changes in the shape of which can result in significantly different skeletal structures [169]. ImageJ's implementation of a thinning algorithm is based on that of Zhang and Suen [170], in which pixels are iteratively removed, by way of a look-up table, until a skeleton remains. Some of the limitations of this approach will be addressed in the next section.

## 3.4 System development II: Quantification of microbial structures

ImageJ, like most image processing software packages, is well-equipped to conduct the image pre-processing described in the previous section. However, for the quantification of binary representations of filamentous microbes, additional functionality was required. This section provides a description of the plug-ins that were devel-

oped to this end, together with a summary of the complete analysis procedure for fungal spores and hyphal elements at the microscopic level and, on the macroscopic scale, fungal pellets. All routines described in this study were written in Java, incorporating ImageJ classes and methods where appropriate.

### 3.4.1 Microscopic analysis

While image pre-processing is similar regardless of the object of interest, the analysis of hyphal elements is more extensive than that of spores. The steps involved in each case are presented (Fig. 3.11). It is assumed that a colour (RGB colour-space) image is provided as input, but this is not strictly necessary.

The image is divided into three, 8-bit grey-scale images, representing the three primary colour components (red, green and blue). The red component exhibits the greatest contrast for images of lactophenol cotton blue-stained samples (a common mycological preparation) and is retained for image processing; the green and blue components are discarded. Image pre-processing begins with filtering of the image to compensate for low-frequency, uneven illumination using an implementation of the Rolling Ball algorithm [160]. The radius of the filter was set to the pixel equivalent of 40 $\mu$m (40 pixels for images of hyphae, 200 pixels for spores), which is large relative to the width of a typical hypha (approximately 2 – 4 $\mu$m). Any high-frequency speckle noise was subsequently removed by median filtering. A grey-level threshold, calculated using the iso-data algorithm was then applied, resulting in a binary image.

The next stage of the routine is dependent on whether spores or hyphae are the primary object of study. It is unlikely that viable spores and hyphae will be present in the same image: results from this study indicated that the majority of spores had germinated by approximately 8 hours after inoculation (data not shown). Any spores present in a sample taken after this time were considered to be non-viable

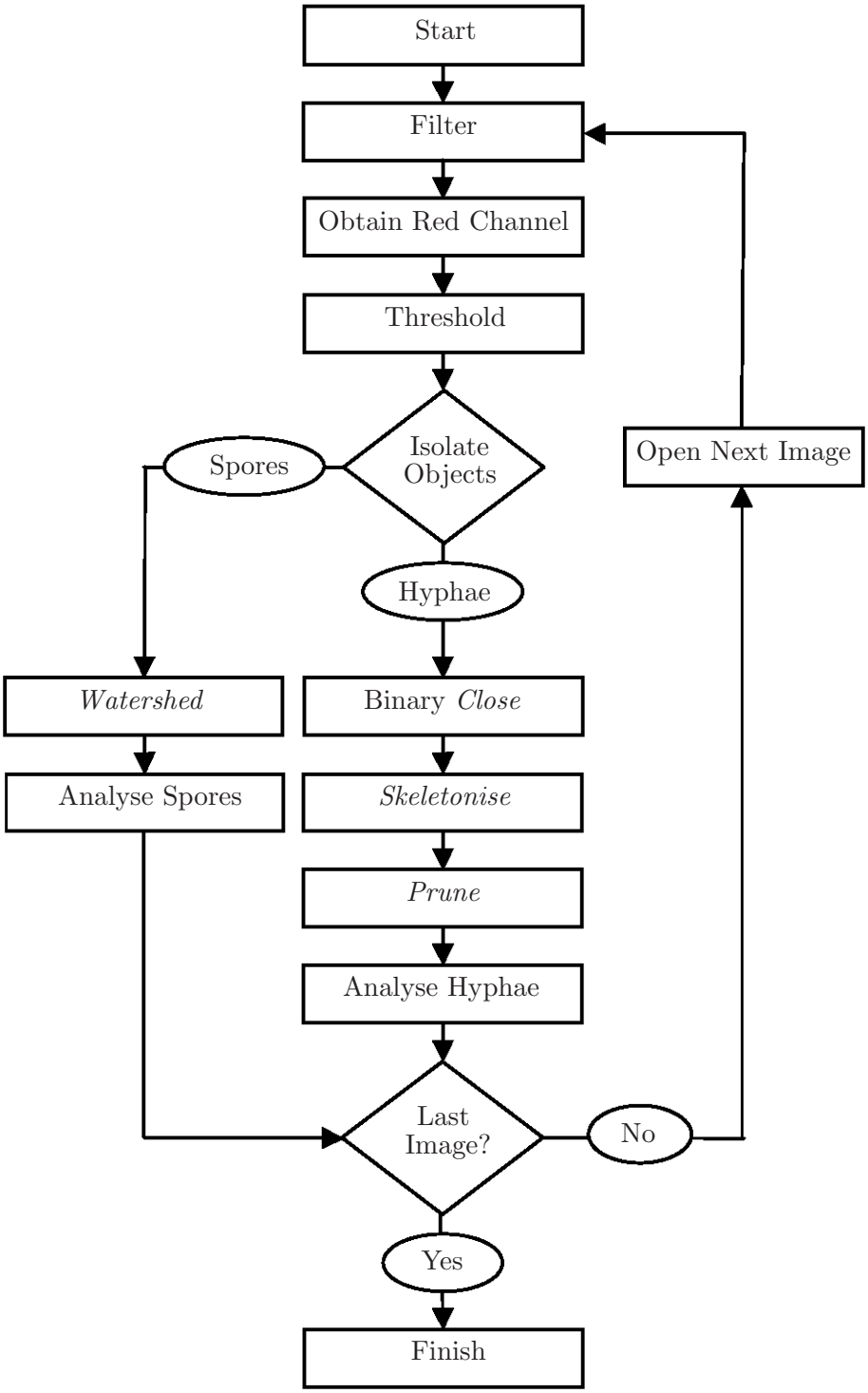


**Figure 3.11:** Algorithm used for characterization of fungal micro-morphology

and were treated by the system as artifacts.

*Analysis of spores*

In the case of spores, a *watershed* operation was used to separate any touching objects. Objects were then classified based on projected area and circularity[2]. Spores of many industrially relevant fungi, such as *Aspergillus*, are relatively spherical [4]. Therefore, objects with a projected area above a specified minimum ($A_{p,\,min}$) and with a circularity greater than a threshold value ($C_{s,\,min}$) were considered to be spores; remaining objects were considered to be artifacts and were excluded from the analysis.

*Analysis of mycelia*

When hyphae are the objects of interest, a single binary *close* operation (a single *dilation* operation followed by a single *erosion*) is performed to remove any small breaks (or holes) in the objects. All objects with a projected area below $A_{p,\,min}$ or a circularity greater than a second threshold value ($C_{h,\,max}$) are excluded from the analysis. The binary image of the hyphal elements is then *skeletonised*, which reduces the objects in the image to a series of lines one pixel in width.

The *skeletonisation* of an object during image analysis can occasionally result in artifactual points or branches [4, 9, 171]. Artifactual points (sites where the skeleton is greater than one pixel in width) can lead to the incorrect classification of branch-points, while artifactual branches can lead to an over-estimation of hyphal length and the number of hyphal tips. These may be removed by way of *pruning* (Fig. 3.12), which also has the effect of removing any remaining small artifacts from the image.

[2]In the case of a circle, $A_p = \pi r^2$ and $P = 2\pi r$, and so $C = 1$. The larger $P$ becomes with respect to $A_p$, the less circular the object becomes and so the value of $C$ decreases

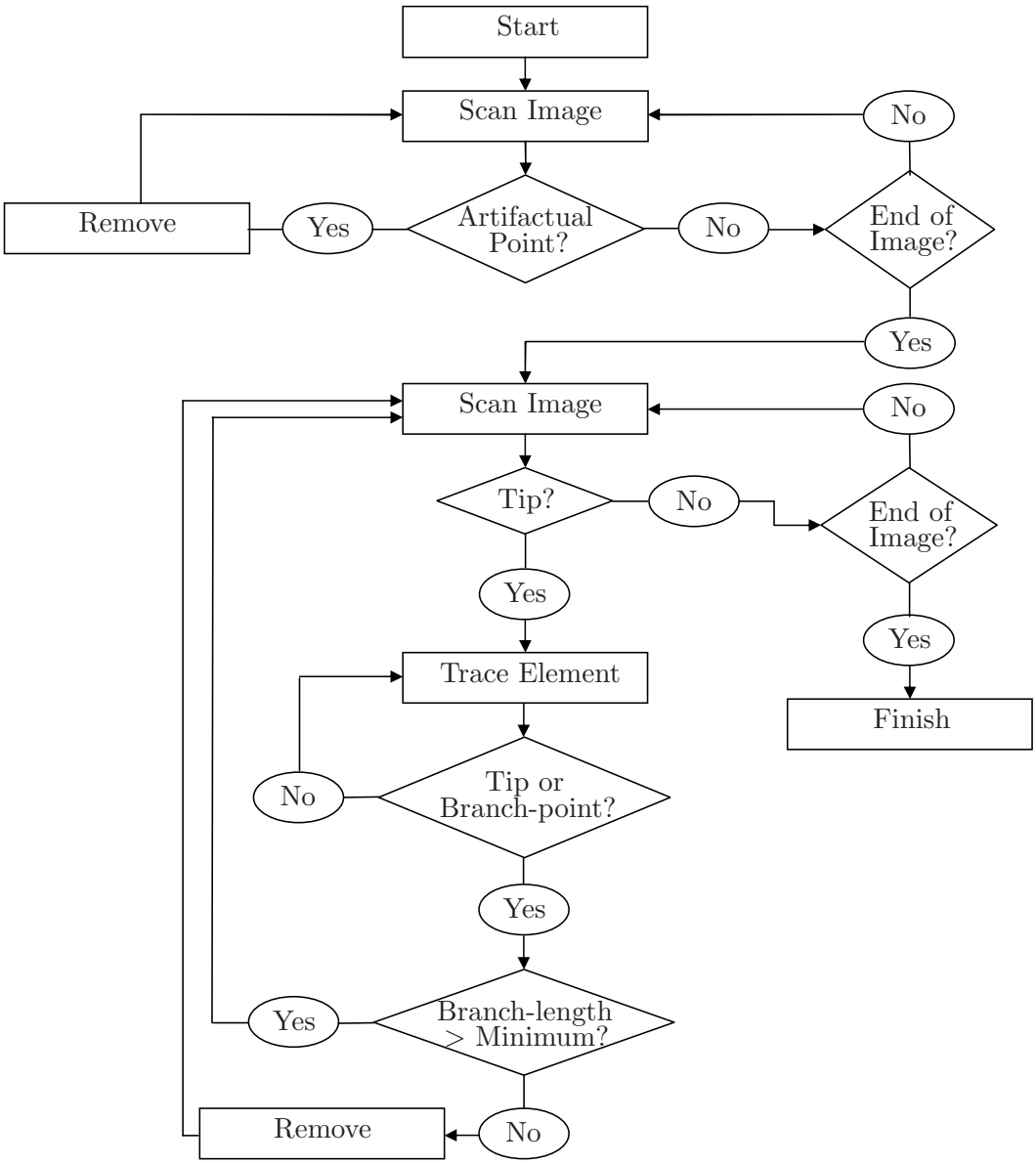


**Figure 3.12:** Algorithm used for the *pruning* of skeletal hyphal structures prior to measurement

The *pruning* routine begins by scanning the image in a raster fashion until a black pixel is located. If this pixel is deemed artifactual (by way of a look-up table), then it is removed. This process continues until the end of the image has been reached. The second stage begins by scanning the image in a raster fashion until a hyphal tip is located. A tip is defined as a black pixel with just one other black pixel in the immediate neighbourhood (Fig. 3.13). The location of the tip is recorded and the skeleton is then traced from this tip along the hyphal length until either another tip or branch-point is reached. A branch-point is defined as a black pixel with three or more black pixels in the immediate neighbourhood, with no two of these neighbours joined. The length of the branch is then calculated based on the number of pixels traversed. If the length of the branch is less than the specified minimum ($L_{b,\,min}$) it is removed. The scan of the image then resumes from the point where the initial tip was located and the process continues until the end of the image has been reached. All pre-processing of mycelia is illustrated in Figure 3.14.

Once *pruned*, the *skeletonised* hyphae are suitable for analysis (Fig. 3.15). The routine begins by scanning the image in a raster fashion until a hyphal tip is located. The location of the tip is noted and the skeleton is then traced from this tip along the hyphal length until either another tip or branch-point (collectively termed *end-points*) is reached. At this point, the length of the branch is recorded, along with the position and classification of the end-points. This combined information describes a hyphal *segment*. For example, unbranched hyphae will consist of a single *segment* with two tips as *end-points*.

If a branch-point is located, tracing continues along the first *segment* found branching away from this point; any additional *segments* branching from this point are *pushed* onto a *stack*, containing *segments* yet to be traced. If a hyphal tip is reached, the current *segment* is recorded and the most recently encountered, non-

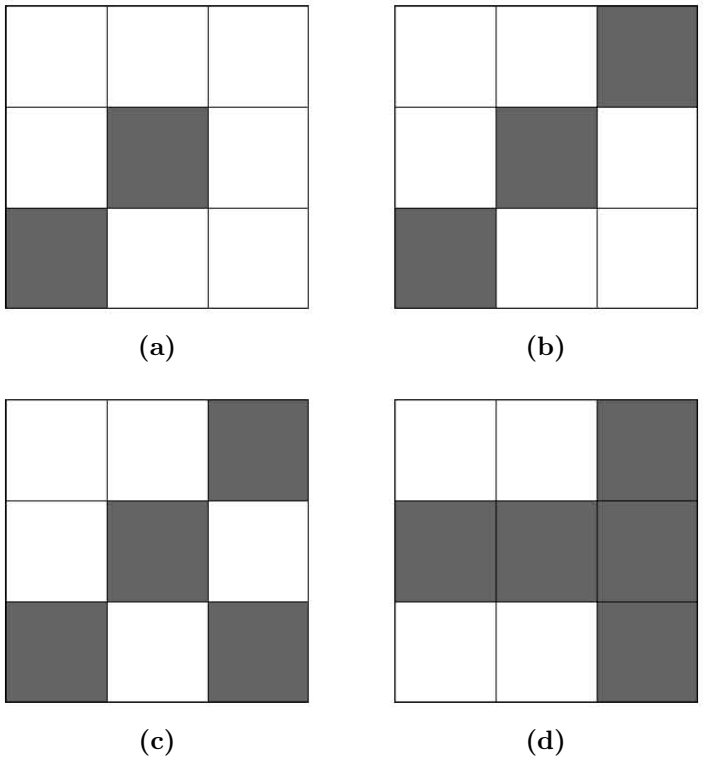


**Figure 3.13:** Classification of points on a skeletal hyphal structure. (a) A pixel is defined as a hyphal tip if all but one of the neighbouring pixels is white. (b) If two of the neighbouring pixels are black, the current pixel is deemed an internal component of a hyphal *segment*. (c) A branch-point is defined if at least three neighbouring pixels that do not share a common edge are black. (d) Conjoined neighbouring black pixels indicate the current pixel is adjacent to a branch-point

traced *segment* is *popped* from the top of the *stack*, and the routine continues tracing from there.

If a tip is reached and all *segments* in the current hyphal element have been traced, the measured data (total hyphal length, number of tips, and hyphal growth unit) is outputted to the results table. The algorithm then returns to the point in the image where the last hyphal element was first located and continues to scan until either another element is detected or the end of the image is reached.

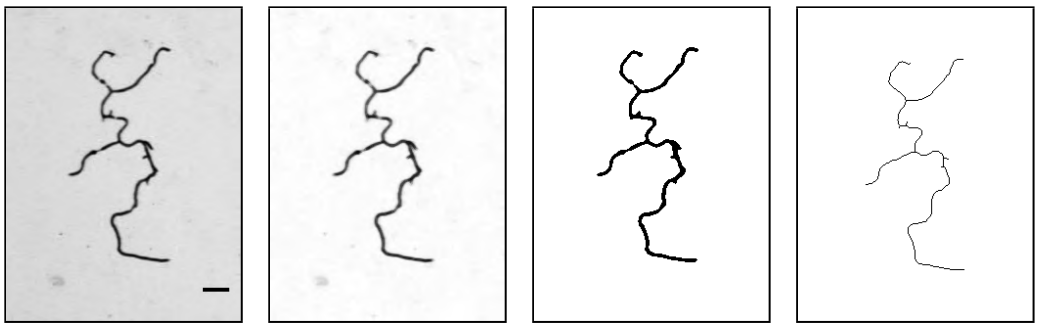

**(a)** **(b)** **(c)** **(d)**

**Figure 3.14:** (a) Original image of stained mycelium produced using the protocols described in Sections 2.4 & 2.5 (Bar 30 $\mu$m) (b) Background subtracted and median filtered (c) Resultant binary image (d) *Pruned*, *skeletonised* mycelium.

*Generation of Mycelium Graph*

The compiled information on the individual *segments* of a mycelial structure may be thought of as a mycelium graph or network (Fig. 3.16). Each tip and branch-point represent the vertices of the graph, connected by edges whose length is that of the hyphal *segment* from which it was derived. Such a representation of a mycelium is of use in calculating, for example, the length of the 'main' hypha [72], or the distribution of tips or branch-points with respect to other branch-points. By fixing such a graph to a co-ordinate plane, it may also be used to geometrically map foraging strategies of the microbe.

*Analysis of a population*

Typically, the morphological characterisation of a single hyphal structure is of limited value and with this in mind, the plug-ins described here have been adapted to process a series of images and derive population statistics. The programme begins by requesting a set of parameters from the user, along with the directory in which the bank of images to be analysed is contained. The routine then proceeds

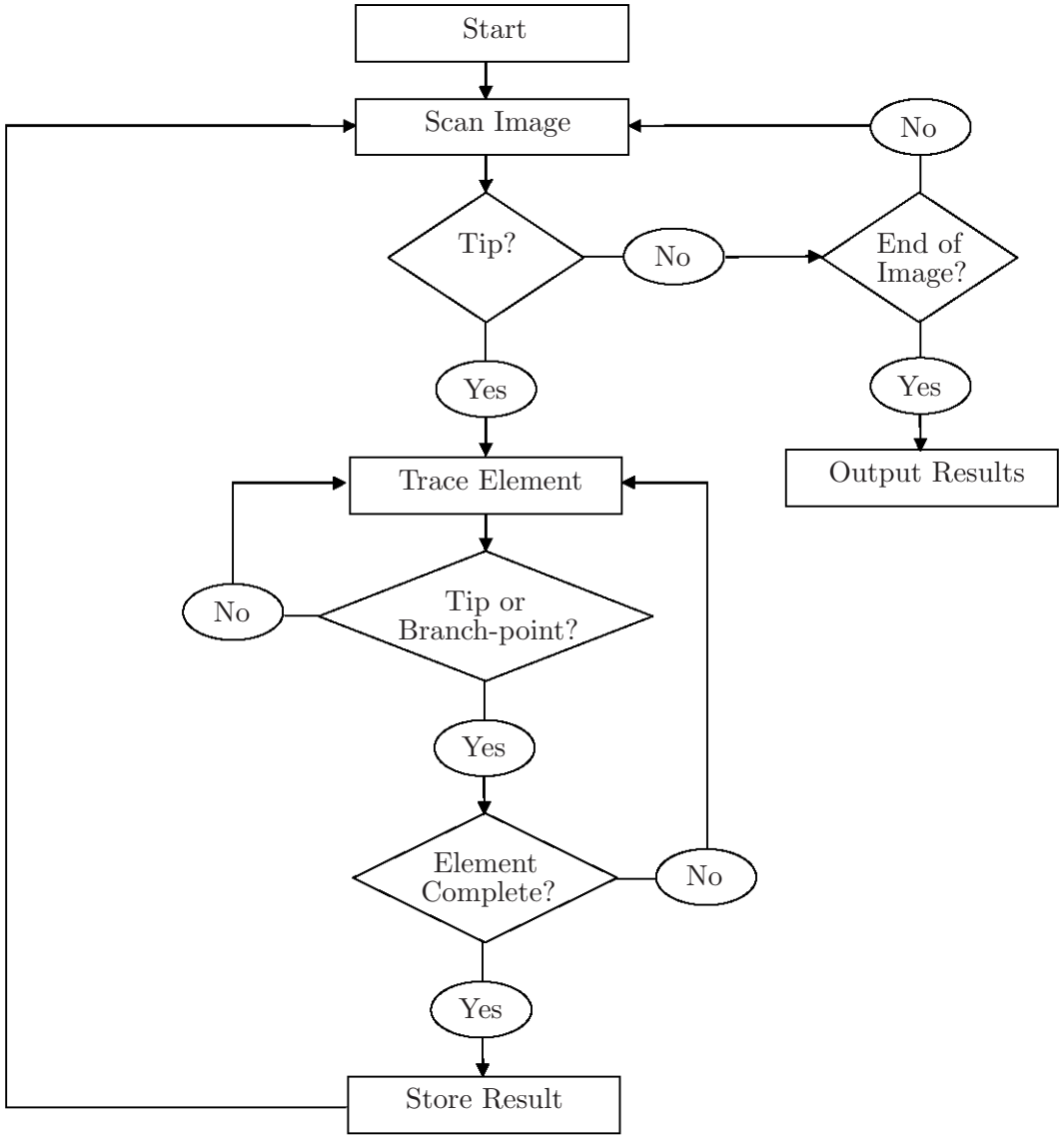


**Figure 3.15:** Algorithm used for the analysis of skeletal hyphal elements

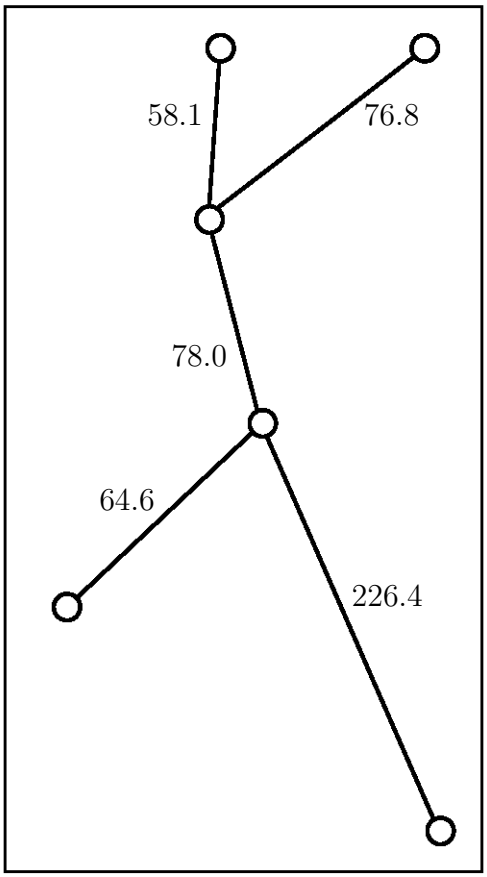


**Figure 3.16:** Graph of the mycelium in Figure 3.14 with small branches omitted for clarity.

automatically until all images in the specified directory have been processed. An example of data output following the analysis of a population of mycelia is shown in Figure 3.17.

### 3.4.2 Macroscopic analysis

Analysis of pellet images commences in a similar manner to that described above. The red channel of the RGB image is isolated and subject to the same filtering procedures as those used for microscopic images, albeit with a larger filter radius for background subtraction (8 mm). Prior to thresholding, it is necessary to locate the Petri dish in the image, so that a region-of-interest (ROI) may be specified

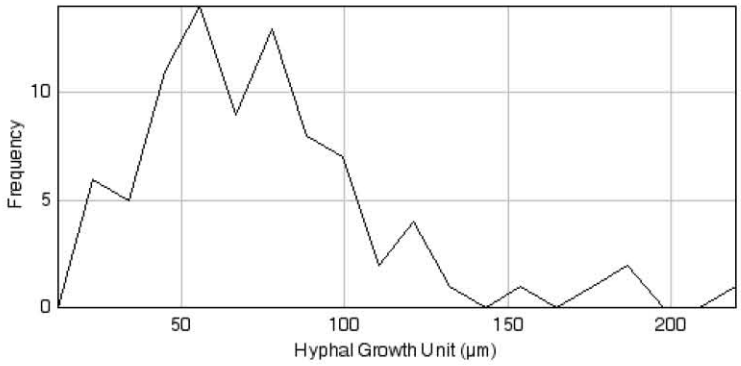


| | |
|---|---|
| Population Size: | 86 |
| Mean Hyphal Growth Unit: | 68.942 +/- 8.076 µm |
| Minimum: | 12.920 µm |
| Maximum: | 219.077 µm |
| Mode: | 55.789 µm |

**Figure 3.17:** Distribution and statistics on hyphal growth unit values produced in a typical analysis of a population of mycelial elements.

within the Petri dish. This was achieved using a method similar to that described by Dörge and colleagues [158]. To begin, a Sobel filter is applied to the image ($I$):

$$G_x = \begin{bmatrix} 1 & 2 & 1 \\ 0 & 0 & 0 \\ -1 & -2 & -1 \end{bmatrix} * I \qquad \text{and} \qquad G_y = \begin{bmatrix} 1 & 0 & -1 \\ 2 & 0 & -2 \\ 1 & 0 & -1 \end{bmatrix} * I \tag{3.8}$$

The resultant 'edge image' is then Gaussian filtered to smooth and remove noise. The Petri dish may then be found by locating the nearest local maximum to a chosen image corner. This assumes that the Petri dish is approximately centrally located in the image. By repeating this operation for two more corners, three different points on the Petri dish circumference may be located, representing three points on a circle ($a$, $b$ and $c$). The centre of the circle ($o$) is then located by forming two chords ($ab$ and $ac$), bisecting them and calculating the point of intersection of the

two perpendicular bisectors ($mo$ and $no$). A ROI, representing the Petri dish, may then be specified with $o$ as centre and $|oa|$ as the radius ($r$). However, considering the digital representation of the Petri dish is not perfectly circular (due to, for example, optical aberration), more accurate elimination is achieved if $r$ is specified as:

$$r = (1 - T)|oa| \tag{3.9}$$

where $T$ is some specified tolerance (typically 0.1). Once the ROI is specified, the region outside is cleared and the image may be thresholded as above. The entire process is illustrated in Figure 3.18. Quantification of objects in the resultant binary image is identical to that described above for spores. The morphological data corresponding to the image in Figure 3.18 is shown in Figure 3.19.

## 3.5 Discussion

The accurate characterisation of fungal morphology remains a key target for industrial biotechnologists and the deployment of image processing systems is central to achieving this goal. While extensive progress has been reported in the use of computer-aided analysis of mycelial structures [8, 136], many implementations of image analysis systems described in the literature depend on significant manual intervention for accurate quantification to be achieved [10–13, 87, 121, 123, 139, 140, 148]. Hence there still exists a need for further development of automated systems for the classification and analysis of filamentous microbial conformations.

In this study a new system has been presented for quantitative analysis of both micro- and macro-morphology. The method obviates the need for purchase of relatively expensive commercial software by adding utility to the publicly available ImageJ platform [114], a system of proven usefulness in this field [140, 159]. The

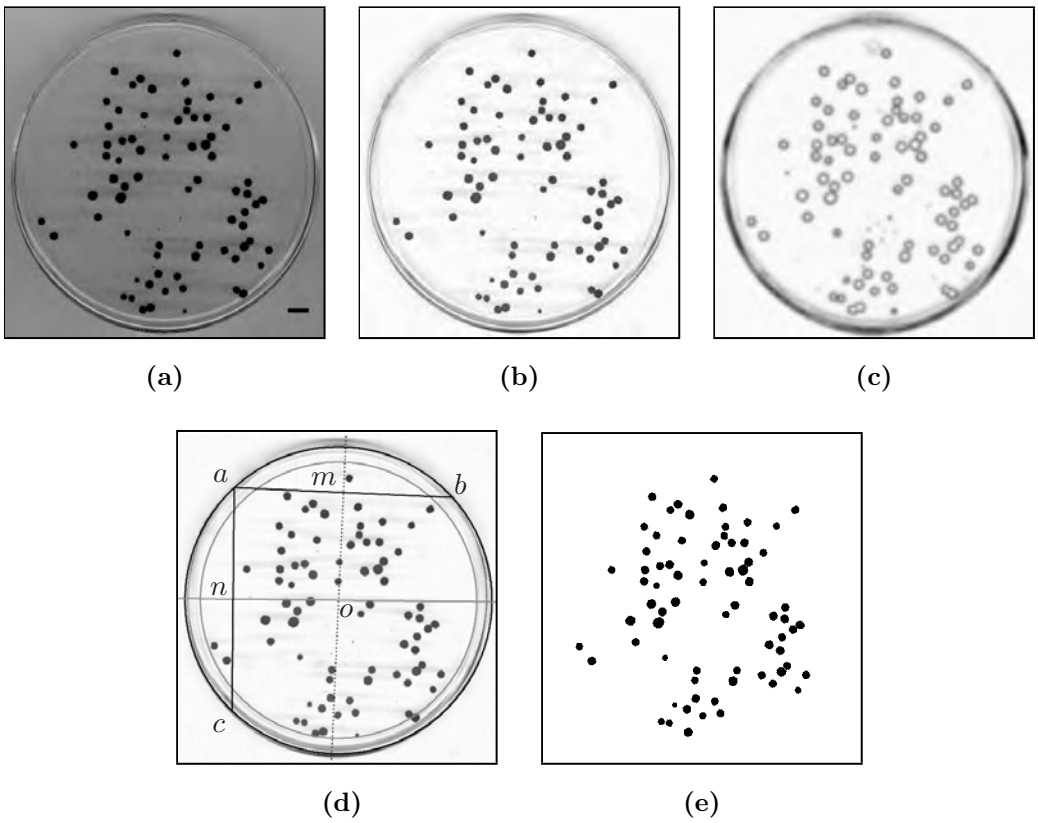


**Figure 3.18:** (a) Original image of stained pellets produced using the protocol described in Section 2.5.1 (Bar 10 mm) (b) Background subtracted and median filtered (c) Gaussian filtered edge image (d) Points $a$, $b$ and $c$ are located on Petri dish circumference, midpoints $m$ and $n$ are found and $o$ is located as the intersection of the perpendicular bisectors of $ab$ and $ac$ (e) Resultant mask image.

prioritisation of speed of execution has yielded a system capable of both rapid and accurate analysis of a large bank of images, permitting near-'real time' assessment of fungal development through the compilation of population data. While the on-line examination of individual hyphal elements has yielded valuable data on apical extension [4], population statistics are essential for the characterisation of bioprocesses, due to the inherent variations in growth kinetics throughout a given population [4, 129].

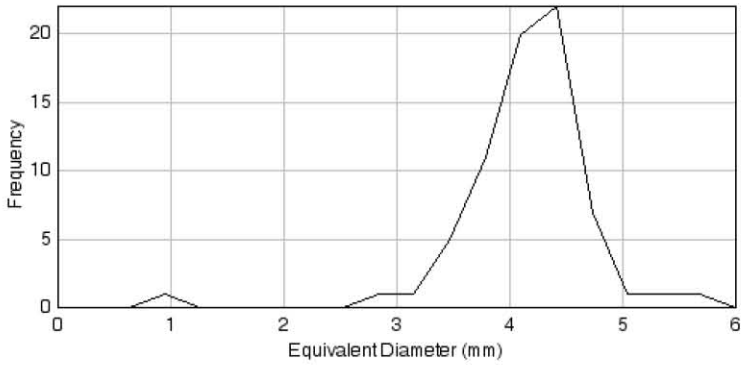


| | |
|---|---|
| Population Size: | 71 |
| Mean Equivalent Diameter: | 4.003 +/- 0.139 mm |
| Minimum: | 0.811 mm |
| Maximum: | 5.450 mm |
| Mode: | 4.421 mm |

**Figure 3.19:** Result of the analysis of the pellets in Figure 3.18.

In common with all image-analysis systems, the routines described here depend on high-quality input images and are sensitive to elevated levels of artifact, low-level or uneven sample illumination and out-of-focus fields of view. Uniform staining of hyphal elements is also essential to ensure against the incorrect classification of mycelial structures. Contiguous, high-contrast staining also permits automatic image segmentation via the application of grey-level thresholding, obviating the requirement for manual segmentation [146] or the specification of a fixed threshold value to be used for all images [172]. While the image pre-processing described alleviates these concerns to some degree, high-quality sample preparation will ensure optimal system performance and the generation of accurate morphological data. The dilution of biomass prior to image capture may also be necessary so as to minimise hyphal overlapping and contact between spores or pellets.

The system described here has much in common with those previously described in the literature. The use of simple morphological thresholds to exclude artifacts is a commonly adopted approach [10, 155]. This simple technique is generally effective

as artifacts tend to be small relative to hyphae and also exhibit a higher circularity index ($C$). The use of morphological filters to remove small breaks in objects has previously been utilised, although caution was advised by Lucumi and colleagues against multiple iterations, which may result in the removal of 'gaps' in mycelial networks [155]. Such an approach was refined by Daniel and colleagues to join small gaps in skeletal structures [173].

*Skeletonisation* has also been widely utilised in the study of hyphal elements [4, 5, 10, 140, 168, 174, 175], as it facilitates rapid enumeration of hyphal lengths and tip numbers. However, such an approach is not without short-comings and, as was the case in this study, the specification of *pruning* algorithms is often necessary [4, 10, 155, 168, 171], although in some cases this is due to the presence of solid particles in the media and a need to ensure such artifacts are not interpreted as small branches. Another dimension was added to the analysis of skeletal structures by Drouin and colleagues, as the use of the binary skeleton as a mask allowed the precise quantification of 'full' and 'empty' hyphal zones, together with septation, in filaments of *Streptomyces ambofaciens* [171]. Such an approach could potentially be utilised to delineate 'active' and 'non-active' regions in calcofluor white-stained preparations [84]. Other authors have avoided using *skeletonisation* algorithms as small changes in hyphal boundaries can have a significant impact in the performance of the algorithm [169]. This is particularly true when swollen hyphal tips are the object of study, but the omission of such a thinning step has generally resulted in the necessity for manual tip counts [152], resulting in a considerable increase in processing time. In the absence of *skeletonisation*, the automatic detection of hyphal tips may be implemented using either the application of morphological filters to the binary mask of the mycelium, or an interpretation of the mycelium boundary, in which tips would manifest themselves as sharp turning points.

The production of a mycelial graph could be potentially applied to the study

of a microbe's foraging strategy on a solid substrate or the response to changes in environmental conditions. A similar 'segmental' approach to mycelial characterisation was previously described in the analysis of *Trichoderma viride* colonies [172]. Such an approach permits an estimation of the order in which branches were formed on 'free' elements, previously determined by iterative erosion [4, 5, 10]. The inclusion of hyphal width in such a graph would add further utility and permit the modelling of the mycelium as a 'fungal network' [176]. However, the estimation of hyphal width from images in which the hyphae are perhaps 2 – 3 pixels in width (which is sensitive to the grey-level threshold) is difficult, considering the width can only be measured to within one pixel. The average width could be estimated by dividing the projected area by the total length of the structure, but this is of little value in the context of a network. An alternative means of estimating hyphal width was proposed by Hitchcock and colleagues, which involved convolution with a Gaussian point-spread function and subsequently summing over the resultant grey levels based on the location of the hyphae in the binary mask [172].

More extensive characterisation of pellets has been described in other reports. Müller and colleagues estimated the 'compactness' of pellet structures by calculating the ratio of projected area to projected convex area, which was defined as the projected area after filling any internal voids and any concavities in the external perimeter [152]. Papagianni and Mattey quantified pellets in terms of their eccentricity, a measure of the degree to which a shape deviates from a circle [72]. Other generally-applicable measures include the dimensions of the object's bounding box and the convex perimeter [10]. A more thorough assessment of pelleted morphologies is possible with the system described here. However, it has been assumed here that images of pellets to be analysed are captured macroscopically, using either a camera or, preferably, a flatbed scanner. For more extensive examinations and the derivation of data beyond the projected area, it is recommended that microscopic

imaging be utilised, permitting the isolation of individual hyphae and the accurate localisation of the pellet perimeter.

As with pellets, an analysis of mycelial aggregates is also possible with the system described here, using parameters such as projected area and circularity. Other parameters, such as those mentioned above, could easily be incorporated if necessary. Lucumi and colleagues described a useful algorithm for the extensive quantification of such aggregates, which involved the object's separation into core and filamentous fractions and a subsequent estimate of hyphal growth unit based on the number of tips found [155]. A common measure that has been applied to the dispersed growth form is the 'main' hyphal length [5], which Wongwicharn and colleagues described simply as the tip-to-tip length of the longest hyphal length in a mycelium [148]. While the identification of the main hypha is trivial for free elements (no hyphal 'crossovers'), the utility of such a measure in the assessment of mycelial aggregates is limited. The use of more universally applicable measures, such as projected area, is more appropriate; projected area was described by Li and colleagues as being particularly useful for the determination of fragmentation in a bioreactor [177]. Projected area has also been demonstrated to correlate well with measures of dry-cell weight in submerged culture, due to the relative constant width of hyphae in these processes [45, 106]. Measures such as projected area have the added advantage of obviating the need to discriminate between different morphological forms, a capability that has been described in detail in some studies [5, 72]. However, the information that may be garnered from such simple measures is obviously extremely limited and, given the evidence for metabolite excretion occurring primarily at hyphal tips [84, 105, 107], an accurate evaluation of branching is vital in studies of filamentous microbial development.

The image-processing system does have some difficulty in distinguishing between 'young' hyphae (recently germinated spores) and spore clusters, because of their

morphological similarity in terms of projected area and circularity (in the approximate range 0.4 – 0.8). As such, these young hyphae and spore clusters are typically excluded from the results. In order to fully characterise this transition from spore to hypha (as would be necessary in studies of germinative potential, for example), a means of distinguishing between these different objects is required. Boundary shape descriptors [143, 165] could be utilised in conjunction with the morphological thresholds used in the current study to this end. A means of breaking up clumps of spores in the inoculum, such as sonication, may also help to alleviate the problem. However, restrictions posed by such limitations should be minimal, as the development of spores and the development of hyphae are typically subject to separate analyses, due to the different nature of their respective growth mechanisms (swelling versus polarised tip extension). It should however be noted that in the analysis of spore morphology, the use of *watershed* techniques to separate touching objects is not recommended for images containing germinated spores, as it is likely that the germ tubes will be segmented from the parent spore and both objects interpreted as separate objects.

## 3.6 Conclusions

Image analysis systems represent essential enabling tools for the accurate quantification of filamentous microbial morphology. Despite the significant progress that has been achieved in producing such systems, a requirement for manual intervention is still commonplace and, as such, further development, with an emphasis on process automation, is necessary. The system described here is capable of rapidly and accurately producing population statistics derived from a large bank of images of either fungal spores or mycelia at the microscopic level, or pellets at the macroscopic level. Such data can then be utilised to derive information on the growth kinetics,

by presenting multiple image banks representing different stages in the organism's development.

The parameters used in quantifying morphology in this study (projected area, circularity, total hyphal length and number of hyphal tips) are similar to those utilised in other studies of filamentous microbes. However, other measures (eccentricity, convex area, bounding rectangle) can be easily incorporated if necessary. The analysis of mycelia is more extensive than that typically reported in other studies and allows a more complete characterisation of the microbe beyond the conventional hyphal growth unit. The basic utility of the system has been demonstrated, but more extensive application will be detailed in the subsequent chapters of this thesis, as image processing is employed in the derivation of growth kinetics on solid substrates and development in submerged systems.

# Chapter 4

# Nitrocellulose as a Tool for Microscopic Examination of Filamentous Microbes

## 4.1 Introduction

A large number of products of commercial significance are produced using filamentous microbes, such as enzymes, antibiotics and organic acids [8]. The majority of these compounds are produced in the submerged culture format (SmF), due to the greater ease with which such fermentations may be controlled and the metabolite of interest separated from biomass. However, recent reports suggest elevated metabolite expression by filamentous microbes when cultured in solid-state culture (SSF) compared to submerged [65, 68]. Furthermore, SSF is not without merits, such as low energy requirements and cheap raw materials, which has led to the utilisation of this fermentation format in the production of a range of bioactive compounds, organic acids and industrial enzymes [64].

Key to fostering an understanding of metabolite expression in SSF is an ability to accurately and rapidly assess the spatial distribution of the organism. Relationships between productivity and gross morphology are well-established in many processes [8], with some studies also suggesting links between metabolite expression and micro-morphological indicators, such as branch formation [84, 107]. However,

the vast majority of these studies have been restricted to the SmF format and there is therefore a need to develop methods suitable for use in examining hyphal growth on solid culture. Conventional techniques for microscopically studying moulds, such as those employed in clinical mycology laboratories, include 'tease-mounts', whereby a small amount of biomass is torn from a solid culture with needles and 'wet-mounted' in a suitable stain (such as lactophenol cotton blue), or a variety of 'tape-touch' methods [178, 179]. These techniques require a considerable level of skill, often incur significant disruption to the fungal conformations and are typically suited to the isolation of characteristic reproductive structures for specific strain identification, rather than the examination of early hyphal differentiation.

### 4.1.1 Assessment of two-dimensional microbial development

One of the chief difficulties associated with studying the morphology of filamentous microorganisms is their significant three-dimensional character, even in solid culture, where the microbe may produce both aerial hyphae and penetrative structures that bore down into the substrate. Such three-dimensional arrangements complicate the visualisation of fungal conformations, as capturing morphological features in a single focal plane is often impossible, particularly at high magnification. One of the more successful means of managing this particular problem has been to cultivate the microbe of interest in a 'flow-through cell', a small chamber designed specifically to restrict the growth of the organism to two dimensions in a controlled environment. Such devices have been successfully applied to the study of *Mucor circinelloides* [13, 123], *Aspergillus oryzae* [4, 107, 147] and various *Mortierella* species [124, 125]. While such studies have provided invaluable data on the development of individual hyphal elements, they only permit the simultaneous study of a very small population and, as such, derivation of global, species-specific statistics is difficult. Furthermore, such an apparatus is only suitable for the study of submerged growth.

### 4.1.1 ASSESSMENT OF TWO-DIMENSIONAL MICROBIAL DEVELOPMENT

In designing a means of visualising fungal hyphae, of principal concern is the provision of a field of view that is predominantly free of artifact, provides a high-magnification, high-resolution representation of the microbe and provides good contrast between the hyphae and background, particularly if the intention is for the resultant images to be analysed automatically. While the cultivation of filamentous microbes in SSF has received considerable attention in the literature, many of the methods utilised for the visualisation of hyphal development do not meet the above criteria. Many studies of SSF have been of a relatively low-magnification capability, with assessment of mycelia often limited to the macroscopic scale and morphological measures have typically been limited to 'global' parameters, such as projected area of biomass [156, 180], colony fractal dimension [180, 181] or colony expansion rate, derived from manual measures of colony diameter [140, 180, 182, 183]. Other studies have focussed directly on quantification of metabolite production rather than on hyphal growth. Olsson reported a means of mapping the glucose and phosphorus uptake by *Fusarium oxysporum* on agar [40], while Jones and colleagues focussed on evaluating dye biotransformation by *Pycnoporus cinnabarinus* and *Phanerochaete chrysosporium* [131].

Where microscopic assessments have been made, efforts to restrict growth to two dimensions often involve the inoculation of cover-slips, microscope slides or Petri dishes with minimal volumes of media, which are subsequently viewed with bright-field optics [26, 108, 140, 184, 185]. Some methods involve the fixing and staining of the cultured cover-slip prior to observation [186]. Many require the application of a cover-slip on top of the culture to be scrutinised [118, 186, 187], 'compressing' the biomass, which inevitably results in disruption of the hyphae present. Nevertheless, this form of approach has yielded good quality, high-magnification images in some cases [118, 187], providing detailed information on hyphal extension. However, the population studied is typically very small and substantial manual intervention was

required in the analysis of the images. In other cases, samples of agar are excised from an existing culture and observed using bright-field or fluorescence microscopy [27, 28, 188]. Microscopic examination on substrates such as leaves often resulted in significant levels of artifact, requiring the development of imaging routines specifically for the purpose of recognising certain artifactual features, such as stomata [173]. More specialised techniques, such as confocal microscopy, have also been employed to visualise the penetration of hyphae into a solid substrate [189].

### 4.1.2 Membrane-immobilisation of filamentous microbes

An alternative approach involves the cultivation of filamentous microbes immobilised on an inert membrane, placed on top of a solid nutrient medium. Such an arrangement permits an ease of separation of biomass from the medium following a suitable period of incubation, which can then be processed as required prior to microscopic analysis. An additional advantage of such a system is the planar nature of the resultant fungal growth, as the presence of the membrane presents a physical barrier to hyphal extension into the substrate. Restricting growth to two-dimensions in such a manner facilitates ease of microscopic examination and subsequent imaging, as all biomass is predominantly presented in a single focal plane.

There are a limited number of studies in the literature involving the use of membranes in the culturing of filamentous microbes (Table 4.1). In some cases, the cultured membranes were subjected to image processing [157, 172], but the resultant images were typically of a low resolution and often contained significant levels of artifact. In the case of the method described by Reichl and colleagues, the skilful transfer of *S. tendae* mycelia from cellophane membranes to a microscope slide (by bringing the slide into contact with the membrane) was required prior to analysis with fluorescence microscopy, which may have incurred disruption to the hyphae [190]. However, the ability of the membrane to restrict growth to two dimensions

has been documented [110, 157, 172], although in some cases, this involved 'sandwiching' the culture between two membranes [157, 191], which may have incurred damage to the hyphae upon the destructive sampling of the microcosm. However, further potential application of such a system has been demonstrated in the production of high-magnification images of laccase localisation in *Pycnoporus cinnabarinus* hyphae by treating the membrane with microscopy-immersion oil, permitting the use of oil-immersion objective lenses [192]. The advantages of membrane-immobilisation outlined in these studies suggest that such a system warrants further investigation. The potential clearly exists for the production of planar, two-dimensional hyphal structures that may be routinely examined using high-magnification oil-immersion microscope lenses.

### 4.1.3 Aim of the work in this chapter

The principal aim of the work described in this chapter was to develop a two-dimensional growth assay by immobilising fungal spores on cellulose nitrate membranes, using *A. oryzae* as the model organism. The suitability of the assay for producing samples appropriate for the image analysis system described in Chapter 3 was investigated. Such a sample should consist of a low level of background and artifact while yielding contiguous high-contrast staining of fungal hyphae. As nitrocellulose membranes are rendered transparent with microscopic immersion oil, the use of high-magnification oil objective lenses is possible. Such examinations were pursued with a view to identifying fine details in hyphal structure, such as septation.

Means of optimising the assay were investigated, concentrating specifically on minimising processing time, maximising the contrast between stained hyphae and sample background, while minimising any disruption to the hyphal architecture. Finally, the use of membrane-immobilisation as a means of analysing samples of

**Table 4.1:** Reports in the literature of membrane-immobilisation of filamentous microbes

| Organism | Material | Report | Reference |
|---|---|---|---|
| Various | Cellophane | Growth kinetics of filamentous microbes determined by continuous monitoring of immobilised cultures | [1] |
| *S. tendae* | Cellophane | Cultivated on membranes prior to transfer to microscopic slides for fluorescent examination | [190] |
| *A. niger* | Polycarbonate | Membranes utilised to restrict growth to a layer of agarose | [105] |
| *T. viride* | Cellophane | Measures of local fractal dimension and branching complexity derived | [172] |
| *P. cinnabarinus* | Polycarbonate | Fractal dimension of membrane-immobilised cultures related to phenol-oxidase yield in SmF | [110] |
| *P. cinnabarinus* | Cellophane & polycarbonate | Laccase detected histochemically in hyphae by growing on membranes overlaid on agar | [192] |
| *N. crassa* | Cellophane | Cultivated between two sheets of cellophane in analysis of hyphal branching | [191] |
| *T. virens* | Cellulose acetate | Investigated effects of temperature on growth | [157] |

biomass taken from submerged culture was investigated, using both the conventional lactophenol cotton blue stain and calcofluor white, with a view to identifying sub-cellular details and active regions in the hyphae.

## 4.2 Materials & methods

For the initial 'proof-of-principle' experimentation, nitrocellulose squares (approximately 4 × 4 mm) were aseptically cut from a proprietary membrane (Millipore HAWG 047 SO; 0.45 $\mu$m) by use of a sterile scissors. Each nitrocellulose square was overlaid evenly onto the surface of a malt agar plate and then inoculated with 5 $\mu$L of a standardized conidial suspension ($1 \times 10^6$ spores ml$^{-1}$; Fig. 4.1). The plates were incubated at 25°C and test squares removed after various time intervals for drying, staining, and microscopic visualization. Membranes were dried in sterile Petri dishes (3 h, 25°C air incubator) and stained with lactophenol cotton blue (BBL Diagnostic Systems PL7054). The membranes were rinsed in PBS-Tween 80, re-dried at 25°C (3 h), and placed on microscope slides; a minimum volume of immersion oil was added (Olympus AX 9602), and images were captured at various magnifications (stated in figure legends). The optimised assay is described in Section 2.4.

### 4.2.1 Assessment of image background

Ten regions of background (320 × 240 pixels), defined as an area within an image devoid of any biomass, were manually selected in ten randomly selected images of membrane-immobilised hyphae. The green and blue bands of the RGB images were discarded and a 256-bin luminance histogram computed for the resultant 8-bit greyscale images. Each distribution was then aligned and plotted.

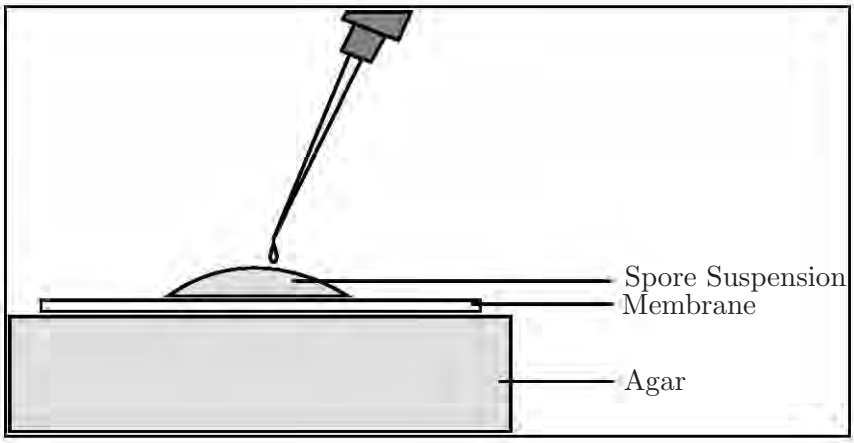


**Figure 4.1:** Schematic representation of inoculation of membrane on agar with spore suspension.

## 4.3 Results

### 4.3.1 Proof of concept

The oil-treated nitrocellulose membrane was found to provide a uniform background relatively free of artifact for the purposes of imaging. The grey-level distributions of ten samples of 'background' were plotted (Fig. 4.2) and found to approximate a scaled Gaussian distribution:

$$\frac{a}{\sqrt{2\pi\sigma^2}} \exp\left(\frac{-(x-\bar{x})^2}{2\sigma^2}\right) \tag{4.1}$$

where $a$ is a scaling factor, $\bar{x} = 164$ and $\sigma = 4$. This narrow distribution represents a relatively uniform image background, which is essential for accurate grey-level thresholding, whereby the object and background are partitioned based on an analysis of a bi-modal histogram (see Fig. 3.6).

The rudimentary assay was used to identify key developments in the growth of *A. oryzae* on a solid substrate. Spore germination was first noted at 8 hours but was not widespread until 9 hours post-inoculation (Fig. 4.3a); germ tubes emerging

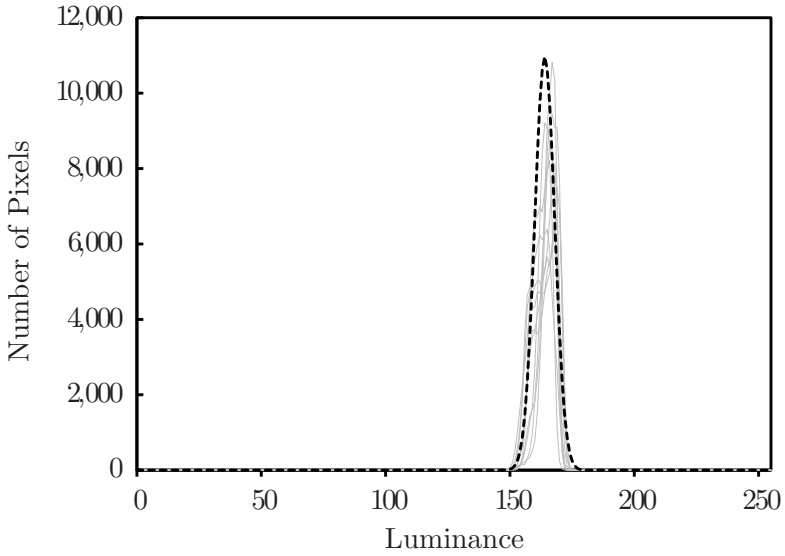


**Figure 4.2:** Distribution of grey-level luminance values (*in grey*) for 10 background samples (320 × 240 pixels). The histograms approximate a Gaussian distribution (*black dashes*) with $\bar{x} = 164$ and $\sigma = 4$.

from a cluster of spores appear to radiate away from the cluster's centre of mass (Fig. 4.3b). The beginnings of hyphal branching were first noted at 16 hours when small nodules began to form on the primary hyphae (Fig. 4.3c). The emergence of a second germ tube from the spore was often observed at this time (Fig. 4.3d).

The application of immersion oil permitted the use of oil immersion lenses directly on the sample, thereby allowing high-power magnification and the imaging of fine details (Fig. 4.4). While useful for the identification of septae, the imaging of hyphae at high magnification may also be of interest as a means of tracking hyphal morphogenesis [137], thus potentially providing kinetic data on the evolution of apical and sub-apical regions over time. Such analyses may be of value in studying the response of hyphae to changes in environmental conditions and/or metabolic activity. It has previously been demonstrated, for example, that the shape of the apical compartment of certain *Aspergilli* varies with the specific growth rate [90], while Haack and colleagues reported an increase in hyphal tip size during the feeding

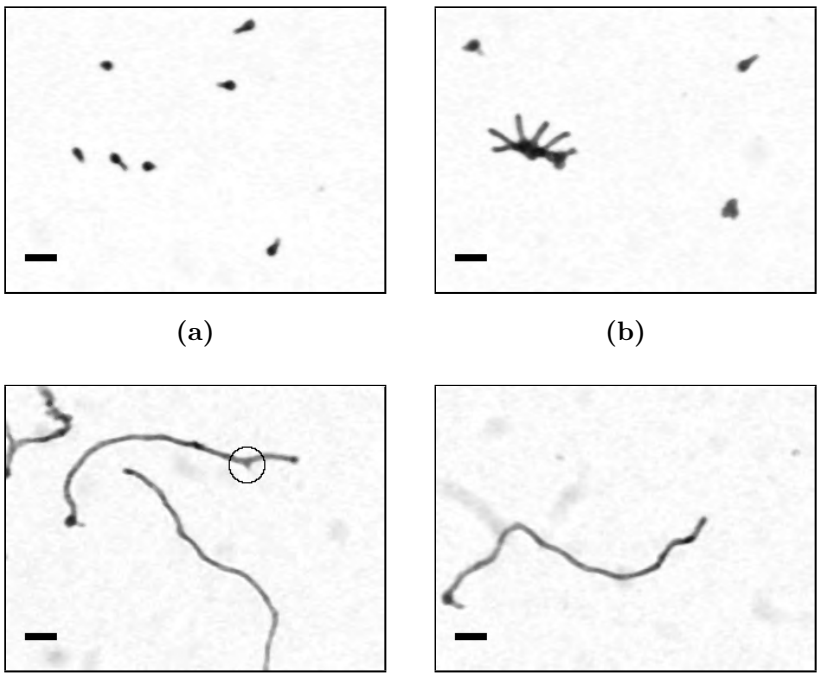


**Figure 4.3:** (a) Germ tube emergence from individual spores at 9 h (b) Germ tube emergence from spore cluster; the germ tubes appear to radiate outward away from the centre of mass (c) Emergence of branching hypha at 16 h (d) Emergence of 2nd germ tube at 16 h. All images captured at $\times$400 magnification (Bars: 15 $\mu$m).

phase of fed-batch culturing of *A. oryzae* [109]. Further studies have found that the hyphal diameter of *A. oryzae* is significantly reduced when the organism is starved of glucose [147]. However, such investigations were beyond the scope of this study.

### 4.3.2 Assay optimisation

Further development of the assay was undertaken in an attempt to maximise both the resultant image quality and the speed of assay execution, without compromising cell integrity or disrupting morphological conformations. Investigations focussed on minimising sample drying time and evaluating the effects of this accelerated drying on cell structure.

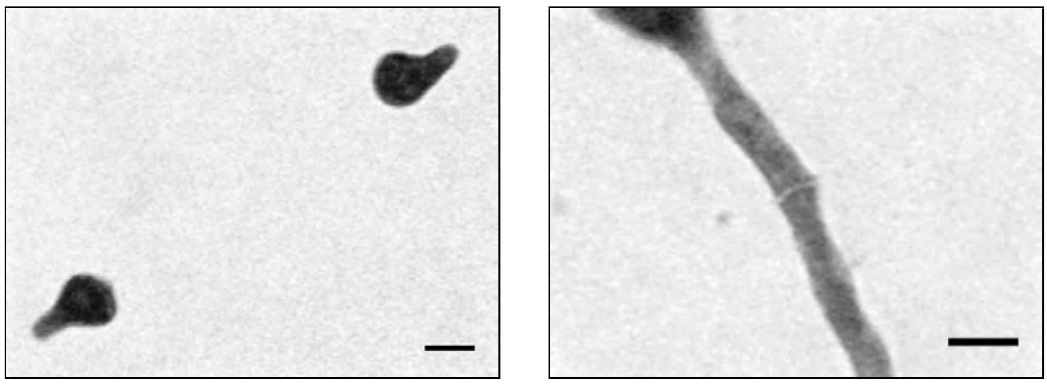

**(a)** **(b)**

**Figure 4.4:** (a) Germ tube emergence and (b) septation in *A. oryzae* visualized on nitrocellulose; the undulating nature of the hyphal surface is also apparent. Images were captured at $\times 1,000$ (Bars: 5 $\mu$m).

Contiguous staining of hyphal elements is essential to avoid misinterpretation of the field of view by the image-analysis routines. Staining of membranes while still wet was found to result in non-uniform, patchy staining of hyphae (Fig.4.5). While this did not pose significant problems for manual, qualitative examinations, it did result in an over-estimation of the number of discrete hyphal elements within a given sample and, consequently, an underestimation of hyphal length and number of tips when subjected to automated analysis. Within a typical experiment, it was found that up to 80% ($n = 50$) of the hyphal elements were misinterpreted as multiple objects within samples that were stained while wet. Drying of membranes before staining reduced the incidence of this artifact to less than 2% of cases.

Within certain limits of time and temperature, the drying of membranes was not found to adversely affect cell morphology. Drying at 25°C for 24 hours was without appreciable effect on spore size, but prolonged exposure (up to 72 h) resulted in a reduction of the mean projected area of the spore population (approximately 8%; Table 4.2). The drying of samples at temperatures up to 105°C had no discernible

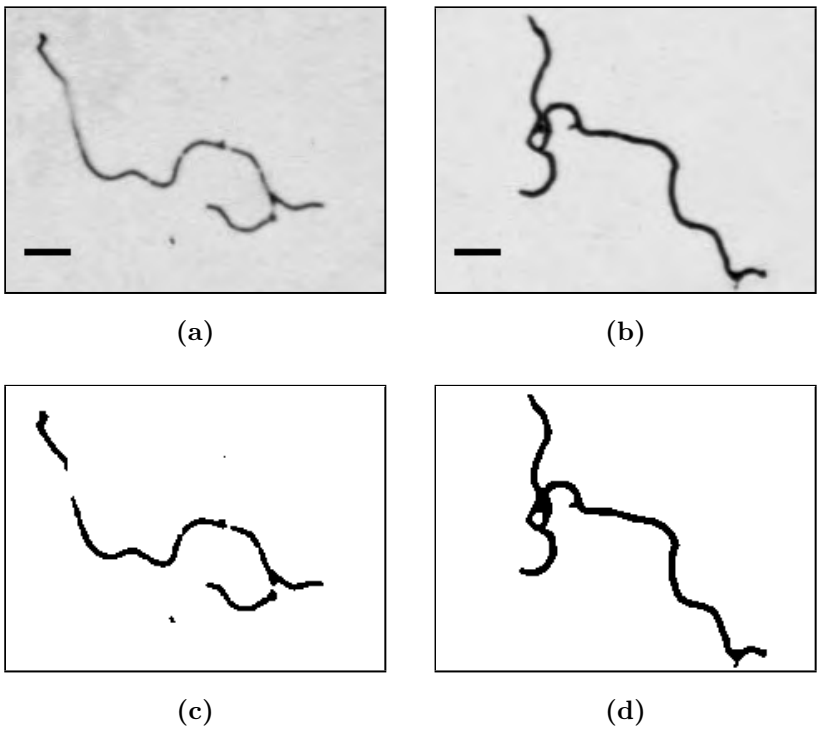


**Figure 4.5:** Staining wet membranes resulted in non-uniform stain uptake. (a) Samples of *A. oryzae* on cellulose nitrate membranes were stained while wet immediately upon removal from agar surface; (b) Samples were fixed and then dried at 65°C for 75 minutes prior to staining; (c) Binary image resulting from grey-level thresholding of 'a' (six distinct structures are produced); (d) Binary image of 'b' (a single hyphal structure produced). Bar: 30 $\mu$m.

impact on spore projected area or circularity if performed for a short time (10 min), but caused the cellulose nitrate membrane to wilt. No significant change in spore circularity was observed with any treatment.

An analysis of the size distributions of each population of spores subjected to these treatments provides an additional insight into the impact of accelerated drying (Fig. 4.6). Maintaining the spores at 25°C for 24 hours does not result in an appreciable change in the overall shape of the distribution, but extended exposure (72 hours) causes the histogram to narrow significantly, with a considerable reduc-

**Table 4.2:** Mean projected area ($A_p$) and mean circularity ($C$) of *A. oryzae* spores subjected to various drying treatments prior to staining, where $n$ is the size of each population. Errors represent 95% confidence intervals

| Drying temperature (°C) | Drying time (h) | $A_p$ ($\mu$m$^2$) | $C$ | $n$ |
|---|---|---|---|---|
| N/A | 0 | 7.7 ± 0.3 | 0.895 ± 0.003 | 726 |
| 25[1] | 24 | 8.2 ± 0.3 | 0.888 ± 0.003 | 2,915 |
| 25 | 72 | 7.1 ± 0.2 | 0.882 ± 0.003 | 768 |
| 65 | 1.25 | 8.1 ± 0.1 | 0.887 ± 0.002 | 2,505 |
| 105 | 0.17 | 8.4 ± 0.1 | 0.886 ± 0.002 | 2,315 |

[1] Average of two independent experiments.

tion in the number of spores recorded at larger projected areas. Drying spores at higher temperatures seems to result in a slight increase in projected area for the population overall. This may be a result of an increase in internal pressure within the spores arising from the increase in temperature, which produces a subsequent increase in volume. However, there is little change in the height or position of the mode of each distribution. A drying treatment of 65°C for 1.25 hours was selected for routine use; this enabled acceptable speed of processing without compromising cell morphology or the integrity of the membrane.

An important caveat to the use of drying procedures was found to be that a fixative be employed to maintain cell structure. Apparent rupturing of hyphal tips was observed in non-fixed samples that were dried prior to staining, with the effect being most pronounced when samples were dried at 65°C (Fig. 4.7). This rendered hyphal elements unsuitable for analysis, because the affected tips were incorrectly classified by the image-analysis system. Typically it was found that approximately 60% ($n = 70$) of hyphal elements exhibited at least one ruptured tip when dried at 65°C, but when samples were fixed before drying, this figure was reduced to

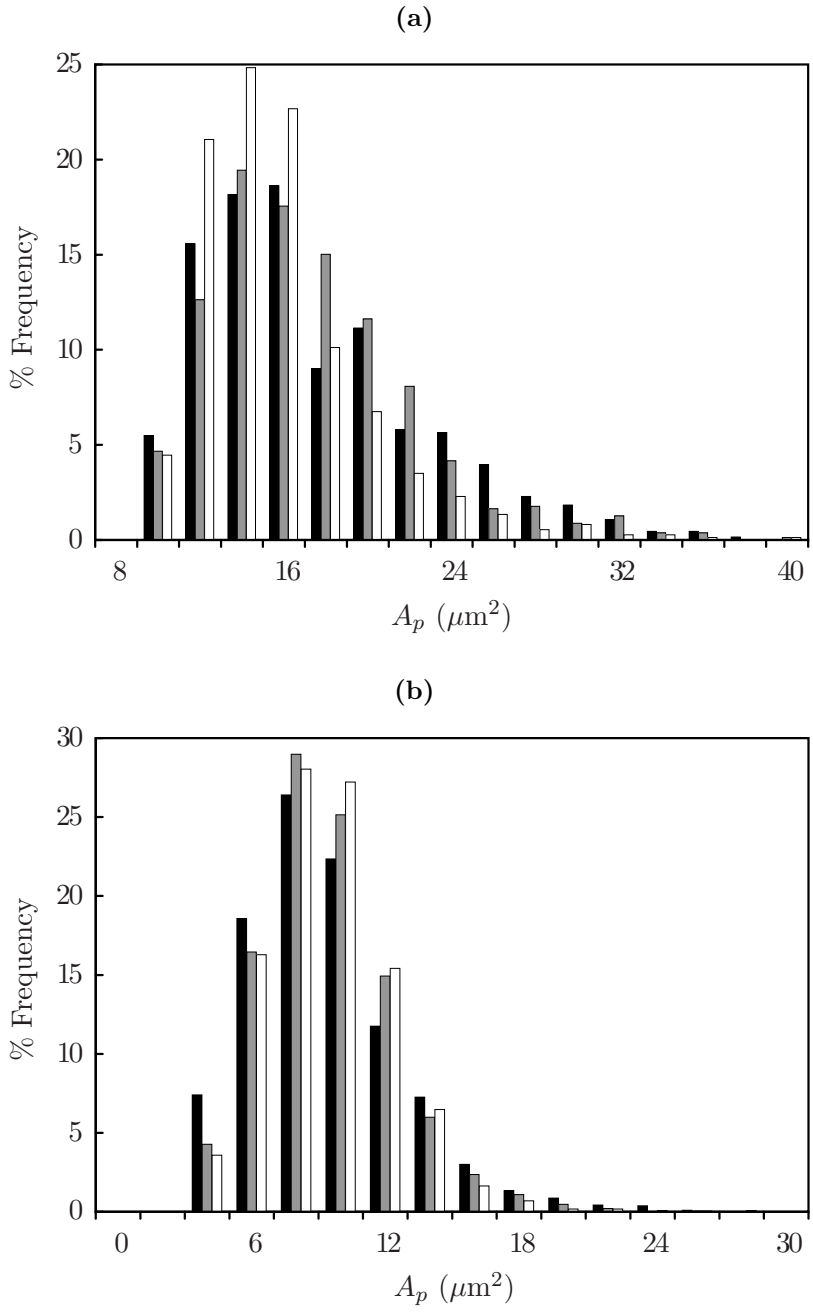


**Figure 4.6:** Comparisons of size distributions of populations of *A. oryzae* spores subjected to (a) 25°C for 0 (■), 24 (■) and 72 hours (□) ($n \approx 700$) and (b) 25°C for 24 hours (■), 65°C for 75 minutes (■) and 105°C for 10 minutes (□) ($n \approx 2,000$).

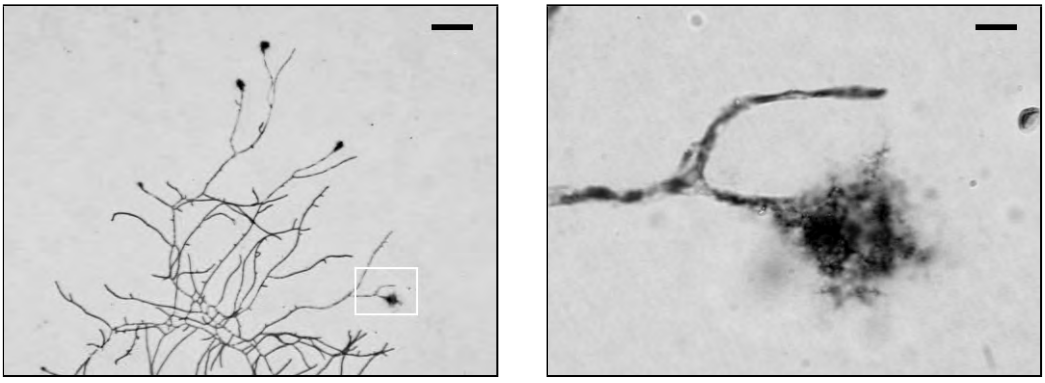

**(a)** **(b)**

**Figure 4.7:** Appearance of hyphal tips of *Aspergillus oryzae* when samples are dried without fixative prior to staining. (a) ×100; bar 100 $\mu$m. (b) ×1,000; bar 10 $\mu$m.

approximately 5% (based on manual observation). Exposure to lacto-phenol cotton blue or fixative caused the membrane to wilt slightly on contact, but extended exposure (up to 30 min) was not found to have any additional impact.

The influence of membrane composition on morphology was investigated and found to be significant (Fig. 4.8). While cellulose acetate membranes successfully confined the growth to two dimensions, the membranes were not sufficiently durable and were found to deform easily during processing. Cellulose nitrate membranes with pore sizes greater than 0.45 $\mu$m were also found to be unsuitable, as considerable three-dimensional growth resulted, which is difficult to image and quantify (Fig. 4.9). This may suggest that the fungus is capable of penetrating certain membranes, although the mechanism involved is not clear.

A modification of the assay for the examination of samples taken from submerged culture was also evaluated and found to be suitable for preparations stained with lactophenol cotton blue or calcofluor white (Fig. 4.10 & 4.11), a fluorescent stain that has previously been utilised to visualise septation and discriminate between

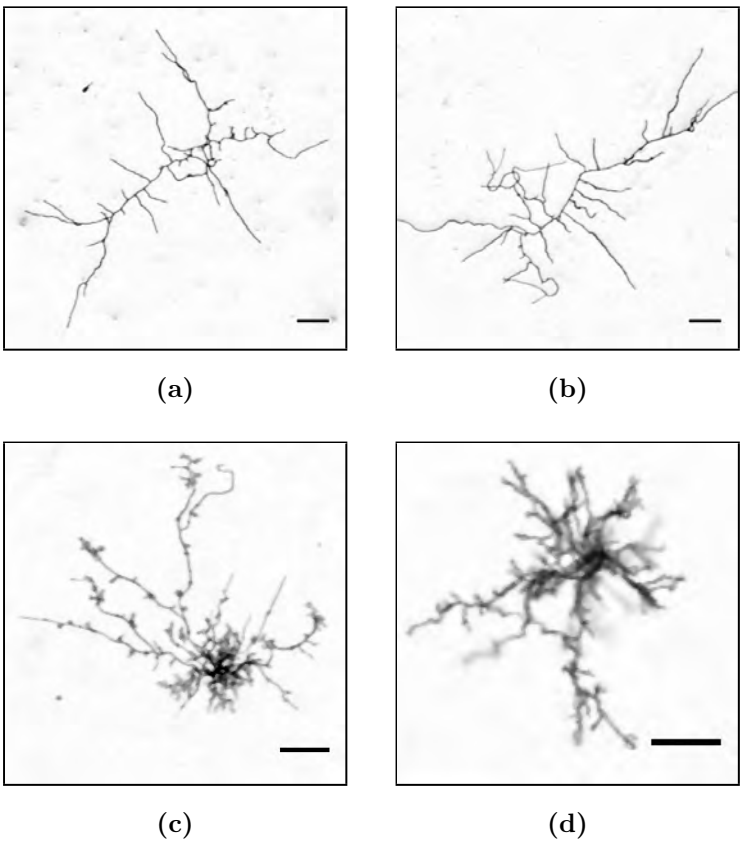


**Figure 4.8:** Variation in morphological form of *A. oryzae* when grown on different membranes: (a) 0.2 $\mu$m cellulose acetate (Sartorius 11107) (b) 0.45 $\mu$m cellulose acetate (Sartorius 11106) (c) 0.8 $\mu$m cellulose nitrate (Sartorius 11404) (d) 3.0 $\mu$m cellulose nitrate (Sartorius 11302). Bars 100 $\mu$m.

active and non-active hyphal tips in *A. oryzae* [84]. The filtration of material and subsequent immobilisation on a membrane reduced the complexity of the conformations from three dimensions to a single focal plane, permitting analysis of the structures present using the routines described in the previous chapter.

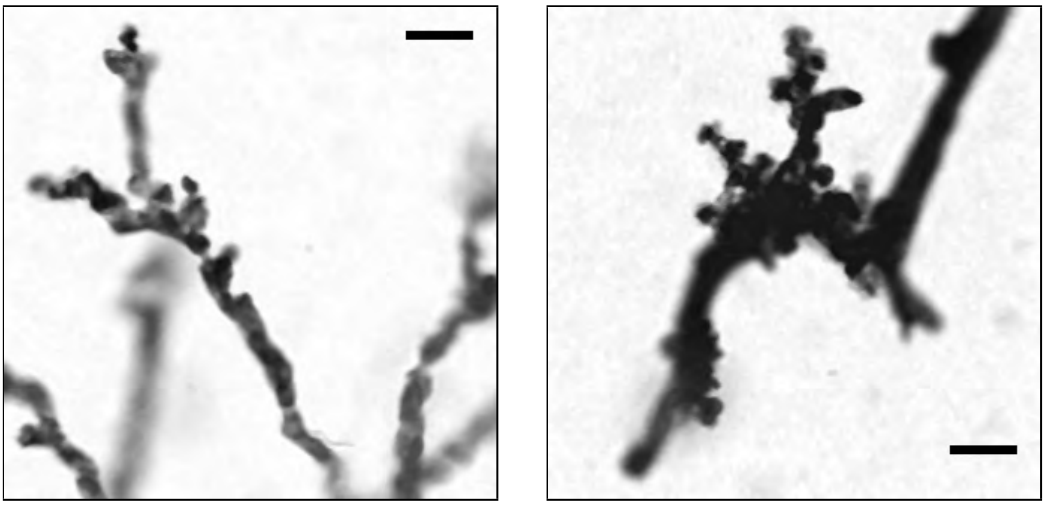

**(a)** **(b)**

**Figure 4.9:** High-magnification images ($\times 1,000$) of *A. oryzae* show extensive three-dimensional growth when cultivated on (a) cellulose nitrate (3.0 $\mu$m pore size) and (b) mixed cellulose ester membranes (0.45 $\mu$m pore size). Bars 10 $\mu$m.

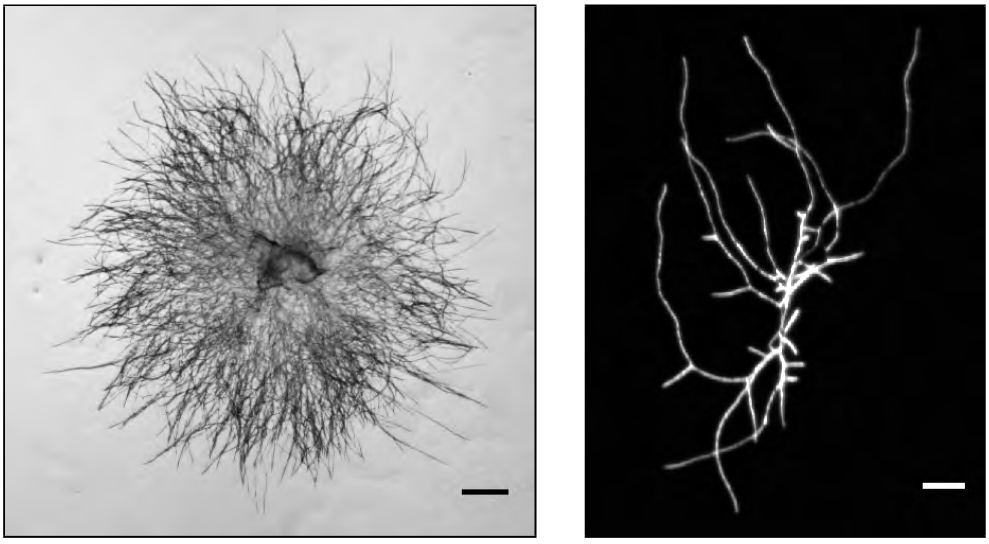

**(a)** **(b)**

**Figure 4.10:** Samples of *A. oryzae* grown in submerged culture stained with (a) lactophenol cotton blue (bar 50 $\mu$m) and (b) calcofluor white (bar 25 $\mu$m) and immobilised on cellulose nitrate membranes.

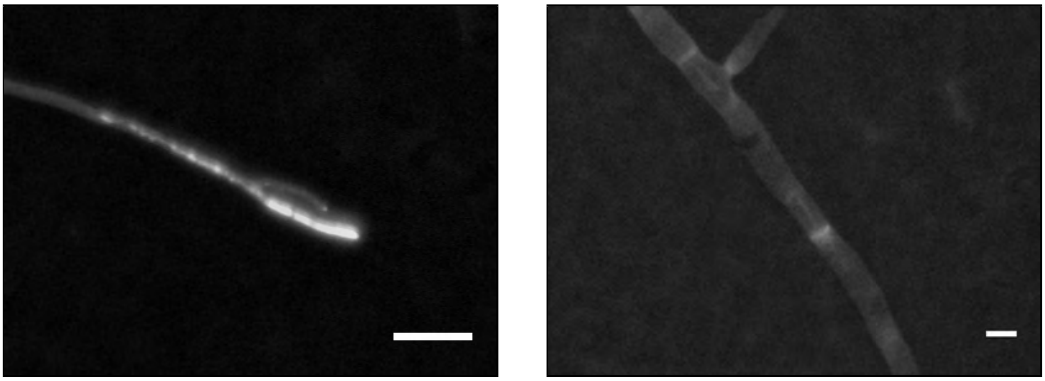

**(a)** **(b)**

**Figure 4.11:** Samples of membrane-immobilised *A. oryzae*, cultivated in submerged medium and stained with calcofluor white, showing (a) 'active' hyphal region (Bar 20 $\mu$m) and (b) septation (Bar 5 $\mu$m).

## 4.4 Discussion

There is currently a dearth of techniques available for the study of filamentous microbial development on solid substrates, particularly for analysis of early-stage differentiation ($<$ 24 hours post-inoculation). While reports of microscopic examination of fungi have been common in the literature [136], the majority have focussed on the submerged culture format. Conventional techniques for the examination of filamentous microbes on solid culture, such as those involving 'tape-lifts' [178, 179], require considerable skill and experience to master and often incur significant disruption to the fungal conformations. Given the potential for differential gene and protein expression in solid culture compared to the submerged format [65, 68, 193], the ability to study the growth of filamentous microbes in detail in such a system would be highly advantageous and may lead to a greater understanding of the relationship between morphology and productivity.

In presenting complex fungal conformations in an essentially two-dimensional format, membrane immobilization confines cultures to a single focal plane, while

maintaining the natural spatial arrangement of vegetative mycelia encountered in solid state culture. The membrane also presents a very low level of background or artifact (Fig. 4.2), which is highly advantageous for images that are to be analysed automatically, assuming the biomass present is uniformly stained. In such a scenario, the image histogram will be characterised by two well-separated peaks (bimodal; Fig. 3.6) and object segmentation is easily achieved by calculating a single grey-level threshold. While eliminating artifact completely is obviously impossible, minimising the occurrence of small particles is desirable. The system developed in Chapter 3 is capable of identifying objects that conform to a certain morphological description, but a small level of artifact will inevitably be incorrectly classified as hyphae and/or spores and included in the results. As such, measures to minimise the occurrence of artifact within the sample preparation should always be exploited. Due to the use of filtration in sample preparation, the possibility exists that sediment may accumulate on the membrane surface during processing and/or inoculation. It is therefore important to ensure that all solutions used are completely clarified so as to minimise the levels of artifact present in the resultant sample.

Perhaps the most significant advantage of this method of fungal examination is the ability to use high-power oil-immersion objective lenses, which permit the identification of fine details in the hyphae (Fig. 4.9 & 4.11). The versatility of the assay is further emphasised by the demonstrated compatibility with fluorescent staining (Fig. 4.10b & 4.11). Studies of filamentous microorganisms in solid culture using fluorescent stains have been quite rare, so such a system is of considerable potential benefit in, for example, quantifying active regions of hyphae in solid culture using calcofluor white staining. Furthermore, combining fluorescence microscopy with high-power magnification provides potential new perspectives on solid-state development.

Additional advantages of this system include the ability to modify the nutri-

ent environment by simple membrane transfer. Such was employed by Ishida and colleagues in their investigation of gene expression by *A. oryzae* [193]. It is also well suited to investigating diffusion-mediated processes, such as antimicrobial susceptibility testing, or trophic responses to substrate gradients, for example. Other potential applications include investigations of germinative potential of populations of spores in response to various stimuli [26].

Membrane-immobilisation also permits the simultaneous examination of a relatively large number of hyphal elements, the size of the population being limited only by the area of the membrane. All elements on a single membrane are subjected to the same treatments during sample preparation, thus ensuring consistency within the population. Archiving of membrane-bound material is also possible, as the culture is fixed, stained, and killed during specimen preparation. It was found that samples stored for up to three years after preparation were still suitable for imaging.

The assay is, however, highly sensitive to the choice of membrane used as support (Fig. 4.8). This is an important consideration as it has been demonstrated that membranes with similar product descriptions produced by different manufacturers can result in different growth patterns (not shown). In some cases, it has been found that even the orientation of the membrane can influence the morphology of the organism. Indeed, Jones and colleagues claimed that membrane orientation can affect both cellular attachment and stain uptake [194], while a difference in membrane pore size was found to alter gene expression in recombinant *A. oryzae* [193]. Membrane-immobilisation also involves a considerable amount of time devoted to sample processing (approximately 3 hours). However, this compares very favourably with other reports of processing times for membrane-bound cultures of up to 24 hours, which also involved a much greater degree of subtle sample manipulation and sophisticated equipment [194].

It has been reported that the use of membranes in SSF is not representative of growth in the absence of a support, with oxygen diffusion in particular being restricted and, as a result, growth and metabolite production being limited [195]. However, the study in question examined growth from approximately 20 hours post-inoculation onwards, and significant deviation between the membrane-bound culture and the control were not observed until approximately 40 hours post-inoculation. While these findings should obviously be considered when membrane-immobilised cultures are a target of study, the aim in the development of the assay reported here was to provide, in particular, a means of analysing early-stage hyphal differentiation (0 - 24 hours). As such, concerns regarding oxygen limitations are somewhat unwarranted in this context.

Of further consideration is the use of lactophenol cotton blue (LPCB) as a means of enhancing contrast for the visualisation of fungal preparations. It has been noted that only young, recently developed hyphae tend to stain intensely when exposed to LPCB, such as those at the periphery of a colony, for example. Those hyphae that are more distal to the colony perimeter tend to remain completely unstained, or else take on a very pale blue appearance. This may be explained by a transformation in the composition of the cell wall as hyphae mature [7]. As such, LPCB may only be suitable for staining actively-growing hyphae. Such an observation has been made in cultures of *A. oryzae* stained with calcofluor white [84]. Considering the mechanisms of stain uptake to be similar for both compounds, this may infer that LPCB is also not suitable for staining older, 'non-active' regions. However, such a phenomenon could prove useful in SSF, whereby the actively growing region at the colony periphery could be easily identified. The prevalence of 'patchy' uptake of LPCB noted in this study on hyphae that are not dried prior to staining (Fig. 4.5) calls into question the use of LPCB-stained wet-mounts and their suitability for image analysis [109, 119, 122, 175].

The system has also been demonstrated as an effective means of examining fungal growth in submerged culture. By filtering samples through a membrane, rather than, for example, drying directly onto a microscope slide, any solutes present in the broth are removed, reducing the level of artifact in the subsequent field of view. This also results in the fungal conformations being presented in essentially two dimensions, facilitating an ease of analysis. While fungal biomass cultivated in submerged medium often has a significant 3-dimensional character, it is common for the sample to be 'compressed' into two dimensions, generally by 'wet-mounting' between a microscope slide and cover-slip [49, 119, 122, 149]. Compared to pipetting samples onto a slide, decanting a sample into a filtration device also obviates any concern about selectively sampling objects below a certain size and also aids in the uniform distribution of biomass across the membrane surface. Membrane immobilisation also obviates the need for multiple slide preparations (depending on membrane area), thus ensuring further consistency. This may be particularly relevant in the event that calculations of biomass per unit volume are being derived.

Examination of the development of filamentous microbes on solid substrates has typically been of low resolution capability and the subsequent analysis may involve considerable human intervention [145]. However, membranes have previously been used in the assessment of fungal growth on solid substrates and have been combined with image processing and light microscopy, but generally with low magnification, low resolution capability. Cellulose acetate membranes have been used to study the growth of *Trichoderma virens* [157] in conjunction with a dissecting microscope. Image analysis has been used in the enumeration of the fractal dimension of *Pycnoporus cinnabarinus* [110] and *Trichoderma viride* [172] colonies immobilized on polycarbonate and cellophane membranes, respectively. The quantification of septation in *Streptomyces tendae* was achieved using cellophane membranes in conjunction with image analysis [190], but this method involved the highly skilful transfer of mycelial

matter from the membrane to a microscope slide. Polycarbonate membranes were also used in the immobilisation of *Pycnoporus cinnabarinus* prior to histochemical laccase detection [192] and to limit growth to two dimensions in the localisation of protein secretion by *A. niger* in solid culture [105].

## 4.5 Conclusions

There is renewed interest in the solid culture format, due in part to recent findings suggesting differential metabolite expression compared to submerged culture. While a variety of organisms have been studied in the literature in order to relate morphology to metabolite excretion, the vast majority of these studies have focussed on the submerged culture format. Those that have investigated the solid culture format have generally been of a low-resolution, low-magnification capability, or else are suited to the study of just a small population. There is thus a need to develop systems suitable for the study of filamentous microbes on solid substrates, particularly with a view to generating samples suitable for presentation to an image analysis system.

The use of inert membranes to restrict growth of filamentous microbes to two dimensions has been reported in the literature and their use was investigated here. The oil-treated membrane-immobilised culture presented a high-contrast, low-artifact field of view, suitable for imaging and automatic analysis. A low level of background artifact was encountered and, when dried prior to staining, hyphae exhibited high-contrast elements, easily segmentable from the background. The effect of drying of samples prior to staining was not significant.

Of particular significance is the provision of an ability to observe solid-cultured samples with high-power, oil-immersion objective lenses, permitting the capture of fine details. Such a capability may be of particular use in the study of hyphal mor-

phogenesis. The utility of the method in the examination of samples taken from submerged culture was also demonstrated, reducing the complex conformations found in a typical fermentation from three down to two dimensions, facilitating an ease of imaging and subsequent analysis. A compatibility with fluorescent staining was also shown, with fine details such as active hyphal regions and septation illustrated.

The utility of the membrane-immobilisation system demonstrated here suggests that, in conjunction with image processing, such a culture format would prove useful for quantitative assessment of early filamentous microbial development. The examination of a large population of mycelia is facilitated, each of which is simultaneously subjected to the same treatment (ensuring sample consistency), resulting in high-contrast samples with low levels of artifact, suitable for accurate automated analysis. There currently exists a pressing need for such studies, given the lack of computational methods for solid-state fermentations.

# Chapter 5

# Examination of the Growth Kinetics of *Aspergillus oryzae* in Solid-State Fermentation

## 5.1 Introduction

An understanding of the kinetics of fungal development is fundamental to the rigorous design of fermentation processes, as the time-course of production is intrinsically linked to the rate and mode of growth. Perturbations to the rate at which biomass is produced, or alterations to the morphological form that this biomass takes, will have implications for productivity. Furthermore, there is emerging evidence suggesting a fundamental link between kinetic parameters of growth at the microscopic level and resultant macroscopic conformations [107, 125, 152]. Hence, there is significant potential utility in the quantification of structural variation at the microscopic level.

### 5.1.1 The temporal analysis of micro-morphological development

The life-cycle of filamentous microbes generally commences as a single spore, which is typically a few microns in diameter. Upon activation, the spore begins to grow in size, with the increase in diameter generally being linear with respect to time [4, 7]. When a critical size is attained, a germ tube emerges, the tip of which accelerates away from the spore until a constant linear rate of elongation has been reached [4].

When the germ tube reaches a certain length, a lateral branch is formed behind the advancing apex, which accelerates to the same constant rate of elongation [7]. This process continues as long as conditions to support this linear rate of tip extension are met. Exponential growth is attained as a result of each branch producing further branches at a constant specific rate, all of which attain the same constant linear rate of growth, and a composite structure termed a 'mycelium' develops. The increase in biomass ($x$) may thus be described as:

$$\frac{dx}{dt} = \mu x \tag{5.1}$$

where $\mu$ is described as the specific growth rate ($h^{-1}$). The critical branch length that results in a new branch being spawned is referred to as the hyphal growth unit ($L_{hgu}$), which is approximately equal to the total hyphal length ($L_{th}$) divided by the total number of tips ($N$) of any given mycelium [38]:

$$L_{hgu} = \frac{L_{th}}{N} \tag{5.2}$$

This value will tend to be approximately constant across all mycelia within a given population.

Considering that mycelial growth involves the duplication of a constant hyphal growth unit, then $L_{th}$ and $N$ must increase exponentially at approximately the same specific growth rate. This was first demonstrated experimentally by Trinci [1], who cultivated colonies on cellophane-covered solid media and obtained morphological measures from enlarged photographic prints. After an initial period of discontinuous branch production, exponential growth was observed, with measured specific growth rates varying from approximately 0.25 $h^{-1}$ for *A. nidulans* up to 0.60 $h^{-1}$ for *Mucor hiemalis*. Spohr and colleagues produced similar metrics in their study of *A. oryzae* mycelia, cultivated submerged in a small 'flow-through cell' [4]. The principle advantage of such a system is the ability to monitor the develop-

ment of individual elements, and even individual hyphae, from a single spore, up to a mycelium several millimetres in length. Similar systems have since been used to analyse the early growth stages of *M. circinelloides* [13, 123] and various *Mortierella* species [124, 125]. However, the continuous monitoring of individual mycelia, while providing valuable physiological data, does not permit the examination of large populations, which is essential for the statistical characterisation of fermentation processes.

Evidence exists for a link between micro-morphological development of filamentous microbes and macro-morphological form. For example, Park and colleagues concluded that species of *Mortierella* exhibiting a high branch formation rate formed 'pellet-like' aggregates with a distinct core, while species attributed with a low branch formation rate formed hyphal aggregates without cores [125]. In addition, Müller and colleagues found that a mutant strain of *A. oryzae* that exhibited a greater degree of hyphal branching (with respect to a wild-type strain) was less likely to form large, inseparable clumps in submerged culture [107]. It was also suggested that the positioning of branches (apically or sub-apically) may affect the formation and dimension of macroscopic structures. It has also been demonstrated that biomass aggregation is directly related to the specific growth rate in the early stages of *Aspergillus niger* submerged cultivation [196, 197].

Recently, digital image processing has been utilised as a means of elucidating kinetic data [4, 45, 106, 107, 123, 125, 126, 140, 147, 156, 157, 175, 198]. Conventionally, parameters such as the specific growth rate were calculated based on, for example, physical measurements of biomass content per unit volume of fermentation broth. However, it is possible to derive the same rate measurements from an analysis of digital images, whereby the projected area or length of these elements is considered to be proportional to the biomass present in the system. This obviously assumes that the density of all elements in the population is constant and that the

diameter of all hyphae in the population is approximately equal. While there is evidence that individual hyphae approximate ellipsoids rather than cylinders [137] and that hyphal diameter appears to be proportional to the specific growth rate [126, 147], studies have demonstrated a close relationship between growth rates derived from image analysis and those derived from measures of dry cell weight [45, 106].

By employing image processing techniques, which permit the rapid quantification of fungal morphology, the growth kinetics of a large population of mycelia (such as that present within a bioreactor) may be accurately determined. Carlsen and colleagues successfully characterised the development of *A. oryzae* in batch culture using such an approach, producing data such as the specific growth rate, the specific branching rate and the mean tip extension rate [45]. Similar data was produced by Spohr and colleagues in their comparative assessment of different strains of *A. oryzae* and it was suggested that a more densely branched strain may have been favourable for protein production [106]. While particular kinetic parameters can vary from one individual hyphal element to the next [4, 187, 198], simple equations can be derived to describe the average kinetic properties of a large population of hyphal elements, thus permitting the kinetic analysis of fermentation processes involving filamentous microbes.

### 5.1.2 Influences on growth kinetics

There is evidence in the literature suggesting that the specific rates of development may be influenced by a variety of factors. These include, but are not limited to, pH [45], temperature [45, 157], available oxygen concentration [140] and agitation speed in submerged culture [79, 81]. The morphological form adopted by an organism in submerged culture can also affect the specific growth rate, due to substrate limitations in pellets [45]. Variations in temperature, pH and water activity have also

been reported as significant in determining rates of spore swelling and germination in *Penicillium chrysogenum* [26] and *Rhizopus oligosporus* [28].

Variations in substrate concentration are one of the more common means of effecting a change in the growth kinetics of microbes. Available evidence suggests that in many organisms, the response of the growth rate to changes in carbon source concentration may be described using Monod kinetics, where a saturation constant, typically denoted $K_s$, is the rate controlling factor [4]. A relationship between dilution rate and the specific growth rate of *A. niger* in chemostat culture has been demonstrated [199], while Pollack and colleagues noted that the growth of a glucoamylase producing strain of *A. oryzae* ceased when starved of glucose, before growth recommenced at a significantly reduced specific growth rate, fuelled by endogenous carbon [147]. Müller and colleagues noted a small decrease in the specific growth rate of both a wild-type strain of *A. oryzae* and a mutant strain at a low glucose concentration [107].

Variations in media composition have also been demonstrated as a successful means of inducing a change in the dynamics of hyphal development. The specific growth rate of *A. niger* was higher in the presence of sucrose compared to glucose and fructose [175], while it has also been reported that the addition of kaolin had a positive effect [98]. McIntyre and colleagues described an influence of media composition on the maximum specific growth rate of *Mucor circinelloides* (syn. *racemosus*) [200], but the specific growth rate of *M. circinelloides* was later reported to be relatively independent of both carbon source type and concentration [123]. Meanwhile, the concentration of both carbon and nitrogen sources was found to have a significant impact on the growth kinetics of *Mortierella alpine* [124].

### 5.1.3 Aims of the work in this chapter

Despite this significant progress in elucidating relationships between kinetic parameters of growth in filamentous microbes, the majority of the aforementioned studies have focussed on the submerged culture format. As such, there is currently a dearth of 'micro-analyses' of filamentous microorganisms on solid substrates. The aims of the work presented in this chapter were to (a) examine the kinetic development of *A. oryzae* on a solid substrate, using the system described in Chapters 3 and 4 (b) establish the basic kinetic parameters for this system and (c) investigate whether a change in media composition results in a change in kinetic parameters.

## 5.2 Materials & methods

Solid state fermentation of *A. oryzae* was carried out on either malt agar or the basal medium (BM) described in Section 2.3 supplemented with 17.0 g $L^{-1}$ Agar No. 1 (Lab M, Lot Q28626/207), 5 g $L^{-1}$ yeast extract (Oxoid, Lot 876584) and 2.0% (w/v) soluble starch ($BM_S$) or glucose ($BM_G$). The media were adjusted to pH 7.0 (unless otherwise stated) prior to sterilisation. Immobilisation of fungal spores for solid culturing and the processing of solid-state-cultured membranes for image analysis was as described in Section 2.4.

Fungal micro-morphology was quantified using automated image analysis, as described in Section 3.4.1. Semi-automatic image analysis was also performed to validate the automatic system. Noise removal was performed according to the automatic method. Grey-level thresholding and selection of hyphal elements from the image were both performed manually, as was artifact removal and the filling of any breaks or holes in the hyphal elements. The elements were then skeletonised and quantified according to the automatic method; the pruning of the skeleton was omitted from the semi-automatic method as artifact removal was performed prior

to skeletonisation.

## 5.3 Results

### 5.3.1 Kinetics of spore swelling

In an effort to establish appropriate values for the threshold variables, $A_{p,\,min}$ and $C_{s,\,min}$, a series of analyses was performed with $A_{p,\,min} = 0.0$ and $C_{s,\,min} = 1.0$, which resulted in all objects present within a given image being included in the output data (Fig. 5.1). All of the area ($A_p$) distributions have a small mode in the approximate range 2 – 4 $\mu$m$^2$ (Fig. 5.1a). It is likely that the objects that fall in this range are predominantly artifacts, as the shape of all sixteen distributions is very similar over this interval. A value of 3.0 $\mu$m was therefore considered suitable for $A_{p,\,min}$ to exclude artifacts.

Distributions compiled to compare circularity values presented a more complex picture. Four of the distributions are comparatively flat in the approximate range $0.2 < C < 0.8$, before rising to a sharp peak at $C \approx 0.95$. These represent samples containing germinated spores, the analysis of which did not involve the application of the 'watershed' algorithm to separate touching objects (see Section 3.3.4), hence the wide range of $C$ values, resulting from hyphae, clumps of spores and other artifacts. However, most of the other distributions appear to display a similar peak at $C \approx 0.95$. Most artifacts tend to be rather small and approximately circular, so discriminating between spore and artifact in terms of circularity is virtually impossible. However, evidence in the literature suggests a relatively high value of $C$ ($\sim 0.94$) for spores [4]. Given this fact and the data presented in Figure 5.1b, an initial value of 0.8 was chosen for $C_{s,\,min}$ and the effect of varying this between 0.70 and 0.85 is discussed later in this section.

With these thresholds in place, the system was used to study the development of

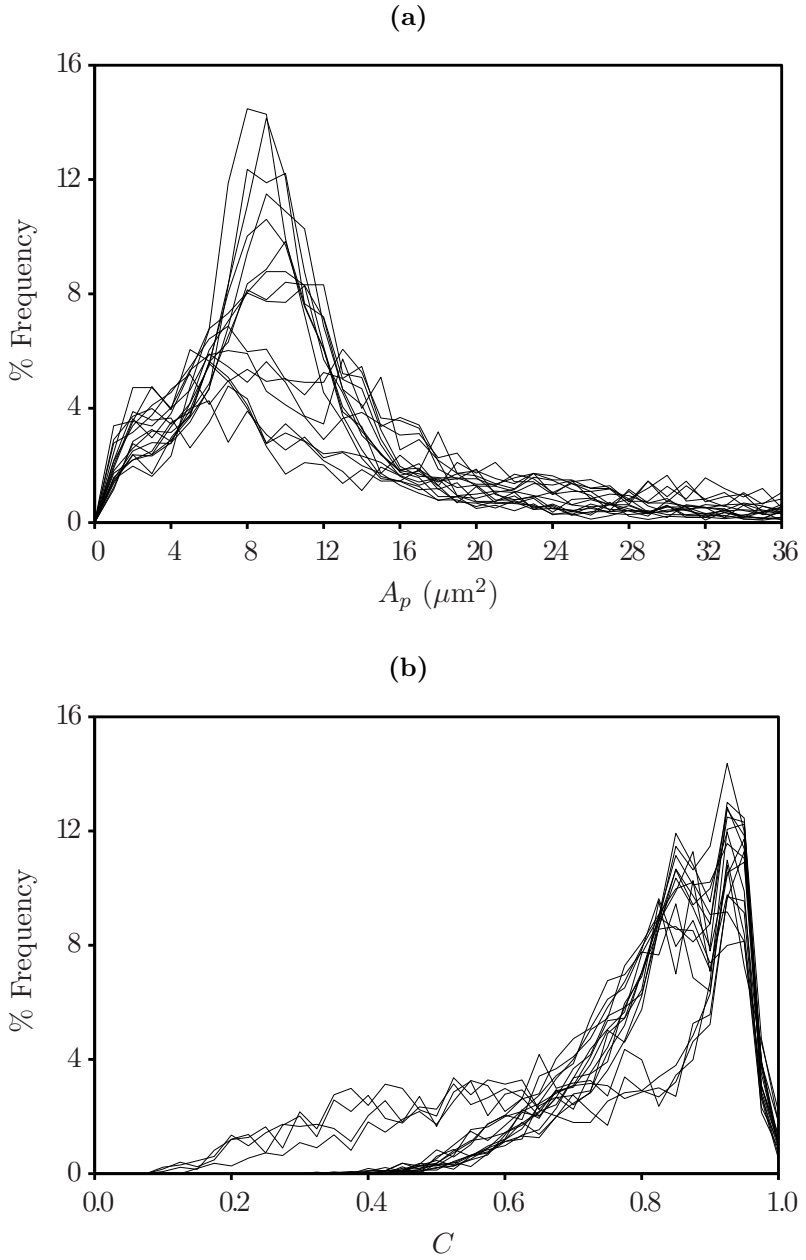


**Figure 5.1:** Distribution of (a) the projected area ($A_p$) and (b) circularity ($C$) of *A. oryzae* spores, based on an analysis of sixteen different samples 0 – 8 hours post-inoculation.

*A. oryzae* spores on malt agar from 0 to 8 h (Fig. 5.2). Similar to the value of 4 $\mu$m reported by Agger and colleagues [126], the initial mean spore projected area of 8.5± 0.1 $\mu m^2$ at inoculation corresponds to an equivalent spore diameter of $3.3 \pm 0.4$ $\mu$m. An increase in mean spore projected area of approximately 30% was observed from 0 to 6 h, corresponding to an increase in mean equivalent spore diameter of 0.45 $\mu$m (and a linear swelling rate of 0.08 $\mu m\ h^{-1}$). Germ tube emergence from a large number of spores had occurred by 8 h, resulting in a circularity value of less than 0.8 and their subsequent exclusion from the analysis. Removal of such large objects resulted in a decrease in the measured mean projected area at this time point. The circularity of the spores was found to remain relatively constant as projected area increased from 0 to 6 h, as previously reported for individual *A. oryzae* spores in submerged culture in a flow-through cell [4].

The mean projected area of spores may not give an accurate representation of the swelling process, as each sample was found to contain a wide range of spore sizes, particularly at later time points (Fig. 5.3). The projected area of most spores in the inoculum (0 h) was in the range 5 – 13 $\mu m^2$. Additionally, it was known from the routine preparation of spore stock suspensions that approximately 60% of spores were non-viable when thawed from frozen (as judged by a failure to germinate over 48 h during the total viable count procedure on malt agar, compared with an original total count performed using a Neubauer chamber). After incubation for 8 h, the projected area of such non-viable spores should not have increased, and it is reasonable to assume that most non-viable spores still occupied the size range of 5 – 13 $\mu m^2$. However, the possibility of viable spores exhibiting a small projected area in the same range, even after 8 h, cannot be eliminated, as it is apparent from the size distributions that swelling rates can vary to a large extent among different spores. Consequently, excluding non-viable spores from the analysis is difficult to achieve, because they cannot be distinguished on the basis of size alone.

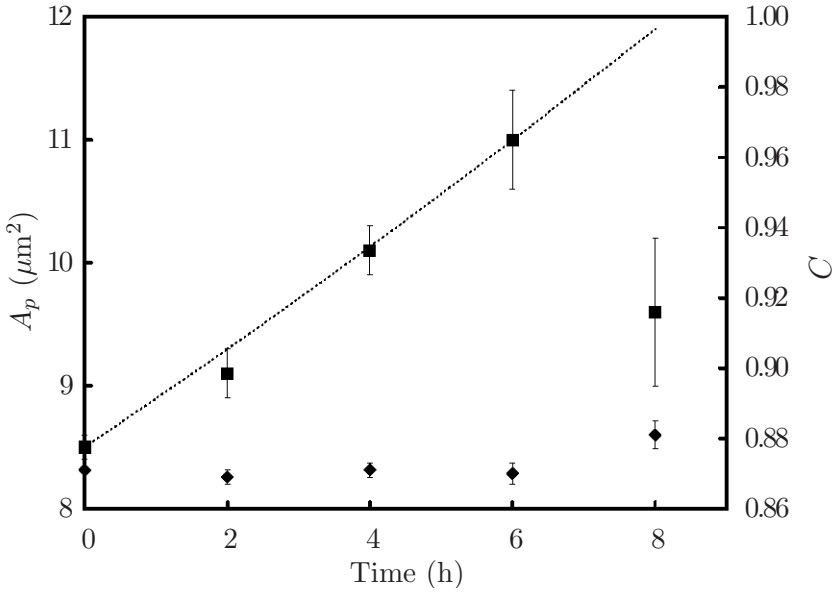


**Figure 5.2:** Mean projected area ($A_p$; ■) and mean circularity ($C$; ♦) of *A. oryzae* spores incubated on cellulose nitrate membranes on malt agar at 25°C. $A_{p,min}$ = 3 $\mu$m$^2$, $C_{s,min}$ = 0.8. The increase in mean equivalent spore diameter ($D_s$) was approximately linear at a rate of 0.08 $\mu$m h$^{-1}$ (dotted line). An average of approximately 1,500 spores were analysed per time-point from 0 to 6 h and 350 at 8 h. Error bars represent 95% confidence intervals.

Specifying a minimum projected area threshold to exclude these non-viable spores would most likely also exclude an unknown number of viable spores. Such a wide variation in spore sizes and swelling rates has previously been reported in the study of *Penicillium chrysogenum* in submerged culture [129].

*Influence of media composition on kinetic parameters*

The use of different substrates was found to have little influence on the swelling rate of *A. oryzae* spores (Fig. 5.4a). There were no statistically significant differences in mean spore projected area ($A_p$) at 2, 4 or 6 hours post-inoculation. The average rate of increase was found to be approximately 0.4 $\mu$m$^2$ h$^{-1}$, corresponding to an increase in spore diameter of approximately 0.07 $\mu$m h$^{-1}$. There was however, a considerable

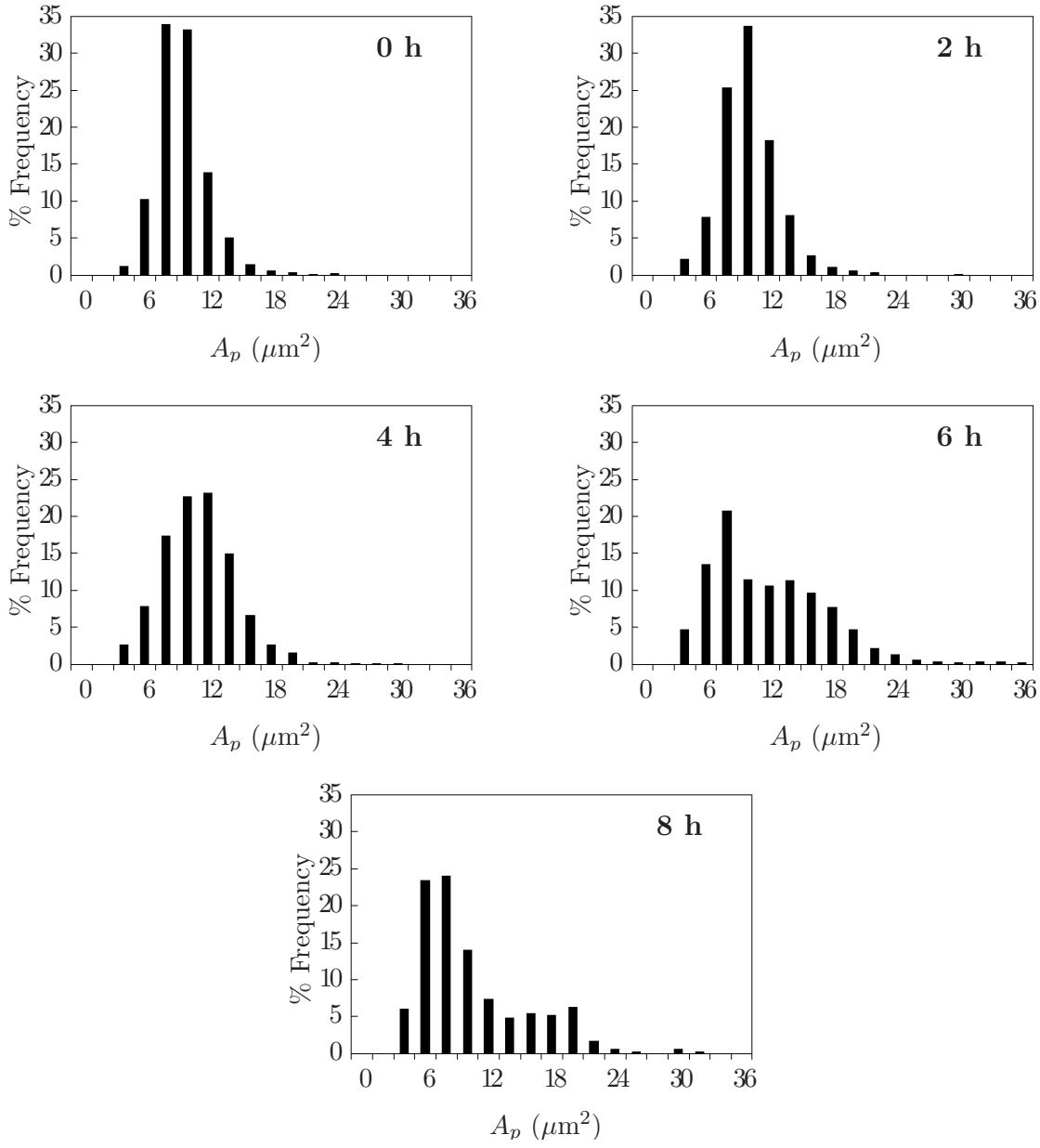


**Figure 5.3:** Comparisons of size distributions of populations of *A. oryzae* spores. Spores were incubated on mixed cellulose ester membranes on malt agar at 25°C and analysed at the time intervals shown ($A_{p,min} = 3$ $\mu$m$^2$, $C_{s,min} = 0.8$).

difference apparent at 8 hours, where those spores that had not germinated were substantially larger on $BM_G$ compared to both BM and $BM_S$. This may suggest that spores on $BM_G$ have taken longer to germinate and a comparison of the size distributions of those spores incubated on malt agar for 6 hours and those incubated on $BM_G$ for 8 hours indicates that the two populations are at a similar stage of development (Fig. 5.5). However, it must be remembered that the analysis of these two populations was not identical, with no watershed applied in the case of the 8-hour-old $BM_G$ sample. The circularity profiles for all three media were similar to that on malt agar, with the slight increase in circularity observed at 8 hours likely owing to the omission of the watershed algorithm in the analysis of these samples (Fig. 5.4b).

*Validation of results*

It was found that small variations in the value of $C_{s,\,min}$ did not have a significant impact on the measured average spore projected area or mean spore circularity (Fig. 5.6). In the analysis of samples taken at 6 h, a decrease of 0.05 in the value of $C_{s,\,min}$ resulted in an increase of approximately 0.75 $\mu$m$^2$ in the measured mean spore projected area (for $C_{s,\,min} > 0.7$). This is possibly a result of a greater number of clumped spores (relatively large artifacts) being included in the analysis as the circularity threshold is lowered. This variation may be reduced by placing an upper limit on the projected area of objects included in the analysis.

Reducing the value of $C_{s,\,min}$ also had the effect of reducing the mean spore circularity at each time-point, as objects of a lower circularity are included in the measurement. In the analysis of samples taken at 6 h, a decrease of 0.05 in the value of $C_{s,\,min}$ resulted in a decrease of approximately 0.02 in the measured mean spore circularity.

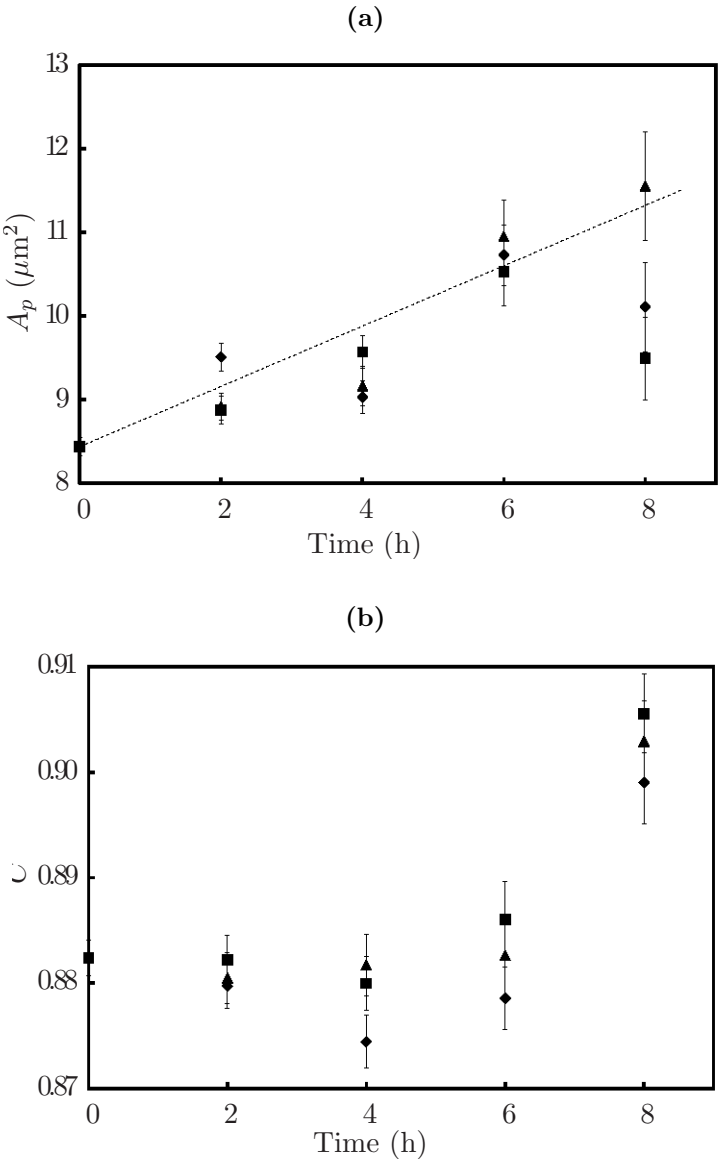


**Figure 5.4:** (a) Average projected area ($A_p$) and (b) average circularity ($C$) of *A. oryzae* spores incubated on mixed cellulose ester membranes on BM supplemented with 2% (w/v) glucose ($BM_G$; ▲), BM supplemented with 2% (w/v) starch ($BM_S$; ♦) and BM without sugar supplementation (■) at 25°C. $A_{p,min} = 3$ $\mu$m$^2$, $C_{s,min} = 0.8$. The increase in mean equivalent spore diameter ($D_s$) was approximately linear at a rate of 0.07 $\mu$m h$^{-1}$ (dotted line). Error bars represent 95% confidence intervals. An average of approximately 800 spores were analysed per time-point for each media type.

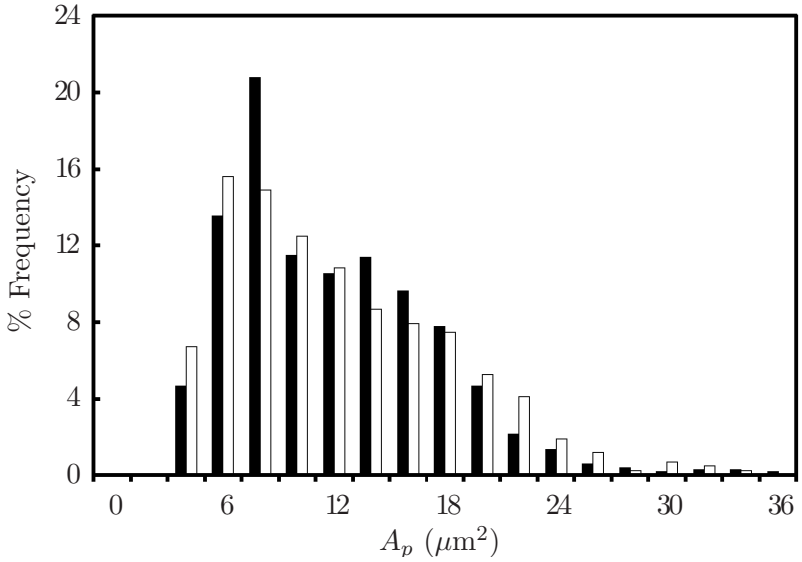


**Figure 5.5:** Comparison of size distributions of populations of *A. oryzae* spores. Spores were incubated on mixed cellulose ester membranes on malt agar for 6 hours (■) and $BM_G$ for 8 hours (□) at 25°C ($A_{p,min} = 3$ $\mu$m$^2$, $C_{s,min} = 0.8$).

### 5.3.2 Kinetics of hyphal development

The development of *A. oryzae* hyphal elements was characterised over a 10-hour period from 14 to 24 h after inoculation (Fig. 5.7). Assuming hyphae to be cylinders of approximately constant radius ($r$) and density ($\rho$), then biomass ($X$) is directly proportional to the total hyphal length ($L_{th}$):

$$X = \pi r^2 \rho L_{th} \tag{5.3}$$

The specific growth rate ($\mu$) can then be estimated according to:

$$\mu = \frac{2.3(\log L_{th} - \log L_{th0})}{t} \tag{5.4}$$

where $L_{th}$ is the total hyphal length at time $t$ and $L_{th0}$ is the total hyphal length at time $t = 0$. A value of approximately 0.27 h$^{-1}$ was calculated for $\mu$ on the basis of data acquired using semi-automatic image analysis and 0.24 h$^{-1}$ for the fully

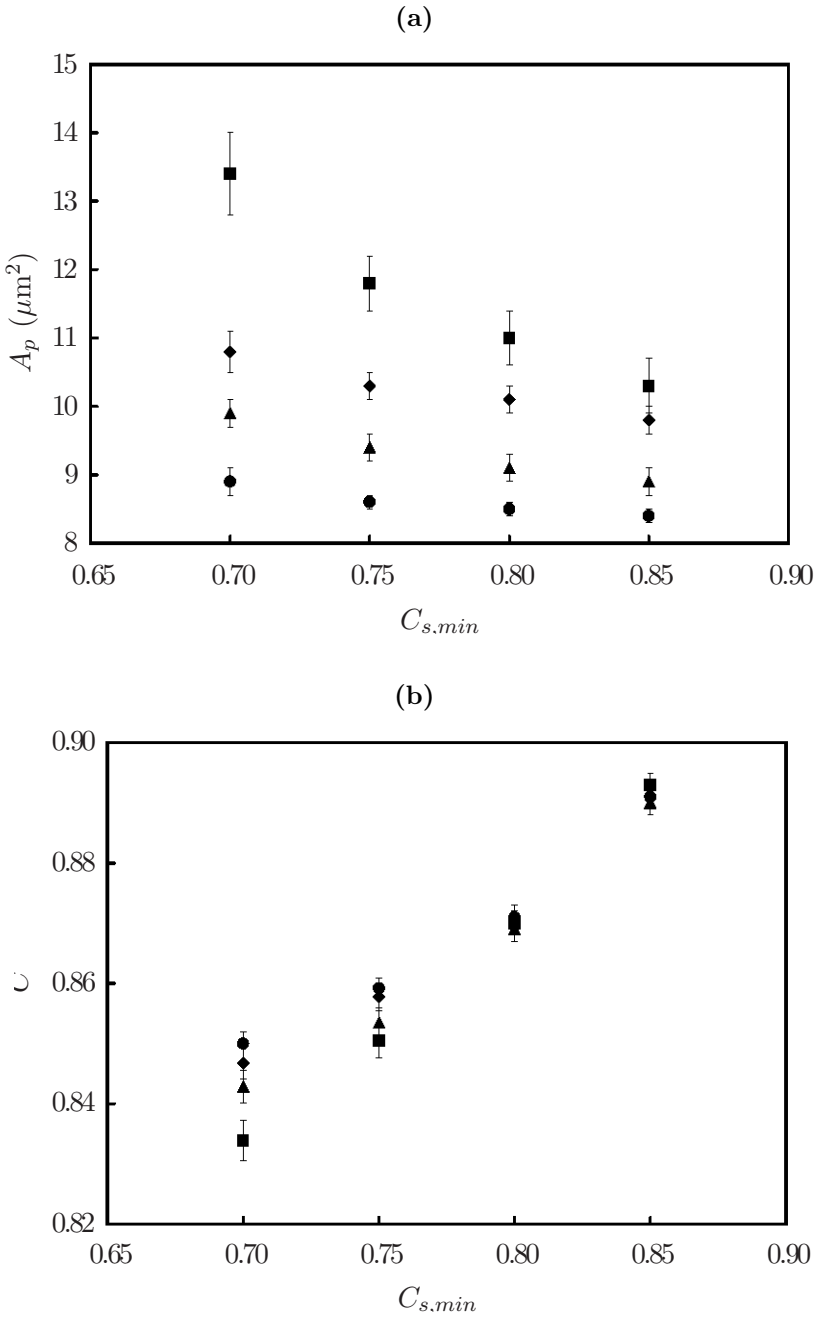


**Figure 5.6:** Variations in (a) mean spore projected area ($A_p$) and (b) mean spore circularity ($C$) at different time intervals. Automatic image analysis was performed for different values of $C_{s,min}$. The times used were 0 (•), 2 (▲), 4 (♦) and 6 h (■). Error bars represent 95% confidence intervals.

automatic method (Fig. 5.7a). Specific growth rates were calculated on the basis of total hyphal length in a previous study of *A. oryzae* using a flow-through cell [4], where the immersion of the fungus in a glucose-rich medium resulted in values of $\mu$ of up to 0.37 $h^{-1}$. However, a specific growth rate of 0.258 $h^{-1}$, derived from measures of $L_{th}$, was reported by Carlsen and colleagues for batch cultivations of *A. oryzae* (grown as freely dispersed elements), which corresponded well with an estimation of $\mu$ from dry weight measurements (0.266 $h^{-1}$). The hyphal growth unit in this work can be seen to be tending towards a constant value of approximately $72 \pm 8$ $\mu$m (Fig. 5.7b).

Using this data, an expression for the mean number of tips as a function of time ($n_t$) may be derived. Spohr and colleagues described this process as follows [106]:

$$\frac{dn_t}{dt} = \begin{cases} 0 & L_{th} < 150\mu\text{m} \\ k_b L_t = k_b . L_{th0} e^{\mu t} & L_{th} \geq 150\mu\text{m} \end{cases} \tag{5.5}$$

where $L_t$ is $L_{th}$ expressed as a function of time ($L_t = L_{th}(t)$) and $k_b$ is the specific branching frequency. In other words, significant branching does not commence until a minimum mean total hyphal length of 150 $\mu$m has been attained [45]. Integration of Equation 5.5 gives (for $L_{th} \geq 150$ $\mu$m):

$$n_t = \frac{k_b}{\mu} . L_{th0} e^{\mu t} + n_0 \tag{5.6}$$

A value of $k_b$ may be estimated as the product of $\mu$ and the rate of change of $N$ with respect to $L_{th}$ (Fig. 5.8):

$$k_b = \mu . \frac{dN}{dL_{th}} \tag{5.7}$$

which yields $k_b = 2.3 \times 10^{-3}$ tips $\mu m^{-1}$ $h^{-1}$, identical to the value reported by Spohr and colleagues for a wild type strain of *A. oryzae* [106].

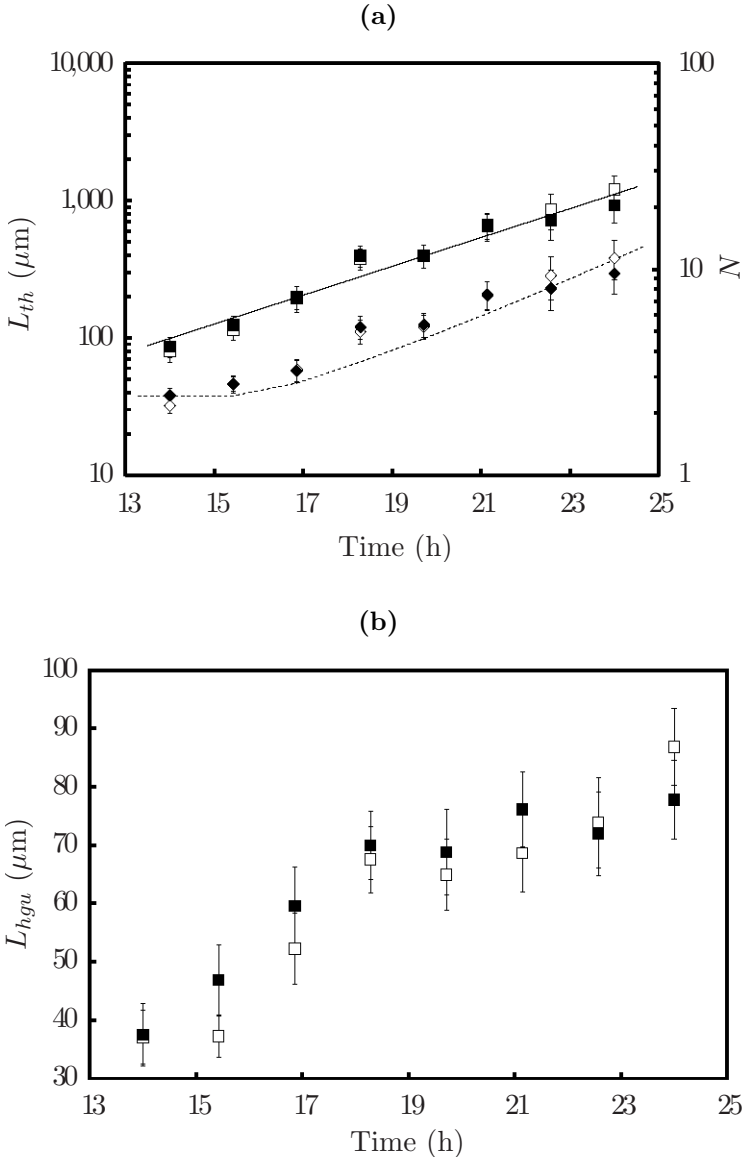


**Figure 5.7:** (a) Mean total hyphal length ($L_{th}$; ■, □), mean number of tips ($N$; ♦, ◊) and (b) mean hyphal growth unit ($L_{hgu}$) of *A. oryzae* on malt agar as determined by automatic (■, ♦; $L_{b,min} = 2.5$ $\mu$m and $C_{h,max} = 0.35$) and semi-automatic (□, ◊) image analysis. The solid line represents exponential growth with a specific growth rate of 0.24 $h^{-1}$ as determined by linear regression ($R^2 = 0.96$). The dotted line is a simulation of Equation 5.6 with $k_b = 2.3 \times 10^{-3}$ tips $\mu m^{-1}$ $h^{-1}$, $L_{th0} = 3.35$ $\mu$m and $n_0 = 0.96$. Approximately 100 elements were analysed for each time-point. Error bars represent 95% confidence intervals.

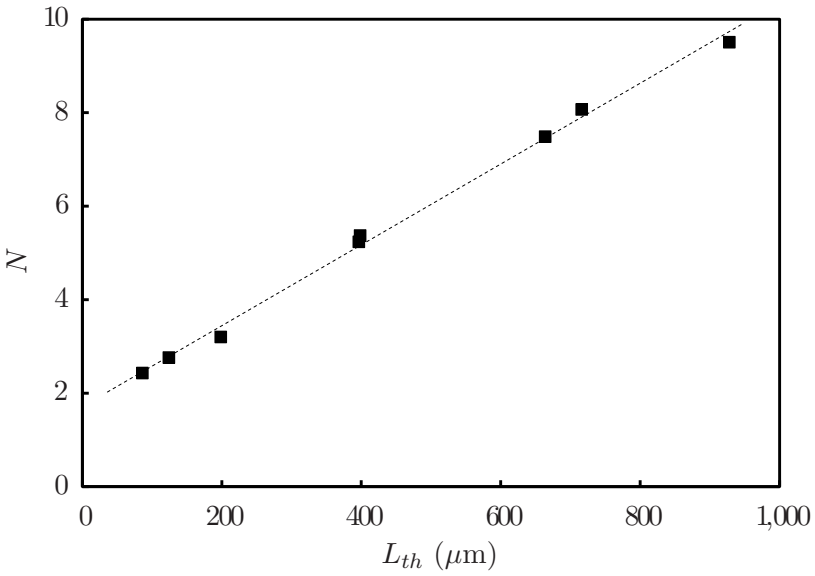


**Figure 5.8:** Mean number of tips ($N$) versus mean total hyphal length ($L_{th}$) of various *A. oryzae* mycelial populations cultivated on malt agar for different periods of time. A specific branching constant ($k_b$) of $2.3 \times 10^{-3}$ tips $\mu$m$^{-1}$ h$^{-1}$ was estimated by multiplying the slope of this plot (0.0086 tips $\mu$m$^{-1}$; $R^2 = 0.996$) by $\mu$.

The acquired data on $N$ and $L_{th}$ can be used to determine other kinetic parameters of use when comparing the growth of fungi in different environmental conditions. The average tip extension rate at a given point in time ($q_{tip}$; $\mu$m tip$^{-1}$ h$^{-1}$), for example, may be calculated according to [106]:

$$q_{tip} = \mu . \frac{L_{th}}{N} \tag{5.8}$$

which is plotted as a function of $L_{th}$ (Fig. 5.9), but may also be correlated with the total hyphal length by saturation kinetics [106]:

$$q_{tip} = k_{tip} . \frac{L_{th}}{L_{th} + K_t} \tag{5.9}$$

where $k_{tip}$ ($\mu$m tip$^{-1}$ h$^{-1}$) is the maximum tip extension rate and $K_t$ ($\mu$m) is a saturation constant.

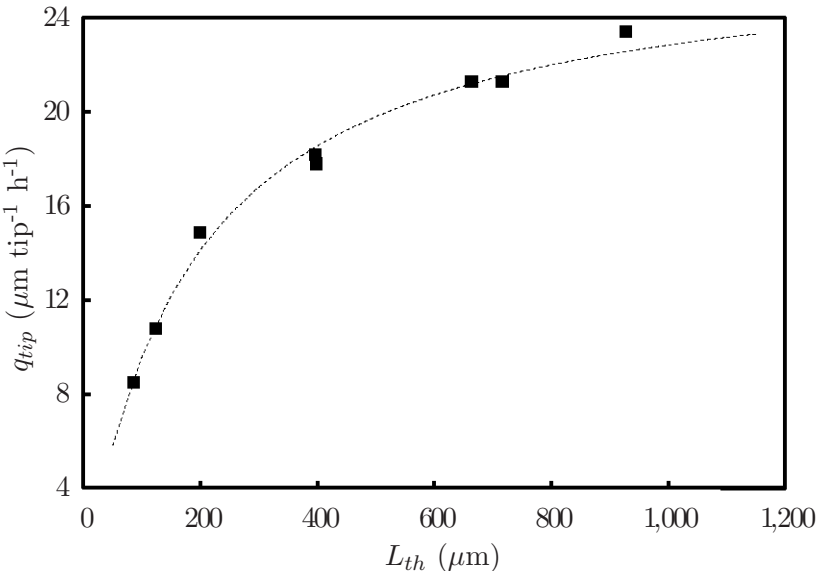


**Figure 5.9:** Mean tip extension rate ($q_{tip}$) as function of the mean total hyphal length ($L_{th}$) of *A. oryzae* as determined by Equation 5.8. The dotted line represents Equation 5.9 with $k_{tip} = 27$ $\mu$m tip$^{-1}$ h$^{-1}$ and $K_t = 148$ $\mu$m.

A large distribution in the size of individual hyphal elements was discernible at each time-point, with the distribution being greatest in the later stages of the analysis (Fig. 5.10). This may be a result of variations in the specific growth rate of different hyphal elements within a given sample. Differences in spore swelling rate and germination time would also make a contribution to the observed variation in the sizes. Considering the increase in total hyphal length as an exponential function, a difference of as little as 10% in the specific growth rate of two hyphal elements would be expected to result in a significant variation in total hyphal length after 24 h of growth. Variations in the specific growth rate well in excess of this figure have been reported in an online study of *A. oryzae* in submerged culture [4].

*Influence of media composition on kinetic parameters*

The influence of different carbon substrates on growth kinetics was investigated and the growth rates on each of three different media compared (Fig. 5.11). Glucose

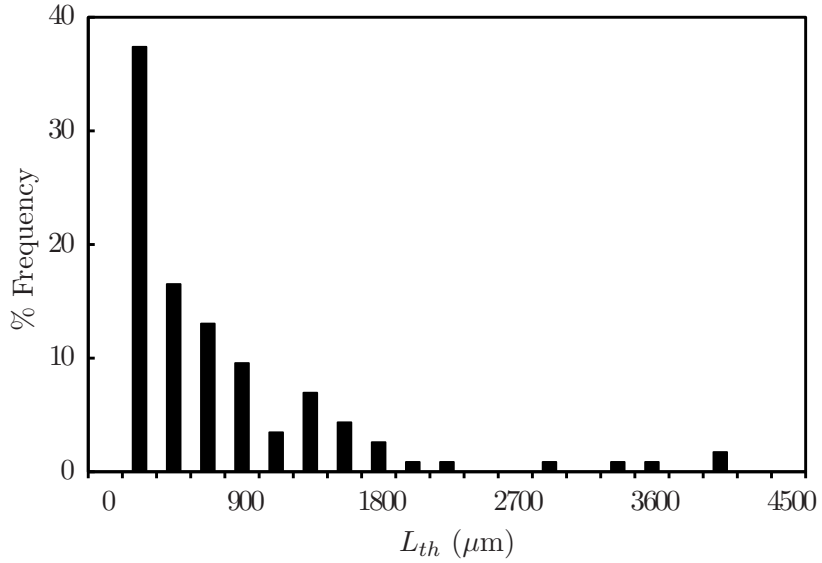


**Figure 5.10:** A 21-hour old sample of *A. oryzae* cultivated on cellulose nitrate membranes on malt agar shows a wide variation in total hyphal length ($L_{th}$). $L_{b,min} = 2.5$ $\mu$m, $C_{h,max} = 0.35$.

was found to yield a marginally higher growth rate of 0.29 $h^{-1}$ compared to 0.24 and 0.25 $h^{-1}$ on starch and the basal medium respectively. However, it is clear from the figure that at any given point in time, there is no statistically significant difference between the three measured values of $L_{th}$. It may therefore be concluded that there was no appreciable difference in growth rates on the three different media, with all three being similar to that observed on malt agar.

*Validation of results*

The effect of varying $C_{h,\,max}$ by $\pm 0.10$ was tested and was found to have little influence on the results (Fig. 5.12). Reducing the value of $C_{h,\,max}$ will have the effect of excluding a greater number of artifacts from the analysis. However, it will also result in the exclusion of small unbranched hyphae, which typically have a circularity of 0.3 – 0.4, depending on their size. By excluding these small hyphae, the mean total hyphal length and the mean number of tips per hyphal element will

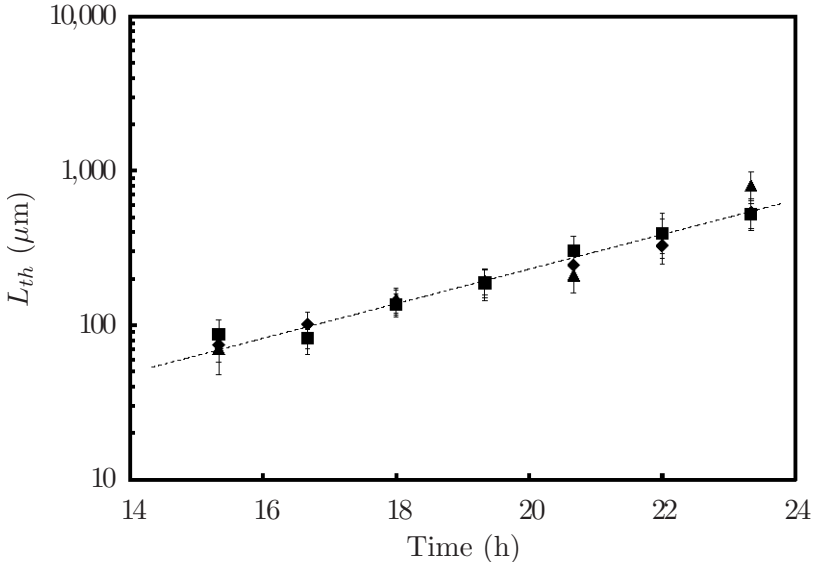


**Figure 5.11:** Average total hyphal length ($L_{th}$) of *A. oryzae* elements growing on mixed cellulose ester membranes on BM supplemented with 2% (w/v) glucose ($BM_G$; ▲), starch ($BM_S$; ♦) and without sugar supplementation (■) at 25°C. The specific growth rate ($\mu$) was estimated as approximately 0.29 $h^{-1}$ on $BM_G$ ($R^2$ = 0.95), 0.24 $h^{-1}$ on $BM_S$ ($R^2 = 0.99$) and 0.25 $h^{-1}$ on BM ($R^2 = 0.97$). The dotted line represents exponential growth with a specific growth rate of 0.26 $h^{-1}$ ($R^2 = 0.96$). Error bars represent 95% confidence intervals. An average of approximately 100 elements were analysed per time-point for each media type.

be slightly over-estimated, particularly for earlier time-points.

The effect of varying $L_{b,\,min}$ by $\pm 2.0$ $\mu$m was also tested and was found to have little influence on the measured mean number of tips (Fig. 5.13) and virtually no impact on the mean total hyphal length (not shown). Increasing the value of $L_{b,\,min}$ will result in smaller branches being excluded from the analysis and an underestimation in the number of tips. A large increase in the value of $L_{b,\,min}$ would be necessary to cause a significant decrease in the mean total hyphal length. Removing branches 2 – 4 $\mu$m long is unlikely to have an appreciable effect on the final result when quantifying structures that are hundreds, or even thousands, of

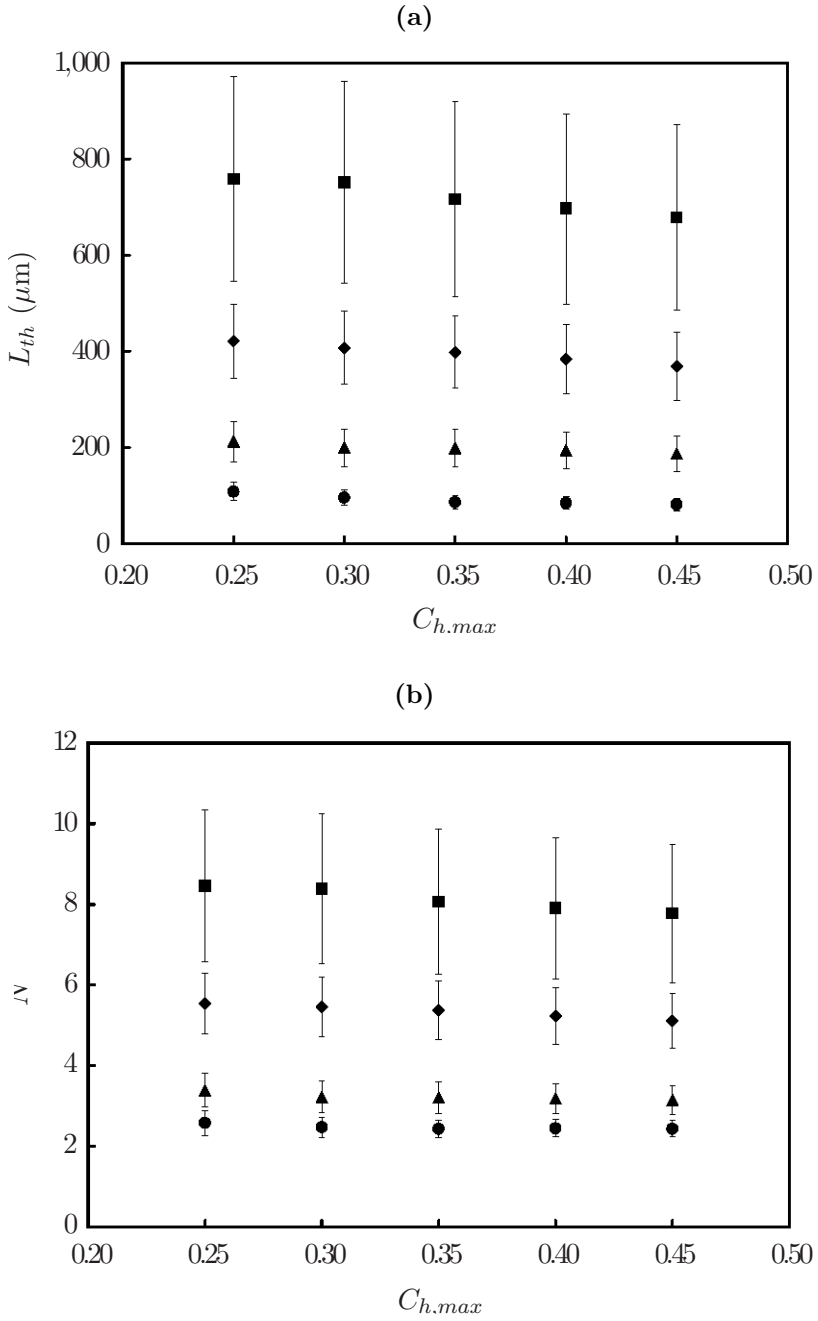


**Figure 5.12:** Variations in (a) mean total hyphal length ($L_{th}$) and (b) mean number of tips ($N$) at different time intervals. Automatic image analysis was performed for different values of $C_{h,max}$. The times used were 14 (•), 16.9 (▲), 19.7 (♦), and 22.6 h (■). Error bars represent 95% confidence intervals.

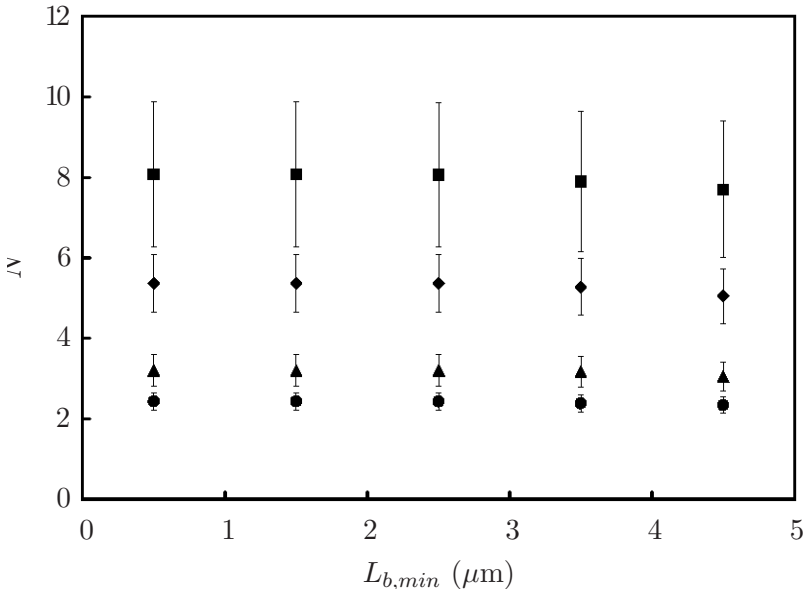


**Figure 5.13:** Variations in mean number of tips ($N$) as determined by automatic image analysis for different values of $L_{b,min}$. The times used were 14 (•), 16.9 (▲), 19.7 (♦), and 22.6 h (■). Error bars represent 95% confidence intervals.

microns in length.

## 5.4 Discussion

The ability to derive kinetic parameters to describe industrial fermentations is a powerful tool in facilitating process optimisation. A link between microscopic and macroscopic kinetics has long been established [41, 42], but more recently, detailed examinations of growth kinetics have been linked to specific macro-morphological forms [107, 125, 152]. Relationships between micro-kinetics and metabolic activity have also been identified, suggesting that knowledge of microscopic parameters is crucial to furthering an understanding of metabolite production [45, 79, 81, 126]. Indeed, many of these dependencies have been expressed in mathematical form and combined to yield model simulations, which have proved extremely useful in describing the time-course of development [119, 126, 157, 198, 201].

While there have been numerous detailed studies of the growth kinetics of filamentous organisms reported in the literature, the majority have focused on the development of microbes in submerged culture [4, 45, 106, 107, 123, 125, 126, 147, 175, 198]. Examinations of growth on solid culture have tended to be restricted to low-resolution assessments of the rate of change of colony projected area [156, 157], for example. More detailed investigations of individual hyphae in solid culture have been limited to a very small number of hyphae or hyphal elements [1, 140, 187].

The same is also true of many 'on-line' studies of microbial development in submerged culture using some form of a flow-through cell [4, 107, 123, 125, 147, 198]. While these chambers offer the advantage of a homogeneous environment that can be easily modified and controlled, deriving population statistics from such a small number of examinations is difficult. Indeed, many of these studies have illustrated that growth parameters can vary from one hypha or hyphal element to the next. In the on-line study of a single element of *A. oryzae*, for example, Christiansen and colleagues found that values for $K_t$ can vary significantly between individual hyphae, even within a single mycelium; when apical branching occurred, it was observed that the tip extension rate decreased temporarily [4, 198]. These variations in the growth rate of individual tips invariably lead to inter-mycelial variations in the specific growth rate [4], further evidence for which is presented here (Fig. 5.10). However, by averaging over a large population, an accurate estimate of growth rate may be derived, as demonstrated both here (Fig. 5.7a) and in studies of *A. oryzae* in submerged culture [45, 106].

### 5.4.1 Kinetics of spore swelling

The approximately linear increase in *A. oryzae* spore diameter described here, together with an invariant spore circularity (Fig. 5.2), is in general agreement with other reports [4]. The increase in spore diameter is relatively modest compared

to increases of 2.0 $\mu$m in 6 hours for spores of *A. niger* [175] and approximately 7.0 $\mu$m in *Rhizopus oligosporus* sporangiospores [28]. Spohr and colleagues reported an equivalent diameter of approximately 8.6 $\mu$m for spores of *A. oryzae* just prior to germination [4]. However, in all of these cases, the examination was conducted in submerged culture. Little difference in spore swelling rates was observed between *A. oryzae* spores on different substrates (Fig. 5.4a). It has previously been found that virtually no uptake of nutrients occurs during the swelling of *A. niger* spores [175], which may explain the absence of any detectable influence in this study. However, a carbon source was deemed necessary for the commencement of swelling of *R. oligosporus* sporangiospores while both carbon and nitrogen were required for germination - the spores did not contain sufficient endogenous carbon to support either process [28].

The germination of spores of *A. oryzae* took place 6 – 8 hours post inoculation in this study, which is in approximate agreement with the germination time of 6 hours reported by Carlsen and colleagues [45]. A germination time of just 4 hours has also been found for *A. oryzae* [4], while spores of other *Aspergilli* can take up to 10 hours to produce germ tubes [175]. In this study, glucose was found to prolong the spore swelling process compared to other substrates (Fig. 5.4a). Media composition has also been suggested to have a significant influence on the germination of *Penicillium chrysogenum*, as did inoculum age [129], while water activity and temperature were also demonstrated to have a considerable effect [26]. Both pH and temperature were reported to have a substantial impact on the germination of *R. oligosporus* [28].

### 5.4.2 Kinetics of hyphal development

The description of growth kinetics presented here utilised the same basic principles previously described in other population studies involving filamentous microbes [45, 106]. While the derived values of $k_{tip}$, $k_b$ and $K_t$ have no mechanistic basis, they

are useful for comparing the behaviour of organisms under different environmental conditions. To the best of the author's knowledge, this is the first such analysis involving a large population of hyphal elements cultivated on a solid substrate. However, the artificial environment in which the organism was grown must be taken into consideration when comparing with kinetic parameters derived in other systems. Rahardjo and colleagues contended that the presence of membrane filters reduces the maximum respiration rate and, consequently, the growth rate of *A. oryzae* [195]. However, differences in activity were not observed until well in excess of 24 hours post-inoculation, indicating that oxygen limitations were unlikely to have been significant in this work. Furthermore, the similarity of kinetic parameters derived here to those reported in other studies involving *A. oryzae* suggest that, while an influence of the membrane cannot be ruled out, it does not appear to have been significant.

The use of digital image processing to derive information on growth rates has been found to be accurate with respect to the conventional means of deriving kinetics from dry cell weight measures in submerged cultures of *A. oryzae* [45, 106]. However, the morphological form adopted by the fungus can influence the growth rate derived from biomass measurements; pelleted biomass may result in a lower specific growth rate due to substrate limitation compared to filamentous growth [45]. A caveat to the use of measures of hyphal length as a means of deriving kinetic data is that hyphal diameter is relatively constant throughout the population being analysed, as has been demonstrated in submerged batch fermentations of *A. oryzae* [45, 106, 119]. However, it appears that this only holds true for a constant specific growth rate. Hyphal diameter has been shown to be directly proportional to the specific growth rate [126], while it was also noted that the growth of a glucoamylase producing strain of *A. oryzae* starved of glucose was characterised by significant reduction in hyphal diameter and a reduced growth rate [147].

A variety of factors have been reported as significant in influencing the growth rate of filamentous microbes, but the most commonly employed regulator is substrate concentration. Jørgensen and colleagues demonstrated a relationship between dilution rate and the specific growth rate of *A. niger* in chemostat culture [199]. Pollack and colleagues noted that the growth of *A. oryzae* ceased when starved of glucose, before growth recommenced, fuelled by endogenous carbon, following a defined lag-time [147]. Specific growth rate, specific branching rate and final tip extension rate of *A. oryzae* have all been modelled using Monod kinetics with respect to glucose concentration [4], while Müller and colleagues also noted increases in the specific growth and branching rates in the presence of increased glucose concentration [107].

While no discernible influence of media composition on specific growth rate was noted in this study, reports in the literature have demonstrated otherwise. Ali described a significant increase in specific growth rate resulting from the addition of kaolin in the submerged culturing of *A. niger* [98]. The concentration of both carbon and nitrogen sources had a substantial impact on the growth kinetics of *Mortierella alpine* and it was suggested that growth is inhibited at high nutrient concentrations [124]. However, the specific growth rate of *Mucor circinelloides* was found to be relatively independent of both carbon source type and concentration [123], although McIntyre and colleagues had earlier documented the effect of media composition on the maximum specific growth rate of *Mucor circinelloides* (syn. *racemosus*) [200].

## 5.5 Conclusions

Detailed analysis of the kinetics of filamentous microbial growth is essential for the understanding of a process time-course. Metabolite production is dependent on the specific rates of biomass and branch formation - understanding precisely how fungal

biomass develops over time is therefore crucial for the purposes of optimisation and reproducibility. While a number of studies of the growth kinetics of filamentous microbes have been reported, the vast majority have focussed on the submerged culture format.

The analysis of *A. oryzae* spores conducted here, the results of which were found to be reliable within a certain tolerance of the pre-selected circularity threshold, confirms earlier findings suggesting that the rate of increase in spore diameter during the swelling process is linear with respect to time. However, the possible distribution of swelling rates within a population, coupled with the prevalence of non-viable spores within the population, presents a considerable complication. Differences in germination times may also have some bearing on the result. Cultivating the spores on different media does not seem to have a significant influence on spore development, although spores did seem to take slightly longer to germinate on glucose.

Detailed information on the hyphal development of *A. oryzae* on a solid substrate was derived, which approximated previously reported data for this organism. While these kinetic parameters and associated empirical expressions have no physiological basis, they are useful for comparing different environmental conditions, or for comparing with other organisms. The specific growth rate on a glucose-rich medium was slightly higher when compared to starch or malt agar, but the difference was not deemed to be statistically significant. The results produced by the image analysis system were tested and found to be stable over a range of input parameters.

# Chapter 6

# Investigation into the Morphological Development of *Aspergillus oryzae* in Submerged Fermentation

## 6.1 Introduction

The optimisation of submerged fermentations involving filamentous microbes, which are employed in the production of a wide variety of compounds of economic importance [6–8], relies heavily on a knowledge of the morphology of the process microorganism, as specific phenotypes are often associated with maximum productivity. A degree of progress has been made in elucidating correlations between fungal morphology and metabolite production in fungal fermentations and the topic has been extensively reviewed [8, 23, 202]. Despite such progress, significant obstacles remain in developing reproducible relationships in many cases, due to the complex architectures manifested in submerged culture.

### 6.1.1 Morphological variation in submerged culture

While the previous chapters of this thesis detailed work on the characterisation of mycelial growth restricted to two dimensions using membrane immobilisation, the configuration adopted by filamentous microbes often exhibits a significant three-dimensional character (Fig. 6.1). For example, in submerged culture, a microbe may

manifest itself in the form of approximately spherical pellet structures, which may be several millimetres in diameter. Morphologically quantifying such a convoluted architecture represents a considerable challenge, particularly at the microscopic level. As a result, 'free' hyphal elements are often targeted for microscopic analysis, as their architecture is easily confined to two dimensions (between a microscope slide and cover-slip, for example), facilitating ease of imaging.

The morphological form that results in a particular fermentation depends on environmental parameters (such as agitation speed, medium composition and pH [8]) and also on the physiology of the process microbe. For example, pellet formation can result from the aggregation of spores prior to germination, aggregation of spores and germ tubes or the aggregation of mycelia. There is evidence that conidiospores of *A. oryzae* are of the agglomerative variety and tend to form aggregates as they swell, prior to germination [45], while the development of pellets of *A. terreus* from agglomerates of spores was graphically illustrated by Bizukojc and Ledakowicz [47]. Other organisms, such as *Rhizopus nigricans*, do not agglomerate during swelling and form mycelial aggregates post-germination [203]. Carlsen and colleagues suggested that spore agglomeration is the principle driver of pellet formation in *A. oryzae* as pellets did not result when cultures were inoculated with dispersed mycelia [45], but other studies have since demonstrated that mycelia of *A. oryzae* can agglomerate to form clumps and/or pellets [88, 152].

In investigating the influence of environmental variables on microbial development, many researchers have demonstrated reproducible relationships between product yield and macro-morphology for a particular process [45, 46, 50, 72, 74, 96, 97, 104]. However, some reports have indicated that under certain conditions, product yield is seemingly independent of morphological form [73, 83, 84, 107, 112, 115]. There also exist conflicting results, such as for the production of citric acid from *A. niger*. A filamentous growth form had been considered to favour maximal pro-

**(a)** Free element **(b)** Clump **(c)** Pellet

**Figure 6.1:** Different morphological forms adopted by filamentous microbes in submerged culture. These range from simple, branched, 'free' hyphal structures (hyphal diameter is typically of the order of $10^{-6}$ m) to complex, composite architectures frequently termed 'clumps'. The agglomeration of biomass can also result in the formation of dense, approximately spherical, macroscopic aggregates termed 'pellets', which may be up to several millimetres in diameter.

duction [44] and a correlation between clump perimeter and citric acid titre derived [80], but more recently, pelleted biomass has been suggested as optimal [98]. Either dispersed, filamentous growth [45, 97, 104] or comparatively small, compact pellets [46, 50, 74, 96] are the most common growth forms associated with process optimisation, but occasionally, large pellets have been proposed as the preferred phenotype [72].

Fundamental to furthering the understanding of morphological influence on product yield is the elucidation of a relationship between hyphal branching and metabolite production, as evidence in the literature points to protein secretion occurring almost exclusively at the hyphal apex [105, 107]. Facilitating an increase in branch formation may therefore be favourable for many processes; branching complexity has been correlated with metabolite production in *A. oryzae* [106, 108] and *Pycnoporus cinnabarinus* [110], while a swelling of hyphal tips was found to coincide with increased metabolite excretion in *A. oryzae* [109] and *A. niger* [48]. Some

studies have also indicated dependencies of macro-morphological form on micro-morphological parameters and there is emerging evidence suggesting a fundamental link between kinetic parameters of growth at the microscopic level and the resultant macroscopic conformations [107, 125, 152]. For example, Müller and colleagues found that a mutant strain of *A. oryzae* that exhibited a greater degree of hyphal branching (lower hyphal growth unit with respect to a wild-type strain) was less likely to form large, inseparable clumps in submerged culture [107]. It was also suggested that the positioning of branches (apically or sub-apically) may affect the formation and dimension of macroscopic structures. Detailed microscopic analysis is also essential to understanding development during exponential growth, an important growth phase for the production of industrial products such as biomass and growth-associated metabolites (amylases, cellulases and proteases, for example).

### 6.1.2 Challenges associated with the morphological quantification of submerged cultures

The complex nature of aggregates such as clumps and pellets often presents difficulties in isolating individual hyphae for the accurate quantification of branching behaviour. Furthermore, microscopic examination of composite structures such as pellets can only be performed if the size of the pellet is sufficiently small to fit within the field of view of a microscope objective lens, which is often not the case. For example, Carlsen and colleagues found that pellets of *A. oryzae* grew up to 1.6 mm in diameter [45], while pellets of *A. terreus* up to 4 mm in diameter were measured by Bizukojc and Ledakowicz [47]. This clearly presents difficulties for conducting simultaneous assessment at the micro- and macroscopic levels when a microbe adopts such a morphology. Papagianni and Mattey used a macro-viewer connected to a CCD camera to image large pellets [48], as did Paul and colleagues, who suspended pellets in a Petri dish filled with water, to preserve the three-dimensional archi-

tecture [44]. O'Cleirigh and colleagues focused exclusively on macroscopic analysis by suspending pellets of *S. hygroscopicus* var. *geldanus* in a Petri dish containing water and imaging with a flatbed scanner [77].

Given the relatively large size of the agglomerates that can result in the submerged culturing of filamentous microbes, apparently trivial tasks such as obtaining a representative sample of biomass can prove problematic. In the case of unicellular organisms such as *Saccharomyces cerevisiae*, probes have been successfully developed for *in situ* culture analysis [132], but such devices are not suited to the study of filamentous growth, which is not easily captured within a single focal plane. However, an automated sampling mechanism was described by Treskatis and colleagues for use in the quantification of *Streptomyces tendae* Tü 901/8c fermenter cultures [204]. The system performed automatic dilution and subsequent imaging (using a microscope stage-mounted chamber, similar in construction to a flow-through cell), but the analysis was restricted to macroscopic criteria ($\times$1.25 objective), with the results consisting of classifications (rough pellets, smooth pellets, mycelial flocks, other components) assigned to biomass fractions; no morphological data beyond this was presented.

The difficulties associated with the analysis of macroscopic structures has led many researchers to focus exclusively on the dispersed growth form, using experimental arrangements such as the immobilisation of spores within a flow-through cell to study micro-morphological development in detail [4, 13, 125]. While the observations made using these simple experimental environments may be extrapolated to the more complex fermenter setting, such approaches are limited to the physiological study of a relatively small number of elements. Nonetheless, there may be potential for the utilisation of spore-immobilisation in submerged culture to provide a two-dimensional surface to support microbial growth for subsequent microscopic examination of individual elements. While such a cultivation format represents a

significant deviation from conventional submerged cultivation conditions, the use of solid supports in submerged fermentations has recently been demonstrated to result in elevated metabolite production. Papagianni and Mattey found that the use of nylon supports in the cultivation of *A. niger* resulted in higher citric acid production compared to a control submerged culture [48]. A beneficial effect was also reported by Bigelis and colleagues, who found that the use of polymeric membranes in liquid culture resulted in elevated metabolite production in cultures of *Penicillium* sp. *LL*-WF159 [54].

### 6.1.3 Influences on morphology

A wide range of parameters have been utilised as a means of modifying the morphological form of filamentous microbes, including variations in medium pH [52, 94], agitation intensity [46, 50, 51, 80, 83, 84, 88] and temperature [205]. Further efforts at phenotypic manipulation have involved experimentation with media composition, such as varying the nitrogen source [154, 205, 206], phosphate source [205], the addition of metal ions [95–97] or the modification of broth viscosity [81, 103]. A more invasive approach involved forcing the fermentation broth through a screen to remove pellets above a desired size [207].

One of the more common means of influencing morphological variation involves modifying the type or concentration of the inoculum. A very large concentration of spores provides a large number of growth centres and a very limited amount of growth from each can result in nutrient exhaustion. Conversely, if the initial spore concentration is low, substantial growth may be required before nutrient exhaustion occurs. The distribution of biomass may thus be varied between a large number of small elements and a small number of large elements. Various reports have indicated the macroscopic impact of inoculum concentration, which is typically characterised by a decrease in mean pellet diameter for increasing initial spore concentration [74].

Larger increases in inoculum concentration have been demonstrated to induce completely dispersed growth in some cases [72]. More abrupt transitions from pelleted to dispersed growth [72, 75, 76, 208] have also been documented, in which inoculum effects are characterised by a sudden state change in morphology, rather than a gradual variation in one particular parameter such as projected area or pellet diameter. A microscopic response has also been described, with increasing inoculum concentration found to cause an increase in the hyphal growth unit in cultures of *A. awamori* [73] and *A. niger* [159].

There is also evidence in the literature of morphological variation induced by altering the carbon source concentration in a defined medium. For example, it has been found that glucose concentration is an effective regulator of pellet size in *A. niger* [48]. At the microscopic level, it has been demonstrated that apical volume of *Aspergilli* may be regulated by the surrounding glucose concentration [90] and further reports indicate the size and shape of mycelial clumps of *A. niger* may be influenced by glucose levels [209]. Sub-cellular effects have also been reported, such as increased vacuolation at low substrate concentrations [79, 210], which can result in increased hyphal fragmentation.

### 6.1.4 Chapter overview

Having successfully applied the newly-developed image processing system (Chapter 3) to membrane-immobilised cultures on solid substrates (Chapter 5), a transition to the industry standard of submerged fermentation was now required, with a view to characterising the morphology of *A. oryzae* at the microscopic level and relating microscopic form to macro-morphology and $\alpha$-amylase production (Fig. 6.2). The isolation of 'free' mycelial elements was a prerequisite for the application of the imaging system, necessitating the identification of a submerged culture format in which the growth form could be reproducibly controlled.

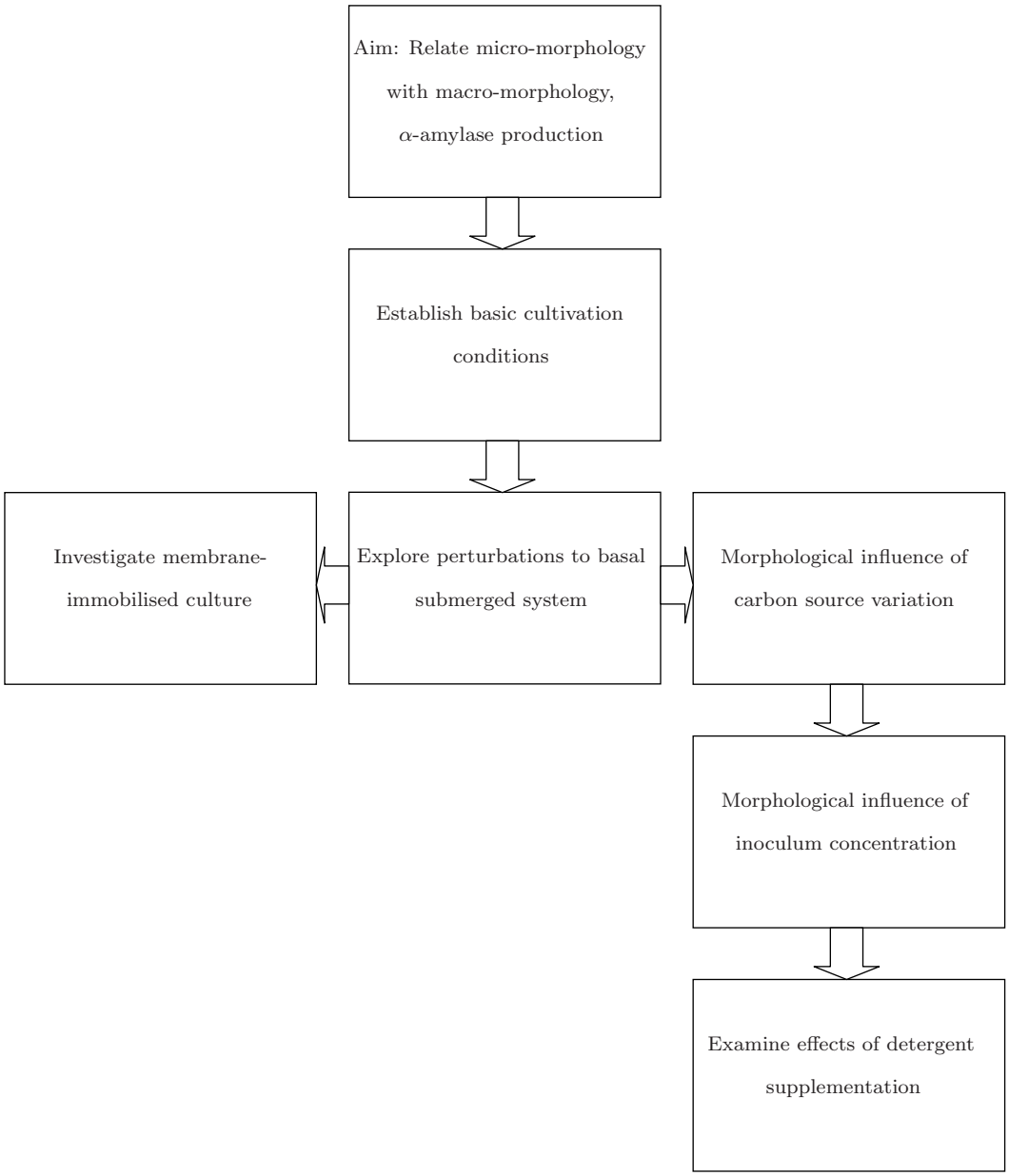


**Figure 6.2:** Overview of the results presented in this chapter.

Initial qualitative investigations of the effect of inoculum concentration were necessary in order to determine a spore level that reproducibly resulted in the formation of a morphology suitable for image processing (such as distinct pellets), with other culture parameters (media composition, temperature) based on previously published reports. Once these basic parameters were established, the development of *A. oryzae* over time in shake-flask culture could be assessed in order to establish reference points for biomass growth and $\alpha$-amylase production. Subsequently, the effect of perturbations to the basal submerged system was examined by quantifying responses to changes in the carbon source, variations in inoculum concentration and supplementation with non-ionic detergents; relationships between micro-morphology, macro-morphology and $\alpha$-amylase production were explored. In parallel with this, a novel 'mixed-phase' culture format, consisting of immobilised biomass in submerged culture, was investigated, with a view to establishing a submerged culture format in which microscopic structures (early-stage hyphal development, in particular) could be routinely visualised.

## 6.2 Materials & methods

### 6.2.1 Micro-organism cultivation

The basal medium (BM; see Section 2.3) used for all fermentations was that described for batch cultivation of *A. oryzae* by Amanullah and colleagues [122], with soluble starch (Sigma S-9765, Lot 93H0243 or Difco 0178-17-7, Lot FJ0041XA; concentration specified in individual experiments) used in place of maltodextrin and Pluronic P6100 omitted. Cultivations were conducted at pH 6 (reported by Carlsen and colleagues as optimal for maximal specific $\alpha$-amylase production [45]) unless otherwise stated and a temperature of 25 – 30°C. For investigations of non-ionic detergents and polymers, Nonidet P-40, Triton X-100, Tween-80, carboxymethyl-

cellulose (CMC), Ficoll, diethylaminoethyl cellulose (DEAE), Sephadex G-75 and Sephadex G-200 were added to a final concentration of 0.05 – 1.0% (w/v). In all shake-flask fermentations, 250 ml Erlenmeyer flasks, with a working volume of 20%, were incubated in a Lh Fermentation Mk X Incubator Shaker at 200 rpm. Inoculum consisted of 500 $\mu$L of $1 \times 10^7$ spores ml$^{-1}$ unless otherwise stated.

Investigations into particle agglomeration were conducted using malt extract broth: malt extract (Difco 0186-17, Lot 138225XD), 17.0 g L$^{-1}$; bacteriological peptone (Oxoid LP0037, Lot 239324), 3.0 g L$^{-1}$. Solid state cultivation was conducted on BM supplemented with Agar No. 1 (17.0 g L$^{-1}$) and immobilisation of fungal spores was performed as described in Section 2.4.

*Mixed-phase cultivation*

Cellulose nitrate membranes were overlaid onto the surface of Sabouraud dextrose agar (SDA): Sabouraud liquid medium (Lab M LAB033), 30.0 g L$^{-1}$; Agar No. 1 (Lab M), 17.0 g L$^{-1}$. The membranes were inoculated with 500 $\mu$L of $1 \times 10^7$ spores ml$^{-1}$ and incubated at 30°C for 16 hours. The membranes were then aseptically removed from the surface of the agar and transferred into Erlenmeyer flasks containing 50 ml of pre-autoclaved medium. The cultivation conditions for the shake-flask phase are referred to in individual experiments.

### 6.2.2 Visualisation of fungal morphology

Fungal macro-morphology was imaged by either photographing unstained biomass against a black background, or by using the method described in Section 2.5.1. The analysis of these images was performed as described in Section 3.4.2. Visualisation of fungal micro-morphology and the processing of solid-state-cultured membranes for image analysis was as described in Section 2.4. Fungal micro-morphology was quantified as described in Section 3.4.1. The effect of detergents on particle dispersal

in submerged media was evaluated using a variation of the approach adopted by Grimm and colleagues [196]; samples taken from shake-flasks were processed and imaged as above, then, using the routines developed for the quantification of spore morphology described in Chapter 3, the number of particles (any object detected within field of view) per unit volume of media was calculated.

### 6.2.3 Processing of shake-flask cultures

*Estimation of dry-cell weight*

The dry-cell weight of biomass per unit volume was estimated in one of two ways. In the first method, flask contents were transferred to a clean, dry, pre-weighed plastic universal and centrifuged at 3,000 rpm for 35 minutes at 4°C. Any wall-adherent biomass from the original flask was removed by washing with PBS containing Tween-80 (0.1% v/v). The universal containing biomass was dried in an oven for 24 hours at 105°C, then allowed to cool in a desiccator for 30 – 60 minutes before being re-weighed.

In the second method, flask contents were vacuum-filtered through a glass microfibre filter (Whatman GFC 1822-110). Any wall-adherent biomass from the flask was removed by washing with PBS-T80 (0.1% w/v). The filter and biomass were transferred to a pre-weighed universal and dried for 24 hours at 105°C, then allowed to cool in a desiccator for 30 – 60 minutes before being re-weighed. The weight of the filter (determined by drying three filters at 105°C for 24 h, then weighing) was subtracted from the final result.

*Estimation of $\alpha$-amylase activity and extra-cellular protein concentration*

Thimerosal (Sigma T8784) and protease inhibitor cocktail (Sigma P8340) were added to culture supernatants at final concentrations of 0.01% w/v and 0.001% v/v (of stock concentration) respectively. The samples were then stored at $-20$°C

prior to analysis.

$\alpha$-amylase activity was estimated with the use of a ceralpha assay kit (Megazyme K-CERA). The ceralpha procedure employs as substrate the defined oligosaccharide 'non-reducing-end blocked *p*-nitrophenyl maltoheptaoside' in the presence of excess levels of $\alpha$-glucosidase. On hydrolysis of the oligosaccharide by $\alpha$-amylase, the excess quantities of $\alpha$-glucosidase results in hydrolysis of the *p*-nitrophenyl maltosaccharide fragment to glucose and free *p*-nitrophenol, which may be quantified by measuring absorbance at 400 nm. The assay procedure (including preparation of assay 'blank') was conducted according to the manufacturer's manual [211]. Absorbance values were measured in plastic cuvettes (Sarstedt 67.742) using a Pharmacia LKB Ultraspec III spectrophotometer blanked against distilled water. Activity was expressed in international units (IU), derived from ceralpha units (CU) according to the manufacturer's manual:

$$\mathrm{IU} = 0.94 \times \mathrm{CU} \tag{6.1}$$

Extra-cellular protein concentration was determined using the Bradford colourimetric protein assay (Bio-Rad 500-0006) with bovine serum albumin (Sigma A7906, Lot 115K0714) as standard [212]. The assay was conducted in plastic micro-titre plates (Sarstedt 82.1582) and absorbance values measured using a Labsystems Multiskan Plus plate reader.

## 6.3 Results

### 6.3.1 Qualitative investigation of the relationship between inoculum concentration and macro-morphology

An initial 'range-finding' investigation into the effect of inoculum concentration on the macroscopic form of *A. oryzae* was performed to study the effect of spore

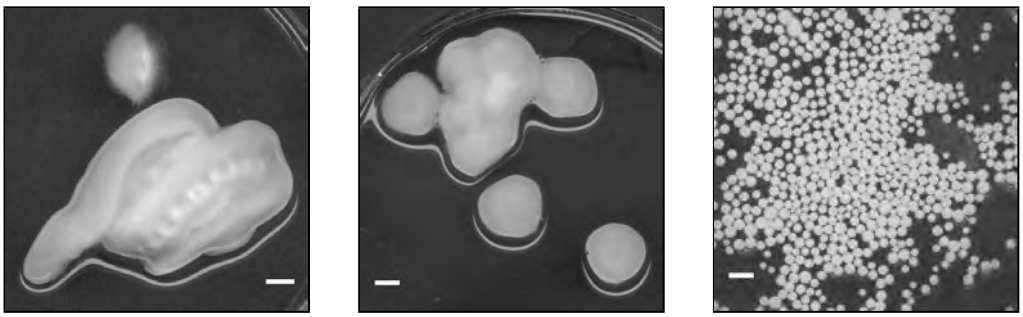

**(a)** **(b)** **(c)**

**Figure 6.3:** Variation in macroscopic morphological forms of *A. oryzae* for inoculum concentrations of (a) $1 \times 10^4$, (b) $1 \times 10^6$ and (c) $1 \times 10^7$ spores ml$^{-1}$ ($34.1 \pm 5.8\%$ viability). Bars: 5 mm.

concentration on pellet formation. The initial selection of spore concentrations was based on a review of studies involving shake-flask culturing of *Aspergilli* [45, 49, 72, 74]. Inoculum concentrations of less than $1 \times 10^7$ spores ml$^{-1}$ frequently resulted in the formation of large agglomerates of biomass (Fig. 6.3). Based on Pirt's theory of pellet growth, which states that actively-growing hyphae are restricted to a narrow region (estimated as $<\sim 350$ $\mu$m deep in *A. oryzae* [45]) at a pellet's surface [43], such large agglomerates would be expected to contain a very high proportion of diffusion-limited biomass. Furthermore, such agglomerates do not lend themselves to meaningful morphological analysis. While pellets were sometimes produced with an inoculum of $1 \times 10^6$ spores ml$^{-1}$, the inherent variability of the submerged culture format resulted in frequent biomass aggregation at this inoculum level (Fig. 6.3b). A minimum inoculum concentration of $1 \times 10^7$ spores ml$^{-1}$ was therefore chosen for subsequent study of *A. oryzae* in submerged culture to maximise morphological reproducibility between flasks.

### 6.3.2 Characterisation of morphological development and product formation in submerged culture over time

The variation in the macro-morphology of *A. oryzae* was evaluated over the course of a 7-day shake-flask fermentation (Fig. 6.4a), the development of which is illustrated in Figure 6.4b to 6.4f. The pellets attained their maximum diameter 45 – 72 hours post-inoculation and appeared to degrade from this point on. This may have been a result of nutrient exhaustion (depletion of starch was confirmed by observing the reaction between samples of fermentation broth and Lugol's iodine - not shown) and a subsequent weakening of cell structure, resulting in hyphal fragmentation at the pellet periphery; low levels of substrate have previously been demonstrated to lead to increased vacuolation and subsequent hyphal fragmentation in *A. niger* [79]. This fragmentation resulted in a large increase in mycelial 'clumps' in the media, depicted by the 'cloudy' nature of Figure 6.4e and 6.4f. These clumps were observed using light microscopy, but analysis and quantification was not possible as staining with lactophenol cotton blue proved problematic (Fig. 6.5).

The assessment of pellet sizes is complicated somewhat in this scenario as accurate image segmentation (separation of pellets from background) is more difficult and an evaluation of pellet size alone does not provide complete morphological quantification of the organism. Up to 72 hours post-inoculation, biomass exists in almost exclusively pelleted form and, as such, a measure of the size of these pellets provides an accurate representation of the organism's phenotype. However, beyond this point, a variety of structures are present, the smallest of which may be excluded from the analysis by virtue of the limited resolution of the scanner (and limited stain uptake), and therefore the mean size of biomass elements (expressed as mean pellet diameter) is possibly over-estimated beyond 72 hours.

The fragmentation of pellets is further illustrated in Figure 6.6. Overall pellet

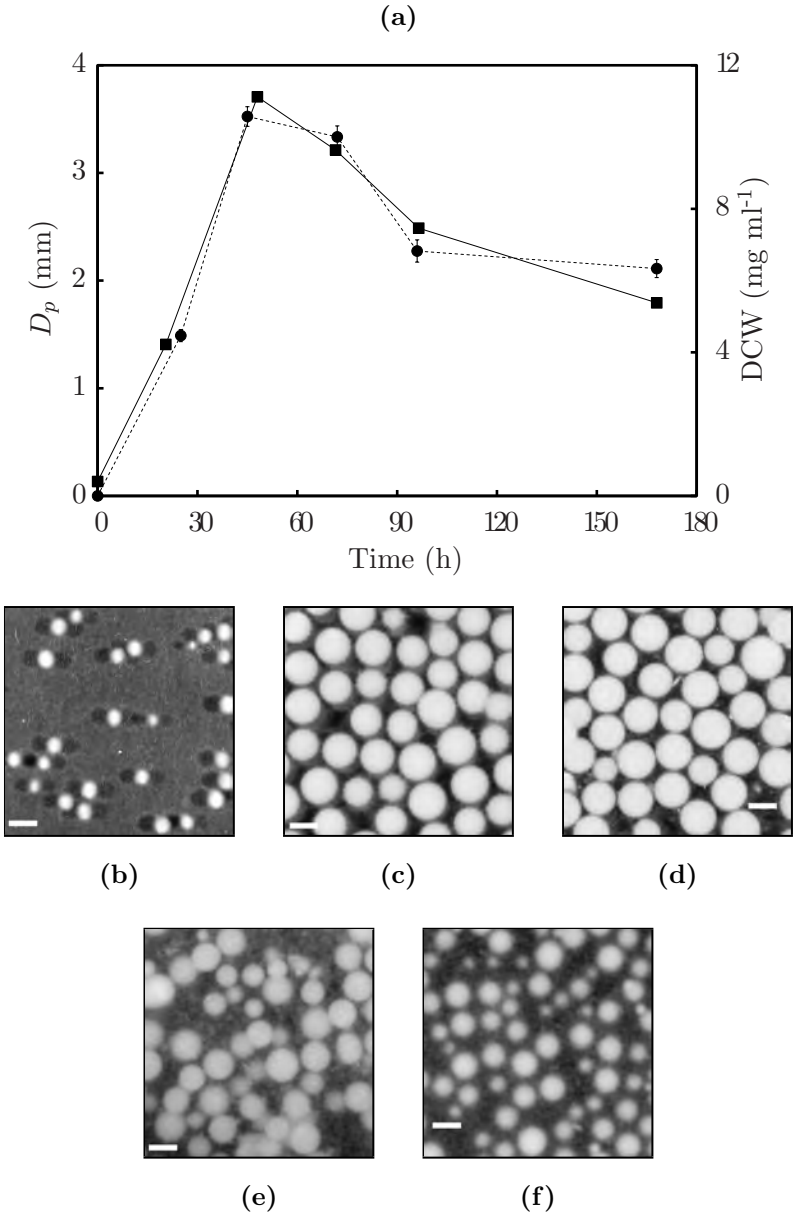


**Figure 6.4:** (a) Variation in mean pellet diameter ($D_p$; •) and dry-cell weight (DCW; ■) during a 'standard' submerged fermentation of *A. oryzae*. Error bars represent 95% confidence intervals. Images of macro-morphology were captured at (b) 24, (c) 45, (d) 72, (e) 96 and (f) 168 hours (Bars: 2 mm). Organism cultivated in BM (pH 7.0) supplemented with yeast extract (0.5 % w/v) and starch (0.8 % w/v). Each data point represents a single flask terminated at the indicated time. All flasks incubated at 25°C, spore viability = 34.1 ± 5.8%.

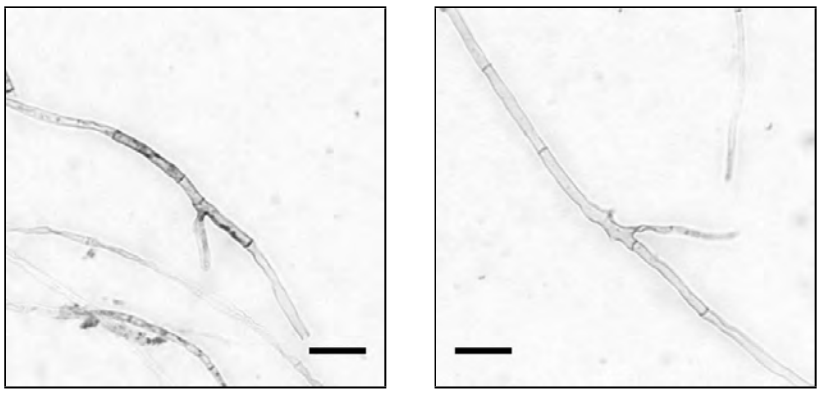

**(a)** **(b)**

**Figure 6.5:** Conventional lactophenol cotton blue 'wet-mounts' of 72-hour-old samples showed limited stain uptake (a), or in some cases, none at all (b). Bars: 25 $\mu$m.

diameter of a sample population increased from 24 – 45 hours and remained relatively constant until 72 hours. Thereafter, a large increase in the number of objects with an equivalent diameter below $\sim$ 2 mm coincided with a reduction in the number of objects with diameters above $\sim$ 3 mm. This suggests that larger pellets had begun to fragment, forming smaller pellet-like structures and clumps.

In their study of *A. oryzae* in the form of pellets, Carlsen and colleagues estimated that oxygen limitation set in 23 hours post-inoculation, when the pellets were approximately 600 – 800 $\mu$m in diameter [45]. The pellets continued to increase in size until approximately 35 hours, when mean pellet diameter began to decline, the number of pellets per unit volume increased rapidly and an increase in ethanol concentration was noted. No ethanol was detected in cultures grown as freely dispersed hyphal elements, indicating ethanol production was limited to the dense pellet core, where anaerobic conditions predominated. This may suggest that autolysis contributed to the decline in pellet diameter and biomass concentration illustrated in Figure 6.4, given that the measured diameters were well in excess of

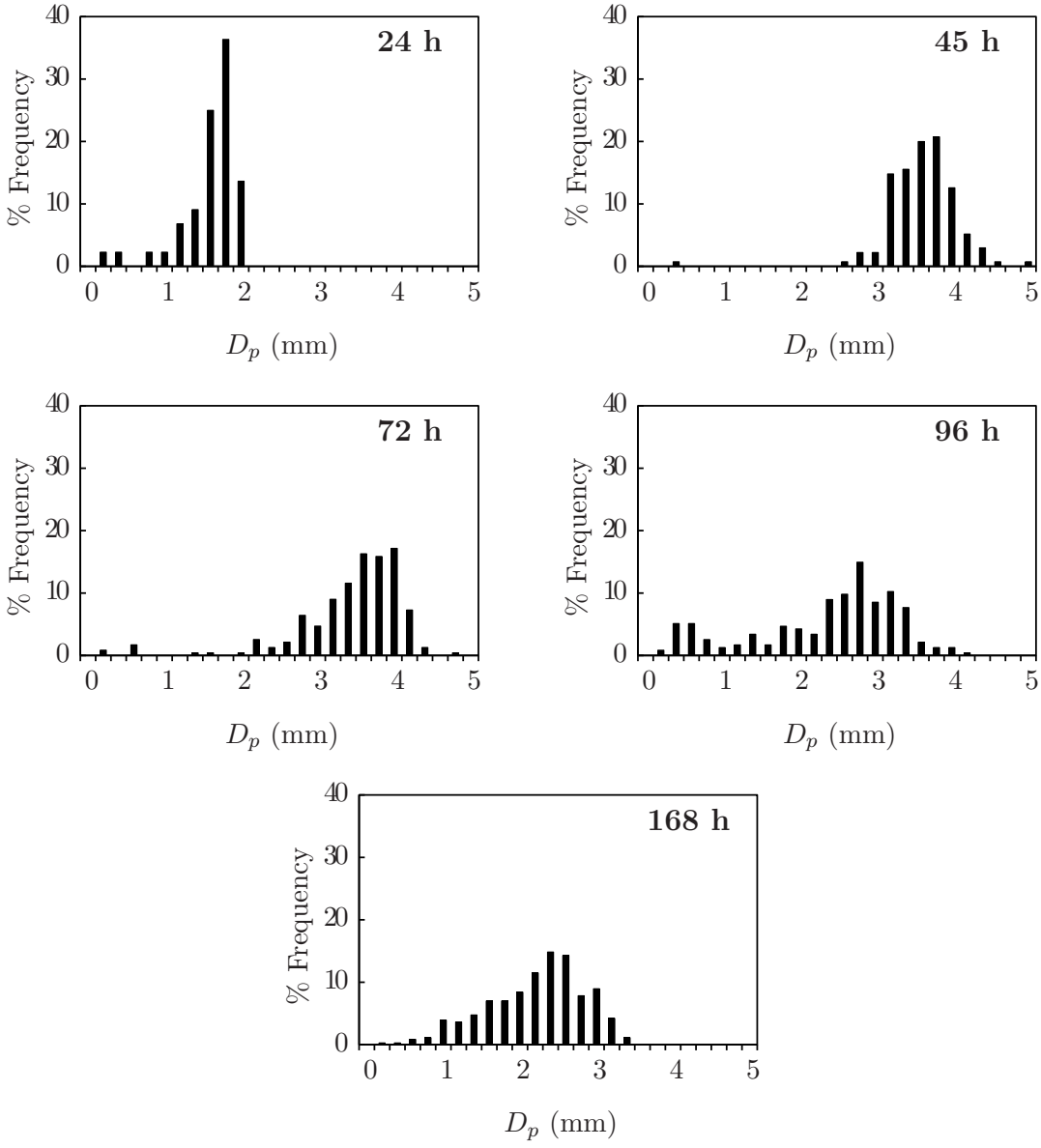


**Figure 6.6:** Variation in distributions of pellet diameter ($D_p$) over time in shake-flask cultures of *A. oryzae* ($44 \leq n \leq 357$). Cultivation conditions were as described in Figure 6.4.

those reported by Carlsen and colleagues.

The rate of $\alpha$-amylase production slowed considerably once maximum pellet diameter and maximum biomass levels had been attained (Fig. 6.7a), suggesting that production of this enzyme is primarily growth-associated. Carlsen and colleagues demonstrated a similar concurrent increase in biomass and $\alpha$-amylase production in batch cultivations of *A. oryzae* (specific $\alpha$-amylase production was constant) [45] and it was later reported that $\alpha$-amylase synthesis was closely coupled to the growth of the fungus [111]. However, Spohr and colleagues found that the specific $\alpha$-amylase secretion rate seemed to decrease with time during batch cultivation, although no explanation was offered for this observation [106]. Exhaustion of starch (an inducer of $\alpha$-amylase production in *A. oryzae* [213]) may have been responsible for the decline in $\alpha$-amylase production observed here. It is also possible that the presence of glucose, resulting from total starch degradation, had repressed $\alpha$-amylase production, as has been previously documented [111]. Peak specific $\alpha$-amylase activity (IU $mg^{-1}$ extra-cellular protein) occurred at 45 hours (Fig. 6.7b), coinciding with peaks in pellet diameter and biomass levels and indicating a reduction in $\alpha$-amylase production beyond this point in the fermentation.

The results of these preliminary experiments provided a baseline understanding of the development of *A. oryzae* in shake-flask culture and permitted the design of further experiments examining the relationship between morphology and $\alpha$-amylase production. This result suggested that a sampling time of 45 – 72 hours was optimal for comparing different shake-flask conditions, given that growth and primary metabolite production of the organism had peaked by this time.

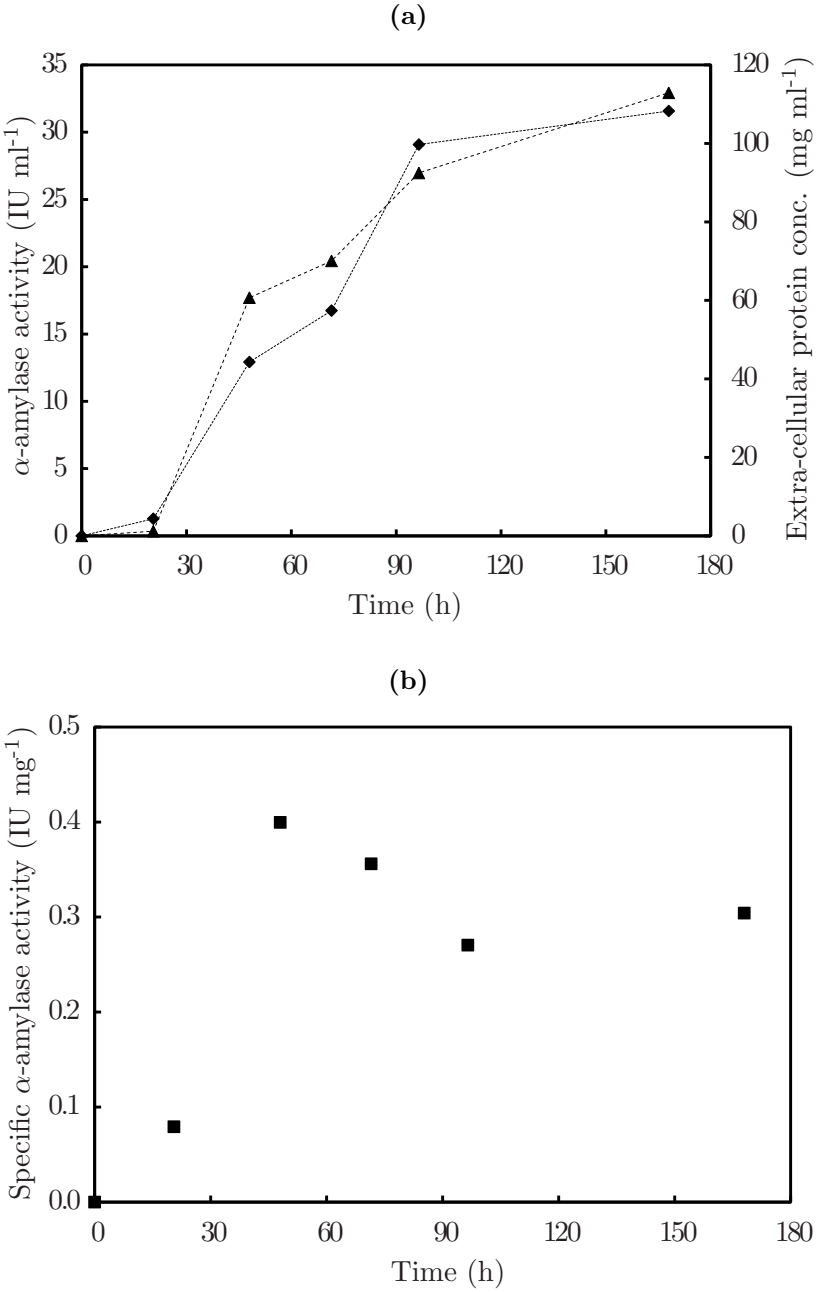


**Figure 6.7:** Typical submerged fermentation of *A. oryzae* showing (a) $\alpha$-amylase activity (▲), extra-cellular protein concentration (♦) and (b) specific $\alpha$-amylase activity (IU $mg^{-1}$ protein). Cultivation conditions were as described in Figure 6.4.

### 6.3.3 Investigation into the use of solid supports in submerged fermentation

In an attempt to garner an insight into the early stages of hyphal development in liquid media, initial work on the characterisation of submerged fermentations was combined with the assay described in Chapter 4 to provide a novel 'mixed-phase' cell-immobilisation culture format. In addition to possible facilitation of micro-morphological observation, the use of solid supports in submerged culture has shown potential for both increased metabolite yield [48] and differential protein expression [54]. A series of shake-flask fermentations were conducted to determine the effect of starch concentration on both the mixed-phase and conventional submerged systems.

When cultivated in the mixed phase format, virtually all biomass remained adhered to the membrane (Fig. 6.8a to 6.8d) - the absence of mycelial elements or pellets in the broth was confirmed by both visual and microscopic inspection. However, acquiring any morphological data from such agglomerates, other than projected area (a proxy indicator of biomass levels), was not possible. Other authors have availed of scanning electron microscopy to visualise immobilised biomass, but the resultant morphological descriptions were qualitative in nature [48]. However, it is interesting to note the lack of a filamentous or annular region around the periphery of the agglomerates, as would often be visible on pellets, which may suggest that peripheral hyphae were compacted by fluid eddies, as described by Rodríguez Porcel and colleagues [51].

Increasing substrate concentration was found to have a significant impact on the gross, macroscopic form of the organism in the submerged format (Fig. 6.8e to 6.8h), with dispersed growth becoming more common as the substrate concentration was increased, complicating the quantification of the resulting macro-morphologies. It is possible that this dispersed growth may be explained by the presence of a greater

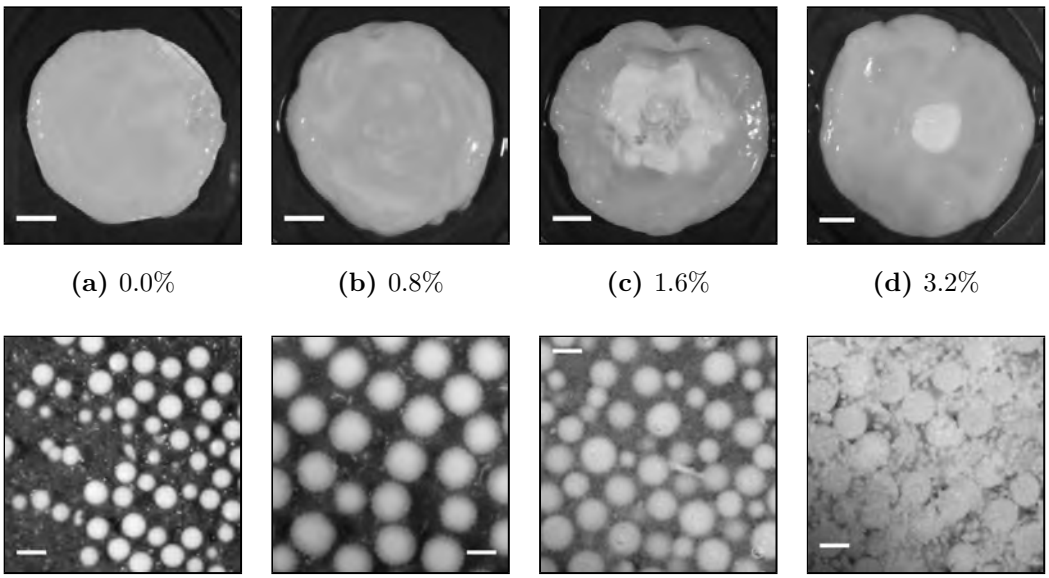

**(a)** 0.0% **(b)** 0.8% **(c)** 1.6% **(d)** 3.2%

**(e)** 0.0% **(f)** 0.8% **(g)** 1.6% **(h)** 3.2%

**Figure 6.8:** Morphological form of *A. oryzae* 120 hours post-inoculation in mixed-phase ('a' - 'd', bars: 10 mm) and submerged fermentations ('e' - 'h', bars: 3 mm) supplemented with the indicated starch concentrations (w/v). Following incubation of membrane culture on SDA for the mixed-phase system, the organism was cultivated in BM (pH 7.0) supplemented with yeast extract (0.5% w/v) and starch (at the indicated concentrations). All flasks and membranes were inoculated with $1 \times 10^7$ spores $ml^{-1}$ ($34.1 \pm 5.8\%$ viability).

number of 'growth centres', provided for by the increased substrate concentration. Starch is not completely soluble at room temperature and, as its concentration in the media was increased, it is possible that a greater number of starch 'particles' were present in the media. These may have provided sites onto which germinating spores adhered themselves, resulting in a more dispersed growth at higher starch concentrations. Such a mechanism has previously been documented in the culturing of *A. oryzae* [154] and *A. awamori* [214] in complex media containing solid particles. Alternatively, the increase in viscosity that resulted from increasing sub-

strate concentration may have been responsible for this observed change in biomass distribution. Indeed it has been reported that regulating apparent broth viscosity (through the addition of xanthan gum) resulted in a decrease in the volume of *Streptomyces hygroscopicus* var. *geldanus* pellets [103]. In this study, a microscopic examination was complicated by the presence of starch particles, particularly at higher concentrations, which obscured the field of view and made the isolation of individual hyphae for analysis difficult to achieve.

A direct relationship was found between substrate concentration and biomass yield (Fig. 6.9), with the dry-cell weight increasing linearly with increasing substrate concentration in both the mixed-phase ($R^2 = 0.96$) and submerged systems ($R^2 = 0.98$). However, the same did not appear to be true of $\alpha$-amylase yield. While biomass levels increased by 85% when starch concentration was increased from 0.8 to 1.6% in the submerged system, $\alpha$-amylase yield increased by just 47%, equating to a drop in $\alpha$-amylase activity per unit dry cell weight (DCW) of approximately 20% (Fig. 6.10). Other reports in the literature have indicated that increasing substrate concentration above 1% (w/v) had no discernible effect on $\alpha$-amylase production by *A. oryzae* [215] or *A. ochraceus* [206]. The levels of $\alpha$-amylase produced in the mixed phase system were similar to those produced in the submerged, which is surprising given the sub-optimal morphological form adopted by the organism when immobilised; it would be expected that such large agglomerates would consist of a relatively low proportion of 'active' biomass. However, a higher biomass yield at a starch concentration of 0.8% (w/v) resulted in a significant reduction in yield per DCW at this substrate concentration in the mixed-phase system.

The difficulties associated with morphological analysis of biomass in the mixed-phase system and the limited influence on $\alpha$-amylase production led to the conclusion that further study of this culture format, in the context of relating morphology to metabolite yield, was not feasible. Furthermore, given the difficulties associated

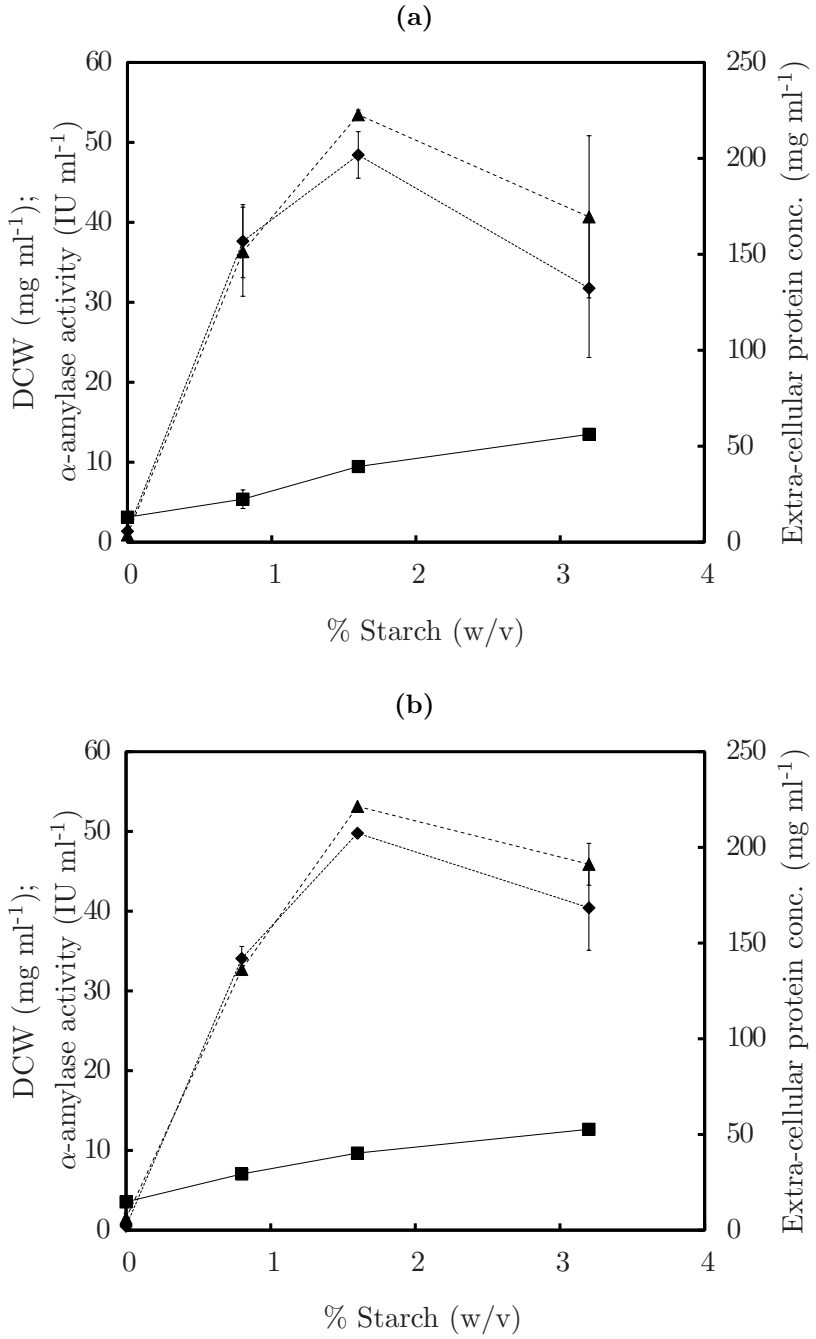


**Figure 6.9:** Dry-cell weight (DCW; ■), $\alpha$-amylase activity (▲) and extra-cellular protein concentration (♦) for varying starch concentrations in the (a) submerged and (b) mixed-phase fermentation of *A. oryzae* 120 hours post-inoculation. Cultivation conditions were as described in Figure 6.8. Error bars represent standard deviation of two independent results.

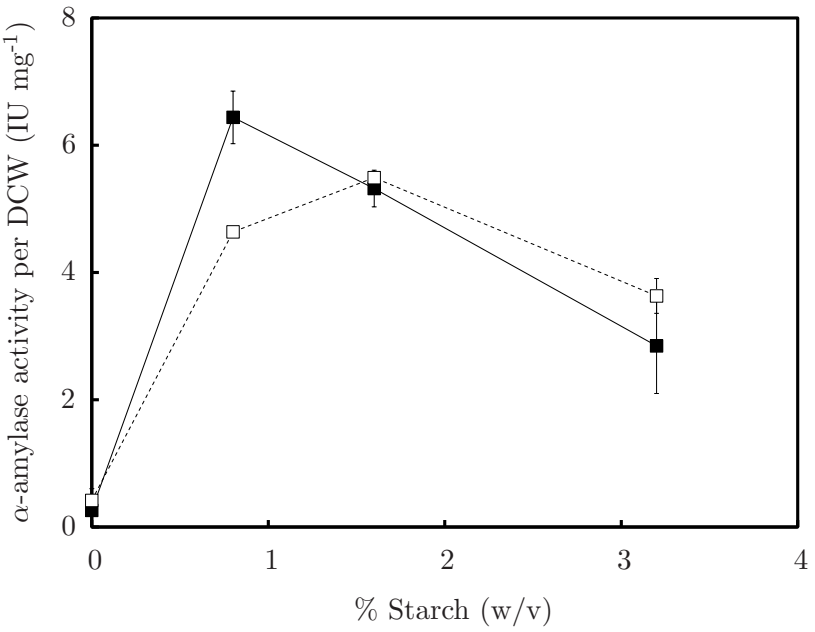


**Figure 6.10:** $\alpha$-amylase activity per unit dry-cell weight for varying starch concentrations in the submerged (■) and mixed-phase fermentation (□) of *A. oryzae* 120 hours post-inoculation. Cultivation conditions were as described in Figure 6.8. Error bars represent standard deviation of two independent results.

with microscopic examination and the apparent lower $\alpha$-amylase yield per DCW at higher substrate levels in the submerged system, there was deemed to be little benefit in increasing starch concentration above approximately 1% (w/v). All subsequent fermentations were conducted with a carbon source concentration at or below this level.

### 6.3.4 Investigation into the effect of carbon source variation on morphology in submerged culture

As a means of perturbing the submerged system to induce micro-morphological change (which may translate into macro-morphological variation) without indirectly impacting other process parameters (such as the increased heterogeneity of the medium resulting from the presence of solid particles described in the previous

section), the effect of utilising different carbon sources in a defined medium was investigated. The early-stage hyphal development of the organism was assessed by imaging submerged culture samples immobilised on membranes (see Section 2.4) and a relationship between micro-morphology and macro-morphology was examined. The substrates chosen were based on reports in the literature suggesting that $\alpha$-amylase yield may be increased by employing lactose and maltose rather than starch [215].

While the development of the fungus on glucose seemed to result in a larger hyphal growth unit compared to other substrates (Table 6.1), the elements were relatively small and unbranched and, as such, the difference is possibly owing to the more limited growth on maltose and starch (reflected in the lower value of $L_{th}$). Virtually no hyphal elements were detectable in basal medium and, as such, a micro-morphological analysis was not possible. Little macro-morphological influence was noted as a result of carbon source variation, with slightly smaller pellets resulting from cultivation on starch compared to maltose and glucose (Fig. 6.11). Starch was found to be the most suitable substrate for $\alpha$-amylase production, while also producing slightly less biomass. The growth of *A. oryzae* on lactose was limited (not shown), the resulting biomass and $\alpha$-amylase yields being similar to those produced in the basal medium (without carbon source supplementation).

Studying the micro-morphological development of *A. oryzae* in submerged culture had associated practical difficulties. The organism's spores tended to agglomerate prior to germination (Fig. 6.12) and this resulted in the presence of free mycelia in the media being rare, particularly so when starch was used as substrate. A large sample of the media was therefore required (approximately 10% of the total volume) in order to provide a sufficient number of elements to yield a statistically significant result; such a large reduction in culture volume may well have affected the outcome of the fermentation.

**Table 6.1:** Mean total hyphal length ($L_{th}$), mean number of tips ($N$) and mean hyphal growth unit ($L_{hgu}$) of *A. oryzae* mycelia 16 hours post-inoculation when cultivated in BM (pH 7.0) supplemented with 1% (w/v) of the indicated carbon source. Errors represent 95% confidence intervals.

| Substrate | $L_{th}$ ($\mu$m) | $N$ | $L_{hgu}$ ($\mu$m) | n |
|---|---|---|---|---|
| Glucose | 344.1 ± 57.7 | 4.9 ± 0.7 | 67.8 ± 5.6 | 71 |
| Maltose | 171.5 ± 33.0 | 3.1 ± 0.4 | 50.8 ± 6.3 | 80 |
| Starch | 208.7 ± 40.1 | 3.9 ± 0.5 | 50.3 ± 5.1 | 73 |

Given the limited growth of the mycelia presented here (Table 6.1), the experiment was repeated in an attempt to analyse the microscopic form of the organism at a later point in time (24 hours post-inoculation). However, obtaining a large enough population of mycelia from which to derive a statistically relevant result, without sampling more than 10% of the culture, was not feasible (data not shown). It is possible that as the mycelia increased in size, a degree of agglomeration occurred, further reducing the concentration of free mycelia in the media; agglomeration of *A. oryzae* mycelia has previously been described by Amanullah and colleagues [88]. It was therefore concluded that microscopic examination of such cultures was not achievable and subsequent experimentation focussed on attempts to induce a greater degree of filamentous growth to enable quantification of micro-morphology.

### 6.3.5 Influence of inoculum concentration on morphology and alpha-amylase production

Increasing inoculum concentration has previously been demonstrated as an effective means of inducing filamentous growth in both *A. niger* [72] and *Rhizopus chinensis* [76]. As a dispersed growth form would permit a more extensive microscopic analysis, the effects of increasing the initial inoculum concentration above

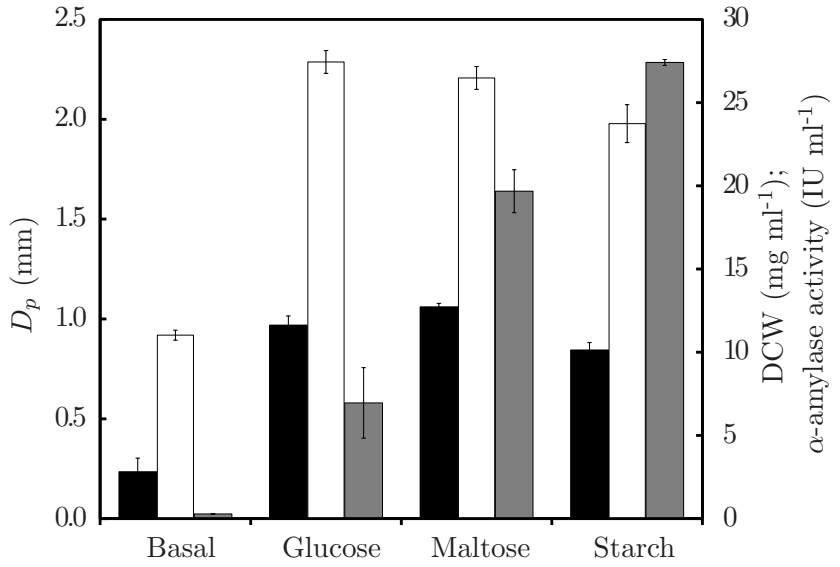


**Figure 6.11:** Dry-cell weight (DCW; ■), $\alpha$-amylase activity (■) and mean pellet diameter ($D_p$; □) for different carbon sources in the submerged fermentation of *A. oryzae* 60 hours post-inoculation. Organism cultivated in BM (pH 7.0) supplemented with 1% (w/v) of the indicated carbon source. All flasks inoculated with $1 \times 10^7$ spores ml$^{-1}$ ($33.6 \pm 5.9\%$ viability). Error bars represent standard deviation of two independent results.

$1 \times 10^7$ spores ml$^{-1}$ on morphology and $\alpha$-amylase production in the submerged fermentation of *A. oryzae* were investigated.

While pelleted biomass was found to predominate at all inoculum concentrations (and as a result, micro-morphological examination of 'free' elements was not feasible), relationships between inoculum concentration ($C_i$), pellet diameter ($D_p$) and $\alpha$-amylase yield were observed. $\alpha$-amylase activity per unit dry-cell weight (IU mg$^{-1}$ DCW) appeared to be directly proportional to inoculum concentration ($R^2 = 0.95$; Fig. 6.13a), while mean pellet diameter was found to be inversely proportional to inoculum concentration ($R^2 = 0.96$).

In an attempt to establish a preliminary link between metabolite yield and morphology, $\alpha$-amylase activity per DCW was expressed as a function of $D_p$ (Fig. 6.13b),

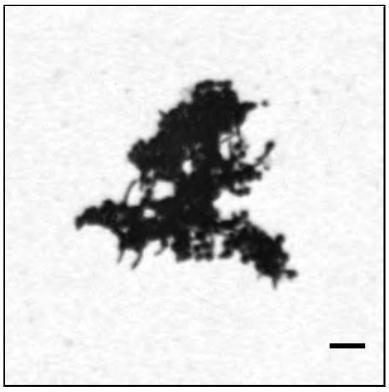

**Figure 6.12:** An aggregate of *A. oryzae* spores sampled from a shake flask approximately 7 hours post-inoculation. Bar: 25 $\mu$m.

which is derived from the measured projected area ($A_p$; mm$^2$) of each pellet by calculating the equivalent radius ($r = \sqrt{A_p \pi^{-1}}$). Given the evidence in the literature for metabolite excretion occurring primarily at hyphal tips [107, 216] and productive biomass being limited to the outer layer of pellets [43, 46], it seems reasonable that $\alpha$-amylase activity per DCW would be directly proportional to the mean pellet surface area times the number of pellets present in the media ($n$):

$$\alpha\text{-amylase activity per DCW} \propto n 4\pi r^2 \tag{6.2}$$

This is based on the assumption that the product of the number of hyphal tips ($N$) per unit area of pellet surface and the amount of $\alpha$-amylase produced by each tip is relatively independent of inoculum concentration:

$$\frac{\alpha\text{-amylase activity}}{N} \times \frac{N}{4\pi r^2} = c \tag{6.3}$$

where $c$ is a constant. For a given level of biomass, $n$ is inversely proportional to pellet size (or pellet volume):

$$n \propto \frac{1}{\frac{4}{3}\pi r^3} \tag{6.4}$$

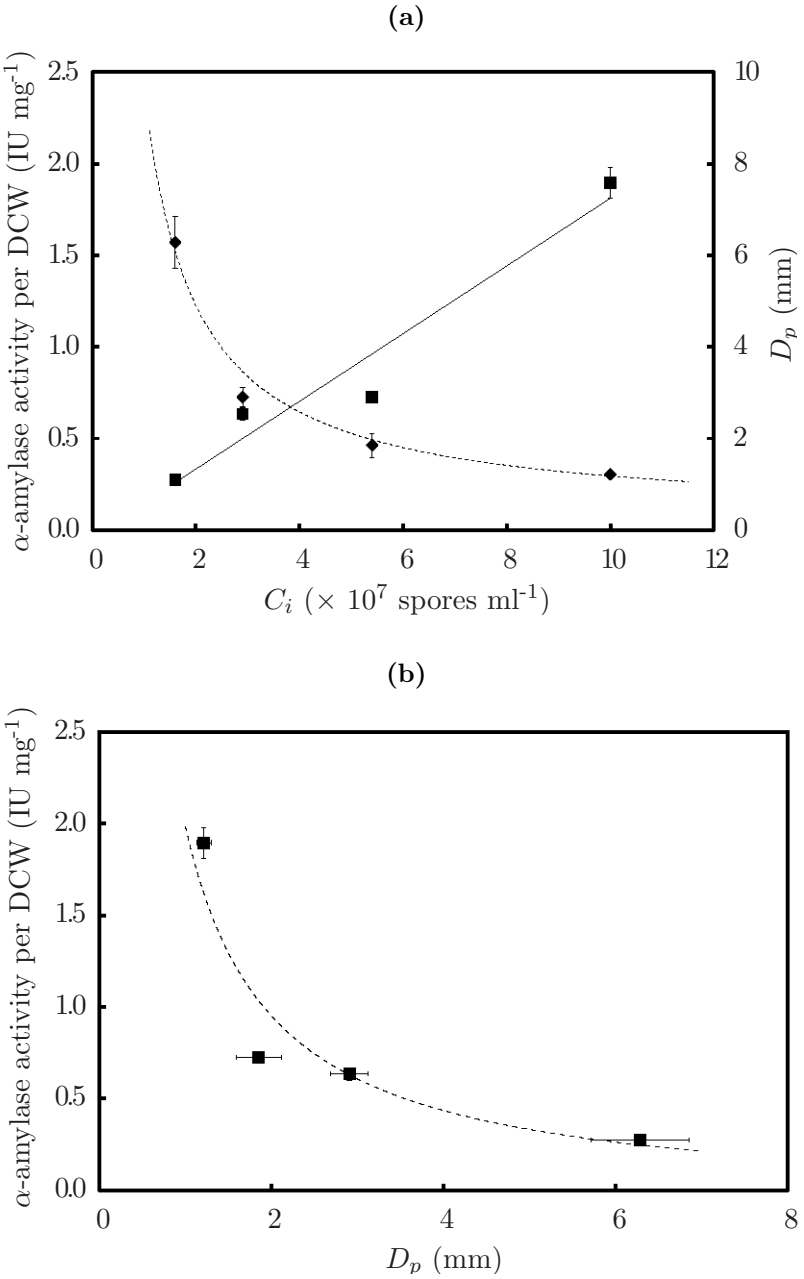


**Figure 6.13:** (a) $\alpha$-amylase activity per DCW (■) and mean pellet diameter ($D_p$; ♦) versus inoculum concentration ($C_i$) in the submerged fermentation of *A. oryzae* 65 hours post-inoculation. (b) $\alpha$-amylase activity per DCW is inversely proportional to mean pellet diameter ($D_p$). The dotted line represents Equation (6.5) with $a_{D/X} = 2.07$ IU mm mg$^{-1}$ ($R^2 = 0.88$). Error bars represent standard deviation of two flasks. Spore viability = $35.7 \pm 7.1\%$.

Combining equations 6.2 and 6.4 and substituting for $r$:

$$\alpha\text{-amylase activity per DCW} = \frac{a_{D/X}}{D_p} \tag{6.5}$$

where $a_{D/X}$ (IU mm mg$^{-1}$) is a proportionality constant. This relationship is illustrated graphically in Figure 6.13b.

These results are in general agreement with reports in the literature that suggest a low inoculum concentration results in larger pellets [49, 72, 100] and that smaller pellets result in higher metabolite yields in *Aspergilli* [46, 74, 96, 98]. While a correlation between pellet size and $\alpha$-amylase production appeared to exist in this study, the microscopic examination of pellets using light microscopy was not feasible, due to their three-dimensional structure and relatively large size ($D_p \leq 7$ mm). The potential for obtaining micro-morphological insights into enzyme production using inoculum concentration as a process variable was therefore deemed to be limited.

### 6.3.6 Influence of surfactant compounds on morphology and metabolite yield

During the course of this work, studying *A. oryzae* at the microscopic level was often complicated by the lack of 'free' mycelia present in submerged culture due to the agglomerative nature of the organism's conidiospores. However, several studies have reported successful attempts to regulate morphology by supplementing media with various polymers and surfactant (surface active agent) compounds [14, 15, 100–102]. The effect of some of these substances on cultures of *A. oryzae* was therefore investigated.

*Influence of Tween-80 on morphology and $\alpha$-amylase production*

In an attempt to counteract the agglomeration of spores, without adversely affecting growth or metabolite production, Tween-80, a surfactant routinely used in

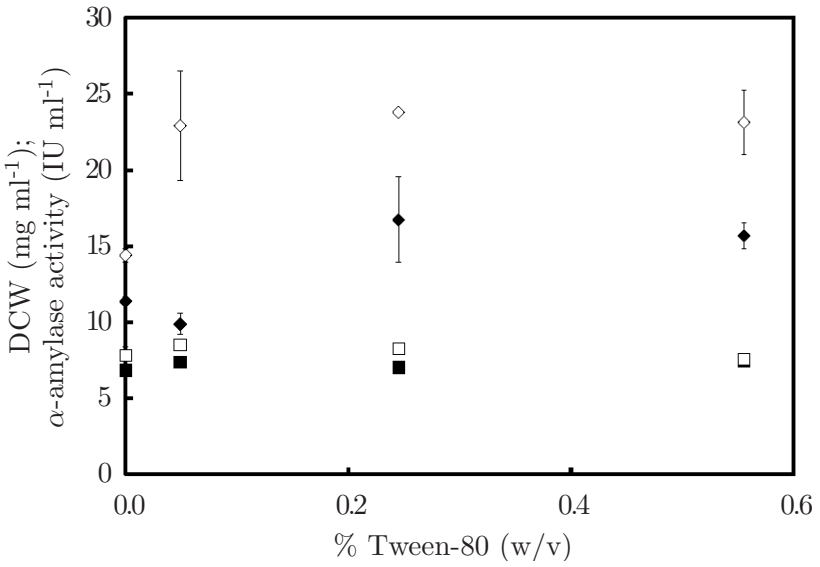


**Figure 6.14:** Impact of supplementing *Aspergillus oryzae* fermentation broth with Tween-80 on $\alpha$-amylase activity (⧫, ◊) and dry cell weight (■, □) for inoculum concentrations of $1 \times 10^7$ (⧫, ■) and $1 \times 10^8$ spores ml$^{-1}$ (◊, □) 65 hours post-inoculation. Error bars represent standard deviation of two flasks. Spore viability = $52.8 \pm 11.7\%$.

fungal conidial preparations to aid spore dispersal, was incorporated into submerged culture and its impact on morphology and $\alpha$-amylase yield was quantified. The addition of 0.05% (w/v) Tween-80 resulted in an increase in $\alpha$-amylase activity of approximately 59% in flasks inoculated with $1 \times 10^8$ spores ml$^{-1}$ (Fig. 6.14); further increasing the concentration of Tween-80 up to 0.56% (w/v) had little additional effect. In flasks inoculated with $1 \times 10^7$ spores ml$^{-1}$, $\alpha$-amylase activity was slightly reduced in the presence of 0.05% (w/v) Tween-80, but increasing the concentration to 0.25% (w/v) resulted in an increase in activity of approximately 47%. Biomass levels appeared to be relatively independent of Tween-80 concentration.

The addition of 0.05% (w/v) Tween-80 resulted in a significant increase in pellet size at the lower inoculum concentration (Fig. 6.15a), which may explain the observed reduction in $\alpha$-amylase activity at this concentration. However, despite

**Table 6.2:** Mean projected area ($A_p$) and mean circularity ($C$) of *A. oryzae* pellets 24 hours post-inoculation when cultivated in media supplemented with Tween-80 as indicated. Flasks were inoculated with $1 \times 10^7$ spores ml$^{-1}$ (viability = 35.5%) and incubated at 30°C. Errors represent 95% confidence intervals.

| Tween-80 (% w/v) | $A_p$ ($\times 10^6$ $\mu$m$^2$) | $C$ | $n$ |
|---|---|---|---|
| 0.0 | $1.50 \pm 0.28$ | $0.032 \pm 0.007$ | 12 |
| 0.5 | $1.28 \pm 0.28$ | $0.028 \pm 0.005$ | 12 |
| 1.0 | $1.51 \pm 0.25$ | $0.027 \pm 0.004$ | 10 |

producing slightly larger pellets, flasks inoculated with $1 \times 10^8$ spores ml$^{-1}$ produced higher yields of $\alpha$-amylase per DCW in the presence of Tween-80. This complex relationship is emphasised in Figure (6.15b), where no clear correlation between pellet size and $\alpha$-amylase activity per DCW is apparent ($R^2 = 0.52$ for linear regression).

The higher yield of $\alpha$-amylase obtained in the presence of Tween-80 may be evidence of an influence at the micro-morphological level, such as an increase in hyphal branching. A microscopic analysis of pellets (Fig. 6.16) suggests that this is not the case, as similar values of circularity ($C = 4\pi A_p P^{-2}$) were obtained for pellets cultivated with or without Tween-80 supplementation (Table 6.2). However, a more extensive microscopic examination was required to generate a more conclusive result.

*Influence of Tween-80 on micro-morphological development in solid culture*

The effect of Tween-80 on the early-stage, microscopic development of *A. oryzae* was investigated on solid substrate using membrane-immobilisation in order to isolate individual mycelia for subsequent image analysis. The inclusion of Tween-80 in the media resulted in a small decrease in the hyphal growth unit compared to the control, although this decrease was not statistically significant (Fig. 6.17a). Furthermore, given the reasonable correlation between $L_{hgu}$ and $L_{th}$ evident in Figure 6.17,

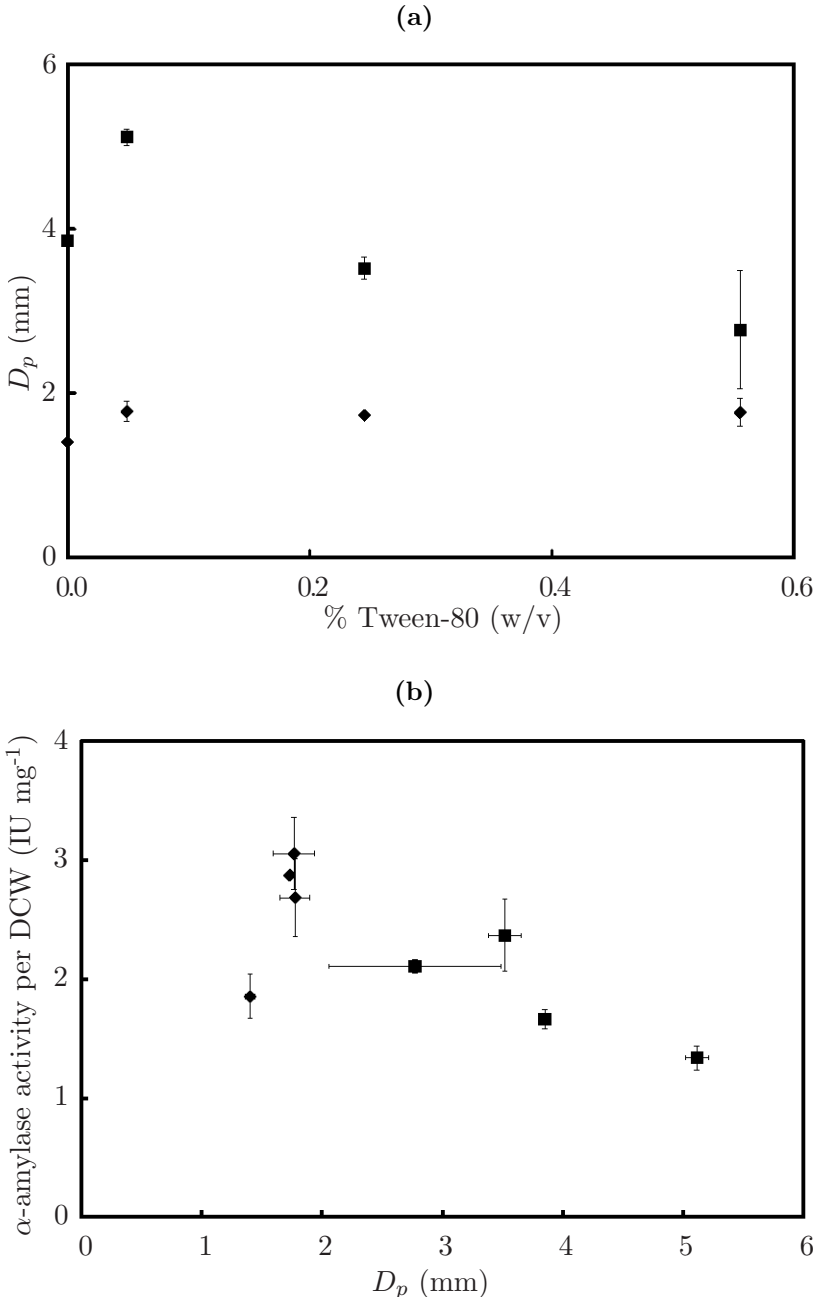


**Figure 6.15:** Impact of supplementing *Aspergillus oryzae* fermentation broth with Tween-80 on (a) mean pellet diameter ($D_p$) after 65 hours' incubation for inoculum concentrations of $1 \times 10^7$ (■) and $1 \times 10^8$ spores ml$^{-1}$ (⧫). (b) No direct relationship between $\alpha$-amylase activity per DCW and $D_p$ was found. Error bars represent standard deviation of two flasks. Spore viability $= 52.8 \pm 11.7\%$.

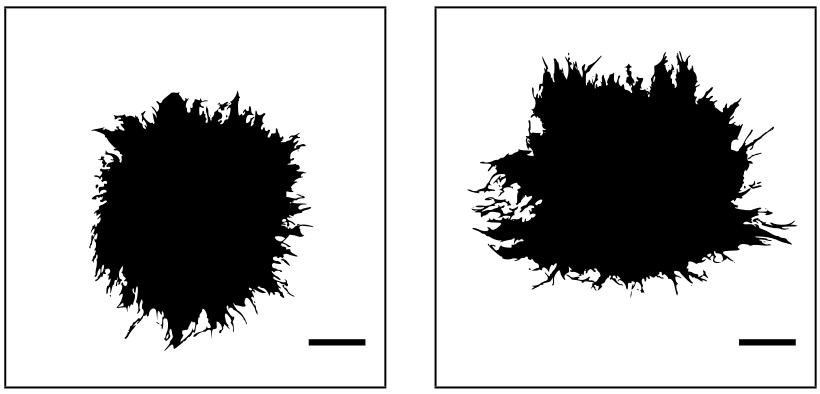

**(a)** $A_p = 1.68 \times 10^6$ $\mu$m$^2$, $C = 0.027$ **(b)** $A_p = 1.64 \times 10^6$ $\mu$m$^2$, $C = 0.025$

**Figure 6.16:** Morphology of *A. oryzae* pellets cultivated in the presence of (a) 0% and (b) 1.0% (w/v) Tween-80. Cultivation conditions were as described in Table 6.2. Bars: 0.4 mm.

it is probable that this lower value of $L_{hgu}$ was related to a decrease in the extent of growth, rather than any change in the morphology of the organism (Fig. 6.17b). It was therefore concluded that no appreciable influence of Tween-80 on hyphal extension was evident, but the increase in pellet size observed at some concentrations in submerged culture was still without explanation.

*Effect of Tween-80 on spore agglomeration*

The observed influence of Tween-80 on pellet diameter (Fig. 6.15a) was investigated at the microscopic level by assessing the effect of the surfactant on particle agglomeration. Approximately 2 hours post-inoculation, the number of particles present in the media was up to 45% higher in the presence of the Tween-80, the difference being even more pronounced at 4 hours post-inoculation (Fig. 6.18). The lower of the two Tween-80 concentrations (0.05% w/v) resulted in a greater degree of dispersal, but from 6 hours onwards, there was no significant difference in particle dispersal

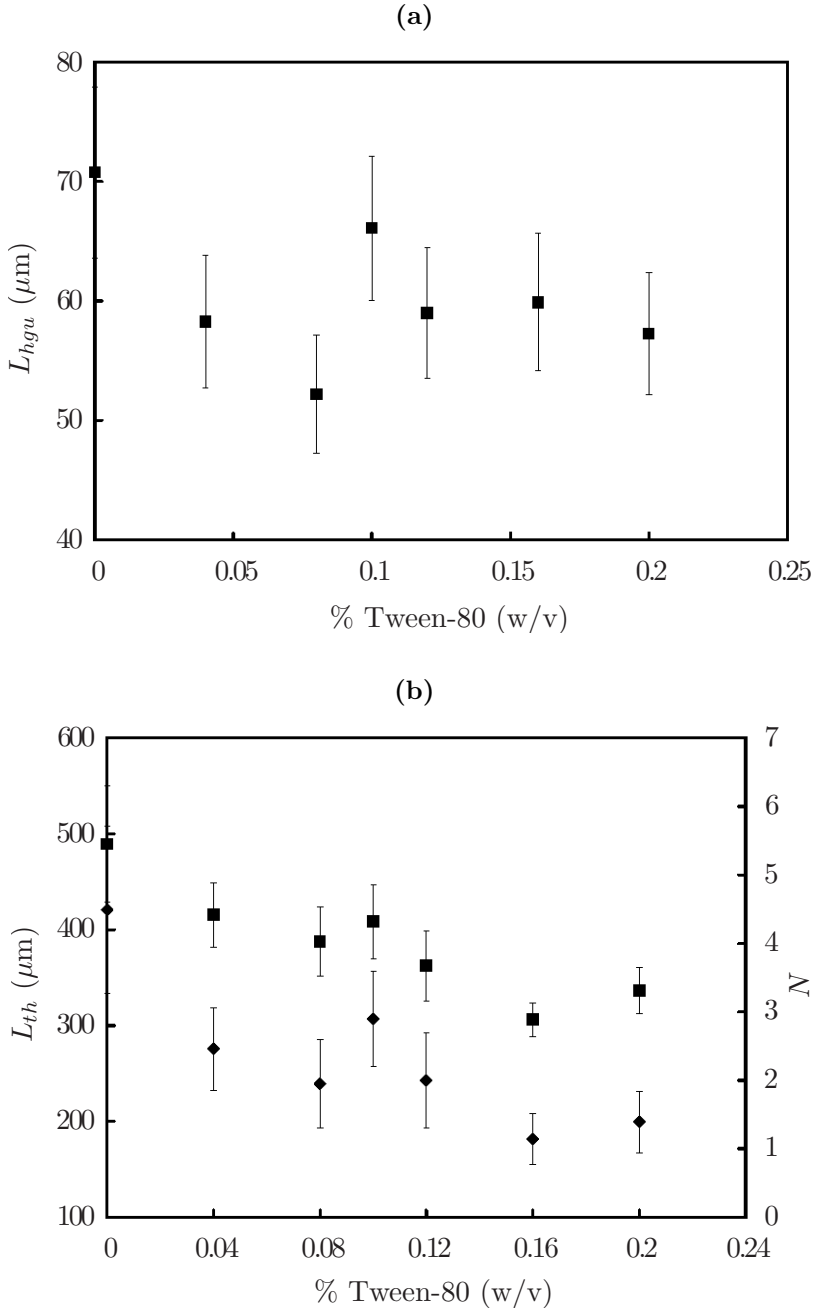


**Figure 6.17:** Variation in (a) the mean hyphal growth unit ($L_{hgu}$) and (b) the mean total hyphal length ($L_{th}$; ♦) and mean number of tips ($N$; ■) of populations of *Aspergillus oryzae* mycelia cultivated on malt agar supplemented with varying concentrations of Tween-80 (30°C, 20 h). Error bars represent 95% confidence intervals.

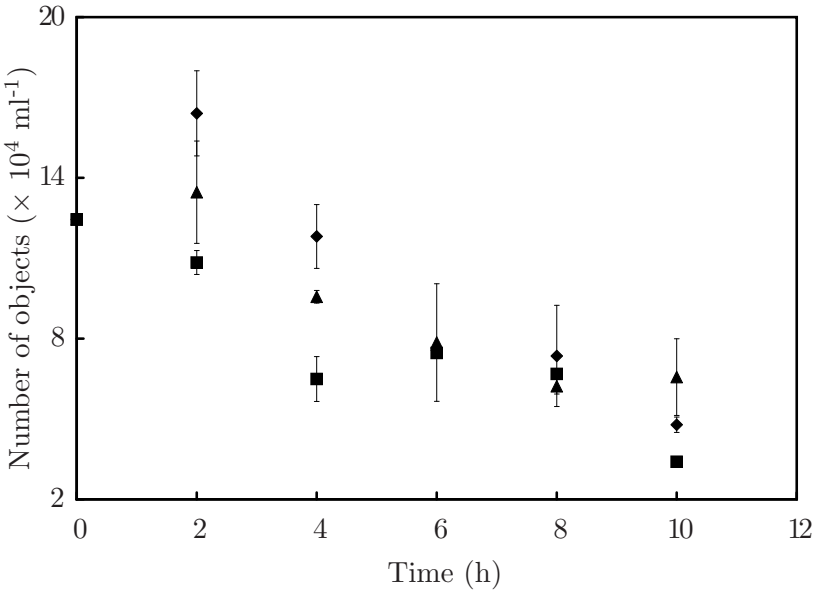


**Figure 6.18:** Time-course of aggregation in the submerged fermentation of *Aspergillus oryzae* in the presence of 0 (■), 0.05 (♦) and 0.1 (▲) % Tween-80 (w/v). All flasks inoculated with $2 \times 10^7$ spores $ml^{-1}$. Error bars represent standard deviation of two flasks, with approximately 27 fields of view examined for each flask.

between the three different media, suggesting that any impact was short-lived.

There is evidence that suggests the surface properties of fungal spores are altered during the swelling and germination process. Investigations using atomic force microscopy have shown that the hydrophobicity of *A. oryzae* and *A. fumigatus* conidia decreases as they swell and germinate [217, 218]. This may offer an explanation as to why the influence of Tween-80 does not seem to be visible 6 hours post-inoculation.

*Does Tween-80 influence the morphology of* Aspergillus oryzae*?*

Based on the series of investigations conducted here, it was concluded that Tween-80 had a limited influence on pellet formation in submerged cultures of *A. oryzae*. Although Tween-80 has been found to inhibit pellet formation in *T. reesei* [14], it has also been found to cause an increase in pellet size in cultures of *R. nigricans* [15],

although in the case of the latter, a degree of filamentous growth was also induced at higher concentrations. However, no inducement of filamentous growth was observed here and, as such, a thorough microscopic examination of submerged culture was not possible, and no relationship between the increase in $\alpha$-amylase production and micro-morphological parameters (such as $L_{hgu}$) was obtainable. Subsequent experimentation focussed on investigations of other surfactants and polymers that had been previously reported to inhibit pellet formation.

*Further qualitative assessment of the morphological influence of polymers and surfactants*

The potential of a number of other polymers and surfactant compounds to disrupt pellet formation in cultures of *A. oryzae* was investigated. The majority of compounds tested resulted in the formation of pellets of either smaller (Ficoll) or larger diameter (diethylaminoethyl cellulose, Sephadex G-75) than the control (data not shown). However, other compounds seemed to inhibit pellet formation to some extent, producing filamentous structures (together with pellets) that were potentially suited to routine microscopic analysis (Fig. 6.19). However, polymers such as carboxymethylcellulose (CMC) and Sephadex caused the media to exhibit a paste-like consistency, which complicated dry-cell weight determination and for this reason they were deemed unsuitable for further study. Subsequent experiments examined the effect of the non-ionic detergents, Triton X-100 and Nonidet P-40.

*Influence of Triton X-100 and Nonidet P-40 on macro-morphology and metabolite yield*

The addition of 0.1% (w/v) Triton X-100 resulted in an increase of approximately 149% in $\alpha$-amylase activity; higher concentrations had no further effect (Fig. 6.20a). The addition of Triton X-100 also caused a reduction in biomass levels of up to 51%,

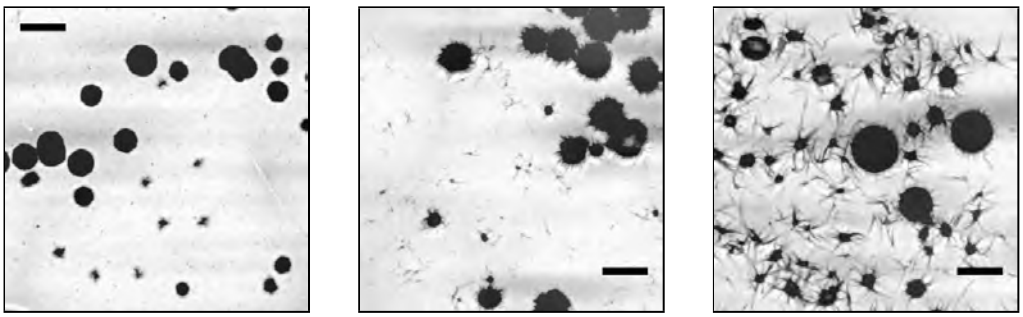

**(a)** **(b)** **(c)**

**Figure 6.19:** Variation in morphology of *A. oryzae* after 72 hours resulting from supplementation with 0.6% w/v (a) Triton X-100, (b) carboxymethylcellulose and (c) Sephadex G-200. Bars: 5 mm.

resulting in increases in $\alpha$-amylase per DCW of up to 184%. Lower biomass yields may suggest a negative physiological impact of the detergent and an inhibition of growth. The addition of Nonidet P-40 caused similar reductions in biomass levels, but the resultant increases in $\alpha$-amylase activity were significantly less.

In the case of both Nonidet P-40 and Triton X-100, no correlation was found between $\alpha$-amylase per DCW and pellet size (Fig. 6.20b). Evidence in the literature suggests that smaller pellets should result in a higher metabolite yield [46, 74, 96, 98, 100], but $\alpha$-amylase activity was lower in flasks supplemented with Nonidet P-40 compared to those supplemented with Triton X-100 (but still higher than the control), even though the latter produced larger pellets. This may be explained by the lower dry-cell weights observed in the presence of detergents; the smaller pellet sizes may be partly caused by inhibition of growth rather than dispersal of biomass. Evidently, a macro-morphological analysis alone is not sufficient to explain the effect of non-ionic detergents on *A. oryzae*.

The detergents may have had a micro-morphological effect; an increase in hyphal branching may have been responsible for the observed increase in $\alpha$-amylase yield.

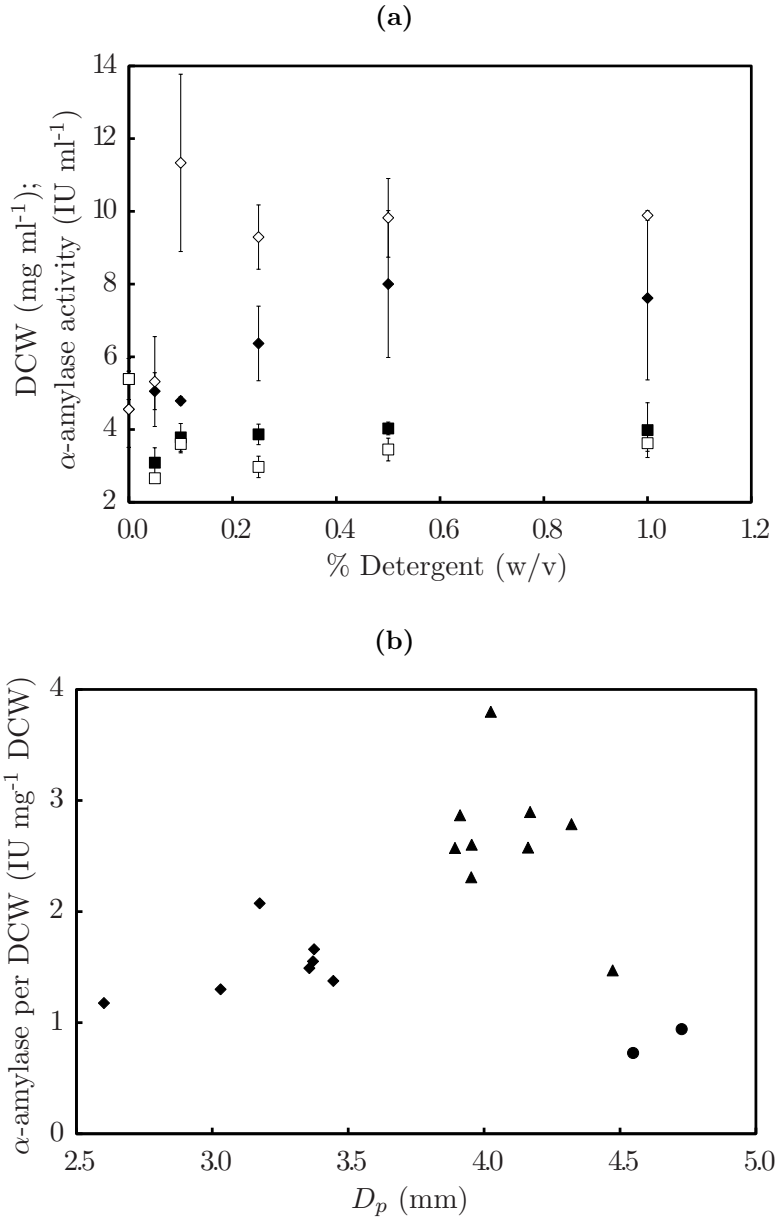


**Figure 6.20:** (a) Impact of supplementing *Aspergillus oryzae* fermentation broth with different concentrations of Nonidet P-40 (■, ⧫) and Triton X-100 (□, ◊) on $\alpha$-amylase activity (⧫, ◊) and dry cell weight (DCW; ■, □). Average of two independent results is shown. Error bars represent standard deviation. (b) Mean pellet diameter ($D_p$) versus $\alpha$-amylase activity per unit dry cell weight in the presence of Nonidet P-40 (⧫), Triton X-100 (■) and without supplementation (•). All flasks inoculated with $9 \times 10^6$ spores ml$^{-1}$ (viability = $45.3 \pm 2.9\%$).

However, microscopic examination of the fungus in the presence of either Triton X-100 or Nonidet P-40 was not possible, as samples taken from these fermentations exhibited poor stain uptake (lactophenol cotton blue; not shown). Whether this was a result of an inhibition of staining by the detergents, or a physiological influence of the detergents on the cells, resulting in variations in cell wall composition, is not clear. Alternatively, it is possible that the presence of non-ionic detergents in the media caused an increase in cell permeability, leading to greater mass diffusion into the pellets [14, 15]. This may have resulted in a wider 'active' region in the pellet, causing an increase in metabolite production. The increase in $\alpha$-amylase activity observed in the presence of non-ionic detergents may also have been a result of enhanced activation of the enzyme by the surfactants, rather than an increase in enzyme production by *A. oryzae*. Supplementing a solution containing porcine pancreatic $\alpha$-amylase with 0.02% w/v Triton X-100 has been shown to result in an increase in activity of approximately 40% [219].

## 6.4 Discussion

The yield from fermentation processes involving filamentous micro-organisms are heavily influenced, both directly and indirectly, by the phenotype adopted by the microbe [8, 220]. While many reports have indicated success in elucidating reproducible relationships between morphology and metabolite production [45, 46, 50, 72, 74, 80, 96, 97, 100, 154], conflicting reports do exist [44, 95, 98], while others have failed to demonstrate any significant dependence [73, 83, 84, 107, 112]. The optimisation of submerged fermentations through the computation of morphological parameters therefore remains a considerable challenge for fungal biotechnologists. While growth on solid culture may be essentially restricted to two dimensions (using membrane-immobilisation), filamentous micro-organisms cultivated in liquid

medium typically exhibit significant three-dimensional character, resulting in complex conformations that are not easily quantified. Consequently, 'free' filaments are generally targeted for detailed microscopic analysis, as individual hyphae and branches may be isolated and an accurate description of morphological parameters produced. However, the presence of such free elements may be rare, depending on the culture conditions. Nevertheless, given the evidence for metabolite excretion occurring primarily at hyphal tips [105, 107], microscopic characterisation is essential for a thorough description of microbial growth.

Furthermore, there is evidence that the microscopic development of an organism can have a significant influence on the macroscopic form. For example, a 'hyper-branched' mutant of *A. oryzae*, which exhibited a lower projected area per hyphal tip, resulted in more compact clumps and pellets compared to a wild-type strain, resulting in lower broth viscosity [107, 152]. Park and colleagues also demonstrated relationships between micro-morphological parameters and macroscopic form in different species of *Mortierella*, although the resultant macro-morphologies were not quantitatively assessed [125]. Species exhibiting a high branch formation rate formed 'pellet-like' structures with a distinct core, while species attributed with a low branch formation rate formed hyphal aggregates without cores. Microscopic analysis of early hyphal development is therefore essential if the formation of diverse phenotypes is to be understood.

### 6.4.1 Growth and fragmentation of pellets in shake-flask culture

The characterisation of shake-flask culture conducted here indicated that the distribution of pellet sizes at any given point in time is dependent on both growth and fragmentation. The depth of the 'active' region of *A. oryzae* pellets has been estimated to be of the order of 100 – 300 $\mu$m [45], meaning that by 24 hours post-inoculation, when pellets had attained a mean diameter of approximately 1.5 mm

(Fig. 6.4), oxygen limitation had almost certainly set in at the pellet core. Furthermore, considering that Carlsen and colleagues demonstrated a sharp increase in ethanol concentration (indicating anaerobic metabolism) at the onset of pellet fragmentation in *A. oryzae* just 35 hours post-inoculation [45], it seems likely that in the shake-flask culturing conducted here, anaerobic conditions existed at the pellet core by the time fragmentation was observed (when $t \geq 72$ h). Autolysis and subsequent 'hollowing' of pellets may also offer an explanation for the reduction in biomass, which was concurrent with pellet fragmentation.

However, if autolysis was solely responsible for pellet fragmentation, then it might be expected that the fragmented pellets would continue to grow and biomass would continue to increase. This was clearly not the case (Fig. 6.4a), suggesting that the culture was nutrient-limited. Under these conditions, vacuolation of hyphae at the pellet periphery may have weakened the structure of these cells [79], resulting in shearing of the pellet boundary and a subsequent reduction in pellet size, while also causing an increase in the number of relatively small mycelial objects in the media (Fig. 6.6). It is possible that pellet fragmentation resulted from a combination of mass-transfer limitations (perhaps leading to autolysis) and nutrient exhaustion.

As discussed in Chapters 3 and 4, contiguous, high-contrast staining of hyphae is essential for accurate quantification of hyphal architectures using automated image analysis. As such, quantification of pellet/hyphal fragments at the microscopic level was not possible due to limited stain uptake by hyphae (Fig. 6.5). Indeed, comprehensive assessment of micro-morphology in batch culture over a period of days (rather than hours) are rare in the literature. One such study was conducted by Müller and colleagues, who characterised the microscopic development of *A. oryzae* up to 60 hours post-inoculation [152]. However, a relatively low resolution was employed (×4 objective) and manual counts of hyphal tips were required. A higher resolution examination was conducted by Carlsen and colleagues, but was restricted

to the first 18 hours of growth [45]. However, examination of microscopic structures that result from pellet/hyphal fragmentation may be of limited value as such objects will exhibit artificial 'tips' resulting from hyphal fragmentation. While it may be of interest to identify points on hyphae at which breakage has occurred, discriminating between 'true' tips and artificial tips using bright-field microscopy would be difficult to achieve. However, an analysis of such fragments at the microscopic level could be used to provide more complete data on the projected area of biomass elements than that which was presented here.

More extensive morphological data could also be gathered through the microscopic examination of pellets (such as that presented in Table 6.2). Pellet diameter and circularity were quantified by Paul and colleagues by suspending pellets of *A. niger* in water (to preserve the three-dimensional structure) in a Petri dish and imaging with a macro-viewer [44]. However, given the problems associated with hyphal staining encountered here, it is likely that stain uptake around the pellet periphery would be poor in the latter stages of the fermentation. Furthermore, the pellets encountered in this work were often far too large to microscopically image in a single field of view, with pellet diameters of up to $\sim$ 7 mm measured at low inoculum concentrations.

### 6.4.2 Limitations of mixed-phase culture format

Investigations into the feasibility of a mixed-phase culture format were limited by a lack of morphological data; there was little potential for analysis of the macroscopic form adopted by the organism (Fig. 6.8a to 6.8d). While microscopic examination of membrane-immobilised cultures is possible (Chapters 3 & 4), the situation is complicated somewhat when a liquid medium is employed, as the fungus must be allowed to establish itself on the membrane (for the purpose of adherence). This establishment prior to submerged incubation limits the 'window' during which mi-

croscopic visualisation may be conducted, although a 'snapshot' at a particular point in time is still possible. This difficulty may potentially be overcome by employing some form of 'adhesive' to fix spores to the membrane, such as poly-D-lysine [4], obviating the requirement for pre-establishment. This may permit a detailed assessment of early hyphal development in the mixed-phase system, although based on the results presented here, it seems likely that the resultant growth would exhibit a significant three-dimensional character.

There are reports in the literature of successful attempts to incorporate solid supports into liquid fermentation systems. While no significant influence on metabolite production was found in this investigation, the use of polymeric membranes in liquid culture has recently been discovered to result in elevated production in cultures of *Penicillium* sp. *LL*-WF159 [54]. In addition, nylon supports were found to substantially increase citric acid yield when employed in submerged cultures of *A. niger* [48]. The increased production was attributed to the considerably lower diffusion path in the immobilised mycelium compared to pelleted cultures. However, morphological characterisation of immobilised biomass was limited to qualitative assessment of images produced using scanning electron microscopy.

### 6.4.3 Macro-morphological influence of starch concentration

A significant macroscopic response was observed when the concentration of starch in the media was increased (Fig. 6.8e to 6.8h). While it was not possible to investigate this influence at the microscopic level (due to high levels of artifact resulting from suspended starch), evidence in the literature suggests that increasing substrate concentration serves only to increase growth rate, without affecting micro-morphological parameters. For example, Park and colleagues reported that the branch formation rate of *Mortierella alpine* was independent of carbon concentration [124]. A similar conclusion was reached by Spohr and colleagues in the study

of *A. oryzae*, where Monod kinetics were used to illustrate the effect of substrate concentration on growth parameters [4]. However, Müller and colleagues reported that, in *A. niger* and *A. oryzae*, the length of the apical compartment, the number of nuclei in the apical compartment and the hyphal diameter were regulated in response to the surrounding glucose concentration [90]; variations in length of approximately 100 $\mu$m were recorded for different growth rates. However, the concentrations of starch used in this study were likely to be high enough to ensure that $\mu$ approximated $\mu_{max}$. Hence, variations in apical volume caused by changes in specific growth rate seem unlikely.

The provision of additional substrate resulted in an approximately linear increase in biomass levels (Fig. 6.9a); a similar linear increase in biomass for increasing starch concentration was reported by Nahas and Waldemarin in the culturing of *A. ochraceus* [206]. However, it is clear that not only did an increase in starch concentration result in additional biomass, but a significant influence on morphology was also observed, which may offer an explanation for the lower yields of $\alpha$-amylase per DCW. The growth form that resulted at high starch concentrations (Fig. 6.8h) produced a much more turbid medium compared to that which prevailed at lower substrate concentrations (Fig. 6.8e). The predominance of this 'pulpy' growth may have caused mixing problems in the broth, resulting in mass transfer limitations and a subsequent reduction in metabolite production.

A macro-morphological influence of substrate concentration has been reported in other studies. For example, an increase in the pellet size of *Mortierella alpina* was described for increasing carbon to nitrogen ratios (for $C/N > 20$), but when the medium was enriched at a fixed $C/N$ ratio of 20, the whole pellet size and the width of the pellet annular region decreased with increasing nutrient concentration [93]. Papagianni and Mattey found that mean equivalent pellet diameter was inversely related to glucose concentration in shake-flask fermentations of *A. niger* [48].

### 6.4.4 Impact of carbon source variation

A limited macro-morphological influence of carbon source variation was observed (Fig. 6.11), with the mean equivalent diameter of pellets cultivated in the presence of starch being slightly less than that in the presence of maltose (approximately 10%) and glucose (15%). It was also noted that biomass yield was 15 – 20% lower on starch compared to maltose and glucose, which may suggest that the differences in pellet size were linked to variations in the extent of mycelial growth. Although differences in both pellet size and $\alpha$-amylase production were discernible, relating both of these parameters is not feasible in this case given the physiological implications of varying carbon sources. A significant micro-morphological effect of carbon source variation was not evident, although the mycelia analysed were relatively small and unbranched (Table 6.1).

The high yield of $\alpha$-amylase on starch compared to the low yield obtained on glucose (Fig. 6.11) is consistent with other investigations into the effects of different substrates. Agger and colleagues found that starch was the best inducer of $\alpha$-amylase production in both batch and continuous cultivation of different strains of *A. nidulans*, compared with glucose, maltose and various mixtures of carbon sources [213], while glucose has been shown to significantly repress $\alpha$-amylase production in *A. oryzae* [111]. Repression of $\alpha$-amylase production by glucose was also reported by Nahas and Waldemarin, who suggested lactose, maltose, xylose and starch as suitable substrates for inducing $\alpha$-amylase production in stationary culturing of *A. ochraceus* [206].

### 6.4.5 Influence of inoculum concentration on morphology and metabolite production

The influence of inoculum concentration on both macro-morphology and $\alpha$-amylase production was significant (Fig. 6.13); a high inoculum concentration was preferable for the formation of small pellets and, consequently, higher $\alpha$-amylase activity. It may be the case that a further increase in inoculum concentration beyond $1 \times 10^8$ spores ml$^{-1}$ leads to further reductions in pellet size and concomitant increases in $\alpha$-amylase yield, but whether filamentous growth (which has been found to be preferable for $\alpha$-amylase production from *A. oryzae* [45]) may be induced in such a manner is unclear. Bizukojc and Ledakowicz proposed a linear relationship between inoculum concentration ($C_i$) and the number of pellets per unit volume ($n_{pellets}$) that resulted in cultures of *A. terreus* [47]:

$$n_{pellets} = a.C_i \tag{6.6}$$

It was proposed that a constant number of spores ($a \approx 10,400$) formed the core of each pellet. This indicated that while an increase in inoculum concentration would result in a decrease in pellet size, this decrease was owing to a reduction in available nutrients per pellet (and consequently, a reduction in the extent of growth) rather than increased spore dispersal. This suggests that increasing the inoculum concentration in cultures of *A. terreus* is unlikely to induce filamentous growth and the same may also be true of *A. oryzae*, given that pellets are formed by this organism through a similar agglomerative process [45]. Furthermore, if the number of spores forming each pellet is constant, then the mean amount of biomass ($X$) produced by each pellet is equal to the available nutrient concentration ($S$) divided equally among all pellets:

$$X = SY_{X/S} \cdot \frac{1}{n_{pellets}} \tag{6.7}$$

where $Y_{X/S}$ is the yield of biomass per unit volume of media. Taking the projected area of pellets ($A_p$) to be proportional to biomass ($A_p = b.X$, $b$ is a constant) and substituting for $n_{pellets}$:

$$A_p = \frac{bSY_{X/S}}{a} \cdot \frac{1}{C_i} \tag{6.8}$$

This is similar in form to the relationship between $D_p$ and $C_i$ shown in Figure 6.13a.

What is striking is the sensitivity of the system to relatively small changes in the initial spore concentration, emphasising the need for strict maintenance of inoculum suspensions and the accurate evaluation of spore viability. A large reduction in the diameter of *A. oryzae* pellets for an increase in inoculum concentration of approximately one order of magnitude was also reported by Truong and colleagues, without having an appreciable effect on the 'hairiness' of the pellets (ratio of area of outer filamentous zone to that of the core) [154]. However, the cultivations were conducted in cassava starch processing waste-water, containing suspended solids, which were shown to influence pellet formation. A similar range of variation in inoculum concentration was also investigated by Xu and colleagues in the fermentation of *A. niger* and while the observed differences in pellet size were significant, the variation was approximately linear [74].

It should also be noted that a micro-morphological influence of variation in inoculum concentration cannot be discounted, as it has been demonstrated that increasing spore concentration causes an increase in the hyphal growth unit of *A. niger* [159] and *A. awamori* [73], which may have implications for the relationship proposed in Equation 6.3. However, the specific rate of $\alpha$-amylase production (IU $mg^{-1}$ DCW $h^{-1}$) has been reported as being closely coupled to the growth of *A. oryzae* [111]. Furthermore, it was suggested by Carlsen and colleagues that the

product of the specific hyphal branching rate ($k_b$) and the maximal hyphal tip extension rate ($k_{tip}$) may be related to the square of the specific growth rate of freely dispersed cultures [45]:

$$\mu^2 = k_{tip}.k_b \tag{6.9}$$

The branching kinetics of an organism can be reasonably described using $k_{tip}$ and $k_b$ and, therefore, if specific $\alpha$-amylase production is proportional to $\mu$ and $\mu$ is independent of the inoculum concentration, then Equation 6.5 should hold true, independent of variations in branching rates. However, in the case of pelleted growth, specific amylase production would be expected to decrease as the fermentation proceeds and more biomass becomes diffusion limited, which would also result in a reduction in the specific growth rate. It must therefore be assumed that both $\mu$ and the specific amylase production rate are dependent on $C_i$ and microscopic analysis is required to confirm the relationship between morphology and metabolite production.

### 6.4.6 Supplementation of cultures with surfactant compounds

The lack of a reduction in pellet size in fermentations supplemented with Tween-80 (Fig. 6.15a) is in disagreement with evidence in the literature suggesting that the inclusion of surfactant compounds leads to smaller pellets and/or dispersed growth. The presence of Tween-80 was found to have a dispersive effect in the fermentation of *T. reesei*, with a 'pulpy' growth form resulting from its inclusion [14]. However, a slight increase in the size of *R. nigricans* pellets was observed by Žnidaršič and colleagues when cultures were supplemented with Tween-80, although higher concentrations also resulted in some dispersed growth [15].

The increase in the number of suspended particles in the presence of Tween-80 may indicate that the dispersal of the hydrophobic spores is aided by the inclusion of

surfactant compounds (Fig. 6.18). However, the resultant increase in pellet size for some concentrations of Tween-80 (Fig. 6.15a) may suggest that hydrophobicity is not the primary driver of pellet formation under these conditions. The hydrophobic nature of dormant spores has been confirmed in investigations using atomic force microscopy, but it has also been demonstrated that the surface properties of spores is altered during the swelling process [217]. Indeed, Dague and colleagues have offered evidence that spores of *A. fumigatus* become hydrophilic as they swell [218]; cell surface hydrophobicity can have a significant influence on morphology in submerged cultures [97]. However, Dynesen and Nielsen concluded that both electrical charge and hydrophobicity affects pellet formation of *A. nidulans*, but spore agglomeration cannot be attributed to these factors alone [94].

In cultures supplemented with Nonidet-P40 and Triton X-100, a reduction in pellet size was observed (Fig. 6.20b), although, given the low levels of biomass, this reduction may be owing to inhibited growth of the pellets, rather than a dispersive effect (although some flasks did contain a considerable amount of free mycelia; not shown); Triton X-100 was also reported to inhibit the growth of *S. hygroscopicus* [100]. However, all three surfactants yielded increases in $\alpha$-amylase yield, which did not appear to be directly related to pellet size (Fig. 6.15b and 6.20b), as was the case in modifying morphology via variations in inoculum concentration. It is possible that the surfactants affected the microscopic development of the organism, but examination of hyphal elements isolated from cultures supplemented with Nonidet P-40 or Triton X-100 was not possible, as the detergents apparently inhibited the staining of the hyphae (not shown). However, quantification of the growth of *A. oryzae* on solid substrate in the presence of Tween-80 would seem to suggest that the surfactants did not have a significant microscopic influence (Fig. 6.17). However, given the different chemical structures and the inhibitory effects of Triton X-100 and Nonidet-P40, coupled with the inherent environmental differences be-

tween the submerged and solid-state systems, an influence at the microscopic level (and possibly a physiological influence) cannot be ruled out.

There also exists the possibility that the presence of non-ionic detergents caused an increase in cell permeability, resulting in greater diffusion into pellets and subsequently raising the proportion of 'active' biomass. Such a conclusion was reached in studies involving *R. nigricans* [15] and *T. reesei* [14], in which cultures were supplemented with surfactants and an increase in metabolite production or biomass yield (or both) was recognised. Correlations between the level of active biomass in a culture and metabolite production have been demonstrated for *A. niger* [46] and *S. fradiae* [221]. Alternatively, the increase in $\alpha$-amylase activity observed in the presence of non-ionic detergents may have been a result of enhanced activation of the enzyme by the surfactants, rather than an increase in enzyme production by *A. oryzae*. Yoon and Robyt found that supplementing a solution containing porcine pancreatic $\alpha$-amylase with 0.02% w/v Triton X-100 resulted in an increase in activity of approximately 40% [219]. Furthermore, the activity of Triton-supplemented solutions remained stable over time, while the activity of a control solution (without surfactant supplementation) declined rapidly.

## 6.5 Conclusions

Fungal morphology is a critically important fermentation parameter, impacting metabolite production and environmental conditions both directly and indirectly. While the relationship between growth form and metabolite yield is sometimes ambiguous, there is a substantial body of evidence suggesting that many processes may be optimised through the selection of environmental variables that favour one particular growth form over others. The original aim of the experimentation described in this chapter was to translate the successful quantification of microscopic

development on solid substrates (Chapter 5) into the submerged culture format; characterising the morphology of *A. oryzae* in a basal system, then by effecting perturbations, influencing variation at the microscopic level that may provide an insight into macroscopic structure formation and $\alpha$-amylase production. While variations in pellet formation were observed in response to changes in certain parameters (varying substrate concentration, inoculum concentration, supplementation with surfactants), microscopic characterisation of branching behaviour was complicated by a variety of factors (presence of solid particles, spore agglomeration, poor stain uptake). However, while the original aim of relating microscopic architecture to macroscopic form was ultimately unattained, several significant findings were reported.

Cultivation of *A. oryzae* in a basal submerged format resulted in a relatively homogeneous population of pellets, the sizes of which were approximately normally distributed prior to the onset of fragmentation. An exhaustion of nutrients seems to be the likely cause of pellet break-up, although oxygen limitations within the pellets and the onset of autolysis may also have been responsible. Investigations involving different carbon sources support the consensus that starch is the preferred substrate for inducement of $\alpha$-amylase activity in *A. oryzae*, while the presence of glucose is associated with low levels of expression. However, increasing starch concentration above approximately 1.0% (w/v) seemed to have a negative impact on $\alpha$-amylase activity per unit dry-cell weight, possibly due to limited mixing at higher substrate concentrations. The influence of inoculum concentration demonstrated here is in general agreement with other reports in the literature; higher spore concentrations result in smaller pellets, which are favourable for metabolite production. The supplementation of fermentation media with surfactant compounds was favourable for increased $\alpha$-amylase activity per unit dry cell weight, although lower biomass levels were recorded in the presence of Triton X-100 and Nonidet P-40. The reason for

this increase in $\alpha$-amylase expression is not fully understood, although an effect on micro-morphological development cannot be ruled out; a physiological influence is also possible. No significant variations in microscopic parameters were observed when cultivations were conducted on a solid substrate in the presence of Tween-80, although the possibility that surfactant compounds effected micro-morphological variation cannot be completely discounted.

Accurate morphological quantification often depends on the presence of free mycelial elements for characterisation of the branching behaviour of the organism. However, many organisms, such as *Aspergillus oryzae*, typically grow in the pelleted form, as the spores of this fungus agglomerate as they swell when cultivated in submerged medium; some means of disrupting this mechanism is therefore required in order to analyse microscopic architectures. A lowering of the culture pH has been utilised in other studies as a means of achieving this, but an acidic medium has also been shown to adversely affect both growth and product formation. Furthermore, the pelleted growth form has been demonstrated as optimal for many processes and is therefore an industrially-relevant phenotype, demanding of attention in itself. Some form of universal measure that may be applied to all growth forms would obviate the requirement for the presence of 'free' mycelia in the culture and allow direct comparison of different phenotypes, without the need for classification of these structures.

# Chapter 7

# Characterisation of the Relationship Between Fractal Dimension and Branching Behaviour in Filamentous Microbes

## 7.1 Introduction

The optimisation of fermentation processes involving filamentous microorganisms requires an in-depth knowledge of the relationship between biomass and metabolite production. The specific morphological form adopted by an organism, which is dependent on a variety of factors [220], is of critical importance to the clarification of this dependency, as particular phenotypes are associated with maximum productivity. In particular, the extent to which an organism forms branches is often of interest, as evidence in the literature suggests that metabolite excretion occurs primarily at hyphal tips [107, 216]. With the advent of image analysis systems, significant progress has been made in furthering the understanding of the link between morphology and productivity [48]. However, the accurate quantification of complex morphologies still represents a major challenge in process optimisation.

At the macroscopic level, the dispersed mycelial morphological form may dominate, or an aggregation of 'free' hyphal elements may result in mycelial 'clumps'

being predominant. Alternatively, dense pellet structures, which may be up to several millimetres in diameter, may result from the aggregation of spores prior to germination, the aggregation of spores and germ tubes or the aggregation of mycelia. In fermentations of certain microorganisms, such as *Aspergillus oryzae* and *Aspergillus terreus*, there is evidence that pellet-formation is driven by spore agglomeration [45, 47] and, as such, the occurrence of 'free' mycelia may be rare. The characterisation of these complex macro-morphologies represents a far greater challenge to the fungal biotechnologist, as individual hyphae cannot be isolated and enumerated. As such, the accurate determination of the extent of branching of the organism is often impossible. These large aggregates of biomass are conventionally characterised in terms of projected area ($A_p$), perimeter length ($P$), circularity ($C = 4\pi A_p P^{-2}$), or various other interpretations thereof [5, 72, 177]. As different morphological parameters are often utilised depending on the growth form present, a considerable amount of effort has been expended in designing imaging systems capable of discriminating between these different phenotypes [5, 72]. An alternative approach to morphological quantification employs the use of fractal geometry to characterise the spatial distribution of an organism.

### 7.1.1 What are fractals?

The term 'fractal' geometry, derived from the Latin *fractus* meaning 'broken' or 'fractured', was first used by Mandelbrot [222] to describe objects that are 'self-similar' (similar at different scales). More specifically, Mandelbrot described a fractal as '*a rough or fragmented geometric shape that can be split into parts, each of which is (at least approximately) a reduced-size copy of the whole.*' There are many examples of such objects in nature, such as clouds, mountain ranges, coastlines and snow-flakes. One of the more commonly cited examples of a naturally-occurring fractal is perhaps the fern (Fig. 7.1), which displays a similar morphology at differ-

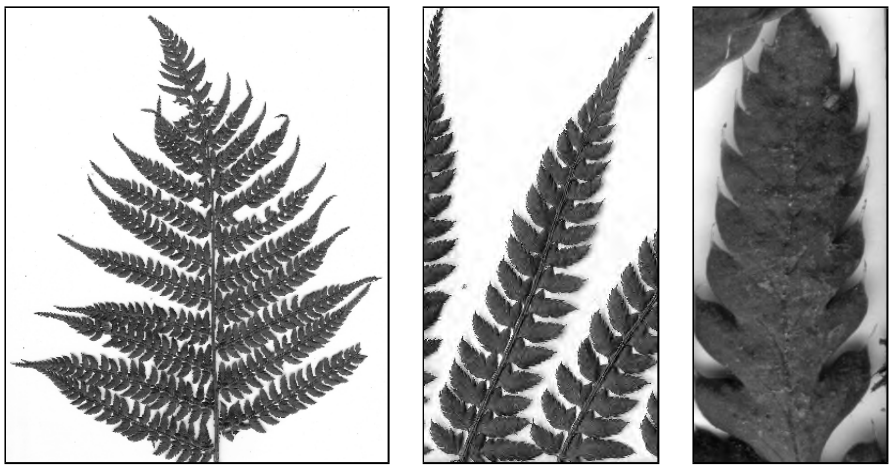

**Figure 7.1:** A fern is an example of a naturally-occurring fractal, exhibiting a similar form at different scales.

ent scales: a central 'stem' from which pointed 'leaves' emerge. Fractal geometry has also been made use of in art (Fig. 7.2), long before the concept was formalised mathematically.

Several studies have also demonstrated that certain filamentous microorganisms can be considered self-similar structures [110, 159, 172, 183, 205, 223, 224], as do several bacterial strains of Gram-negative rods, under certain conditions [225]. Effects of different grazing densities of collembolans on colonies of the fungus *Hypholoma fasciculare* [180] and trophic responses of *Phanerochaete velutina* mycelial systems to nutrient stimuli [181] were also quantified in the same manner. Fractal geometry has also been used as a means of standardising mycelial inocula for submerged fermentations [226].

The concept of fractal or fractional dimension may be considered as follows [227]. Consider a straight line of dimension one and of length $X$. For any positive integer $N$, the segment may be exactly decomposed into $N$ non-overlapping segments of length $X/N$. Each sub-segment may then be considered a scaled version of the original, where $r(N) = 1/N$ is the scaling ratio. This concept may be extended to

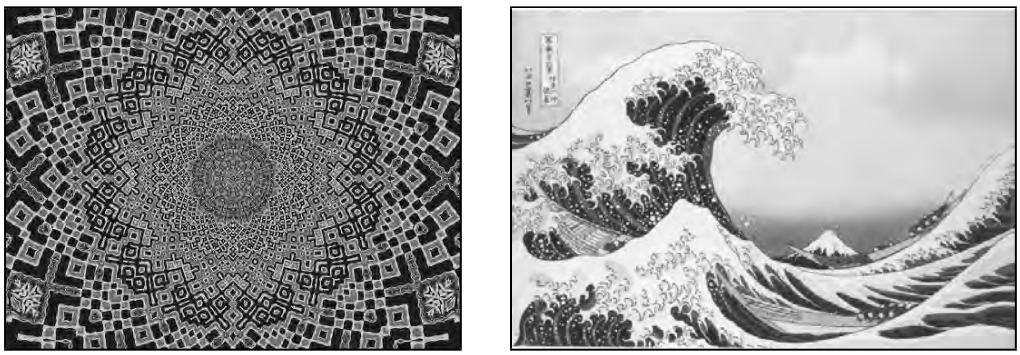

**Figure 7.2:** Many examples of Islamic art exhibit fractal properties (left), while self-similarity is clearly visible in Hokusai's *The Great Wave off Kanagawa* (right).

two dimensions, whereby a rectangle of length $X$ and breadth $Y$ may be sub-divided into $N$ smaller rectangles, each of length $X/\sqrt{N}$ and breadth $Y/\sqrt{N}$, in which case the scaling ratio is $r(N) = 1/\sqrt{N}$. This relationship may be generalised as follows:

$$r(N) = \frac{1}{N^{1/D}} \tag{7.1}$$

The fractal dimension ($D$) is therefore given by:

$$D = -\frac{\log N}{\log r(N)} \tag{7.2}$$

This principle is illustrated by the construction of the von Koch curves (Fig. 7.3). Beginning with a straight line of length $X$, the line is divided into three segments, each of length $X/3$. A fourth segment of length $X/3$ is added and the four segments are arranged as shown, producing the triadic von Koch curve. In this case, $r(N) = 1/3$, as each of the individual segments is one third the length of the original, and $N = 4$. Therefore:

$$D = -\frac{\log 4}{\log 1/3} = \frac{\log 4}{\log 3} \approx 1.262$$

Alternatively, if $r(N) = 1/4$ and $N = 8$, the result is the quadratic von Koch

curve, for which $D = 1.5$. Iteratively repeating this 'divide and construct' procedure results in curves of increasing visual complexity, which are not easily described using Euclidean measures. However, the basis for their construction is relatively simple, as is their subsequent decomposition into elementary, geometrically identical substructures, and a single dimension ($D$) may be used to describe the curves.

### 7.1.2 Quantifying the fractal dimension

One of the earlier approaches to fractal dimension evaluation, termed the 'Richardson walk' [228], originally described the effect of scale when measuring a coastal perimeter on a map using dividers. As the step size ($s$) is reduced, the measured perimeter ($P$) increases, with more of the coastal irregularities included in the measure. A plot of $\log P(s)$ versus $\log n$ will result in a straight line, the slope of which is related to the fractal dimension ($D$) by:

$$P(s) = as^{1-D} \tag{7.3}$$

where $a$ is a constant. The range of scales over which the expression holds true is obviously limited at the lower end by the resolution of the map and at the upper end by the size of the coastline being measured.

A more accurate implementation of such a method for the analysis of objects in digital images is based on the calculation of a Euclidean distance map (EDM) [229]. The grey-level histogram ($h(x)$) provides the luminance value at each distance ($d$) from the 'ultimate point', the centre of the EDM. The perimeter, $P$, at a distance $d$ from the object's centre may be calculated according to:

$$P(d) = \frac{1}{d}\sum_{x=0}^{d} h(x) \tag{7.4}$$

In this instance, $d$ may be thought of as the scale or step size, as a lower value will effectively result in a lower 'resolution' measure of the object perimeter and vice-

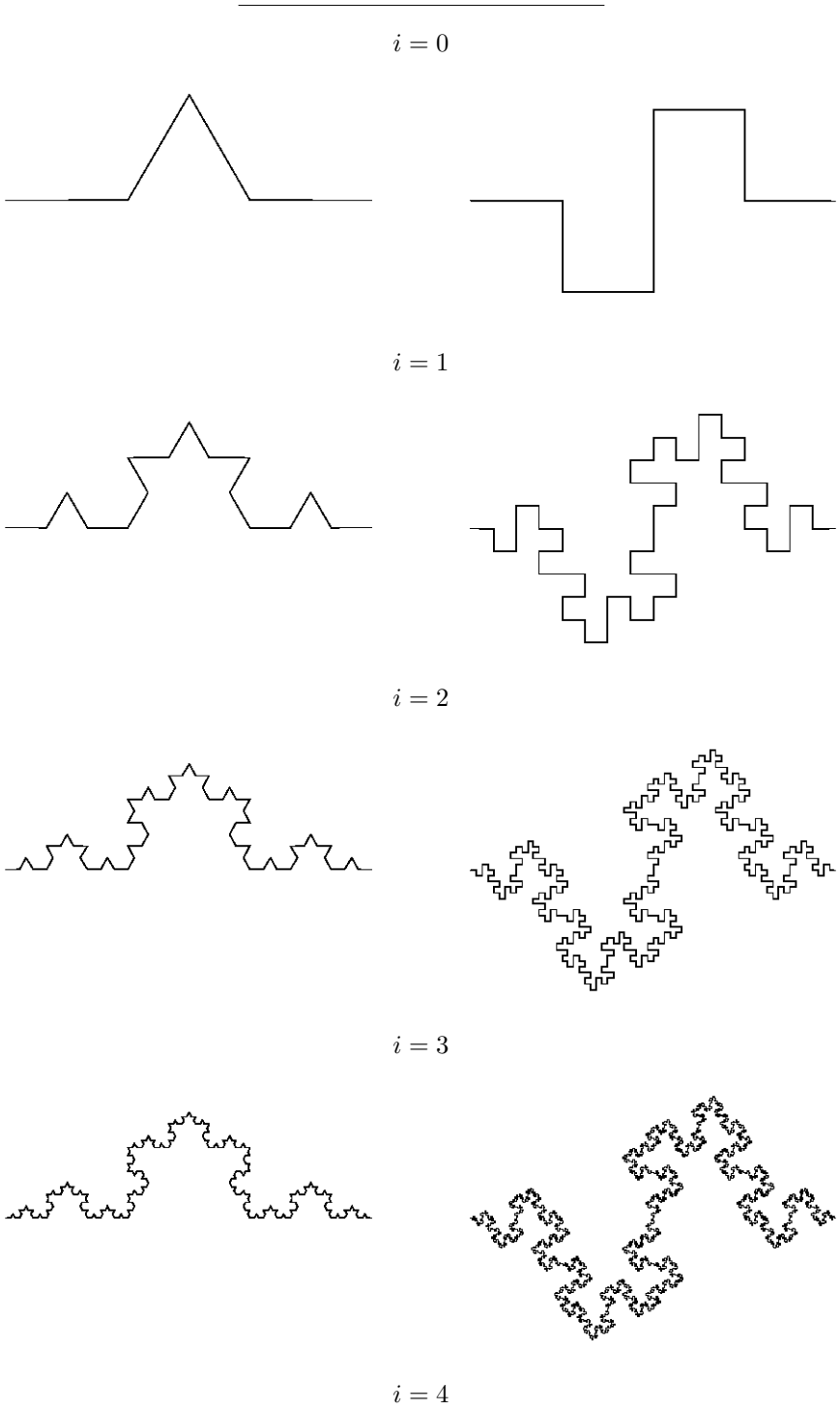


**Figure 7.3:** The triadic (left) and quadratic (right) von Koch curves, where $i$ denotes the number of iterations.

versa. A plot of $\log P(d)$ versus $\log d$ produces a straight line (Fig. 7.4). However, such an approach is not suitable for the analysis of hyphae, as the EDM of such images typically contains a very small number of grey levels due to the elongated nature of hyphae.

The 'box-counting' method has been by far the most common in the analysis of filamentous microbes [184]. This approach entails covering the mycelium with a grid of side length $\epsilon$ and counting the number of boxes, $N(\epsilon)$, that are intersected by the mycelium. If the mycelium is a true fractal, then a relationship of the following form should be found:

$$N(\epsilon) = c\epsilon^{-D} \tag{7.5}$$

where $c$ is a proportionality constant. The fractal nature of mycelia has been studied at two distinct levels using the measures of the surface fractal dimension ($D_{BS}$), effectively allowing discrimination between systems which are fractal only at their boundaries, and the mass fractal dimension ($D_{BM}$) [159, 184]. However, it has been suggested that the fractal dimension is often not sufficient for morphological characterisation, as microorganisms can sometimes appear to have different branching patterns, despite having similar values for fractal dimension [230].

### 7.1.3 Aim of the work in this chapter

While numerous studies have been conducted in which fractal analysis is utilised to quantify morphology, few have attempted to link fractal dimension with conventional morphological parameters. Fractal analysis is of significant potential value in the study of filamentous microorganisms, particularly as it lends itself to the assessment of all gross morphological forms that may be encountered. However, there is a need to develop further the relationship between the fractal dimension within a population of mycelia and the branching behaviour within that population. The

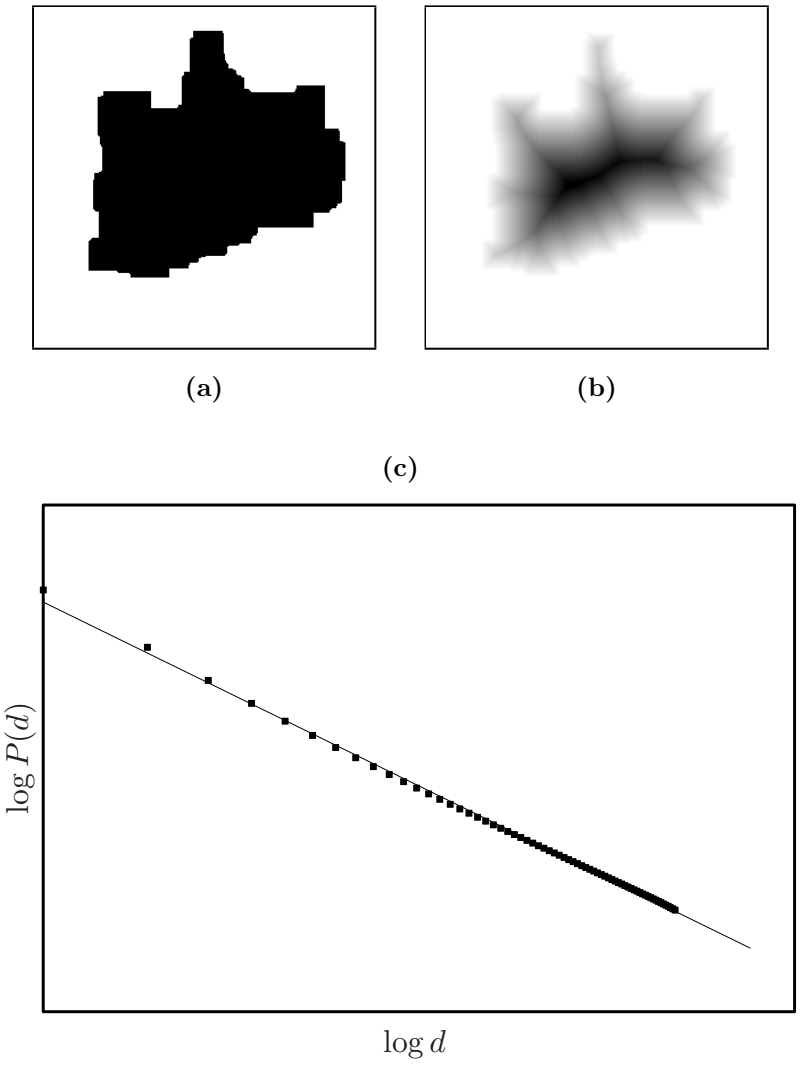


**Figure 7.4:** Enumeration of the fractal dimension based on the Euclidean distance map (EDM). (a) Binary representation of object to be analysed. (b) EDM of object in 'a', in which grey values are inversely proportional to the distance from the nearest background (white) pixel. (c) The fractal dimension may be taken as the slope of a $\log P(d) - \log d$ plot (from Equation 7.4).

aim of this chapter was to investigate an alternative approach to fractal analysis, based on a survey of the mycelial boundary, and attempt to correlate directly the hyphal growth unit ($L_{hgu}$) to the fractal dimension. In order to provide a greater range of $L_{hgu}$ values, *Penicillium chrysogenum* was included in this investigation, as it has been reported to exhibit a more densely branched mycelium with respect to the strain of *A. oryzae* characterised in Chapter 5 [104, 121].

## 7.2 Materials & methods

### 7.2.1 Inoculum preparation

*Penicillium chrysogenum* (IMI 321325) spores were harvested from malt agar (Lab M) slant cultures by addition of 5 ml phosphate-buffered saline (PBS; pH 7.2, Oxoid Dulbecco 'A'; 0.85% w/v) containing Tween 80 (0.1% v/v). Conidiospores were dislodged using a sterile swab, briefly mixed, and the suspension was filtered through sterile glass wool to remove hyphae. The inoculum was standardized using a Neubauer chamber to yield a stock concentration of $2 \times 10^6$ spores $ml^{-1}$, glycerol added to a final concentration of 20% (v/v) and aliquots stored at $-20°C$. The viability of spores after freezing was found to be approximately 47% of stock concentration (pour plate method, malt agar, 36 h incubation).

### 7.2.2 Microorganism cultivation

The basal medium used for solid state fermentation of *A. oryzae* was as described in Section 2.3 with 10.0 g $L^{-1}$ soluble starch and 17.0 g $L^{-1}$ Agar No. 1. Nonidet P-40 or Triton X-100 were added to yield a final concentration of either 0.1% or 5.0% w/v. The media was adjusted to pH 6.0 before autoclaving. Solid state fermentation of *P. chrysogenum* was carried out using the following: malt agar, malt agar supplemented with $CaCl_2.2H_2O$ (0.08% w/v) or $FeCl_2.4H_2O$ (0.11% w/v),

rice, orange and a mixture of rice and bulgar wheat (1:1 w/w). Rice and rice-bulgar wheat were prepared by steeping in water and autoclaving (121°C for 15 minutes) before transfer to sterile Petri dishes. Orange was prepared for use by surface swabbing with alcohol and dissection with a sterile knife. Cell immobilisation, cultivation conditions and processing of culture for image analysis were as described in Section 2.4.

Submerged fermentation of *A. oryzae* was carried out in a 2 L Benchtop Fermenter (BioFlo 110, New Brunswick Scientific). The approximate internal diameter of the vessel was 0.13 m and it had a working volume of 1.5 L. Agitation was provided by two Rushton turbines with a $D_i/T$ ratio[1] of 0.4 operated at 200 rpm. A pipe sparger was used to aerate the culture at an initial rate of 1.0 vvm. The fermenter was run without dissolved oxygen or pH control and the broth temperature was maintained at 30°C. Inoculum work-up consisted of three shake flask cultures (250 ml, 20% working volume) inoculated with $5 \times 10^7$ spores $ml^{-1}$ and incubated at 30°C (200 rpm for 48 hours). The medium used for fermentation and inoculum work-up was as described above (Agar No. 1 and detergents omitted). Sample preparation for fluorescent microscopy and image capture were as described in Section 2.4.

### 7.2.3 Enumerating the fractal dimension

In all cases, only 'free' mycelial elements, exhibiting minimal overlapping of hyphae, were considered for image analysis, so that comparisons could be drawn between the fractal dimension and the hyphal growth unit. The generation of binary images and the enumeration of the hyphal growth unit were as described in Chapter 3. In the case of calcofluor white-stained samples, a pre-set grey-level threshold was used, as the non-uniform nature of the stain uptake complicated automated segmentation.

[1] $D_i$ is the impeller diameter and $T$ represents the vessel's internal diameter.

The fractal dimension, $D$, of an object, $O$, was determined by first locating the object boundary in a binary image (all foreground pixels bordering background), which can be thought of as a curve consisting of a set of $N$ coordinates, $(x_n, y_n)$. From this series of points, a signal, $f(n)$, can be constructed as follows:

$$f(n) = \sqrt{(x_n - x_c)^2 + (y_n - y_c)^2} \quad \text{for all} \quad 0 < n < N \tag{7.6}$$

where $(x_c, y_c)$ is the average location of all $(x, y) \in O$ (Fig. 7.5). If $f(n)$ is a 'fractal signal', then the following relationship holds true [231]:

$$P(\omega) = \frac{c}{\omega^\beta} \tag{7.7}$$

where $P(\omega) = |F(\omega)|^2$, $F(\omega)$ is the Fourier transform of $f(n)$, $\beta = 2q$, $q$ is the Fourier Dimension and $c$ is a constant. Taking the log of this equation yields:

$$\log P(\omega) = -\beta \log \omega + c \tag{7.8}$$

$D$ is related to $\beta$ by [231]:

$$D = \frac{5 - \beta}{2} \tag{7.9}$$

A value for $\beta$ can therefore be determined by linear regression of a plot of $\log P(\omega)$ against $\log \omega$, excluding the DC component (Fig. 7.6). All algorithms were implemented in Java using ImageJ [114].

## 7.3 Results & discussion

An analysis of the development of *A. oryzae* on malt agar showed that both $D$ and $L_{hgu}$ increased over time and both tended towards approximately constant values (Fig. 7.7). This suggests that the value of $L_{hgu}$ specific to *A. oryzae* under these growth conditions is reflected in the fractal dimension of the mycelia. The

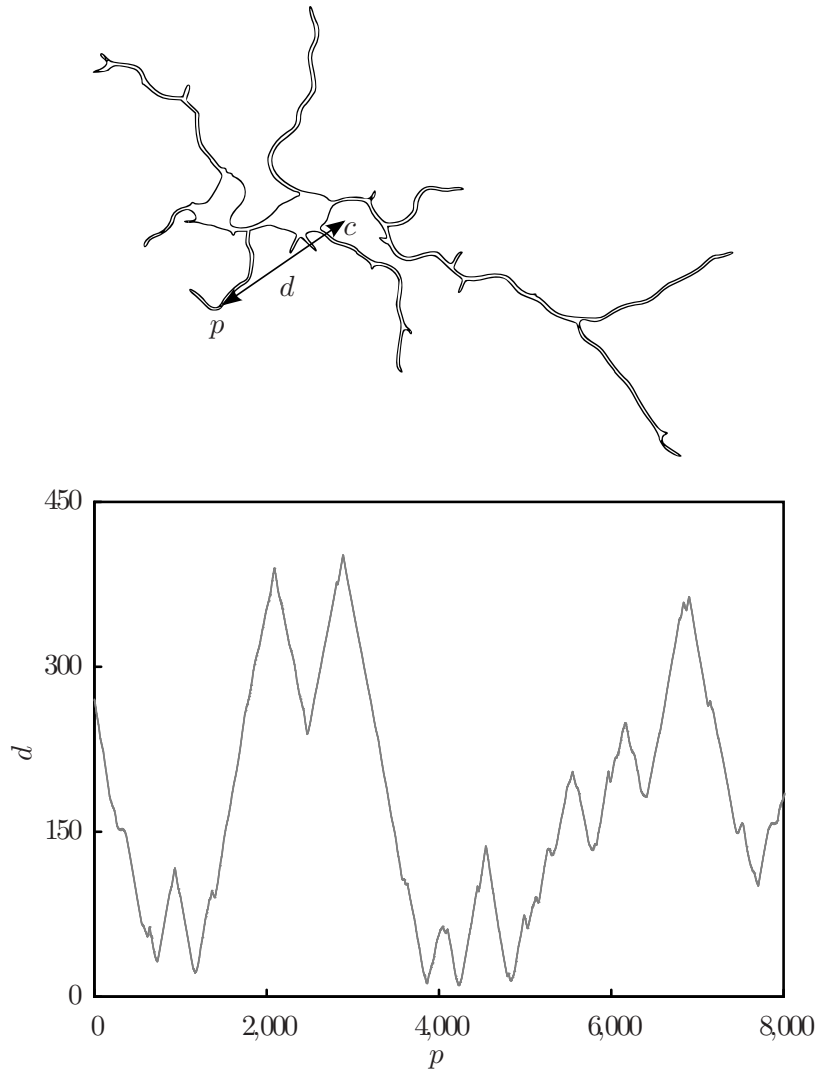


**Figure 7.5:** Illustration of algorithm for determination of fractal dimension ($D$) of mycelial structures. Distance, $d$, between the centroid, $c$, and the boundary is plotted for each position on the boundary, $p$.

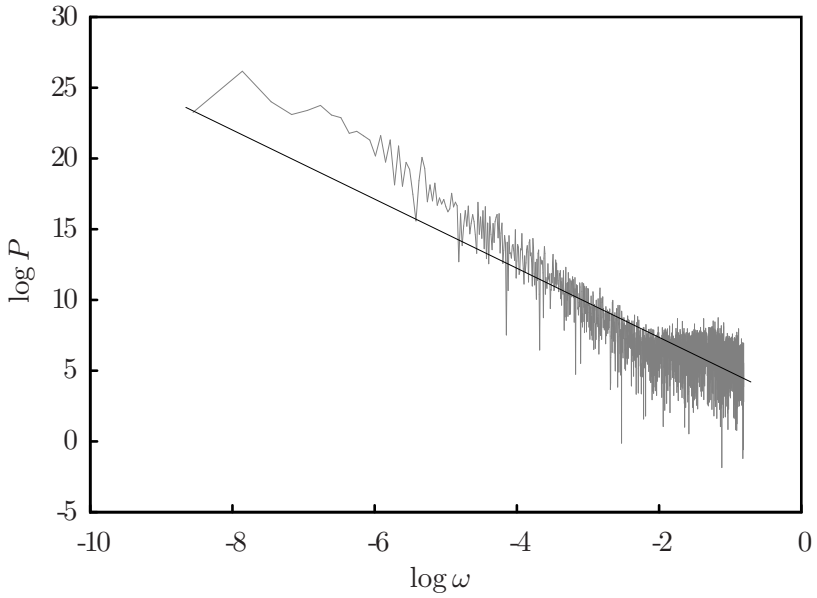


**Figure 7.6:** Illustration of algorithm for determination of fractal dimension ($D$) of mycelial structures. The fractal dimension is derived from a log-log plot of the Fourier domain representation of the signal.

fractal dimension of *Ashbya gossypii* and *Streptomyces griseus* were also found to increase with time during the colonisation of solid substrates [184]. *A. oryzae* and *P. chrysogenum* were grown under a variety of different conditions (Table 7.1), producing mycelia of varying size and dimension that were quantified in the same manner. The resultant mean values of $D$ obtained for each population were plotted against the mean values of $L_{hgu}$ to yield an approximately logarithmic relationship (Fig. 7.8):

$$D = a \log L_{hgu} + b \tag{7.10}$$

where $a$ and $b$ are constants. This result demonstrates a strong correlation between the branching behaviour of mycelia and their space-filling properties. However, it has been shown in other studies that fractal dimension tends to increase as projected area of mycelial structures increases [159]. This may also be the case in this study, as

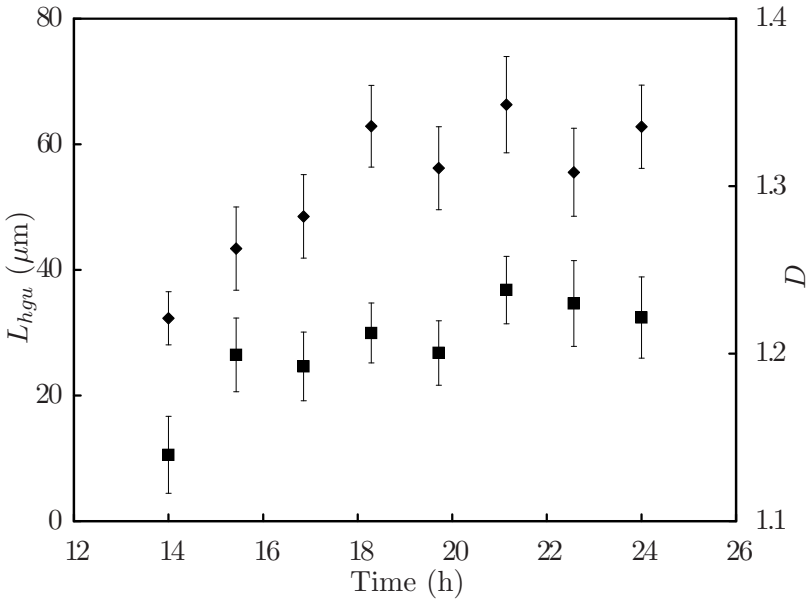


**Figure 7.7:** Temporal variation in mean hyphal growth unit ($L_{hgu}$; ♦) and the mean fractal dimension ($D$; ■) of populations of *A. oryzae* cultivated on malt agar. Error bars represent 95% confidence intervals. Produced using images generated in Chapter 5.

higher values of $D$ tended to be biased toward high values of $A_p$ (Fig. 7.9), but this result is inconclusive, as the sizes of mycelia analysed fell within a comparatively small range.

This result depicts a clear relationship between the branching behaviour of filamentous organisms and the fractal dimension of the resultant mycelial architectures, further emphasising the potential use of fractal analysis in morphological quantification. An ability to extract information on the branching behaviour of an organism by surveying the shape of the mycelial boundary would be highly advantageous in the study of more complex conformations where measures such as the hyphal growth unit are not readily obtainable. Furthermore, as has been demonstrated in other studies [159, 205, 223, 226], fractal analysis can be applied regardless of the gross morphological form that results in a particular process, allowing a more

**Table 7.1:** Populations of filamentous fungi analysed, where $n$ is the number of mycelia in each population and the total hyphal length ($L_{th}$) is presented as mean ±95% confidence interval

| Organism | $t$ (h) | Substrate | $n$ | $L_{th}$ ($\mu$m) |
|---|---|---|---|---|
| *A. oryzae* | 14.0 | Malt Agar[1] | 86 | $85 \pm 16$ |
| ⋮ | 15.4 | ⋮ | 87 | $117 \pm 21$ |
| ⋮ | 16.9 | ⋮ | 82 | $169 \pm 41$ |
| ⋮ | 18.3 | ⋮ | 78 | $341 \pm 71$ |
| ⋮ | 19.7 | ⋮ | 83 | $305 \pm 66$ |
| ⋮ | 21.1 | ⋮ | 67 | $428 \pm 98$ |
| ⋮ | 22.6 | ⋮ | 59 | $336 \pm 101$ |
| ⋮ | 24.0 | ⋮ | 76 | $397 \pm 91$ |
| ⋮ | 18.0 | Solid medium, Nonidet P-40 5.0% (w/v) | 30 | $190 \pm 44$ |
| ⋮ | 24.0 | Solid medium, Nonidet P-40 5.0% (w/v) | 26 | $654 \pm 177$ |
| ⋮ | 15.0 | Solid medium, Triton X-100 0.1% (w/v) | 44 | $177 \pm 39$ |
| ⋮ | 18.0 | Solid medium, Triton X-100 0.1% (w/v) | 35 | $269 \pm 95$ |
| ⋮ | 46.0 | Liquid Medium | 38 | $874 \pm 198$ |
| ⋮ | 72.5 | ⋮ | 56 | $671 \pm 116$ |
| ⋮ | 94.0 | ⋮ | 44 | $527 \pm 126$ |
| *P. chrysogenum* | 20.0 | Malt Agar | 69 | $116 \pm 18$ |
| ⋮ | 27.0 | Malt Agar | 46 | $378 \pm 73$ |
| ⋮ | 20.0 | Malt Agar, $CaCl_2.2H_2O$ 0.08% (w/v) | 68 | $131 \pm 20$ |
| ⋮ | 27.0 | Malt Agar, $CaCl_2.2H_2O$ 0.08% (w/v) | 32 | $296 \pm 52$ |
| ⋮ | 27.0 | Malt Agar, $FeCl_2.4H_2O$ 0.11% (w/v) | 58 | $140 \pm 26$ |
| ⋮ | 20.0 | Orange | 39 | $180 \pm 36$ |
| ⋮ | 19.0 | Rice | 114 | $255 \pm 31$ |
| ⋮ | 20.0 | Rice & Bulgar Wheat | 42 | $400 \pm 121$ |

[1] Results for *A. oryzae* on malt agar were produced using the images generated in Chapter 5.

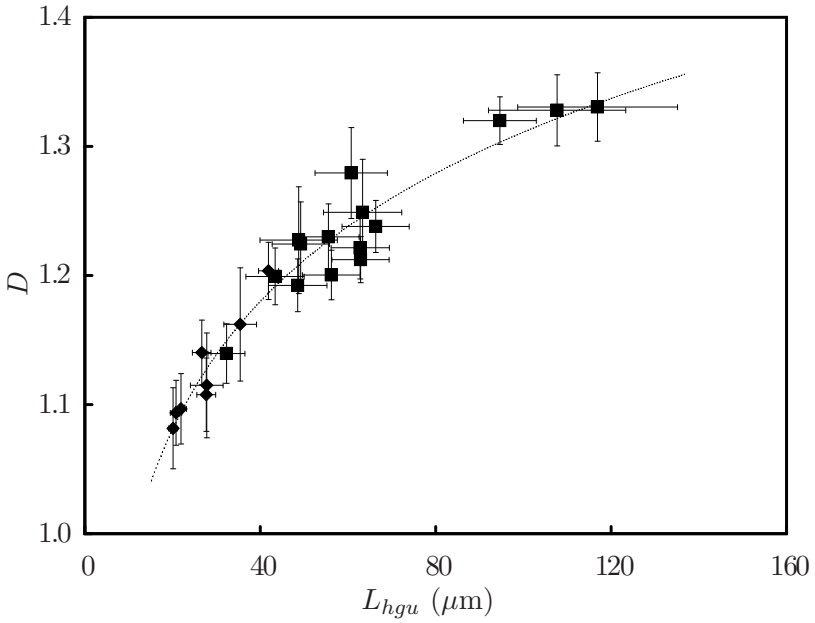


**Figure 7.8:** Relationship between the mean hyphal growth unit ($L_{hgu}$) and the mean fractal dimension ($D$) of populations of *Aspergillus oryzae* (■) and *Penicillium chrysogenum* (♦) mycelia, grown under a variety of different conditions. A logarithmic relationship of the form $D = a \log L_{hgu} + b$ exists between the two parameters, where $a = 0.14$ and $b = 0.65$ (—; $R^2 = 0.95$). Error bars represent 95% confidence intervals.

thorough compilation of data. However, a more complete examination, including more complex structures, is necessary to validate the universal application of fractal analysis.

It has been previously suggested that the box-counting method of fractal dimension enumeration may not be suitable for the analysis of small, relatively unbranched hyphal structures [159, 184]. The accuracy of the box-counting method relies on an object being sufficiently great in size so as to allow a reasonably large variation in $\epsilon$ (approximately one order of magnitude has been proposed [184]). Given a value of approximately 4 $\mu$m for $\epsilon_{min}$ (hyphal width is approximately 2 – 4 $\mu$m), this indicates a minimum value of approximately 40 $\mu$m for $\epsilon_{max}$ in this study, equating

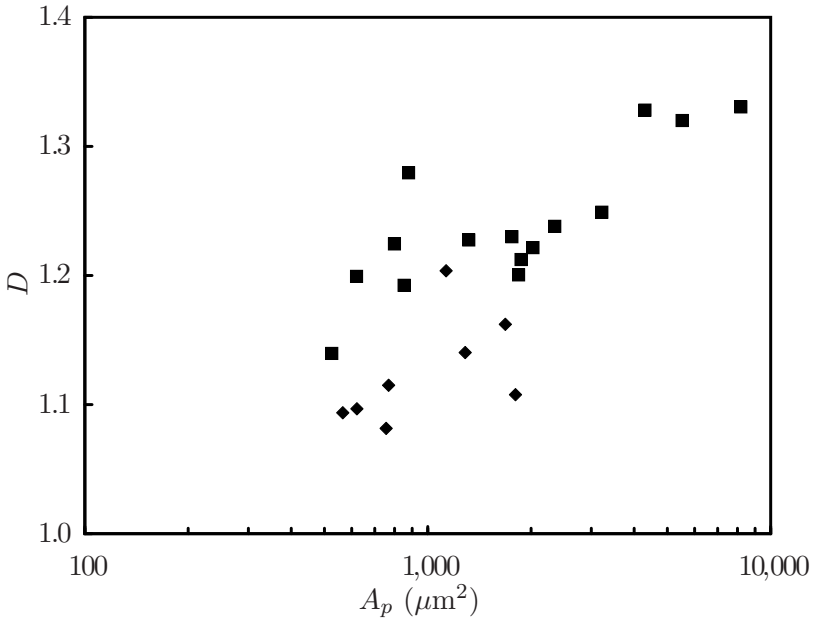


**Figure 7.9:** Relationship between mean fractal dimension ($D$) of populations of *Aspergillus oryzae* (■) and *Penicillium chrysogenum* (♦) mycelia and mean projected area ($A_p$).

to a minimum object 'diameter' ($L$) of 160 $\mu$m (assuming $\epsilon_{max} \leq L/4$ [184]). However, mycelia smaller than this dimension were often encountered, particularly in the case of *P. chrysogenum*. Further, the number of evaluations of $N(\epsilon)$ is restricted by the image resolution (approximately 1 $\mu$m per pixel in this study). This can obviously be overcome by increasing the image resolution, but this in turn results in a significant increase in memory usage and processing time.

By enumerating the fractal dimension based on the object boundary, considerations of resolution are obviated to some degree, as the boundary can be represented geometrically as a series of equations, or indeed as a single spline, to be sampled as often as is necessary to provide sufficient signal resolution. However, image resolution is still an important consideration, as low-resolution images may not contain an accurate representation of the object boundary. Consideration must also be given to the means used to locate the boundary. In this study, hyphae were uniformly

stained and object segmentation from background was accurately performed by grey-scale thresholding. In cases where staining is non-uniform, thresholding may not be suitable and some form of edge-detection algorithm may be required.

A similar examination of spectral periodicity was employed by Jones and colleagues in their study of the positional relationship between acid phosphatase intracellular concentration and hyphal cellular differentiation in *Pycnoporus cinnabarinus*. Acid phosphatase was detected histochemically on membrane-bound colonies, which were imaged using a camera fitted with a macro-lens. In the resulting image, a series of one-dimensional 'walks' were made along random colony radii and the fractal dimension calculated according to the power spectrum of the resultant luminance profile along each 'walk'. Different concentrations of an organic dye were used to effect substrate induction of the enzyme response, which was shown to be statistically correlated according to a fractal power law [232].

While numerous studies have been conducted in which fractal analysis is utilised to quantify mycelial morphology, few have attempted to link fractal dimension with conventional morphological parameters. However, links have been established between fractal dimension and productivity in some processes. For example, in the optimisation of *Funalia trogii* fermentations, both fractal dimension and mean pellet area were monitored; while no link was established between the two parameters, it was suggested that a relationship may exist between fractal dimension and decolourisation of reactive black 5 [205]. A positive correlation was also found between fractal dimension and phenol-oxidase expression by *Pycnoporus cinnabarinus*, with both parameters being regulated by media composition [110].

Where links between fractal dimension and conventional Euclidean measures of morphology have been made, the dependency is often either ambiguous or qualitative in nature. An approximate correlation ($R^2 = 0.614$) was found between the convexity (defined as the ratio between convex perimeter and respective perime-

ter) of *Cupriavidus necator* DSM 545 flocs and $D_{BS}$ [233]. Fractal dimension was shown to be related to broth rheology in the submerged fermentation of *Cephalosporium acremonium* M25 and a link with other morphological measures, such as the number of arthrospores in the media, was also suggested, but not explicitly demonstrated [223]. A relationship between hyphal growth unit and fractal dimension of mycelia was previously noted in submerged fermentations of *Aspergillus niger*, but the differences in the recorded values of $L_{hgu}$ were ambiguous [224]. Further studies of *A. niger* revealed that medium composition had a significant impact on the fractal dimension, the changes in morphology reflected in variations in the size and compactness of mycelial aggregates [159]. The local fractal dimension (determined by the concentric circles method) within a colony of *Trichoderma viride* was found to increase with branching frequency (occurrence of 'loops' in the mycelium), although the result was rather qualitative in nature [172]. However, successful attempts have been made in associating fractal dimension with growth kinetics. While colony expansion rates were found to differ between different strains of *Cryphonectria parasitica*, fractal dimension was found to correlate with the expansion rate, independent of strain [183].

## 7.4 Conclusion

The optimisation of fermentation processes involving filamentous microbes requires extensive knowledge of morphological development, as productivity is heavily influenced by the specific phenotypic form adopted. The accurate quantification of morphological variation in vegetative mycelia is therefore of the utmost importance, but the characterisation of complex morphologies represents a significant challenge. The utility of conventional measures employed in the analysis of these microbes (such as projected area, perimeter length and circularity) is limited, as they reveal

little about the extent of branching of the organism, which is known to be related to metabolite production.

An alternative approach to morphological quantification employs the use of fractal geometry to characterise the spatial distribution of an organism. The self-similar nature of mycelial structures has been demonstrated in numerous studies and there is clearly significant potential benefit in the application of fractal analysis to filamentous microorganisms. What has been lacking in these studies is a firm link between fractal dimension and conventional morphological parameters, such as the hyphal growth unit. This study indicates a strong correlation between these two parameters in the assessment of 'free' mycelial elements and further investigation involving a wide range of complex conformations is necessary. Future work will focus on elucidating a universal relationship between fractal dimension, branching behaviour and productivity, independent of the gross morphological form encountered. It is hoped that this work will lead to a rapid and efficient means of morphological quantification for use in industrial processes.

# Chapter 8

# General Discussion

The principal aim of this study was the design of a system capable of high-speed, high-throughput assessment of the morphology of filamentous microorganisms at both the microscopic and macroscopic levels. The open-source application, ImageJ [114], was selected as the platform for software development and the resulting programme is capable of the rapid analysis of a bank of images, permitting near-'real time' quantification of fungal morphology and the compilation of population data. In parallel with software development, a means of presenting fungal conformations in two-dimensional format using membrane-immobilisation was investigated, facilitating the production of samples amenable to rapid analysis [234]. The newly-created imaging routines were combined with the immobilisation assay to examine the growth kinetics of *Aspergillus oryzae* on a solid substrate [235] and a direct correlation between hyphal growth unit ($L_{hgu}$) and fractal dimension ($D$) was successfully derived for *A. oryzae* and *Penicillium chrysogenum* [236]. Further experimentation focussed on investigating the link between the micro-morphology, macro-morphology and $\alpha$-amylase production of *A. oryzae* in submerged culture; a correlation between pellet size and $\alpha$-amylase production was obtained for various inoculum concentrations (Fig. 6.13). Attempts were subsequently made to induce dispersed mycelial growth in *A. oryzae* by supplementing cultures with var-

ious surfactant compounds. While a significant influence of non-ionic detergents on $\alpha$-amylase production was found (Figs. 6.14 & 6.20b), no direct dependency on morphological variation was determined.

The outcome of fermentation processes involving filamentous microbes depends heavily on the morphological form adopted by the organism, as this can have a significant influence on process productivity, both directly and indirectly [8, 220]. Despite the increase in sophistication of process monitoring equipment since the inception of the biotechnology industry in the early-mid twentieth century, the accurate evaluation of morphological variation only became possible with the increased availability of affordable computer hardware over the last two decades, permitting the use of digital image analysis to fulfil this task. Although the compilation of quantitative data was possible prior to this, the methods involved were typically laborious and time-consuming [1, 3] and, as such, were often overlooked.

However, despite early progress in the development of automated imaging systems for the purpose of morphological quantification [5, 9], many authors still indicate a dependence on manual intervention for the production of accurate results [10–13, 121, 140, 148], prolonging processing time. Furthermore, many recent publications also rely on qualitative morphological descriptors, such as 'smooth', 'fluffy', 'pulpy', 'pelleted' and 'filamentous' [14, 15, 99]. Such descriptions introduce a degree of ambiguity and subjectivity into published results and comparisons between different qualitative reports can result in apparent disagreement. For example, contradictory reports exist in the case of the production of citric acid from *A. niger* [44, 95], but this disagreement may result from the ambiguous classification of fungal conformations in earlier studies, resulting from a lack of image-analysis methods to quantify morphology. As such, a precise relationship between morphology and metabolite production is difficult to ascertain.

The imaging routines described in this study have much in common with those

previously described elsewhere. At the microscopic level, spores were analysed in terms of projected area ($A_p$) and circularity ($C = 4\pi A_p P^{-2}$ or $C = P^2(4\pi A_p)^{-1}$), while hyphal elements were analysed in terms of simple metrics such as their total length ($L_{th}$) and the total number of tips per element ($N$), from which the hyphal growth unit ($L_{hgu} = L_{th}/N$) may be calculated. This simple measure is still often used as a means of comparing the branching behaviour of various organisms under different conditions [72, 104, 159, 175, 185]. At the macroscopic level, pellets were analysed simply in terms of projected area, which may subsequently be expressed as equivalent diameter ($D = 2\sqrt{A_p/\pi}$) if the pellets are considered to be approximately spherical. While this may seem to be of limited value, projected area and/or diameter are common measures of fungal biomass and many studies have derived relationships between one or other of these parameters and metabolite production [46, 50, 72, 74, 96].

For more extensive data on pellet morphology, microscopic analysis is required, given that the pellet perimeter is delineated by hyphae 2 – 3 $\mu$m in diameter. An accurate representation of the pellet at the microscopic level would permit the quantification of parameters such as the perimeter ($P$), the convex perimeter ($P_c$) and the projected convex area (area including 'holes'; $A_c$). These could then in turn be used to calculate other morphological descriptors, such as circularity, roughness ($P^2/A_p$) [151], compactness value ($A_p/A_c$) [50, 107, 152] and convexity ($P/P_c$) [48, 49], providing a more thorough characterisation of the pelleted morphology. However, the pellets of *A. oryzae* observed in this work were typically far too large (up to 6 mm in diameter) to image microscopically and, as such, more detailed measurement is difficult to achieve.

Routines for the microscopic analysis of hyphal elements, however, were designed in such a manner as to allow a more in-depth characterisation of mycelia, should it be required. This was achieved by modelling the mycelium as a 'graph' consisting of

'nodes' or 'vertices' (hyphal tips and branch-points) and 'edges' (inter-nodal hyphal segments). Such a capability would be useful in characterising the foraging strategies of filamentous microbes on solid substrates. While the hyphal growth unit is a useful indicator of the 'average' branching behaviour of a mycelium, it reveals nothing about the spatial arrangement of the individual hyphae (Fig. 8.1), or how this arrangement may be affected by a change in environmental conditions (such as a step-change in nutrient concentration). Hyphal 'spiralling', which can result from a high coefficient of friction between the hyphae and the substrate [32], can also have a significant impact on the morphology of a mycelium cultivated on solid substrate. By recording the specific location of each tip or branch-point (as co-ordinates in a Cartesian plane, for example), an evaluation of tip-to-tip, branchpoint-to-branchpoint or tip-to-branchpoint distances is possible. Although nutrient concentration, for example, is known to influence the directionality of mycelial growth [32], studies of this behaviour are rare. Hitchcock and colleagues demonstrated increased hyphal density in regions of increased nutrient concentration, but the analysis was conducted at a relatively low resolution: fungal colonies were projected onto lith film, which was subsequently imaged using a flat-bed scanner.

While the image processing routines have much in common with those described in other studies, the principle advantage of those described here over others is full automation, which was demonstrated to produce results in close agreement with those produced through semi-automated analysis (Fig. 5.7). Furthermore, the output is stable when input parameters are varied over a small range (Figs. 5.6, 5.12 & 5.13). Image processing applications reported in the literature are sometimes described as 'semi-automatic', but the term can be used rather liberally, as it may refer to manual image segmentation and object detection followed by automated object measurement [79], which is essentially manual analysis.

In parallel with software development, a means of presenting fungal conforma-

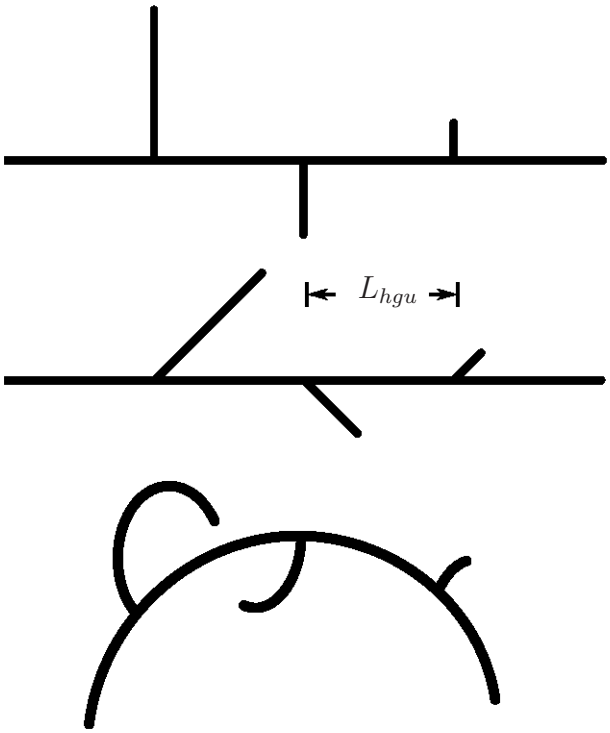


**Figure 8.1:** Two mycelia with the same hyphal growth unit, but with different directionality of growth, and a third exhibiting signs of hyphal 'spiralling'. Although the length of the hyphal growth unit is similar in each case, the spatial distribution of the hyphae is quite different.

tions in an essentially two-dimensional format was investigated [234]. Nitrocellulose-immobilised elements of *A. oryzae* were successfully cultivated on malt agar and key developmental states, such as spore germination and the onset of hyphal branching, were clearly observable (Fig. 4.3). Furthermore, the application of microscope immersion oil permitted the use of high-magnification oil-objectives for routine capture of fine details such as septation (Fig. 4.4). A modification of this immobilisation technique was also found to be useful for examining samples taken from submerged culture, using both conventional light or fluorescence microscopy (Figs. 4.10 & 4.11).

The newly-developed imaging routines were combined with the immobilisation assay to examine the growth kinetics of *Aspergillus oryzae* on a solid substrate

[235]. Detailed analysis was made of a population of spores from inoculation to germination and hyphal elements from 14 to 24 hours post-inoculation, with data calculated for spore swelling rate, biomass specific growth rate and mean hyphal tip extension rate (Figs. 5.2, 5.7 & 5.9). The growth data was consistent with previously-published empirical expressions (Equations 5.4 – 5.9) and the parameters derived, such as the specific growth rate ($\mu = 0.24$ h$^{-1}$) and the specific branching rate ($k_b = 0.0023$ tips $\mu$m$^{-1}$ h$^{-1}$), were in close agreement with previously published figures for *A. oryzae* [45, 106]. To the best of the author's knowledge, this is the first detailed, microscopic study of the growth kinetics of a large population of mycelia in a solid state system and there is potential to extend this work to the examination of other microbes growing under similar conditions. Immobilised cultures have previously been utilised for the study of filamentous moulds, but this involved the continuous monitoring of a small number of colonies to derive kinetic data [1]. While such physiological studies provide invaluable data on the extension rates of individual hyphae, for example, a more extensive population-based analysis is desirable for the characterisation of industrial processes.

Further experimentation focussed on investigating the relationship between the micro-morphology, macro-morphology and $\alpha$-amylase production of *A. oryzae* in submerged culture. A simple measure of pellet projected area was used as a means of quantifying and comparing different morphological forms in the frequent absence of 'free' mycelial elements, the presence of which would have permitted the characterisation of branching behaviour of the organism. However, a correlation between pellet size and $\alpha$-amylase production was derived when increases in inoculum concentration triggered morphological variation (Fig. 6.13). These findings were consistent with other reports in the literature which suggest that smaller pellets typically favour increased metabolite production [46, 50, 74, 96].

The various investigations into the behaviour of *A. oryzae* in submerged culture

were often complicated by the agglomerative nature of the fungus' spores, which typically resulted in low levels of 'free' mycelial elements. Other morphological studies of *A. oryzae* have used a low medium pH during the early stages of incubation to ensure that agglomeration does not occur [45, 107]. However, highly acidic conditions have also been demonstrated to adversely affect growth and product formation [45], and, as a result, such a means of inducing morphological variation was avoided in this study. However, attempts were made to induce dispersed mycelial growth in *A. oryzae* by supplementing cultures with surfactant compounds, which have previously been reported to inhibit pellet formation in filamentous microbes [14, 102]. A significant influence on $\alpha$-amylase production was found when fermentations were supplemented with the non-ionic detergents, Tween-80, Nonidet P-40 and Triton X-100. Tween-80 had little effect on biomass yield and a limited morphological impact (slight increase in mean pellet diameter), but $\alpha$-amylase yields were substantially higher in its presence (Fig. 6.14). Both Nonidet P-40 and Triton X-100 caused a reduction in biomass yield, possibly indicating an inhibition of growth, but levels of $\alpha$-amylase produced per unit dry cell weight were higher than the control (Fig. 6.20b). These increases did not appear to be directly related to the observed morphological variation, although a quantitative analysis of micro-morphology was not possible due to the limited stain uptake of cultures incubated in the presence of detergents.

The positive influence on metabolite production resulting from detergent supplementation has been noted in previous studies, the consensus being that an increase in cell permeability leads to an increase in the diffusion path into pellets [14, 15]. This subsequently causes an increase in the percentage of active biomass in a culture, resulting in increased metabolite yield. However, Reese and Maguire found that supplementation with Tween-80 resulted in an increase in the yield of various enzymes in some organisms, but a reduction in yield for others [237]. For example,

the yield of gluconases and glucosidases obtained from *A. luchuensis* and *A. terreus* increased in the presence of Tween-80, but the yield of gluconases obtained from *P. funiculosum* decreased in the presence of Tween, while the yield of glucosidases increased. Alternatively, the increase in $\alpha$-amylase activity observed in the presence of non-ionic detergents in this study may have been a result of enhanced activation of the enzyme by the surfactants, rather than an increase in enzyme production by *A. oryzae*. Yoon and Robyt found that supplementing a solution containing porcine pancreatic $\alpha$-amylase with 0.02% w/v Triton X-100 resulted in an increase in activity of approximately 40% [219]. Such reports suggest that surfactant supplementation may result in complex physio-chemical effects.

While beyond the scope of this study, one possible approach to investigating the physiological influence of surfactants on filamentous microbes would be the quantification of the 'active' region of pellets (Fig. 8.2). The fluorescent stain acridine orange has been previously utilised for this purpose [46]. Alternatively, a direct evaluation of cell permeability may be possible with the use of SYTOX Green, which permeates non-viable cells and fluoresces green, while viable cells remain unaffected [238, 239]. Staining of inactive pellet cores could permit their measurement and a percentage of 'active' biomass could thus be calculated, allowing comparisons between different culture conditions. However, the success of such an approach would be dependant on fungal pellets being small enough to be examined microscopically, which was typically not the case in this study, in order to obtain sufficiently high resolution images to accurately delineate the intra-pellet regions. Alternatively, the work conducted here investigating the impact of Tween-80 in solid culture (Fig. 6.17) could be expanded upon to determine if the detergent has any effect on cell membrane permeability, which may be visualised using SYTOX Green. However, the processing of membrane-immobilised cultures results in the death of cells and a viable stain such as SYTOX Green may not be compatible with such a procedure.

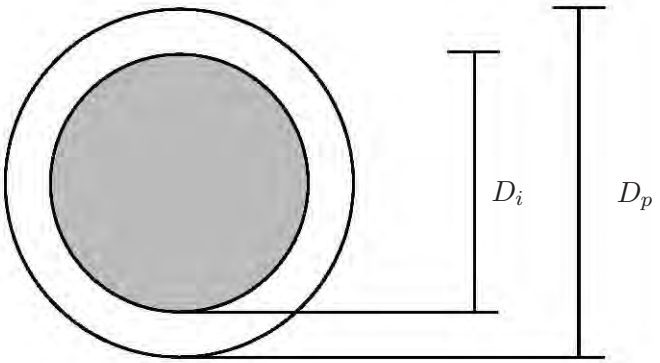


$$V_a = \frac{\pi}{6}(D_p^3 - D_i^3)$$

**Figure 8.2:** Calculation of the 'active' pellet volume ($V_a$), by measuring the total pellet diameter ($D_p$) and the 'inactive' pellet diameter ($D_i$).

It must be concluded from these investigations that inducing tightly-controlled morphological variation is not easily achieved. As such, image processing systems must be designed in such a manner as to permit detailed evaluation of any morphological form that may result in a particular process, rather than relying on the existence of one particular phenotype, such as the freely dispersed form. Some studies have described systems capable of discriminating between different morphological forms and assigning a specific classification to a particular object exhibiting certain features [72, 204]. However, such systems are based on a degree of subjectivity in that the system is typically trained by a human observer who assigns a label (pellet, clump, free mycelia, artifact) to a particular object in an image and this label is subsequently assigned by the automated system to other objects that exhibit similar morphological features. While a description of a culture as predominantly 'pelleted' or 'dispersed', for example, provides little quantitative information on the morphology, it may be possible to subject each of these classes to subsequent image analysis. However, this typically results in different metrics being applied to different 'classes' and a comparison of the morphology of different morphologi-

cal classes is thus not possible. The use of alternative parameters for morphological quantification may be necessary, rather than depending on the existence of a certain morphological form as a prerequisite for the application of an imaging system.

One such parameter investigated here is the fractal dimension ($D$). Fractal geometry has previously been used in a number of studies of the morphology of filamentous microbes [110, 159, 172, 183, 184, 230], but many have been confined to analysis of clumped or pelleted morphologies (or colonies on solid substrates). While it has been proposed that $D$ may be viewed as a measure of branching complexity [110], to the best of the author's knowledge, no direct relationships between $D$ and conventional morphological parameters, such as the hyphal growth unit, have previously been established. The result presented here, indicating a strong correlation between $D$ and $L_{hgu}$ (Fig. 7.8), suggests that $D$, which can be calculated regardless of the morphological form that predominates in a particular process, may be suitable for use as a 'universal measure' of fungal morphology, directly associated with branching behaviour.

In order to verify this association for macroscopic aggregates such as mycelial clumps and pellets, or colonies on solid substrates, a knowledge of the branching behaviour of an organism within such structures is necessary. According to Cox and colleagues, '*it is just possible that in some circumstances the mycelial morphology within clumps might be inferred from the more easily characterized freely dispersed form*' [136], but such requires the presence of 'free' elements in a culture. Should it be possible to relate the hyphal growth unit to the fractal dimension of macroscopic structures (it seems intuitive that a dependency exists; Fig. 8.3), this would obviate the need to induce filamentous growth for accurate assessment of branching behaviour, or the development of systems for the discrimination of different morphological forms. There is some evidence in the literature that microscopic parameters can influence macroscopic form. Park and colleagues found that dif-

ferent *Mortierella* species, which exhibited different morphological features at the microscopic level, produced macroscopic colonies of various shapes and sizes, but no quantitative result was elucidated [125].

While it may be possible to relate the hyphal growth unit of 'young' mycelia cultivated on solid substrates with the fractal dimension of the macroscopic colonies that result, such an investigation must also consider any differing spatial distribution of the different organisms investigated; it is possible that two mycelia can have the same hyphal growth unit while exhibiting different morphological features (Fig. 8.1). As the directionality of hyphal growth is thought to be determined by concentration gradients in the solid substrate [7, 32], cultivation on a membrane placed atop a liquid medium should minimise the impact of this variable and the effect of different medium compositions on hyphal growth unit and, subsequently, colony morphology (fractal dimension) could be examined. However, any differences in foraging strategy (branching angle, for example) would still need to be determined by microscopic assessment. Such an investigation therefore requires the consideration of a large number of variables.

The production of a 'boundary signal', as used here to evaluate $D$, could also prove useful in cases where the application of a skeletonisation routine to mycelial elements is undesirable; such investigations using image analysis systems may rely on manual tip-counts [152]. However, consider the example presented in Figure 7.5; it may be possible to identify the hyphal tips as local maxima in the boundary signal. The enumeration of these local turning points could be used as an indicator of tip location in applications where skeletonisation is unsuitable. There also exists the possibility that an examination of object boundaries could prove useful in discriminating between spore clusters and 'young' hyphae, which can be otherwise morphologically similar (Section 3.5), although it is likely that high-magnification images would be required for such an application to provide sufficiently high reso-

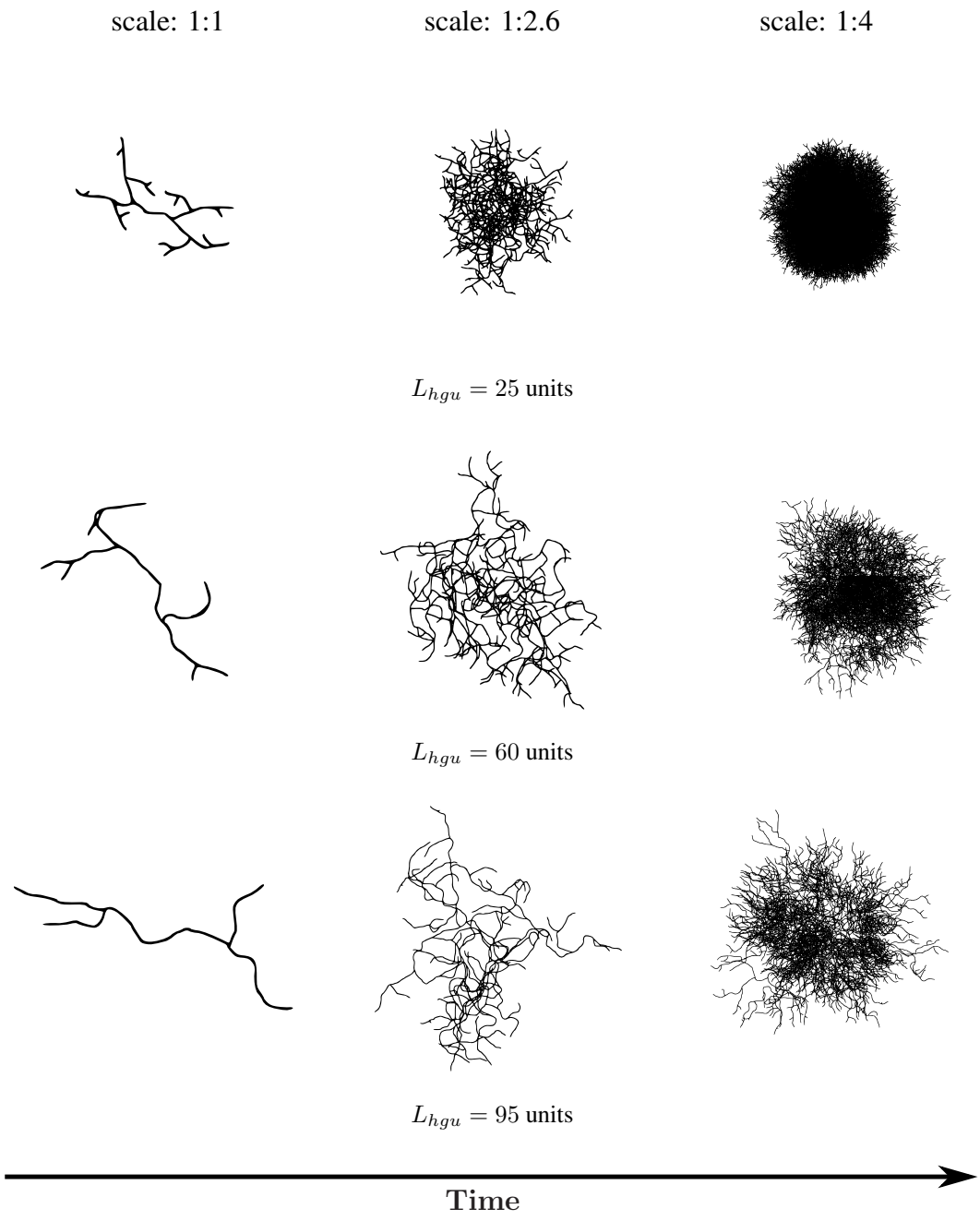


**Figure 8.3:** Simulated effect of increasing hyphal growth unit ($L_{hgu}$) on colony macro-morphology.

lution, resulting in a significant increase in the time necessary for image capture.

Image processing systems represent essential tools for the accurate quantification of fungal morphology, but fully automated systems, designed for this application, are still rare. The system developed in this study has been used in conjunction with a newly-developed immobilisation assay to characterise the growth kinetics of *A. oryzae* on a solid substrate. In addition, published findings on the application of fractal analyses have been expanded upon by relating this parameter to the branching behaviour of the organism using a novel means of fractal dimension evaluation. The growth of *A. oryzae* in shake flask cultures, reports of which are rare in the literature, has also been extensively studied, with data presented on the micro- and macro-morphological form in various different media compositions. The potential exists to combine these research avenues and utilise fractal geometry to further characterise morphological conformations in submerged culture and, subsequently, arrive at a more definitive correlation between phenotypic variation and metabolite production.

# References


[1] A. P. J. Trinci. "A study of the kinetics of hyphal extension and branch initiation of fungal mycelia." *J Gen Microbiol*, vol. 81, no. 1: pp. 225–36, 1974. Doi: 10.1099/00221287-81-1-225.

[2] Y. Chisti and M. Moo-Young. "Bioreactor design." In C. Ratledge and B. Kristiansen, eds., "Basic Biotechnology," pp. 151–72. Cambridge: Cambridge University Press, 2nd ed., 2001.

[3] B. Metz, E. W. de Bruijn and J. C. van Suijdam. "Methods for quantitative representation of the morphology of molds." *Biotechnol Bioeng*, vol. 23, no. 1: pp. 149–62, 1981. Doi: 10.1002/bit.260230110.

[4] A. Spohr, C. Dam-Mikkelsen, M. Carlsen, J. Nielsen and J. Villadsen. "On-line study of fungal morphology during submerged growth in a small flow-through cell." *Biotechnol Bioeng*, vol. 58, no. 5: pp. 541–53, 1998. Doi: 10.1002/(SICI)1097-0290(19980605)58:5<541::AID-BIT11>3.0.CO;2-E.

[5] K. G. Tucker, T. Kelly, P. Delgrazia and C. R. Thomas. "Fully-automatic measurement of mycelial morphology by image analysis." *Biotechnol Prog*, vol. 8, no. 4: pp. 353–359, 1992. Doi: 10.1021/bp00016a013.

[6] D. B. Archer, D. A. Mackenzie and D. J. Jeenes. "Genetic engineering: Yeasts and filamentous fungi." In C. Ratledge and B. Kristiansen, eds., "Basic

Biotechnology," pp. 95–126. Cambridge: Cambridge University Press, 2nd ed., 2001.

[7] M. J. Carlile, S. C. Watkinson and G. W. Gooday. *The Fungi*. New York: Academic Press, 2nd ed., 2001.

[8] M. Papagianni. "Fungal morphology and metabolite production in submerged mycelial processes." *Biotechnol Adv*, vol. 22, no. 3: pp. 189–259, 2004. Doi: 10.1016/j.biotechadv.2003.09.005.

[9] H. Packer and C. R. Thomas. "Morphological measurements on filamentous microorganisms by fully automatic image analysis." *Biotechnol Bioeng*, vol. 35, no. 9: pp. 870–81, 1990. Doi: 10.1002/bit.260350904.

[10] V. Lecault, N. Patel and J. Thibault. "Morphological characterization and viability assessment of *Trichoderma reesei* by image analysis." *Biotechnol Prog*, vol. 23, no. 3: pp. 734–40, 2007. Doi: 10.1021/bp0602956.

[11] N. El-Sabbagh, L. M. Harvey and B. McNeil. "Effects of dissolved carbon dioxide on growth, nutrient consumption, cephalosporin C synthesis and morphology of *Acremonium chrysogenum* in batch cultures." *Enzyme Microb Tech*, vol. 42, no. 4: pp. 315–24, 2008. Doi: 10.1016/j.enzmictec.2007.10.012.

[12] Y. Anikster, T. Eilam, W. Bushnell and E. Kosman. "Spore dimensions of *Puccinia* species of cereal hosts as determined by image analysis." *Mycologia*, vol. 97, no. 2: pp. 474–84, 2005. Doi: 10.3852/mycologia.97.2.474.

[13] T. Lübbehüsen, V. G. Polo, S. Rossi, J. Nielsen, S. Moreno, M. McIntyre and J. Arnau. "Protein kinase A is involved in the control of morphology and branching during aerobic growth of *Mucor circinelloides*." *Microbiology*, vol. 150, no. 1: pp. 143–50, 2004. Doi: 10.1099/mic.0.26708-0.

[14] F. C. Domingues, J. A. Queiroz, J. M. Cabral and L. P. Fonseca. "The influence of culture conditions on mycelial structure and cellulase production by *Trichoderma reesei* Rut C-30." *Enzyme Microb Tech*, vol. 26, no. 5-6: pp. 394–401, 2000. Doi: 10.1016/S0141-0229(99)00166-0.

[15] P. Žnidaršič, R. Komel and A. Pavko. "Influence of some environmental factors on *Rhizopus nigricans* submerged growth in the form of pellets." *World J Microb Biot*, vol. 16, no. 7: pp. 589–93, 2000. Doi: 10.1023/A:1008967519157.

[16] J.-M. Barea, M. J. Pozo, R. Azcón and C. Azcón-Aguilar. "Microbial co-operation in the rhizosphere." *J Exp Bot*, vol. 56, no. 417: pp. 1761–78, 2005. Doi: 10.1093/jxb/eri197.

[17] K. Shalchian-Tabrizi, M. A. Minge, M. Espelund, R. Orr, T. Ruden, K. S. Jakobsen and T. Cavalier-Smith. "Multigene phylogeny of choanozoa and the origin of animals." *PLoS ONE*, vol. 3, no. 5: p. e2098, 2008. Doi: 10.1371/journal.pone.0002098.

[18] D. S. Hibbett, M. Binder, J. F. Bischoff *et al.* "A higher-level phylogenetic classification of the fungi." *Mycol Res*, vol. 111, no. 5: pp. 509–47, 2007. Doi: 10.1016/j.mycres.2007.03.004.

[19] G. Celio, M. Padamsee, B. Dentinger, R. Bauer and D. McLaughlin. "Assembling the fungal tree of life: Constructing the structural and biochemical database." *Mycologia*, vol. 98, no. 6: pp. 850–59, 2006. Doi: 10.3852/mycologia.98.6.850.

[20] J. Heitman. "Sexual reproduction and the evolution of microbial pathogens." *Curr Biol*, vol. 16, no. 17: pp. R711–R725, 2006. Doi: 10.1016/j.cub.2006.07.064.

[21] J. Guarro, J. Gené and A. M. Stchigel. "Developments in fungal taxonomy." *Clin Microbiol Rev*, vol. 12, no. 3: pp. 454–500, 1999.

[22] J. W. Taylor, D. J. Jacobson, S. Kroken, T. Kasuga, D. M. Geiser, D. S. Hibbett and M. C. Fisher. "Phylogenetic species recognition and species concepts in fungi." *Fungal Genet Biol*, vol. 31, no. 1: pp. 21–32, 2000. Doi: 10.1006/fgbi.2000.1228.

[23] L. Wang, D. Ridgway, T. Gu and M. Moo-Young. "Bioprocessing strategies to improve heterologous protein production in filamentous fungal fermentations." *Biotechnol Adv*, vol. 23, no. 2: pp. 115–129, 2005. Doi: 10.1016/j.biotechadv.2004.11.001.

[24] T. Tauro, K. K. Kapoor and K. S. Yadav. *An Introduction to Microbiology*. Singapore: John Wiley and Sons, 1986.

[25] G. M. Walker and N. A. White. "Introduction to fungal physiology." In K. Kavanagh, ed., "Fungi," pp. 1–34. Chichester, UK: John Wiley and Sons, 1st ed., 2005. Doi: 10.1002/0470015330.ch1.

[26] M. Sautour, A. Rouget, P. Dantigny, C. Divies and M. Bensoussan. "Prediction of conidial germination of *Penicillium chrysogenum* as influenced by temperature, water activity and pH." *Lett Appl Microbiol*, vol. 32, no. 3: pp. 131–4, 2001. Doi: 10.1111/j.1472-765X.2001.00872.x.

[27] E. Pardo, U. Lagunas, V. Sanchis, A. J. Ramos and S. Marín. "Influence of water activity and temperature on conidial germination and mycelial growth of ochratoxigenic isolates of *Aspergillus ochraceus* on grape juice synthetic medium. Predictive models." *J Sci Food Agr*, vol. 85, no. 10: pp. 1681–86, 2005. Doi: 10.1002/jsfa.2171.

[28] R. D. Medwid and D. W. Grant. "Germination of *Rhizopus oligosporus* sporangiospores." *Appl Environ Microbiol*, vol. 48, no. 6: pp. 1067–71, 1984.

[29] E. Moore-Landecker. *Fundamentals of the Fungi*. London: Prentice Hall, 4th ed., 1996.

[30] G. D. Robson. "Hyphal cell biology." In "Molecular Fungal Biology," pp. 164–84. Cambridge: Cambridge University Press, 1st ed., 1999.

[31] A. P. J. Trinci. "Exponential growth of the germ tubes of fungal spores." *J Gen Microbiol*, vol. 67, no. 3: pp. 345–48, 1971. Doi: 10.1099/00221287-67-3-345.

[32] J. I. Prosser. "Kinetics of filamentous growth and branching." In N. A. Gow and G. M. Gadd, eds., "The Growing Fungus," pp. 301–18. London: Chapman and Hall, 1st ed., 1995. Doi: 10.1007/978-0-585-27576-5_14.

[33] N. A. R. Gow. "Tip growth and polarity." In N. A. Gow and G. M. Gadd, eds., "The Growing Fungus," pp. 277–299. London: Chapman and Hall, 1st ed., 1995. Doi: 10.1007/978-0-585-27576-5_13.

[34] J. Ruiz-Herrera. *Fungal cell wall: Structure, synthesis, and assembly*. Boca Ranton, Florida: Taylor and Francis, 1991.

[35] G. Paul and C. Thomas. "Characterisation of mycelial morphology using image analysis." In "Relation Between Morphology and Process Performances," vol. 60 of *Advances in Biochemical Engineering/Biotechnology*, pp. 1–59. Berlin: Springer, 1998. Doi: 10.1007/BFb0102278.

[36] S. Bartnicki-Garcia, F. Hergert and G. Gierz. "Computer simulation of fungal morphogenesis and the mathematical basis for hyphal (tip) growth." *Protoplasma*, vol. 153, no. 1: pp. 46–57, 1989. Doi: 10.1007/BF01322464.

[37] A. P. J. Trinci. "Influence of the width of the peripheral growth zone on the radial growth rate of fungal colonies on solid media." *J Gen Microbiol*, vol. 67, no. 3: pp. 325–44, 1971. Doi: 10.1099/00221287-67-3-325.

[38] N. J. B. Plomley. "Formation of the colony in the fungus *Chaetomium*." *Aust J Biol Sci*, vol. 12: pp. 53–64, 1959.

[39] I. Y. Caldwell and A. P. J. Trinci. "The growth unit of the mould *Geotrichum candidum*." *Arch Microbiol*, vol. 88: pp. 1–10, 1973. Doi: 10.1007/BF00408836.

[40] S. Olsson. "Uptake of glucose and phosphorus by growing colonies of *Fusarium oxysporum* as quantified by image analysis." *Exp Mycol*, vol. 18, no. 1: pp. 33–47, 1994. Doi: 10.1006/emyc.1994.1004.

[41] S. Emerson. "The growth phase in *Neurospora* corresponding to the logarithmic phase in unicellular organisms." *J Bacteriol*, vol. 60, no. 3: pp. 221–223, 1950.

[42] K. C. Marshall and M. Alexander. "Growth characteristics of fungi and actinomycetes." *J Bacteriol*, vol. 80: pp. 412–6, 1960.

[43] S. J. Pirt. "A theory of the mode of growth of fungi in the form of pellets in submerged culture." *P Roy Soc Lond B Bio*, vol. 166, no. 1004: pp. 369–73, 1966. Doi: 10.1098/rspb.1966.0105.

[44] G. C. Paul, M. A. Priede and C. R. Thomas. "Relationship between morphology and citric acid production in submerged *Aspergillus niger* fermentations." *Biochem Eng J*, vol. 3, no. 2: pp. 121–29, 1999. Doi: 10.1016/S1369-703X(99)00012-1.

[45] M. Carlsen, A. B. Spohr, J. Nielsen and J. Villadsen. "Morphology and physiology of an alpha-amylase producing strain of *Aspergillus oryzae* during batch cultivations." *Biotechnol Bioeng*, vol. 49, no. 3: pp. 266–76, 1996. Doi: 10.1002/(SICI)1097-0290(19960205)49:3<266::AID-BIT4>3.0.CO;2-I.

[46] H. El-Enshasy, J. Kleine and U. Rinas. "Agitation effects on morphology and protein productive fractions of filamentous and pelleted growth forms of recombinant *Aspergillus niger*." *Process Biochem*, vol. 41, no. 10: pp. 2103–12, 2006. Doi: 10.1016/j.procbio.2006.05.024.

[47] M. Bizukojc and S. Ledakowicz. "The morphological and physiological evolution of *Aspergillus terreus* mycelium in the submerged culture and its relation to the formation of secondary metabolites." *World J Microb Biot*, vol. 26, no. 1: pp. 41–54, 2010. Doi: 10.1007/s11274-009-0140-1.

[48] M. Papagianni and M. Mattey. "Physiological aspects of free and immobilized *Aspergillus niger* cultures producing citric acid under various glucose concentrations." *Process Biochem*, vol. 39, no. 12: pp. 1963–70, 2004. Doi: 10.1016/j.procbio.2003.09.027.

[49] M. Papagianni and M. Moo-Young. "Protease secretion in glucoamylase producer *Aspergillus niger* cultures: Fungal morphology and inoculum effects." *Process Biochem*, vol. 37, no. 11: pp. 1271–78, 2002. Doi: 10.1016/S0032-9592(02)00002-X.

[50] J. P. Park, Y. M. Kim, S. W. Kim, H. J. Hwang, Y. J. Cho, Y. S. Lee, C. H. Song and J. W. Yun. "Effect of agitation intensity on the exo-biopolymer production and mycelial morphology in *Cordyceps militaris*." *Lett Appl Microbiol*, vol. 34, no. 6: pp. 433–38, 2002. Doi: 10.1046/j.1472-765X.2002.01126.x.

[51] E. M. Rodríguez Porcel, J. L. Casas López, J. A. Sánchez Pérez, J. M. Fernández Sevilla and Y. Chisti. "Effects of pellet morphology on broth rheology in fermentations of *Aspergillus terreus*." *Biochem Eng J*, vol. 26, no. 2–3: pp. 139–44, 2005. Doi: 10.1016/j.bej.2005.04.011.

[52] H. J. Hwang, S. W. Kim, C. P. Xu, J. W. Choi and J. W. Yun. "Morphological and rheological properties of the three different species of basidiomycetes *Phellinus* in submerged cultures." *J Appl Microbiol*, vol. 96, no. 6: pp. 1296–1305, 2004. Doi: 10.1111/j.1365-2672.2004.02271.x.

[53] M. Adamczak, U. T. Bornscheuer and W. Bednarski. "The application of biotechnological methods for the synthesis of biodiesel." *Eur J Lipid Sci Tech*, vol. 111, no. 8: pp. 800–13, 2009. Doi: 10.1002/ejlt.200900078.

[54] R. Bigelis, H. He, H. Y. Yang, L. P. Chang and M. Greenstein. "Production of fungal antibiotics using polymeric solid supports in solid-state and liquid fermentation." *J Ind Microbiol Biotechnol*, vol. 33, no. 10: pp. 815–26, 2006. Doi: 10.1007/s10295-006-0126-z.

[55] "Maximising UK opportunities from industrial biotechnology in a low carbon economy." Department of Business Enterprise & Regulatory Reform, London, 2009.

[56] T.-M. Enari. *From Beer to Molecular Biology: The Evolution of Industrial Biotechnology*. Nürnberg: Fachverlag Hans Carl, 1999.

[57] K. Gomi and K. Abe. "Food products fermented by *Aspergillus oryzae*." In S. A. Osmani and G. H. Goldman, eds., "The Aspergilli: Genomics, medical aspects, biotechnology, and research methods," vol. 26 of *Mycology*, chap. 25, pp. 429–40. Boca Raton, Florida: CRC Press, 2008.

[58] A. N. Glazer and H. Nikaido. *Microbial Biotechnology: Fundamentals of Applied Microbiology*. Cambridge: Cambridge University Press, 2nd ed., 2007.

[59] K. Iwashita. "Recent studies of protein secretion by filamentous fungi." *J Biosci Bioeng*, vol. 94, no. 6: pp. 530–35, 2002. Doi: 10.1016/S1389-1723(02)80191-8.

[60] H. Kreuzer and A. Massey. *Biology and Biotechnology: Science, Applications and Issues*. Washington DC: ASM Press, 2005.

[61] B. Kristiansen. "Process economics." In C. Ratledge and B. Kristiansen, eds., "Basic Biotechnology," pp. 239–52. Cambridge: Cambridge University Press, 2nd ed., 2001.

[62] D. A. Mitchell, M. Berovič and N. Krieger. "Solid-state fermentation bioreactor fundamentals: Introduction and overview." In D. A. Mitchell, N. Krieger and M. Berovič, eds., "Solid-State Fermentation Bioreactors: Fundamentals of Design and Operation," pp. 1–12. Berlin: Springer-Verlag, 2006.

[63] A. Pandey, C. Larroche and C. R. Soccol. "General considerations about solid-state fermentation processes." In A. Pandey, C. R. Soccol and C. Larroche, eds., "Current Developments in Solid-state Fermentation," pp. 13–25. New York: Springer-Verlag, 2008.

[64] A. Pandey, C. R. Soccol and D. Mitchell. "New developments in solid state fermentation: I-bioprocesses and products." *Process Biochem*, vol. 35, no. 10: pp. 1153–69, 2000. Doi: 10.1016/S0032-9592(00)00152-7.

[65] R. te Biesebeke, G. Ruijter, Y. S. P. Rahardjo *et al.* "*Aspergillus oryzae* in solid-state and submerged fermentations." *FEMS Yeast Res*, vol. 2, no. 2: pp. 245–48, 2002. Doi: 10.1111/j.1567-1364.2002.tb00089.x.

[66] J. E. Smith, D. R. Berry and B. Kristiansen, eds. *Filamentous Fungi: Fungal Technology*, vol. 4. London: Edward Arnold, 1983.

[67] M. Machida. "Progress of *Aspergillus oryzae* genomics." In A. I. Laskin, J. W. Bennett and G. M. Gadd, eds., "Advances in Applied Microbiology," vol. 51, pp. 81–106. San Diego: Academic Press, 2002.

[68] K. Oda, D. Kakizono, O. Yamada, H. Iefuji, O. Akita and K. Iwashita. "Proteomic analysis of extracellular proteins from *Aspergillus oryzae* grown under submerged and solid-state culture conditions." *Appl Environ Microbiol*, vol. 72, no. 5: pp. 3448–57, 2006. Doi: 10.1128/AEM.72.5.3448-3457.2006.

[69] G. J. G. Ruijter, J. Visser and A. Rinzema. "Polyol accumulation by *Aspergillus oryzae* at low water activity in solid-state fermentation." *Microbiology*, vol. 150, no. 4: pp. 1095–1101, 2004. Doi: 10.1099/mic.0.26723-0.

[70] A. Pandey, P. Selvakumar, C. R. Soccol and P. Nigam. "Solid state fermentation for the production of industrial enzymes." *Curr Sci India*, vol. 77, no. 1: pp. 149–62, 1999.

[71] J. Lenz, M. Höfer, J. Krasenbrink and U. Hölker. "A survey of computational and physical methods applied to solid-state fermentation." *Appl Microbiol Biotechnol*, vol. 65, no. 1: pp. 9–17, 2004. Doi: 10.1007/s00253-004-1592-8.

[72] M. Papagianni and M. Mattey. "Morphological development of *Aspergillus niger* in submerged citric acid fermentation as a function of the spore inoculum level. Application of neural network and cluster analysis for characterization of mycelial morphology." *Microb Cell Fact*, vol. 5, no. 1: p. 3, 2006. Doi: 10.1186/1475-2859-5-3.

[73] C. L. Johansen, L. Coolen and J. H. Hunik. "Influence of morphology on

product formation in *Aspergillus awamori* during submerged fermentations." *Biotechnol Prog*, vol. 14, no. 2: pp. 233–40, 1998. Doi: 10.1021/bp980014x.

[74] J. Xu, L. Wang, D. Ridgway, T. Gu and M. Moo-Young. "Increased heterologous protein production in *Aspergillus niger* fermentation through extracellular proteases inhibition by pelleted growth." *Biotechnol Prog*, vol. 16, no. 2: pp. 222–27, 2000. Doi: 10.1021/bp000006s.

[75] K. G. Tucker and C. R. Thomas. "Mycelial morphology: The effect of spore inoculum level." *Biotechnol Lett*, vol. 14, no. 11: pp. 1071–74, 1992. Doi: 10.1007/BF01021061.

[76] Y. Teng, Y. Xu and D. Wang. "Changes in morphology of *Rhizopus chinensis* in submerged fermentation and their effect on production of mycelium-bound lipase." *Bioprocess Biosyst Eng*, vol. 32, no. 3: pp. 397–405, 2009. Doi: 10.1007/s00449-008-0259-8.

[77] C. O'Cleirigh, P. K. Walsh and D. G. O'Shea. "Morphological quantification of pellets in *Streptomyces hygroscopicus* var. *geldanus* fermentation broths using a flatbed scanner." *Biotechnol Lett*, vol. 25, no. 19: pp. 1677–83, 2003. Doi: 10.1023/A:1025622100475.

[78] X. Jianfeng, S. Zhiguo and F. Pusun. "Suspension culture of compact callus aggregate of *Rhodiola sachalinensis* for improved salidroside production." *Enzyme Microb Tech*, vol. 23, no. 1–2: pp. 20–27, 1998. Doi: 10.1016/S0141-0229(98)00011-8.

[79] M. Papagianni, M. Mattey and B. Kristiansen. "Hyphal vacuolation and fragmentation in batch and fed-batch culture of *Aspergillus niger* and its relation to citric acid production." *Process Biochem*, vol. 35, no. 3–4: pp. 359–66, 1999. Doi: 10.1016/S0032-9592(99)00079-5.

[80] M. Papagianni, M. Mattey and B. Kristiansen. "Citric acid production and morphology of *Aspergillus niger* as functions of the mixing intensity in a stirred tank and a tubular loop bioreactor." *Biochem Eng J*, vol. 2, no. 3: pp. 197–205, 1998. Doi: 10.1016/S1369-703X(98)00032-1.

[81] M. Papagianni, S. E. Nokes and K. Filer. "Submerged and solid-state phytase fermentation by *Aspergillus niger*: Effects of agitation and medium viscosity on phytase production, fungal morphology and inoculum performance." *Food Technol Biotechnol*, vol. 39, no. 4: pp. 319–26, 2001.

[82] S. Kelly, L. H. Grimm, J. Hengstler, E. Schultheis, R. Krull and D. C. Hempel. "Agitation effects on submerged growth and product formation of *Aspergillus niger*." *Bioprocess Biosyst Eng*, vol. 26, no. 5: pp. 315–23, 2004. Doi: 10.1007/s00449-004-0368-y.

[83] A. Amanullah, R. Blair, A. W. Nienow and C. R. Thomas. "Effects of agitation intensity on mycelial morphology and protein production in chemostat cultures of recombinant *Aspergillus oryzae*." *Biotechnol Bioeng*, vol. 62, no. 4: pp. 434–46, 1999. Doi: 10.1002/(SICI)1097-0290(19990220)62:4<434::AID-BIT6>3.0.CO;2-D.

[84] A. Amanullah, L. H. Christensen, K. Hansen, A. W. Nienow and C. R. Thomas. "Dependence of morphology on agitation intensity in fed-batch cultures of *Aspergillus oryzae* and its implications for recombinant protein production." *Biotechnol Bioeng*, vol. 77, no. 7: pp. 815–26, 2002. Doi: 10.1002/bit.10181.

[85] J. A. Rocha-Valadez, M. Hassan, G. Corkidi, C. Flores, E. Galindo and L. Serrano-Carreón. "6-pentyl-$\alpha$-pyrone production by *Trichoderma harzianum*: The influence of energy dissipation rate and its implications on

fungal physiology." *Biotechnol Bioeng*, vol. 91, no. 1: pp. 54–61, 2005. Doi: 10.1002/bit.20489.

[86] E. Galindo, C. Flores, P. Larralde-Corona, G. Corkidi-Blanco, J. A. Rocha-Valadez and L. Serrano-Carreón. "Production of 6-pentyl-$\alpha$-pyrone by *Trichoderma harzianum* cultured in unbaffled and baffled shake flasks." *Biochem Eng J*, vol. 18, no. 1: pp. 1–8, 2004. Doi: 10.1016/S1369-703X(03)00115-3.

[87] A. Wongwicharn, B. McNeil and L. M. Harvey. "Heterologous protein secretion and fungal morphology in chemostat cultures of a recombinant *Aspergillus niger* (B1-D)." *Enzyme Microb Tech*, vol. 24, no. 8–9: pp. 489–97, 1999. Doi: 10.1016/S0141-0229(98)00139-2.

[88] A. Amanullah, E. Leonildi, A. Nienow and C. Thomas. "Dynamics of mycelial aggregation in cultures of *Aspergillus oryzae*." *Bioprocess Biosyst Eng*, vol. 24, no. 2: pp. 101–7, 2001. Doi: 10.1007/s004490100235.

[89] F. X. Prenafeta-Boldú, R. Summerbell and G. S. de Hoog. "Fungi growing on aromatic hydrocarbons: biotechnology's unexpected encounter with biohazard?" *FEMS Microbiology Reviews*, vol. 30, no. 1: pp. 109–30, 2006. Doi: 10.1111/j.1574-6976.2005.00007.x.

[90] C. Müller, A. B. Spohr and J. Nielsen. "Role of substrate concentration in mitosis and hyphal extension of *Aspergillus*." *Biotechnol Bioeng*, vol. 67, no. 4: pp. 390–97, 2000. Doi: 10.1002/(SICI)1097-0290(20000220)67:4<390::AID-BIT2>3.0.CO;2-O.

[91] S. Bhargava, K. S. Wenger, K. Rane, V. Rising and M. R. Marten. "Effect of cycle time on fungal morphology, broth rheology, and recombinant enzyme productivity during pulsed addition of limiting carbon source." *Biotechnol Bioeng*, vol. 89, no. 5: pp. 524–29, 2005. Doi: 10.1002/bit.20355.

[92] E. Y. Park, Y. Koike, H. J. Cai, K. Higashiyama and S. Fujikawa. "Morphological diversity of *Mortierella alpina*: Effect of consumed carbon to nitrogen ratio in flask culture." *Biotechnol Bioproc E*, vol. 6, no. 3: pp. 161–66, 2001. Doi: 10.1007/BF02932544.

[93] Y. Koike, H. J. Cai, K. Higashiyama, S. Fujikawa and E. Y. Park. "Effect of consumed carbon to nitrogen ratio of mycelial morphology and arachidonic acid production in cultures of *Mortierella alpina*." *J Biosci Bioeng*, vol. 91, no. 4: pp. 382–89, 2001. Doi: 10.1016/S1389-1723(01)80156-0.

[94] J. Dynesen and J. Nielsen. "Surface hydrophobicity of *Aspergillus nidulans* conidiospores and its role in pellet formation." *Biotechnol Prog*, vol. 19, no. 3: pp. 1049–52, 2003. Doi: 10.1021/bp0340032.

[95] M. Kisser, C. P. Kubicek and M. Röhr. "Influence of manganese on morphology and cell wall composition of *Aspergillus niger* during citric acid fermentation." *Arch Microbiol*, vol. 128, no. 1: pp. 26–33, 1980. Doi: 10.1007/BF00422301.

[96] S. Couri, G. A. S. Pinto, L. F. de Senna and H. L. Martelli. "Influence of metal ions on pellet morphology and polygalacturonase synthesis by *Aspergillus niger* 3T5B8." *Braz J Microbiol*, vol. 34: pp. 16–21, 2003. Doi: 10.1590/S1517-83822003000100005.

[97] L. Dobson and D. O'Shea. "Antagonistic effect of divalent cations $Ca^{2+}$ and $Mg^{2+}$ on the morphological development of *Streptomyces hygroscopicus* var. *geldanus*." *Appl Microbiol Biotechnol*, vol. 81, no. 1: pp. 119–26, 2008. Doi: 10.1007/s00253-008-1627-7.

[98] S. Ali. "Application of kaolin to improve citric acid production by a ther-

mophilic *Aspergillus niger*." *Appl Microbiol Biotechnol*, vol. 73, no. 4: pp. 755–62, 2006. Doi: 10.1007/s00253-006-0533-0.

[99] A. Ahamed, A. Singh and O. Ward. "Culture-Based strategies for reduction of protease activity in filtrates from *Aspergillus niger* NRRL-3." *World J Microb Biot*, vol. 21, no. 8: pp. 1577–83, 2005. Doi: 10.1007/s11274-005-8121-5.

[100] L. F. Dobson, C. C. O'Cleirigh and D. G. O'Shea. "The influence of morphology on geldanamycin production in submerged fermentations of *Streptomyces hygroscopicus* var. *geldanus*." *Appl Microbiol Biotechnol*, vol. 79, no. 5: pp. 859–66, 2008. Doi: 10.1007/s00253-008-1493-3.

[101] S. Ilić, S. Konstantinović, V. Veljković, D. Savić, M. Lazić and G. Gojgić-Cvijović. "Impact of carboxymethylcellulose on morphology and antibiotic production by *Streptomyces hygroscopicus*." *Curr Microbiol*, vol. 57, no. 1: pp. 8–11, 2008. Doi: 10.1007/s00284-008-9143-7.

[102] S. Lucatero, E. Galindo and C. P. Larralde-Corona. "Quantitative characterisation of the morphology of *Trichoderma harzianum* cultured in shake-flasks and containing Tween 40." *Biotechnol Lett*, vol. 26, no. 1: pp. 41–44, 2004. Doi: 10.1023/B:BILE.0000009458.58602.d9.

[103] C. O'Cleirigh, J. T. Casey, P. K. Walsh and D. G. O'Shea. "Morphological engineering of *Streptomyces hygroscopicus* var. *geldanus*: Regulation of pellet morphology through manipulation of broth viscosity." *Appl Microbiol Biotechnol*, vol. 68, no. 3: pp. 305–10, 2005. Doi: 10.1007/s00253-004-1883-0.

[104] N. El-Sabbagh, B. McNeil and L. M. Harvey. "Dissolved carbon dioxide effects on growth, nutrient consumption, penicillin synthesis and morphology in batch cultures of *Penicillium chrysogenum*." *Enzyme Microb Tech*, vol. 39, no. 2: pp. 185–90, 2006. Doi: 10.1016/j.enzmictec.2005.10.020.

[105] H. A. B. Wösten, S. M. Moukha, J. H. Sietsma and J. G. H. Wessels. "Localization of growth and secretion of proteins in *Aspergillus niger*." *J Gen Microbiol*, vol. 137, no. 8: pp. 2017–23, 1991. Doi: 10.1099/00221287-137-8-2017.

[106] A. Spohr, M. Carlsen, J. Nielsen and J. Villadsen. "Morphological characterization of recombinant strains of *Aspergillus oryzae* producing alpha-amylase during batch cultivations." *Biotechnol Lett*, vol. 19, no. 3: pp. 257–62, 1997. Doi: 10.1023/A:1018361708884.

[107] C. Müller, M. McIntyre, K. Hansen and J. Nielsen. "Metabolic engineering of the morphology of *Aspergillus oryzae* by altering chitin synthesis." *Appl Environ Microbiol*, vol. 68, no. 4: pp. 1827–36, 2002. Doi: 10.1128/AEM.68.4.1827-1836.2002.

[108] R. te Biesebeke, E. Record, N. van Biezen, M. Heerikhuisen, A. Franken, P. J. Punt and C. A. M. J. J. van den Hondel. "Branching mutants of *Aspergillus oryzae* with improved amylase and protease production on solid substrates." *Appl Microbiol Biotechnol*, vol. 69, no. 1: pp. 44–50, 2005. Doi: 10.1007/s00253-005-1968-4.

[109] M. B. Haack, L. Olsson, K. Hansen and A. Eliasson Lantz. "Change in hyphal morphology of *Aspergillus oryzae* during fed-batch cultivation." *Appl Microbiol Biotechnol*, vol. 70, no. 4: pp. 482–7, 2006. Doi: 10.1007/s00253-005-0085-8.

[110] C. L. Jones and G. T. Lonergan. "Prediction of phenol-oxidase expression in a fungus using the fractal dimension." *Biotechnol Lett*, vol. 19, no. 1: pp. 65–69, 1997. Doi: 10.1023/A:1018371121663.

[111] M. Carlsen, J. Nielsen and J. Villadsen. "Growth and $\alpha$-amylase production by *Aspergillus oryzae* during continuous cultivations." *J Biotechnol*, vol. 45, no. 1: pp. 81–93, 1996. Doi: 10.1016/0168-1656(95)00147-6.

[112] M. Papagianni, M. Mattey and B. Kristiansen. "Morphology and citric acid production of *Aspergillus niger* PM 1." *Biotechnol Lett*, vol. 16, no. 9: pp. 929–34, 1994. Doi: 10.1007/BF00128627.

[113] K. Gull and A. P. J. Trinci. "Detection of areas of wall differentiation in fungi using fluorescent staining." *Arch Microbiol*, vol. 96, no. 1: pp. 53–57, 1974. Doi: 10.1007/BF00590162.

[114] W. S. Rasband. "ImageJ.", 1997–2010. URL: http://rsbweb.nih.gov/ij.

[115] O. J. Jayus, B. M. McDougall and R. J. Seviour. "Synthesis of extracellular $(1 \rightarrow 3)$- and $(1 \rightarrow 6)$-$\beta$-glucanase activities in carbon limiting chemostat culture by the fungus *Acremonium* sp. IMI 383068." *Enzyme Microb Tech*, vol. 36, no. 5–6: pp. 680–86, 2005. Doi: 10.1016/j.enzmictec.2004.12.010.

[116] S. M. Martin and M. E. Bushell. "Effect of hyphal micromorphology on bioreactor performance of antibiotic-producing *Saccharopolyspora erythraea* cultures." *Microbiology*, vol. 142, no. 7: pp. 1783–88, 1996. Doi: 10.1099/13500872-142-7-1783.

[117] W. Burger and M. J. Burge. *Digital Image Processing*. New York: Springer, 1st ed., 2008.

[118] S. Bartnicki-García, C. E. Bracker, G. Gierz, R. López-Franco and H. Lu. "Mapping the growth of fungal hyphae: Orthogonal cell wall expansion during tip growth and the role of turgor." *Biophys J*, vol. 79, no. 5: pp. 2382–90, 2000. Doi: 10.1016/S0006-3495(00)76483-6.

[119] Z. J. Li, V. Shukla, A. P. Fordyce, A. G. Pedersen, K. S. Wenger and M. R. Marten. "Fungal morphology and fragmentation behavior in a fed-batch *Aspergillus oryzae* fermentation at the production scale." *Biotechnol Bioeng*, vol. 70, no. 3: pp. 300–12, 2000. Doi: 10.1002/1097-0290(20001105)70:3<300::AID-BIT7>3.0.CO;2-3.

[120] H. L. Adams and C. R. Thomas. "The use of image analysis for morphological measurements on filamentous microorganisms." *Biotechnol Bioeng*, vol. 32, no. 5: pp. 707–12, 1988. Doi: 10.1002/bit.260320516.

[121] M. McIntyre, D. R. Berry, J. K. Eade, P. W. Cox, C. R. Thomas and B. McNeil. "Manual and semi-automated morphological analysis of *Penicillium chrysogenum* chemostat cultures." *Biotechnol Tech*, vol. 12, no. 9: pp. 671–75, 1998. Doi: 10.1023/A:1008856719038.

[122] A. Amanullah, P. Jüsten, A. Davies, G. C. Paul, A. W. Nienow and C. R. Thomas. "Agitation induced mycelial fragmentation of *Aspergillus oryzae* and *Penicillium chrysogenum*." *Biochem Eng J*, vol. 5, no. 2: pp. 109–14, 2000. Doi: 10.1016/S1369-703X(99)00059-5.

[123] T. Lübbehüsen, J. Nielsen and M. McIntyre. "Characterization of the *Mucor circinelloides* life cycle by on-line image analysis." *J Appl Microbiol*, vol. 95, no. 5: pp. 1152–60, 2003. Doi: 10.1046/j.1365-2672.2003.02098.x.

[124] E. Y. Park, T. Hamanaka, K. Higashiyama and S. Fujikawa. "Monitoring of morphological development of the arachidonic-acid-producing filamentous microorganism *Mortierella alpina*." *Appl Microbiol Biotechnol*, vol. 59, no. 6: pp. 706–12, 2002. Doi: 10.1007/s00253-002-1089-2.

[125] E. Y. Park, K. Koizumi and K. Higashiyama. "Analysis of morphological relationship between micro- and macromorphology of *Mortierella species* using

a flow-through chamber coupled with image analysis." *J Eukaryot Microbiol*, vol. 53, no. 3: pp. 199–203, 2006. Doi: 10.1111/j.1550-7408.2006.00094.x.

[126] T. Agger, A. B. Spohr, M. Carlsen and J. Nielsen. "Growth and product formation of *Aspergillus oryzae* during submerged cultivations: Verification of a morphologically structured model using fluorescent probes." *Biotechnol Bioeng*, vol. 57, no. 3: pp. 321–9, 1998. Doi: 10.1002/(SICI)1097-0290(19980205)57:3<321::AID-BIT9>3.0.CO;2-J.

[127] M. Rühl and U. Kües. "Automated image analysis to observe pellet morphology in liquid cultures of filamentous fungi such as the basidiomycete *Coprinopsis cinerea*." *Curr Biotechnol Pharma*, vol. 3, no. 3: pp. 241–53, 2009.

[128] T. Hamanaka, K. Higashiyama, S. Fujikawa and E. Y. Park. "Mycelial pellet intrastructure and visualization of mycelia and intracellular lipid in a culture of *Mortierella alpina*." *Appl Microbiol Biotechnol*, vol. 56, no. 1: pp. 233–38, 2001. Doi: 10.1007/s002530100649.

[129] G. C. Paul, C. A. Kent and C. R. Thomas. "Viability testing and characterization of germination of fungal spores by automatic image analysis." *Biotechnol Bioeng*, vol. 42, no. 1: pp. 11–23, 1993. Doi: 10.1002/bit.260420103.

[130] K.-B. Oh, Y. Chen, H. Matsuoka, A. Yamamoto and H. Kurata. "Morphological recognition of fungal spore germination by a computer-aided image analysis and its application to antifungal activity evaluation." *J Biotechnol*, vol. 45, no. 1: pp. 71–79, 1996. Doi: 10.1016/0168-1656(95)00148-4.

[131] C. L. Jones, G. T. Lonergan and D. E. Mainwaring. "The use of digital image segmentation to quantify an aminoanthraquinone dye biotransformation by white-rot fungi." *Biotechnol Tech*, vol. 7, no. 9: pp. 645–50, 1993. Doi: 10.1007/BF00151863.

[132] N. Wei, J. You, K. Friehs, E. Flaschel and T. W. Nattkemper. "An *in situ* probe for on-line monitoring of cell density and viability on the basis of dark field microscopy in conjunction with image processing and supervised machine learning." *Biotechnol Bioeng*, vol. 97, no. 6: pp. 1489–1500, 2007. Doi: 10.1002/bit.21368.

[133] P. Hough. "Machine analysis of bubble chamber pictures." In "International Conference on High Energy Accelerators and Instrumentation," CERN, 1959.

[134] N. Kharma, H. Moghnieh, J. Yao, Y. Guo, A. Abu-Baker, J. Laganiere, G. Rouleau and M. Cheriet. "Automatic segmentation of cells from microscopic imagery using ellipse detection." *IET Image Process*, vol. 1, no. 1: pp. 39–47, 2007. Doi: 10.1049/iet-ipr:20045262.

[135] F. S. Thatcher and D. S. Clark, eds. *Microorganisms in Foods*, vol. 1: Their Significance and Methods of Enumeration. Toronto, Canada: University of Toronto Press, 1968.

[136] P. W. Cox, G. C. Paul and C. R. Thomas. "Image analysis of the morphology of filamentous micro-organisms." *Microbiology*, vol. 144, no. 4: pp. 817–27, 1998. Doi: 10.1099/00221287-144-4-817.

[137] J. Diéguez-Uribeondo, G. Gierz and S. Bartnicki-García. "Image analysis of hyphal morphogenesis in Saprolegniaceae (Oomycetes)." *Fungal Genet Biol*, vol. 41, no. 3: pp. 293–307, 2004. Doi: 10.1016/j.fgb.2003.10.012.

[138] C. R. Thomas and G. C. Paul. "Applications of image analysis in cell technology." *Curr Opin Biotech*, vol. 7, no. 1: pp. 35–45, 1996. Doi: 10.1016/S0958-1669(96)80092-9.

[139] M. McIntyre and B. McNeil. "Dissolved carbon dioxide effects on morphology,

growth, and citrate production in *Aspergillus niger* A60." *Enzyme Microb Tech*, vol. 20, no. 2: pp. 135–42, 1997. Doi: 10.1016/S0141-0229(96)00108-1.

[140] Y. S. Rahardjo, S. Sie, F. J. Weber, J. Tramper and A. Rinzema. "Effect of low oxygen concentrations on growth and $\alpha$-amylase production of *Aspergillus oryzae* in model solid-state fermentation systems." *Biomol Eng*, vol. 21, no. 6: pp. 163–72, 2005. Doi: 10.1016/j.bioeng.2005.01.001.

[141] J. B. T. M. Roerdink. "An introduction to digital image processing." In M. H. F. Wilkinson and F. Schut, eds., "Digital Image analysis of microbes," pp. 3–36. Chichester, UK: John Wiley and Sons, 1998.

[142] M. Pons and H. Vivier. "Biomass quantification by image analysis." In "Bioanalysis and Biosensors for Bioprocess Monitoring," vol. 66 of *Advances in Biochemical Engineering/Biotechnology*, pp. 133–84. Berlin: Springer, 2000. Doi: 10.1007/3-540-48773-5_5.

[143] M. A. Pazoti, R. E. Garcia, J. D. C. Pessoa and O. M. Bruno. "Comparison of shape analysis methods for *Guinardia citricarpa* ascospore characterization." *Electron J Biotechn*, vol. 8, no. 3, 2005. Doi: 10.2225/vol8-issue3-fulltext-1.

[144] C. L. Jones, G. T. Lonergan and D. E. Mainwaring. "The use of image analysis for spore counts of white-rot fungi." *Biotechnol Tech*, vol. 6, no. 5: pp. 417–22, 1992. Doi: 10.1007/BF02447481.

[145] C. P. Larralde-Corona, F. López-Isunza and G. Viniegra-González. "Morphometric evaluation of the specific growth rate of *Aspergillus niger* grown in agar plates at high glucose levels." *Biotechnol Bioeng*, vol. 56, no. 3: pp. 287–94, 1997. Doi: 10.1002/(SICI)1097-0290(19971105)56:3<287::AID-BIT6>3.0.CO;2-F.

[146] M. McIntyre, J. Dynesen and J. Nielsen. "Morphological characterization of *Aspergillus nidulans*: growth, septation and fragmentation." *Microbiology*, vol. 147, no. 1: pp. 239–46, 2001.

[147] J. K. Pollack, Z. J. Li and M. R. Marten. "Fungal mycelia show lag time before re-growth on endogenous carbon." *Biotechnol Bioeng*, vol. 100, no. 3: pp. 458–65, 2008. Doi: 10.1002/bit.21779.

[148] A. Wongwicharn, B. McNeil and L. M. Harvey. "Effect of oxygen enrichment on morphology, growth, and heterologous protein production in chemostat cultures of *Aspergillus niger* B1-D." *Biotechnol Bioeng*, vol. 65, no. 4: pp. 416–24, 1999. Doi: 10.1002/(SICI)1097-0290(19991120)65:4<416::AID-BIT6>3.0.CO;2-Z.

[149] S. Bhargava, K. S. Wenger and M. R. Marten. "Pulsed addition of limiting-carbon during *Aspergillus oryzae* fermentation leads to improved productivity of a recombinant enzyme." *Biotechnol Bioeng*, vol. 82, no. 1: pp. 111–17, 2003. Doi: 10.1002/bit.10548.

[150] S. Bhargava, K. S. Wenger and M. R. Marten. "Pulsed feeding during fed-batch *Aspergillus oryzae* fermentation leads to improved oxygen mass transfer." *Biotechnol Prog*, vol. 19, no. 3: pp. 1091–94, 2003. Doi: 10.1021/bp025694p.

[151] K. Higashiyama, S. Fujikawa, E. Y. Park and M. Okabe. "Image analysis of morphological change during arachidonic acid production by *Mortierella alpina* 1S-4." *J Biosci Bioeng*, vol. 87, no. 4: pp. 489–94, 1999. Doi: 10.1016/S1389-1723(99)80098-X.

[152] C. Müller, K. Hansen, P. Szabo and J. Nielsen. "Effect of deletion of chitin synthase genes on mycelial morphology and culture viscosity in *As-*

*pergillus oryzae*." *Biotechnol Bioeng*, vol. 81, no. 5: pp. 525–34, 2003. Doi: 10.1002/bit.10491.

[153] Y. Q. Cui, R. G. J. M. van der Lans and K. C. A. M. Luyben. "Effects of dissolved oxygen tension and mechanical forces on fungal morphology in submerged fermentation." *Biotechnol Bioeng*, vol. 57, no. 4: pp. 409–19, 1998. Doi: 10.1002/(SICI)1097-0290(19980220)57:4<409::AID-BIT4>3.0.CO;2-Q.

[154] Q. T. Truong, N. Miyata and K. Iwahori. "Growth of *Aspergillus oryzae* during treatment of cassava starch processing wastewater with high content of suspended solids." *J Biosci Bioeng*, vol. 97, no. 5: pp. 329–35, 2004. Doi: 10.1016/S1389-1723(04)70214-5.

[155] A. Lucumi, C. Posten and M.-N. Pons. "Image analysis supported moss cell disruption in photo-bioreactors." *Plant Biol*, vol. 7, no. 3: pp. 276–82, 2005. Doi: 10.1055/s-2005-865638.

[156] S. Couri, E. P. Mercês, B. C. Neves and L. F. Senna. "Digital image processing as a tool to monitor biomass growth in *Aspergillus niger* 3T5B8 solid-state fermentation: preliminary results." *J Microsc*, vol. 224, no. 3: pp. 290–7, 2006. Doi: 10.1111/j.1365-2818.2006.01699.x.

[157] D. Cross and C. M. Kenerley. "Modelling the growth of *Trichoderma virens* with limited sampling of digital images." *J Appl Microbiol*, vol. 97, no. 3: pp. 486–94, 2004. Doi: 10.1111/j.1365-2672.2004.02310.x.

[158] T. Dörge, J. M. Carstensen and J. C. Frisvad. "Direct identification of pure *Penicillium species* using image analysis." *J Microbiol Methods*, vol. 41, no. 2: pp. 121–33, 2000. Doi: 10.1016/S0167-7012(00)00142-1.

[159] M. Papagianni. "Quantification of the fractal nature of mycelial aggregation

in *Aspergillus niger* submerged cultures." *Microb Cell Fact*, vol. 5, no. 1: p. 5, 2006. Doi: 10.1186/1475-2859-5-5.

[160] S. Sternberg. "Biomedical image processing." *Computer*, vol. 16, no. 1: pp. 22–34, 1983. Doi: 10.1109/MC.1983.1654163.

[161] M. H. F. Wilkinson. "Segmentation techniques in image analysis of microbes." In M. H. F. Wilkinson and F. Schut, eds., "Digital Image analysis of microbes," pp. 135–71. Chichester, UK: John Wiley and Sons, 1998.

[162] G. Zack, W. Rogers and S. Latt. "Automatic measurement of sister chromatid exchange frequency." *J Histochem Cytochem*, vol. 25, no. 7: pp. 741–53, 1977.

[163] T. Ridler and S. Calvard. "Picture thresholding using an iterative selection method." *IEEE T Syst Man Cyb*, vol. 8, no. 8: pp. 630–32, 1978. Doi: 10.1109/TSMC.1978.4310039.

[164] F. Leymarie and M. D. Levine. "Fast raster scan distance propagation on the discrete rectangular lattice." *CVGIP-Imag Understan*, vol. 55, no. 1: pp. 84–94, 1992. Doi: 10.1016/1049-9660(92)90008-Q.

[165] J. Wilson. "Towards the automated evaluation of crystallization trials." *Acta Crystallogr D Biol Crystallogr*, vol. 58, no. 11: pp. 1907–14, 2002. Doi: 10.1107/S0907444902016633.

[166] O. L. Mangasarian, W. N. Street and W. H. Wolberg. "Breast-cancer diagnosis and prognosis via linear-programming." *Oper Res*, vol. 43, no. 4: pp. 570–77, 1995.

[167] L. S. Pinto, L. M. Vieira, M. N. Pons, M. M. Fonseca and J. C. Menezes. "Morphology and viability analysis of *Streptomyces clavuligerus* in industrial

cultivation systems." *Bioprocess Biosyst Eng*, vol. 26, no. 3: pp. 177–84, 2004. Doi: 10.1007/s00449-003-0349-6.

[168] C. R. Denser Pamboukian, L. M. Guimarães and M. C. R. Facciotti. "Applications of image analysis in the characterization of *Streptomyces olindensis* in submerged culture." *Braz J Microbiol*, vol. 33, no. 1: pp. 17–21, 2002. Doi: 10.1590/S1517-83822002000100003.

[169] M. Sonka, V. Hlavac and R. Boyle. *Image Processing, Analysis and Machine Vision*. London: Chapman & Hall, 1st ed., 1993.

[170] T. Y. Zhang and C. Y. Suen. "A fast parallel algorithm for thinning digital patterns." *Commun ACM*, vol. 27, no. 3: pp. 236–39, 1984. Doi: 10.1145/357994.358023.

[171] J. Drouin, L. Louvel, B. Vanhoutte, H. Vivier, M. Pons and P. Germain. "Quantitative characterization of cellular differentiation of *Streptomyces ambofaciensin* submerged culture by image analysis." *Biotechnol Tech*, vol. 11, no. 11: pp. 819–24, 1997. Doi: 10.1023/A:1018429425800.

[172] D. Hitchcock, C. A. Glasbey and K. Ritz. "Image analysis of space-filling by networks: Application to a fungal mycelium." *Biotechnol Tech*, vol. 10, no. 3: pp. 205–10, 1996. Doi: 10.1007/BF00158947.

[173] O. Daniel, F. Schönholzer and J. Zeyer. "Quantification of fungal hyphae in leaves of deciduous trees by automated image analysis." *Appl Environ Microbiol*, vol. 61, no. 11: pp. 3910–18, 1995.

[174] M. Słaba, M. Bizukojć, B. Pałecz and J. Długoński. "Kinetic study of the toxicity of zinc and lead ions to the heavy metals accumulating fungus *Paecilomyces marquandii*." *Bioprocess Biosyst Eng*, vol. 28, no. 3: pp. 185–97, 2005. Doi: 10.1007/s00449-005-0026-z.

[175] M. Bizukojc and S. Ledakowicz. "A kinetic model to predict biomass content for *Aspergillus niger* germinating spores in the submerged culture." *Process Biochem*, vol. 41, no. 5: pp. 1063–71, 2006. Doi: 10.1016/j.procbio.2005.11.016.

[176] M. D. Fricker, J. A. Lee, L. Boddy and D. P. Bebber. "The interplay between structure and function in fungal networks." *Topologica*, vol. 1, no. 1: p. 004, 2008. Doi: 10.3731/topologica.1.004.

[177] Z. J. Li, V. Shukla, K. S. Wenger, A. P. Fordyce, A. G. Pedersen and M. R. Marten. "Effects of increased impeller power in a production-scale *Aspergillus oryzae* fermentation." *Biotechnol Prog*, vol. 18, no. 3: pp. 437–44, 2002. Doi: 10.1021/bp020023c.

[178] J. L. Harris. "Safe, low-distortion tape touch method for fungal slide mounts." *J Clin Microbiol*, vol. 38, no. 12: pp. 4683–84, 2000.

[179] J. L. Rodriguez-Tudela and P. Aviles. "Improved adhesive method for microscopic examination of fungi in culture." *J Clin Microbiol*, vol. 29, no. 11: pp. 2604–05, 1991.

[180] C. Kampichler, J. Rolschewski, D. P. Donnelly and L. Boddy. "Collembolan grazing affects the growth strategy of the cord-forming fungus *Hypholoma fasciculare*." *Soil Biol Biochem*, vol. 36, no. 4: pp. 591–99, 2004. Doi: 10.1016/j.soilbio.2003.12.004.

[181] J. M. Wells, M. J. Harris and L. Boddy. "Encounter with new resources causes polarized growth of the cord-forming basidiomycete *Phanerochaete velutina* on soil." *Microb Ecol*, vol. 36, no. 3: pp. 372–82, 1998. Doi: 10.1007/s002489900123.

[182] S. Marín, E. Companys, V. Sanchis, A. J. Ramos and N. Magan. "Effect of water activity and temperature on competing abilities of common maize fungi." *Mycol Res*, vol. 102, no. 8: pp. 959–64, 1998. Doi: 10.1017/S0953756297005613.

[183] M. R. Golinski, W. J. Boecklen and A. L. Dawe. "Two-dimensional fractal growth properties of the filamentous fungus *Cryphonectria parasitica*: the effects of hypovirus infection." *J Basic Microb*, vol. 48, no. 5: pp. 426–29, 2008. Doi: 10.1002/jobm.200800017.

[184] M. Obert, P. Pfeifer and M. Sernetz. "Microbial growth patterns described by fractal geometry." *J Bacteriol*, vol. 172, no. 3: pp. 1180–5, 1990.

[185] H. Kubo and H. Mihara. "cAMP promotes hyphal branching in *Mucor globosus*." *Mycoscience*, vol. 48, no. 3: pp. 187–89, 2007. Doi: 10.1007/s10267-007-0348-6.

[186] X. Lin and M. Momany. "Identification and complementation of abnormal hyphal branch mutants *ahbA1* and *ahbB1* in *Aspergillus nidulans*." *Biotechnol Prog*, vol. 41, no. 11: pp. 998–1006, 2004. Doi: 10.1016/j.fgb.2004.07.005.

[187] J. Diéguez-Uribeondo, J. C. Hernández-Crespo, R. Cortés, F. López and J. L. Pech. "Towards an automated analysis of video-microscopy images of fungal morphogenesis." *An Jard Bot Madrid*, vol. 62, no. 1: pp. 101–07, 2005. Doi: 10.3989/ajbm.2005.v62.i1.33.

[188] T. Nonomura, H. Tajima, Y. Kitagawa, N. Sekiya, K. Shitomi, M. Tanaka, K. Maeda, Y. Matsuda and H. Toyoda. "Distinguishable staining with neutral red for GFP-marked and GFP-nonmarked *Fusarium oxysporum* strains simultaneously colonizing root surfaces." *J Gen Plant Pathol*, vol. 69, no. 1: pp. 45–48, 2003. Doi: 10.1007/s10327-002-0018-7.

[189] M. Nopharatana, D. Mitchell and T. Howes. "Use of confocal microscopy to follow the development of penetrative hyphae during growth of *Rhizopus oligosporus* in an artificial solid-state fermentation system." *Biotechnol Bioeng*, vol. 81, no. 4: pp. 438–47, 2003. Doi: 10.1002/bit.10482.

[190] U. Reichl, H. Yang, E. D. Gilles and H. Wolf. "An improved method for measuring the interseptal spacing in hyphae of *Streptomyces tendae* by fluorescence microscopy coupled with image processing." *FEMS Microbiol Lett*, vol. 67, no. 1-2: pp. 207–10, 1990. Doi: 10.1111/j.1574-6968.1990.tb13864.x.

[191] T. Sone and A. J. F. Griffiths. "The *frost* gene of *Neurospora crassa* is a homolog of yeast *cdc1* and affects hyphal branching via manganese homeostasis." *Fungal Genet Biol*, vol. 28, no. 3: pp. 227–37, 1999. Doi: 10.1006/fgbi.1999.1169.

[192] C. L. Jones and G. T. Lonergan. "Histochemical detection of laccase in *Pycnoporus cinnabarinus* using microwave-enhanced colloidal gold microcrystallization." *Biotechnol Tech*, vol. 13, no. 12: pp. 871–75, 1999. Doi: 10.1023/A:1008965925940.

[193] H. Ishida, Y. Hata, E. Ichikawa, A. Kawato, K. Suginami and S. Imayasu. "Regulation of the glucoamylase-encoding gene (*glaB*), expressed in solid-state culture (koji) of *Aspergillus oryzae*." *J Ferment Bioeng*, vol. 86, no. 3: pp. 301–07, 1998. Doi: 10.1016/S0922-338X(98)80134-7.

[194] C. L. Jones, G. T. Lonergan and D. E. Mainwaring. "Specimen preparation for high-contrast image-processing and fractal analysis of branching fungal colonies." *Biotechnol Tech*, vol. 8, no. 5: pp. 313–18, 1994. Doi: 10.1007/BF02428973.

[195] Y. Rahardjo, D. Korona, S. Haemers, F. Weber, J. Tramper and A. Rinzema. "Limitations of membrane cultures as a model solid-state fermentation system." *Lett Appl Microbiol*, vol. 39, no. 6: pp. 504–08, 2004. Doi: 10.1111/j.1472-765X.2004.01614.x.

[196] L. Grimm, S. Kelly, J. Hengstler, A. Göbel, R. Krull and D. Hempel. "Kinetic studies on the aggregation of *Aspergillus niger* conidia." *Biotechnol Bioeng*, vol. 87, no. 2: pp. 213–18, 2004. Doi: 10.1002/bit.20130.

[197] L. Grimm, S. Kelly, I. Völkerding, R. Krull and D. Hempel. "Influence of mechanical stress and surface interaction on the aggregation of *Aspergillus niger* conidia." *Biotechnol Bioeng*, vol. 92, no. 7: pp. 879–88, 2005. Doi: 10.1002/bit.20666.

[198] T. Christiansen, A. B. Spohr and J. Nielsen. "On-line study of growth kinetics of single hyphae of *Aspergillus oryzae* in a flow-through cell." *Biotechnol Bioeng*, vol. 63, no. 2: pp. 147–53, 1999. Doi: 10.1002/(SICI)1097-0290(19990420)63:2<147::AID-BIT3>3.0.CO;2-M.

[199] T. R. Jørgensen, P. A. vanKuyk, B. R. Poulsen, G. J. Ruijter, J. Visser and J. J. Iversen. "Glucose uptake and growth of glucose-limited chemostat cultures of *Aspergillus niger* and a disruptant lacking MstA, a high-affinity glucose transporter." *Microbiology*, vol. 153, no. 6: pp. 1963–73, 2007. Doi: 10.1099/mic.0.2006/005090-0.

[200] M. McIntyre, J. Breum, J. Arnau and J. Nielsen. "Growth physiology and dimorphism of *Mucor circinelloides* (syn. *racemosus*) during submerged batch cultivation." *Appl Microbiol Biotechnol*, vol. 58, no. 4: pp. 495–502, 2002. Doi: 10.1007/s00253-001-0916-1.

[201] J. Kim, J. Lim, C. Kim and S. Kim. "Morphology and kinetics studies on cephalosporin C production by *Cephalosporium acremonium* M25 in a 30-l bioreactor using a mixture of inocula." *Lett Appl Microbiol*, vol. 40, no. 5: pp. 307–11, 2005. Doi: 10.1111/j.1472-765X.2005.01682.x.

[202] L. H. Grimm, S. Kelly, R. Krull and D. C. Hempel. "Morphology and productivity of filamentous fungi." *Appl Microbiol Biotechnol*, vol. 69, no. 4: pp. 375–84, 2005. Doi: 10.1007/s00253-005-0213-5.

[203] P. Žnidaršič, R. Komel and A. Pavko. "Studies of a pelleted growth form of *Rhizopus nigricans* as a biocatalyst for progesterone 11$\alpha$-hydroxylation." *J Biotechnol*, vol. 60, no. 3: pp. 207–16, 1998. Doi: 10.1016/S0168-1656(98)00010-8.

[204] S.-K. Treskatis, V. Orgeldinger, H. Wolf and E. D. Gilles. "Morphological characterization of filamentous microorganisms in submerged cultures by on-line digital image analysis and pattern recognition." *Biotechnol Bioeng*, vol. 53, no. 2: pp. 191–201, 1997. Doi: 10.1002/(SICI)1097-0290(19970120)53:2<191::AID-BIT9>3.0.CO;2-J.

[205] C. Park, J.-S. Lim, Y. Lee, B. Lee, S.-W. Kim, J. Lee and S. Kim. "Optimization and morphology for decolorization of reactive black 5 by *Funalia trogii*." *Enzyme Microb Tech*, vol. 40, no. 7: pp. 1758–64, 2007. Doi: 10.1016/j.enzmictec.2006.12.005.

[206] E. Nahas and M. M. Waldemarin. "Control of amylase production and growth characteristics of *Aspergillus ochraceus*." *Rev Latinoam Microbiol*, vol. 44, no. 1: pp. 5–10, 2002.

[207] C.-H. Shu, P.-F. Chou and I.-C. Hsu. "Effects of morphology and oxygen supply on schizophyllan formation by *Schizophyllum commune* using a pellet

size controlling bioreactor." *J Chem Technol Biot*, vol. 80, no. 12: pp. 1383–88, 2005. Doi: 10.1002/jctb.1339.

[208] J.-H. Kim and I. C. Hancock. "Pellet forming and fragmentation in liquid culture of *Streptomyces griseus*." *Biotechnol Lett*, vol. 22, no. 3: pp. 189–92, 2000. Doi: 10.1023/A:1005632929809.

[209] M. Papagianni, M. Mattey and B. Kristiansen. "The influence of glucose concentration on citric acid production and morphology of *Aspergillus niger* in batch and culture." *Enzyme Microb Tech*, vol. 25, no. 8–9: pp. 710–17, 1999. Doi: 10.1016/S0141-0229(99)00102-7.

[210] R. C. Righelato, A. P. J. Trinci, S. J. Pirt and A. Peat. "The influence of maintenance energy and growth rate on the metabolic activity, morphology and conidiation of *Penicillium chrysogenum*." *J Gen Microbiol*, vol. 50, no. 3: pp. 399–412, 1968. Doi: 10.1099/00221287-50-3-399.

[211] Megazyme International Ireland Ltd. *Megazyme alpha-amylase assay procedure (ceralpha method)*, 2004.

[212] M. M. Bradford. "A rapid and sensitive method for the quantitation of microgram quantities of protein utilizing the principle of protein-dye binding." *Anal Biochem*, vol. 72: pp. 248–54, 1976. Doi: 10.1016/0003-2697(76)90527-3.

[213] T. Agger, J. B. Petersen, S. M. O'Connor, R. L. Murphy, J. M. Kelly and J. Nielsen. "Physiological characterisation of recombinant *Aspergillus nidulans* strains with different *creA* genotypes expressing *A. oryzae* alpha-amylase." *J Biotechnol*, vol. 92, no. 3: pp. 279–85, 2002. Doi: 10.1016/S0168-1656(01)00366-2.

[214] Y. Q. Cui, J. N. W. Ouwehand, R. G. J. M. van der Lans, M. L. F. Giuseppin and K. C. A. M. Luyben. "Aspects of the use of complex media for submerged

fermentation of *Aspergillus awamori*." *Enzyme Microb Tech*, vol. 23, no. 1–2: pp. 168–77, 1998. Doi: 10.1016/S0141-0229(98)00038-6.

[215] S. Ramachandran, A. K. Patel, K. M. Nampoothiri, S. Chandran, G. Szakacs, C. R. Soccol and A. Pandey. "Alpha amylase from a fungal culture grown on oil cakes and its properties." *Braz Arch Biol Technol*, vol. 47, no. 2: pp. 309–17, 2004. Doi: 10.1590/S1516-89132004000200019.

[216] C. L. Gordon, D. B. Archer, D. J. Jeenes, J. H. Doonan, B. Wells, A. P. Trinci and G. D. Robson. "A glucoamylase::GFP gene fusion to study protein secretion by individual hyphae of *Aspergillus niger*." *J Microbiol Methods*, vol. 42, no. 1: pp. 39–48, 2000. Doi: 10.1016/S0167-7012(00)00170-6.

[217] B. C. van der Aa, M. Asther and Y. F. Dufrêne. "Surface properties of *Aspergillus oryzae* spores investigated by atomic force microscopy." *Colloid Surface B*, vol. 24, no. 3–4: pp. 277–84, 2002. Doi: 10.1016/S0927-7765(01)00277-6.

[218] E. Dague, D. Alsteens, J.-P. Latgé and Y. F. Dufrêne. "High-resolution cell surface dynamics of germinating *Aspergillus fumigatus* conidia." *Biophys J*, vol. 94, no. 2: pp. 656–60, 2008. Doi: 10.1529/biophysj.107.116491.

[219] S. Yoon and J. F. Robyt. "Activation and stabilization of 10 starch-degrading enzymes by Triton X-100, polyethylene glycols, and polyvinyl alcohols." *Enzyme Microb Tech*, vol. 37, no. 5: pp. 556–62, 2005. Doi: 10.1016/j.enzmictec.2005.04.002.

[220] P. Žnidaršič and A. Pavko. "The morphology of filamentous fungi in submerged cultivations as a bioprocess parameter." *Food Technol Biotechnol*, vol. 39, no. 3: pp. 237–52, 2001.

[221] Y. Park, S. Tamura, Y. Koike, M. Toriyama and M. Okabe. "Mycelial pellet intrastructure visualization and viability prediction in a culture of *Streptomyces fradiae* using confocal scanning laser microscopy." *J Ferment Bioeng*, vol. 84, no. 5: pp. 483–86, 1997. Doi: 10.1016/S0922-338X(97)82014-4.

[222] B. B. Mandelbrot. *The fractal geometry of nature*. New York: W.H. Freeman, 1982.

[223] J. C. Kim, J. S. Lim, J. M. Kim, C. Kim and S. W. Kim. "Relationship between morphology and viscosity of the main culture broth of *Cephalosporium acremonium* M25." *Korea-Aust Rheol J*, vol. 17, no. 1: pp. 15–20, 2005.

[224] D. Ryoo. "Fungal fractal morphology of pellet formation in *Aspergillus niger*." *Biotechnol Tech*, vol. 13, no. 1: pp. 33–36, 1999. Doi: 10.1023/A:1008835529941.

[225] T. Matsuyama and M. Matsushita. "Self-similar colony morphogenesis by gram-negative rods as the experimental model of fractal growth by a cell population." *Appl Environ Microbiol*, vol. 58, no. 4: pp. 1227–32, 1992.

[226] C. L. Jones, G. T. Lonergan and D. E. Mainwaring. "Mycelial fragment size distribution: an analysis based on fractal geometry." *Appl Microbiol Biotechnol*, vol. 39, no. 2: pp. 242–49, 1993. Doi: 10.1007/BF00228613.

[227] B. Mandelbrot. "How long is the coast of Britain? Statistical self-similarity and fractional dimension." *Science*, vol. 156, no. 3775: pp. 636–38, 1967. Doi: 10.1126/science.156.3775.636.

[228] L. F. Richardson. "The problem of contiguity: An appendix to Statistics of Deadly Quarrels." In "General systems: Yearbook of the Society for the Advancement of General Systems Theory," vol. 6, pp. 139–87. Ann Arbor, Michigan: Society for General Systems Research, 1961.

[229] J. C. Russ. *The image processing handbook*. Boca Raton, Florida: CRC Press, 4th ed., 2002.

[230] L. Boddy and D. P. Donnelly. "Fractal geometry and microorganisms in the environment." In "Biophysical chemistry of fractal structures and processes in environmental systems," pp. 239–72. Chichester: John Wiley and Sons, 2008.

[231] J. M. Blackledge. *Digital Image Processing*. Chichester: Horwood Publishing, 1st ed., 2005.

[232] C. L. Jones, G. T. Lonergan and D. E. Mainwaring. "Acid phosphatase positional correlations in solid surface fungal cultivation: A fractal interpretation of biochemical differentiation." *Biochem Bioph Res Co*, vol. 208, no. 3: pp. 1159–65, 1995. Doi: 10.1006/bbrc.1995.1455.

[233] L. Finkler, Y. Ginoris, C. Luna, T. Alves, J. Pinto and M. Coelho. "Morphological characterization of *Cupriavidus necator* DSM 545 flocs through image analysis." *World J Microb Biot*, vol. 23, no. 6: pp. 801–8, 2007. Doi: 10.1007/s11274-006-9300-8.

[234] D. J. Barry, C. Chan and G. A. Williams. "Nitrocellulose as a general tool for fungal slide mounts." *J Clin Microbiol*, vol. 45, no. 3: pp. 1074–5, 2007. Doi: 10.1128/JCM.01609-06.

[235] D. Barry, C. Chan and G. Williams. "Morphological quantification of filamentous fungal development using membrane immobilization and automatic image analysis." *J Ind Microbiol Biotechnol*, vol. 36, no. 6: pp. 787–800, 2009. Doi: 10.1007/s10295-009-0552-9.

[236] D. J. Barry, O. C. Ifeyinwa, S. R. McGee, R. Ryan, G. A. Williams and J. M. Blackledge. "Relating fractal dimension to branching behaviour in filamentous microorganisms." *ISAST T Elec Sig Proc*, vol. 1, no. 4: pp. 71–76, 2009.

[237] E. T. Reese and A. Maguire. "Surfactants as stimulants of enzyme production by microorganisms." *Appl Environ Microbiol*, vol. 17, no. 2: pp. 242–45, 1969.

[238] K. Thevissen, F. R. G. Terras and W. F. Broekaert. "Permeabilization of fungal membranes by plant defensins inhibits fungal growth." *Appl Environ Microbiol*, vol. 65, no. 12: pp. 5451–58, 1999.

[239] T. Theis, M. Wedde, V. Meyer and U. Stahl. "The antifungal protein from *Aspergillus giganteus* causes membrane permeabilization." *Antimicrob Agents Chemother*, vol. 47, no. 2: pp. 588–93, 2003. Doi: 10.1128/AAC.47.2.588-593.2003.

## About this document

The complete manuscript for this thesis was prepared with LaTeX $2_\varepsilon$ using Donald Knuth's Computer Modern fonts. The following additional packages were useful in completing this task: pstool (by Zebb Prime and Will Robertson) for inserting LaTeX constructions into figures; natbib (Patrick W. Daly) for citation and bibliography formatting; fancyhdr (Piet van Oostrum) and titlesec (Javier Bezos) for formatting headings and page layout; tabularx (David Carlisle) and booktabs (Simon Fear) for table formatting. Illustrations were produced using Inkscape, graphs with Microsoft Excel and images with ImageJ.